



Analysis of the Transport and Fate of Metals Released from the Gold King Mine in the Animas and San Juan Rivers

APPENDICES



Cover photo credit:
Southern Ute Indian Tribe

Appendix A.
Information about Acquired Data Sources

Table of Contents

LIST OF ABBREVIATIONS AND ACRONYMS.....	3
TABLE A-1. LINKS TO ACCESS GOLD KING MINE EVENT-RELATED DATA	4
TABLE A-2. LINKS TO ACCESS GOLD KING MINE POST-EVENT RELATED DATA.....	5
TABLE A-3. LINKS TO ACCESS GOLD KING MINE PRE-EVENT RELATED DATA.....	6
TABLE A-4. LINKS TO ACCESS GENERAL SOURCES OF DATA USED TO SUPPORT GROUNDWATER ANALYSIS AND MODELING. 7	
TABLE A-5. LINKS TO ACCESS GENERAL SOURCES OF DATA USED TO SUPPORT ANALYSIS AND MODELING.....	9
TABLE A-6. CONSOLIDATED LIST OF SITES SAMPLED BY DATA PROVIDERS DURING AND AFTER THE GOLD KING MINE RELEASE	10
TABLE A-7. LIST OF METALS LABORATORY METHODS FOR SURFACE WATER SAMPLES BY DATA PROVIDER	21
TABLE A-8. LIST OF METALS LABORATORY METHODS FOR SEDIMENT SAMPLES BY DATA PROVIDER	27
TABLE A-9. ANALYTICAL METHODOLOGY FOR METAL ANALYSES. INCLUDES METHODS USED FOR HISTORIC SAMPLES.	31
TABLE A-10. LIST OF LABORATORY METHODS FOR GENERAL ANALYTES BY DATA PROVIDER.	33
TABLE A-11. LINKS TO QUALITY ASSURANCE DOCUMENTATION FROM DATA PROVIDERS	39

LIST OF ABBREVIATIONS AND ACRONYMS

CDPHE	Colorado Department of Public Health and Environment
CoF	City of Farmington
EC	Electrical conductivity
MSI	Mountain Studies Institute
NGO	non-governmental organization
NMED	New Mexico Environment Department
NNEPA	Navajo Nation Environmental Protection Agency
ODOSat	Optical dissolved oxygen saturation
RCWWN	The Rivers of Colorado Water Watch Network (River Watch)
RDO	Rugged dissolved oxygen (probe)
River Watch	The Rivers of Colorado Water Watch Network (RCWWN)
SADIE	Superfund Analytic Data Integrator & Explorer
STIC	Stream Temperature, Intermittency, and Conductivity logger
SUIT	Southern Ute Indian Tribe
UDEQ	Utah Department of Environmental Quality
UMUT	Ute Mountain Ute Tribe
USEPA	United States Environmental Protection Agency
USGS	United States Geological Survey

Table A-1. Links to access Gold King Mine event-related data

	Data source	Information obtained
Federal	US EPA http://www2.epa.gov/goldkingmine	August-November 2015 surface water and sediment quality data
	US EPA Region 6 https://www.env.nm.gov/river-water-safety/animas-river-data-documents-page	September 2015 sediment core quality data
	USGS Gold King Mine Release Database http://water.usgs.gov/owq/gkm/wq.html	August-December 2015 surface water quality data
	USGS https://www.usgs.gov/	August-September, November 2015 surface water quality data August-September 2015 sonde data
States	Colorado Department of Public Health and Environment https://www.colorado.gov/pacific/cdphe/animas-river-water-quality-sampling-and-data	August, October, December 2015 surface water quality data August 2015 sediment quality data August 2015 fish tissue data
	New Mexico Environment Department https://www.env.nm.gov/riverwatersafety/GoldKingData.html	August 2015 surface water quality data August 2015 sonde data
	Utah Department of Environmental Quality http://www.deq.utah.gov/Topics/Water/goldkingmine/data.htm	August-October 2015 surface water and sediment quality data
City	City of Farmington https://www.env.nm.gov/river-water-safety/animas-river-data-documents-page/	August-November 2015 surface water quality data
Tribes	Navajo Nation Environmental Protection Agency http://waterqualitydata.us/portal/ (Water Quality Portal)	August 2015 surface water quality data
	Southern Ute Indian Tribe ftp://ftp.southernute-nsn.gov (requires password permission) http://waterqualitydata.us/portal/ (Water Quality Portal)	August 2015 surface water quality data August-November 2015 sonde data
	Ute Mountain Ute Tribe https://ofmpub.epa.gov/storpubl/dw_pages.querycriteria (STORET Central Warehouse)	August 2015 surface water quality data
NGO	The Rivers of Colorado Water Watch Network http://waterqualitydata.us/portal/ (Water Quality Portal)	August-October 2015 surface water quality data

Table A-2. Links to access Gold King Mine post-event related data

	Data source	Information obtained
Federal	US Environmental Protection Agency http://www2.epa.gov/goldkingmine	March, June 2016 surface water and sediment quality data
	US Geological Survey http://waterqualitydata.us/portal (Water Quality Portal)	January-August 2016 surface water quality data
States	Colorado Department of Public Health and Environment https://www.colorado.gov/pacific/cdphe/animas-river-water-quality-sampling-and-data	February, April-July 2016 surface water quality data May-July 2016 sediment quality data
	New Mexico Environment Department https://www.env.nm.gov/	February, March 2016 sediment quality data
	Utah Department of Environmental Quality http://www.deq.utah.gov/Topics/Water/goldkingmine/data.htm	February-June 2016 surface water quality data February 2016 sediment quality data
City	City of Farmington https://www.env.nm.gov/river-water-safety/animas-river-data-documents-page/	January-June 2016 surface water quality data
Tribes	Southern Ute Indian Tribe http://waterqualitydata.us/portal (Water Quality Portal) https://www.southernute-nsn.gov/	March-June 2016 surface water quality data March 2016 sediment quality data
NGO	Mountain Studies Institute http://www.mountainstudies.org/animasriver	February-June 2016 surface water quality data

Table A-3. Links to access Gold King Mine pre-event related data

	Data source	General location	Information obtained
Federal	US EPA https://ofmpub.epa.gov/storpubl/dw_pages.QUERYcriteria (STORET Central Warehouse)	San Juan River	2000 surface water quality data for 1 site
	US EPA Superfund Analytic Data Integrator & Explorer (SADIE) https://r8.ercloud.org/sadie (requires password permission)	GKM, Cement Creek, and Animas River in Colorado	2011-2015 surface water quality data 2012-2014 sediment quality data
	USGS Gold King Mine Release Database http://water.usgs.gov/owg/gkm/wg.html	Cement Creek; Animas and San Juan Rivers	1928-2005 surface water quality data 1977-2007 sediment quality data
	USGS National Water Information System (NWIS) Surface Water Data http://waterdata.usgs.gov/nwis	San Juan River in New Mexico	2000-2015 surface water quality data for reference gage
	USGS Open-File Report 97-151 appendices data https://pubs.er.usgs.gov/publication/ofr97151	Cement Creek, Animas River	1995-1996 surface water and sediment quality data (water only on Animas River)
	USGS Professional Paper 1651 database http://pubs.usgs.gov/pp/1651/	Upper Animas River Watershed	1996-2001 surface water and sediment quality data
States	Colorado Department of Public Health and Environment https://ofmpub.epa.gov/storpubl/dw_pages.QUERYcriteria (STORET Central Warehouse)	North Fork Cement Creek, Cement Creek, and Animas River in Colorado	1968-2015 surface water quality data
	New Mexico Environment Department https://ofmpub.epa.gov/storpubl/dw_pages.QUERYcriteria (STORET Central Warehouse) https://www.env.nm.gov/	Animas and San Juan Rivers in New Mexico	2001-2010 surface water quality data 2002 sediment quality data 2010-2014 field data
	Utah Department of Environmental Quality https://ofmpub.epa.gov/storpubl/dw_pages.QUERYcriteria (STORET Central Warehouse)	San Juan River in Utah and Utah/Colorado border	1975-2014 surface water quality data
Tribes	Navajo Nation Environmental Protection Agency http://waterqualitydata.us/portal (Water Quality Portal)	San Juan River in New Mexico and Utah	1999-2015 surface water quality data
	Southern Ute Indian Tribe https://www.southernute-nsn.gov/ http://waterqualitydata.us/portal (Water Quality Portal)	Animas River in SUIT Reservation	1992-2015 surface water quality data 2013-2015 sonde data Summer 2015 fish tissue data
	Ute Mountain Tribe http://www.utemountainutetribes.com/	San Juan River above and below the Colorado/New Mexico border	1996 -2013 surface water quality data
NGO	The Rivers of Colorado Water Watch Network http://waterqualitydata.us/portal (Water Quality Portal)	Cement Creek in Colorado; Animas River in Colorado and New Mexico	1991-2015 surface water quality data

Table A-4. Links to access general sources of data used to support groundwater analysis and modeling

	Data source	Information obtained
Federal	GeoCommunicator http://www.geocommunicator.gov/GeoComm/lsis_home/home/index.htm	Public Land Survey System (PLSS) shapefiles for La Plata and San Juan Counties in Colorado, and San Juan County in New Mexico
	Geospatial Data Gateway https://gdg.sc.egov.usda.gov/GDGOrder.aspx	ground elevation data in raster format at 1/3 arc-second (about 10 meters)
	US EPA Region 6 Scribe database https://www.epaosrc.org/site/SCRIBE (database access requires password permission)	list and location of public water systems sampled by EPA Region 6 in relation to the GKM event GKM event-related water quality data for public water systems
	US EPA Safe Drinking Water Information System (SDWIS) https://www.epa.gov/enviro/sdwis-search	identification of public drinking water systems in Colorado, New Mexico, and Utah
	USGS National Geologic Map Database http://ngmdb.usgs.gov/ngmdb/ngmdb_home.html	New Mexico geology maps
	USGS The National Map http://nationalmap.gov/	ground elevation data in raster format at 1/3 arc-second (about 10 meters)
	USGS National Water Information System (NWIS) Surface Water Data http://waterdata.usgs.gov/nwis/sw	location of stream gages, daily stream discharges
States	Colorado Department of Public Health and Environment https://www.colorado.gov/pacific/cdphe/animas-river-water-quality-sampling-and-data	event-related drinking water quality data collected in Colorado
	Colorado's Decision Support Systems http://cdss.state.co.us/Pages/CDSHome.aspx	records of annual water diversions of Colorado wells map of Colorado wells
	Colorado Division of Water Resources http://www.dwr.state.co.us/wellpermitsearch/	Colorado well permits and driller's logs, static water levels, well yield
	New Mexico Resource Geographic Information System http://rgis.unm.edu/	LiDAR for about the lower third of the Animas HUC 8 (14080104)
	New Mexico Bureau of Geology and Mineral Resources, Aquifer Mapping Program https://geoinfo.nmt.edu/	location and construction information of wells near the Animas and San Juan Rivers located mostly in New Mexico water level measurements for wells GKM event-related and post-event well water quality data
	New Mexico Office of the State Engineer and Interstate Stream Commission http://www.ose.state.nm.us/index.php	New Mexico well driller's logs, water rights, water use, location of wells, water column depth aquifer test data, daily discharge in ditches
	Utah Division of Water Rights http://www.waterrights.utah.gov/	Utah well driller's logs, water rights, water use, location of wells
City	City of Farmington http://www.fmtn.org/DocumentCenter/View/46	Irrigation ditch map

	Data source	Information obtained
County	La Plata County, Colorado GIS http://lpcgis.laplata.co.us/laplatas/	GIS layers for La Plata County, Colorado: streams, lakes/rivers, irrigation ditches, structures, and location of wells by parcel
	San Juan County Office of Emergency Management http://www.sjcoem.com/	floodplain map for San Juan County, New Mexico
Misc.	Animas Water Company, Colorado http://animaswatercompany.com/	event-related data for community wells in Colorado
	The GeoCommunity http://data.geocomm.com/catalog	medium resolution (1:100,000 scale) USGS Digital Line Graphs - Hypsography, Hydrography, and Transportation

Table A-5. Links to access general sources of data used to support analysis and modeling

	Data source	Information obtained
Federal	Better Assessment Science Integrating Point and Nonpoint Sources (BASINS) Version 4.1 http://water.epa.gov/scitech/datait/models/basins/index.cfm	location of USGS streamflow gages
	EnviroAtlas https://www.epa.gov/enviroatlas	reference maps, animation of total metal concentration through time,
	Geospatial Data Gateway https://gdg.sc.egov.usda.gov/GDGOrder.aspx	8- and 10-digit Hydrologic Unit Code (HUC) shapefiles; mid-Animas River ortho-image
	National Atlas of the United States http://nationalatlas.gov	State boundaries
	National Hydrography Dataset (NHD) http://nhd.usgs.gov/index.html	high-resolution (1:24,000 or larger scale) vector stream network
	National Hydrography Dataset Plus (NHDPlus Version 2) http://www.horizon-systems.com/NHDPlus/index.php	medium resolution (1:100,000) vector stream network
	USGS Mineral Resources On-Line Spatial Data http://mrddata.usgs.gov/	mineral resources data, location of active mines, sediment geochemistry data
	USGS National Water Information System (NWIS) Surface Water Data http://waterdata.usgs.gov/nwis/sw	gage field measurements (cross sections), streamflow data
	USGS StreamStats Version 3 (Colorado application) http://streamstatsags.cr.usgs.gov/v3_beta/viewer.htm?stabbr=CO	drainage area shapefiles for the most downstream point of each WASP segment drainage area shapefile for EPA Baker's Bridge sampling site
USGS The National Map http://nationalmap.gov/	ground elevation data in raster format at 1/3 arc-second (about 10 meters)	
States	New Mexico Bureau of Geology and Mineral Resources, Aquifer Mapping Program https://geoinfo.nmt.edu/	feature classes for New Mexico's District 5: district and city boundaries; streams, Places of Use (POUs), and San Juan Basin conveyances New Mexico's Points of Diversion (PODs) feature class
	Automated Surface Observing System (ASOS) https://mesonet.agron.iastate.edu/request/download.phtml	hourly precipitation data
Misc.	Google Earth 7.1.5.1557 https://www.google.com/earth/	aerial imagery, georeference location, elevations

Table A-6. Consolidated list of sites sampled by data providers during and after the Gold King Mine release

Agency	Site ID	Distance from source (km) ¹	Description	Site Type ²	Latitude	Longitude	Media ³
USGS	Gold King-MiniSipper	0.00	NA	Source	37.894583	-107.638358	SW
USEPA	CC06	0.00	NA	Source	37.894583	-107.638358	SW
CDPHE	CO_GKM_0	0.00	Effluent - mine adit (Gold King Mine adit)	Mine Effluent	37.89455	-107.63827	SW, SED
NNEPA	NNEPA-32GOLDKING01	0.00	Gold King Mine adit	Source	37.8946387	-107.6384095	SW
CDPHE	CO_GKM_1	0.79	Gold King Mine effluent	Main	37.895200	-107.6468	SW
CDPHE	CO_GKM_2	0.80	Influent prior to treatment	Main	37.895200	-107.647000	SW
CDPHE	9458	0.82	Cement Creek above Gold King Mine	Reference	37.89605	-107.64696	SW
USGS	375344107384801	0.82	Cement Creek above North Fork Cement Creek near Silverton, CO	Reference	37.89565556	-107.6469389	SW
CDPHE	CO_GKM_3	0.82	(Gold King Mine) Treatment effluent	Reference	37.89572	-107.64714	SW
CDPHE	CO_RI_R2	0.82	Cement Creek above Gold King	Reference	37.89619167	-107.64682	SW
CDPHE	CO_RI_R3	0.82	Cement Creek upstream of GKM treatment	Reference	37.89545	-107.6475	SW
CDPHE	CO_RI_M1	0.87	Cement Creek below Gold King Mine	Main	37.89468	-107.64737	SW
USEPA	GKM13	0.87	NA	Main	37.8946916	-107.647253	SW
NNEPA	NNEPA-32EPAPOND402	0.89	USEPA Gold King Mine Pond 4 outlet	Pond (treatment)	37.8946506	-107.6474652	SW
CDPHE	CO_RI_M2	0.90	Cement Creek (below mine)	Main	37.89456	-107.64774	SW
CDPHE	9456	0.97	Cement Creek below Gold King	Main	37.89396833	-107.647855	SW
CDPHE	CO_RI_M4	0.98	Cement Creek Downstream of GKM treatment	Main	37.8938	-107.64762	SW
USGS	375333107385401	1.13	Cement Creek above American Tunnel below North Fork Cement Creek	Main	37.892575	-107.6483611	SW
USGS	375322107391101	1.75	Cement Creek above South Fork Cement Creek near Silverton, CO	Main	37.8897	-107.6532694	SW
CDPHE	9454	3.06	Cement Creek Ski Resort before entering Las Animas River	Main	37.8848	-107.66526	SW
USGS	09358550	12.41	Cement Creek at Silverton, CO	Main	37.819664	-107.663719	SW
USEPA	CC48	12.54	NA	Main	37.819984	-107.663275	SW, SED
USGS	CC48-MiniSipper	12.55	Cement Creek upstream from Animas	Main	37.82	-107.6631	SW
NNEPA	NNEPA-32CEMENTCR03	12.83	Cement Creek at Silverton Park	Main	37.8181866	-107.6616043	SW
RCWWN	CORIVWCH_WQX-323	13.08	Cement Creek	Main	37.8159	-107.6618	SW
USEPA	CC 14th St Bridge	13.45	NA	Main	37.812475	-107.661401	SW

Gold King Mine Release of Acid Mine Drainage to the Animas and San Juan Rivers

Agency	Site ID	Distance from source (km) ¹	Description	Site Type ²	Latitude	Longitude	Media ³
CDPHE	CEM49	13.78	Cement Creek above Animas River	Main	37.80999333	-107.6606917	SW
CDPHE	9488	13.90	Animas River above Cement Creek	Reference	37.810892	-107.659445	SW, SED
USGS	09358000	13.90	Animas River at Silverton, CO.	Reference	37.810917	-107.658897	SW
USEPA	A68	13.90	NA	Reference	37.811202	-107.659167	SW, SED
USGS	A68-MiniSipper	13.90	14th Street Gauge @ 13th Street Bridge	Reference	37.81120198	-107.6591665	SW
CDPHE	CO_RI_R9	13.90	Animas River above Cement Creek	Reference	37.811065	-107.659232	SW
RCWWN	CORIVWCH_WQX-103	13.90	13th St Bridge	Reference	37.811	-107.6589	SW
RCWWN	CORIVWCH_WQX-467	13.90	Howardsville	Reference	37.8326	-107.6002	SW
CDPHE	9487	14.63	Animas River above Mineral Creek	Main	37.8040225	-107.664772	SW, SED
CDPHE	CO_RI_R8	15.14	Mineral Creek above Animas River	Reference	37.80282	-107.6728217	SW
USEPA	M34	15.14	NA	Reference	37.8028	-107.67222	SW, SED
CDPHE	82	15.56	Animas River near Silverton	Main	37.79700133	-107.6693973	SW, SED
CDPHE	9486	15.66	Animas River below Mineral Creek confluence	Main	37.79625	-107.66942	SW
RCWWN	CORIVWCH_WQX-3579	15.88	Above A72	Main	37.7942	-107.66894	SW
USGS	09359020	16.35	Animas River below Silverton, CO	Main	37.790272	-107.667587	SW
USEPA	A72	16.35	NA	Main	37.79027	-107.667578	SW, SED
USGS	A72-MiniSipper	16.35	Animas gage below Silverton	Main	37.79027049	-107.6675778	SW
RCWWN	CORIVWCH_WQX-3611	16.40	A72	Main	37.78993	-107.66756	SW
CDPHE	AN72	16.42	Animas River at gage above railroad bridge	Main	37.78976717	-107.6675452	SW, SED
USEPA	GKMSE27	24.24	NA NA	Main	37.72437	-107.65405	SED
USEPA	A73	24.48		Main	37.72215833	-107.6548278	SW
CDPHE	9485	24.53	Animas River in Canyon 3 above Elk Creek	Main	37.721807	-107.654554	SW
USEPA	A75D	45.13	NA	Main	37.597779	-107.775621	SW, SED
USGS	Bakers Bridge-MiniSipper	63.44	Baker Bridge 20 miles south of Silverton	Main	37.4589	-107.79955	SW
CDPHE	81	63.50	Animas River at Baker's Bridge	Main	37.45844	-107.7997567	SW, SED
RCWWN	CORIVWCH_WQX-88	63.54	Baker's Bridge	Main	37.4581	-107.8001	SW
USEPA	GKM02	63.83	NA	Main	37.455639	-107.800945	SW
USEPA	GKMSE108	64.00	NA	Main	37.45435	-107.801444	SED
USEPA	Bakers Bridge	64.02	NA	Main	37.454134	-107.801601	SW, SED
CDPHE	CO_DI_1	64.50	Reid Ditch 3	Ditch	37.449806	-107.800564	SED
CDPHE	CO_RI_M16	64.50	Reid Ditch 4 (main river)	Main	37.449814	-107.800797	SED

Gold King Mine Release of Acid Mine Drainage to the Animas and San Juan Rivers

Agency	Site ID	Distance from source (km) ¹	Description	Site Type ²	Latitude	Longitude	Media ³
CDPHE	CO_DI_2	64.52	Reid Ditch 1	Ditch	37.4497	-107.800456	SED
CDPHE	CO_DI_3	64.55	Reid Ditch 2	Ditch	37.44936	-107.800469	SED
CDPHE	9438	65.19	Animas River above James Ditch at headgate pre-flush	Main	37.44421667	-107.8039933	SW
CDPHE	CO_DI_4	65.29	James Ditch - 2nd flush	Ditch	37.44358833	-107.804965	SW
CDPHE	CO_DI_5	65.29	James Ditch - 1st flush	Ditch	37.443595	-107.8049267	SW
CDPHE	CO_DI_6	65.29	James Ditch pre-flush	Ditch	37.44362333	-107.8049783	SW
CDPHE	CO_DI_7	65.31	James Ditch - post flush	Ditch	37.44351667	-107.8050133	SW
USEPA	GKM17	65.55	NA	Off river pond	37.441355	-107.805058	SW
USEPA	GKMSE113	65.69	Animas braid	Off river pond	37.440081	-107.804895	SED
USEPA	GKMSE111	65.71	Animas Valley Consolidated Ditch	Ditch	37.440002	-107.806469	SED
USEPA	GKM16	65.73	NA	Off river pond	37.439878	-107.804945	SW
USEPA	GKM18	65.85	NA	Off river pond	37.438755	-107.805358	SW
USEPA	GKMSE112	65.92	Animas Valley Consolidated Ditch	Ditch	37.438207	-107.807343	SED
CDPHE	CO_PO_1	66.35	Elkhorn Pond	Pond	37.434514	-107.798433	SED
CDPHE	CO_DI_8	67.13	James Creek at James Ranch	Ditch	37.42678167	-107.8150233	SW
USEPA	GKMSE110	68.25	NA	Main	37.419008	-107.814105	SED
USEPA	GKMSE109	71.28	Unnamed ditch	Ditch	37.400369	-107.842508	SED
RCWWN	CORIVWCH_WQX-89	73.84	Trimble Lane Bridge	Main	37.38504872	-107.8366753	SW
CDPHE/USEPA	9426	73.92	Animas River at Trimble Bridge	Main	37.38473666	-107.8374767	SW, SED
CDPHE	CO_DI_9	76.67	River @ Barn Ditch	Ditch	37.373703	-107.838819	SED
USEPA	GKMSE105	76.67	Reid Ditch	Ditch	37.373763	-107.83885	SED
CDPHE	9426A	76.75	River @ Ganzerla property	Main	37.373056	-107.847000	SED
USEPA	GKMSE104	76.80	NA	Main	37.372808	-107.846586	SED
USEPA	GKMSE106	78.76	NA	Main	37.360672	-107.844047	SED
CDPHE	9425	79.36	Animas River north of Durango	Main	37.35618	-107.84412	SW
USEPA	GKMSE100	79.44	NA	Main	37.35543	-107.843991	SED
USEPA	GKMSE101	79.89	Reid Ditch	Ditch	37.353608	-107.842549	SED
USEPA	GKMSE107	79.89	Falls Creek	Reference	37.359627	-107.854338	SED
USEPA	GKMSE102	87.36	NA	Main	37.320016	-107.847591	SED
USEPA	GKMSE103	87.93	NA	Main	37.315999	-107.848961	SED
CDPHE	CO_RI_M21	89.77	Animas River at Oxbow Park and Preserve - Upgradient	Main	37.30844	-107.85479	SED

Gold King Mine Release of Acid Mine Drainage to the Animas and San Juan Rivers

Agency	Site ID	Distance from source (km) ¹	Description	Site Type ²	Latitude	Longitude	Media ³
USEPA	GKMSE01	89.77	NA	Main	37.308403	-107.854738	SED
USEPA	Oxbow Park	89.93	NA	Main	37.309037	-107.855714	SW, SED
CDPHE	9425D	89.95	Animas River at Oxbow Park and Preserve - Downgradient	Main	37.30907	-107.85603	SED
CDPHE	9425E	91.57	Animas River at East 33rd Ave boat launch	Main	37.301667	-107.868056	SED
USEPA	32nd St Bridge	91.76	NA	Main	37.299991	-107.868199	SW, SED
CDPHE	9424A	91.76	Animas River at 32nd Street - post flush	Main	37.30009	-107.86886	SW
RCWWN	CORIVWCH_WQX-3577	91.78	32nd St	Main	37.3001	-107.8691	SW
USEPA	GKMSE02	91.78	NA	Main	37.29985	-107.868733	SED
CDPHE	9424B	92.23	Animas River at 29th Street - post flush	Main	37.295592	-107.870735	SW
USEPA	GKM04	92.38	NA	Main	37.294799	-107.870034	SW
CDPHE	9424C	93.16	Animas River at Memorial Park North	Main	37.290858	-107.869669	SED
CDPHE	9424D	93.20	Animas River at Memorial Park South	Main	37.290539	-107.869667	SED
CDPHE	9424H	93.49	Animas River at Paradise Beach	Main	37.28826	-107.87078	SED
USEPA	GKMSE03	93.50	NA	Main	37.288138	-107.870855	SED
RCWWN	CORIVWCH_WQX-3576	93.82	Hatchery	Main	37.2813	-107.8733	SW
USEPA/MSI	ANIMAS-ROTARY PARK	94.24	NA	Main	37.280718	-107.876927	SW, SED
RCWWN	CORIVWCH_WQX-91	94.61	ANIDURCO	Main	37.2797	-107.8804	SW
CDPHE	9423B	95.55	Animas River at Schneider Park steps	Main	37.276667	-107.883889	SED
CDPHE	9423A	95.77	Animas River at 9th Street	Main	37.27456333	-107.8842733	SW
NNEPA	NNEPA-32ANIMASRI04	95.82	Animas River at 9th Street bridge	Main	37.2741678	-107.8851311	SW
CDPHE	9422A	95.87	Animas River at Schneider Park boat launch	Main	37.273889	-107.885556	SED
CDPHE	CO_RI_M29	95.90	Animas River at Durango - 9th St bridge	Main	37.27365938	-107.8854425	SW, SED
CDPHE	CO_RI_M31	95.95	Animas River at Durango - 9th St bridge - post flush	Main	37.27348183	-107.8856213	SW
USEPA	GKM05	96.48	NA	Main	37.268704	-107.885857	SW, SED
CDPHE	9421	96.50	Animas River at Lightner Creek	Main	37.2683565	-107.8861043	SW, SED
USEPA	GKMSE05	96.66	NA	Main	37.267122	-107.885289	SED
USEPA	GKMSE06	97.20	NA	Main	37.264099	-107.880919	SED
USGS	Durango WTP-Mini-Sipper	97.37	NA	Main	37.262798	-107.8818	SW
USEPA	GKMSE04	97.83	NA	Main	37.259673	-107.877966	SED
CDPHE	9420A	97.85	Animas River at Santa Rita Park	Main	37.259722	-107.877778	SED

Agency	Site ID	Distance from source (km) ¹	Description	Site Type ²	Latitude	Longitude	Media ³
CDPHE	9420	97.86	Animas River below Durango WWTP	Main	37.25952267	-107.8778555	SW
USEPA	GKMSE22	97.88	NA	Main	37.259051	-107.877932	SED
USEPA	GKMSE21	97.91	NA	Intake	37.258796	-107.878004	SED
USEPA	GKMSE23	97.94	NA	Intake	37.258509	-107.877733	SED
CDPHE	9420B	99.18	Animas River at Cundiff Park	Main	37.249025	-107.87255	SED
RCWWN	CORIVWCH_WQX-3590	101.08	High Bridge	Main	37.2355	-107.8691	SW
USEPA	GKMSE09	101.18	NA	Main	37.234729	-107.868651	SED
CDPHE	9418A	101.20	Animas River at Humane Society upgradient	Main	37.2345528	-107.868469	SED
CDPHE	9418B	101.47	Animas River at Humane Society downgradient	Main	37.2320289	-107.868411	SED
USEPA	GKMSE08	102.64	NA	Main	37.222635	-107.86515	SED
CDPHE	9420C	103.16	Animas River at Dallabetta upgradient	Main	37.221319	-107.859603	SED
USEPA	AR19-3_EPA (GKM01)	103.16	NA	Main	37.221297	-107.859598	SW, SED
USEPA	GKM01 (AR 19-3_EPA)	103.16	NA	Main	37.221542	-107.859455	SW
USEPA	GKMSE07	103.18	NA	Main	37.2213	-107.85952	SED
CDPHE	9420D	103.21	Animas River at Dallabetta (Park) downgradient	Main	37.221211	-107.859178	SED
USEPA	GKMSE11	103.95	NA	Main	37.215828	-107.8554	SED
SUIT	AR 19-3 (NAR1)	104.17	Animas River at Southern Ute Tribe AR19-3	Main	37.213842	-107.854161	SW, SED
USEPA	GKMSE10	105.61	First Mesa Ditch	Main	37.203745	-107.846591	SED
USEPA	GKMSE20	105.65	First Mesa Ditch	Ditch	37.2035	-107.846508	SED
SUIT	AR 16-0 (NAR2)	108.95	Animas River at Southern Ute Tribe AR16-0	Main	37.187031	-107.869928	SW, SED
USEPA	GKMSE13	108.95	NA	Main	37.186964	-107.86992	SED
USEPA	GKMSE12	110.11	NA	Main	37.185541	-107.878912	SED
CDPHE	SUIT-AR1	110.11	Animas River at Southern Ute Tribe AR1	Main	37.18547	-107.87904	SED
RCWWN	CORIVWCH_WQX-93	114.42	Weaselskin	Main	37.15185256	-107.8847621	SW
SUIT	Below Little Fishes	116.45	NA	Main	37.137315	-107.892733	SW
USEPA	GKMSE16	116.63	NA	Main	37.136145	-107.891561	SED
CDPHE	9416	116.65	Animas River at Citizens Ditch	Main	37.136157	-107.891243	SW, SED
CDPHE	9416A	117.56	Citizens Ditch	Ditch	37.128853	-107.892015	Sludge
USEPA	GKMSE17	117.56	NA	Ditch	37.128794	-107.892082	SED
CDPHE	AR7-2_CO	123.02	Animas River at Southern Ute Tribe AR7-2	Main	37.08561	-107.87871	SED

Gold King Mine Release of Acid Mine Drainage to the Animas and San Juan Rivers

Agency	Site ID	Distance from source (km) ¹	Description	Site Type ²	Latitude	Longitude	Media ³
USEPA	GKMSE14	123.02	NA	Main	37.085579	-107.878703	SED
CDPHE	AR7-2(2)_CO	123.07	Animas River at Southern Ute Tribe AR7-2(2)	Main	37.08491	-107.87925	SED
SUIT/USEPA	AR 7-2 (NAR4)	123.08	Animas River at Southern Ute Tribe AR7-2	Main	37.084992	-107.878383	SW
CDPHE	AR2-7_CO	123.08	Animas River at Southern Ute Tribe AR2-7	Main	37.08499	-107.87838	SED
CDPHE	66	127.83	Animas River at Bondad Bridge	Main	37.051025	-107.875025	SW
USEPA	GKMSE18	129.60	NA	Main	37.035817	-107.875185	SED
USGS	9363500	129.62	Animas River near Cedar Hill, NM	Main	37.035797	-107.87474	SW
SUIT/USEPA	AR 2-7	130.12	NA	Main	37.03226	-107.8754	SW, SED
USEPA	GKMSE15	130.13	NA	Main	37.032268	-107.875541	SED
USEPA	GKMSE19	130.15	NA	Ditch	37.032261	-107.875651	SED
USEPA	AR2-7a	130.65	NA	Ditch	37.027585	-107.878177	SW, SED
SUIT	NAR 6	131.48	NA	Main	37.02342	-107.87387	SW
USEPA	SA008	134.24	NA	Ditch	36.99963	-107.86906	SED
USEPA	SA007	134.25	NA	Ditch	36.99953	-107.86911	SED
USEPA	SA010	136.39	NA	Ditch	36.98301	-107.86757	SED
USEPA	SA009	136.41	NA	Ditch	36.98296	-107.86756	SED
USEPA	SA012	140.11	NA	Main	36.96348	-107.88013	SED
USEPA	SA013	140.13	NA	Ditch	36.96355	-107.88114	SED
USEPA	SA011	140.61	NA	Ditch	36.95936	-107.88041	SED
USEPA	SA002	142.11	NA	Ditch	36.94713	-107.88186	SED
USEPA	SA003	142.11	NA	Ditch	36.94713	-107.88186	SED
USEPA	SA001	143.22	NA	Ditch	36.94235	-107.87821	SED
NMED	66Animas046.2	146.16	Animas River above Cedar Hill NM 550 bridge	Main	36.9327	-107.894	SW
USEPA	SA015	146.58	NA	Reference	36.96475	-107.90398	SED
USEPA	SA016	147.01	NA	Ditch	36.93461	-107.90331	SED
USEPA	SA014	147.03	NA	Ditch	36.93461	-107.9034	SED
USEPA	ADW-022	147.54	Aztec Domestic Water System, intake sampling location	Main	36.9333	-107.90907	SW, SED
USEPA	ADWS-IT2	147.54	Aztec Domestic Water System, intake sampling location	Main	36.9333	-107.90907	SW
USEPA	SA004	149.22	NA	Ditch	36.91876	-107.9101	SED

Gold King Mine Release of Acid Mine Drainage to the Animas and San Juan Rivers

Agency	Site ID	Distance from source (km) ¹	Description	Site Type ²	Latitude	Longitude	Media ³
USEPA	SA006	149.44	NA	Ditch	36.91667	-107.91152	SED
USEPA	SA005	149.46	NA	Ditch	36.91655	-107.9117	SED
USEPA	NSW-020 (NSW-ARI)	151.58	North Star Water Users Association, intake sampling location	Main	36.900898	-107.917122	SW, SED
USEPA	ADW-021	157.55	Aztec Domestic Water System, intake sampling location	Main	36.872802	-107.96084	SW, SED
USEPA	ADWS-IT1	157.55	Aztec Domestic Water System, intake sampling location	Main	36.87284	-107.96079	SW
USEPA	SA024	157.60	NA	Ditch	36.8726	-107.96107	SED
USEPA	SA023	157.83	NA	Flood plain	36.8726	-107.96548	SED
USEPA	SED02	158.02	Sediment location close to intake sampling locations	Main	36.870511	-107.964815	SED
USEPA	SA025	158.25	NA	Ditch	36.86892	-107.96548	SED
USEPA	SA018	159.29	NA	Ditch	36.86541	-107.97422	SED
USEPA	SA019	159.29	NA	Ditch	36.86541	-107.97425	SED
USEPA	SA017	159.31	NA	Ditch	36.86528	-107.97444	SED
USEPA	ADW-010	162.87	Aztec Domestic Water System, intake sampling location	Main	36.838545	-107.992183	SW, SED
USEPA	ADWS-ARP	162.87	Aztec Domestic Water System, Animas River pump	Main	36.83855	-107.99218	SW
USEPA	AWI-R8R6	162.88	Aztec water intake, ESAT intake sampling location	Ditch	36.838447	-107.992417	SW
USEPA	SED01 (SED-01)	162.91	Sediment location close to intake sampling locations	Main	36.83827	-107.99277	SED
NMED	66Animas029.2	162.99	Aztec drinking water intake	Ditch	36.837463	-107.991684	SW
USEPA	SA020	163.94	NA	Ditch	36.8305	-107.99673	SED
USEPA	SA021	163.94	NA	Ditch	36.83053	-107.99673	SED
NMED	66Animas028.1 (ANIMASAB)	164.09	Animas River above Estes Arroyo, near Aztec	Main	36.82949	-107.997663	SW
USEPA	SA022	164.38	NA	Ditch	36.82861	-107.99974	SED
USEPA	SA027	166.71	NA	Ditch	36.81427	-108.01594	SED
USEPA	SA028	166.71	NA	Ditch	36.81431	-108.01593	SED
USEPA	SA026	166.74	NA	Ditch	36.81409	-108.0163	SED
USGS	9364010	167.39	Animas River below Aztec, NM	Main	36.817767	-108.024407	SW
USEPA	SA029	170.09	NA	Ditch	36.80855	-108.04679	SED
USEPA	SA030	170.09	NA	Ditch	36.80859	-108.04684	SED

Gold King Mine Release of Acid Mine Drainage to the Animas and San Juan Rivers

Agency	Site ID	Distance from source (km) ¹	Description	Site Type ²	Latitude	Longitude	Media ³
USEPA	SA031	170.19	NA	Ditch	36.80836	-108.04782	SED
USEPA	SB007	174.53	NA	Ditch	36.78744	-108.08089	SED
USEPA	SB008	175.02	NA	Ditch	36.78638	-108.08633	SED
USEPA	SB009	175.02	NA	Ditch	36.78637	-108.08632	SED
CoF	FDPS	175.05	Farmer's Ditch pump station	Ditch	36.801878	-108.096829	SW
CoF	WTP #1 raw	175.58	Water Treatment Plant #1 raw sample from lake	Lake	36.799798	-108.103228	SW
CoF	WTP #2 raw	175.58	Water Treatment Plant #2 raw sample from lake	Lake	36.799798	-108.103228	SW
CoF	APS #2	176.56	City of Farmington Animas River Pump Station #2 (drinking water intake)	Main	36.783635	-108.10211	SW
USEPA	FW-012	176.56	Farmington water system, intake sampling location	Main	36.783635	-108.10211	SW, SED
USEPA	FWI-R8R6	176.56	Farmington water intake, ESAT intake sampling locations	Main	36.783476	-108.102056	SW
USEPA	FWS-ARP2	176.56	Farmington Water System, Animas River pump station	Main	36.78357	-108.10214	SW
USEPA	MW-020	178.69	Intake sampling location	Gravel pond	36.771913	-108.118596	SW, SED
USEPA	MWSS-ARI	178.69	Morningstar Water Supply System, Animas River intake	Off river pond	36.77134	-108.11893	SW
USEPA	SB010	183.42	NA	Ditch	36.74627	-108.15439	SED
USEPA	SB011	183.45	NA	Ditch	36.7462	-108.15468	SED
USEPA	SB012	183.45	NA	Ditch	36.7462	-108.15468	SED
USEPA	SB016	185.28	NA	Ditch	36.74034	-108.16943	SED
USEPA	SB013	186.27	NA	Ditch	36.73357	-108.17457	SED
USEPA	SB014	187.81	Willett Ditch	Ditch	36.72753	-108.1855	SED
USEPA	SB015	187.81	Willett Ditch	Ditch	36.72753	-108.1855	SED
NMED	66Animas001.7 (ANIMASFM)	189.39	Animas River at Boyd Park in Farmington	Main	36.72303	-108.201611	SW
USGS	09364500	189.60	Animas River at Farmington, NM	Main	36.721252	-108.201752	SW, SED
USEPA	FW-040	190.16	Intake sampling location	Main	36.719664	-108.207125	SW, SED
USEPA	SB001	191.25	NA	Ditch	36.71469	-108.21644	SED
USEPA	FWS-FDPS	191.27	Farmington Water System, Farmers Ditch Pump Station, Intake sampling location	Main	36.71455	-108.21644	SW
USGS	9355500	191.87	San Juan River near Archuleta, NM	Reference	36.801315	-107.699127	SW
USEPA	SIAR	191.87	NA	Reference	36.707467	-108.150813	SW, SED

Gold King Mine Release of Acid Mine Drainage to the Animas and San Juan Rivers

Agency	Site ID	Distance from source (km) ¹	Description	Site Type ²	Latitude	Longitude	Media ³
USGS	09365000	192.96	San Juan River at Farmington, NM	Main	36.723114	-108.225128	SW, SED
USEPA	SB017	193.52	North Farmington Ditch	Ditch	36.73532	-108.2263	SED
USEPA	SB018	193.52	North Farmington Ditch	Ditch	36.73532	-108.2263	SED
USEPA	SB002	195.15	NA	Ditch	36.72858	-108.24724	SED
USEPA	SB003	195.17	NA	Ditch	36.72858	-108.24734	SED
USEPA	LVW-020	196.05	Lower Valley Water Users Association, intake sampling location	Main	36.730556	-108.251046	SW, SED
USEPA	LVW-WPI	196.20	Lower Valley Water Users Association, Westland Park intake	Main	36.73139	-108.249	SW
NNEPA	NNEPA-10FRUCANAL34	196.60	Fruitland Canal @ first bridge downstream from headgate (sediment on right bank)	Ditch	36.730805	-108.256012	SED
NNEPA	NNEPA-10FRUCANAL35	196.61	Fruitland Canal @ first bridge downstream from headgate (sediment on left bank)	Ditch	36.730779	-108.256072	SED
USEPA	SJLP	196.87	NA	Main	36.73588701	-108.2539868	SW, SED
NNEPA	NNEPA-10FRUCANAL39	198.32	Fruitland Canal near 2nd wasteway	Ditch	36.729082	-108.266056	SED
USEPA	LVW-FD	203.34	Lower Valley Water Users Association, Farmers Ditch, intake sampling location	Ditch	36.73156	-108.31426	SW
NMED	67SanJua088.1 (SJLION)	204.43	San Juan River at Lions Park near Kirtland	Main	36.722136	-108.325619	SW
USEPA	LVW-030	204.48	Lower Valley Water Users Association, intake sampling location	Main	36.721812	-108.325933	SW, SED
USEPA	SB023	213.08	NA	Main	36.73915	-108.40221	SED
USEPA	SB022	213.11	NA	Main	36.73929	-108.4025	SED
USEPA	SB019	213.38	NA	Main	36.74125	-108.4044	SED
USEPA	SB021	213.38	NA	Reference	36.74162	-108.40398	SED
USEPA	SB020	213.43	NA	Main	36.7416	-108.4044	SED
USEPA	SJFP	214.43	NA	Main	36.74815602	-108.4120157	SW, SED
USEPA	SB004	215.33	NA	Ditch	36.74961	-108.42004	SED
USEPA	SB005	217.89	NA	Ditch	36.74278	-108.44241	SED
USEPA	SB006	217.89	NA	Ditch	36.74278	-108.44241	SED
USGS	364446108321510	227.61	San Juan River above Hogback Diversion Channel	Main	36.746217	-108.537725	SW
NNEPA	NNEPA-10SANJUANR25	227.63	San Juan River @ the bottom of the Hogback fish passage	Main	36.7454628	-108.5378488	SW
USEPA	SJHB	227.66	NA	Main	36.74519199	-108.5377578	SW, SED
USGS	09368000	246.12	San Juan River at Shiprock, NM	Main	36.781205	-108.69058	SW

Gold King Mine Release of Acid Mine Drainage to the Animas and San Juan Rivers

Agency	Site ID	Distance from source (km) ¹	Description	Site Type ²	Latitude	Longitude	Media ³
USEPA	SJSR	246.34	NA	Main	36.78162422	-108.6927838	SW, SED
NNEPA	NNEPA-10SANJUANR26	272.48	San Juan River near Canal Creek	Main	36.89325249	-108.8785948	SW
USEPA	SJDS	272.48	NA	Main	36.893312	-108.8786415	SW, SED
NNEPA	NNEPA-02SANJUANR06	295.83	San Juan River near NM/CO border at the Four Corners	Main	36.9962011	-109.0046225	SW
USEPA	SJ4C	295.83	NA	Main	36.99621613	-109.0046838	SW, SED
USGS	09371010	298.53	San Juan River at Four Corners, CO	Main	37.001102	-109.030192	SW
UDEQ	4954000	298.74	San Juan R at US160 Crossing in CO	Main	37.001755	-109.032726	SW, SED
UDEQ	4953880	332.89	McElmo Creek at Hwy U262 Crossing	Reference	37.218048	-109.190111	SW
USEPA	MECT	332.89	NA	Reference	37.21846159	-109.190811	SW, SED
USEPA	SJME	333.21	NA	Main	37.21681097	-109.19615	SW, SED
UDEQ	4953990	345.72	San Juan River at U262 Crossing Phillips Camp Road Crossing (San Juan River at Town of Montezuma)	Main	37.257788	-109.30975	SW, SED
NNEPA	NNEPA-02SANJUANR07	345.80	San Juan River near bridge at Montezuma Creek	Main	37.258277	-109.310476	SW
USEPA	SJMC	345.80	NA	Main	37.25822644	-109.3106036	SW, SED
UDEQ	4953560	348.23	Montezuma Creek at U163 Crossing	Reference	37.272086	-109.327694	SW
UDEQ	4953250	377.05	San Juan River at Sand Island	Main	37.26027863	-109.6137343	SW, SED
NNEPA	NNEPA-02SANJUANR08	377.58	San Juan River at US 191 bridge near Bluff	Main	37.257673	-109.61849	SW
USEPA	SJBB	377.62	NA	Main	37.25737015	-109.6185856	SW, SED
UDEQ	4953020	390.62	Chinle Creek above confluence with San Juan River	Reference	37.199119	-109.715572	SW
USGS	09379500	420.92	San Juan River near Bluff, UT	Main	37.147014	-109.864498	SW
USEPA	SJMH	421.33	NA	Main	37.14999307	-109.8662835	SW, SED
NNEPA	NNEPA-29SANJUANR05	421.39	Immediately upstream from the mouth of McElmo Creek	Main	37.150388	-109.866814	SW
UDEQ	4953000	421.49	San Juan River at Mexican Hat US163 Crossing	Main	37.150758	-109.867672	SW, SED
UDEQ	4952942/4952940	510.74	San Juan River at Clay Hills boat ramp	Main	37.293008	-110.399621	SW, SED
USEPA	SJCH	510.74	NA	Main	37.293336	-110.399293	SW, SED
USEPA	LPCH	543.75	NA	Main	37.25567	-110.66414	SW, SED
USEPA	SJIN	543.85	NA	Main	37.2536	-110.6632	SW
USEPA	SJIN2	545.12	NA	Main	37.2563	-110.67912	SED
USEPA	SJPL	548.53	NA	Lake	37.26238	-110.70908	SED

Agency	Site ID	Distance from source (km) ¹	Description	Site Type ²	Latitude	Longitude	Media ³
USEPA	SJPL2	548.90	NA	Lake	37.25948	-110.711	SED
USEPA	LP-01-I	557.49	NA	Lake	37.213434	-110.664648	SW, SED
USEPA	LPPW	564.01	NA	Lake	37.16278	-110.7085	SW, SED
USEPA	LP-05-I	596.17	NA	Reference	37.676716	-110.485868	SW, SED
USEPA	LP-07-I	596.17	NA	Reference	37.536055	-110.651704	SED
USEPA	LP-10-I	596.17	NA	Reference	37.39395	-110.748414	SW, SED
USEPA	LP-12-I	596.17	NA	Reference	37.31623	-110.90733	SW, SED
USEPA	LP-18-I	625.15	NA	Lake	37.105351	-111.170709	SW, SED
USEPA	LPRC	625.70	NA	Lake	37.13642	-111.19226	SW, SED
USEPA	LP-25-I	632.17	NA	Lake	37.008472	-111.151244	SW, SED
USEPA	LP-19-I	632.58	NA	Lake	37.105511	-111.269176	SW, SED
USEPA	LPGB	633.28	NA	Lake	37.05487	-111.23475	SW, SED
USEPA	LPPC	636.09	NA	Lake	37.06631	-111.26525	SW, SED
USEPA	LP-21-I	646.70	NA	Lake	37.00547	-111.360354	SW, SED
USEPA	LPNC	647.12	NA	Lake	36.939	-111.32459	SW
USEPA	LPDAM	663.55	NA	Lake	36.94436	-111.48691	SW
USEPA	LP-24-I	663.66	NA	Lake	36.94345	-111.486242	SW, SED
USEPA	PAGE	665.79	NA	PWS	36.90847222	-111.4535528	SW

¹Distance from source for **Reference** sites was taken at the confluence of the reference stream and the corresponding main stream affected by the release.

²**Main** - in the path of the GKM plume. **Reference** - not in the path of the GKM plume. **PWS** - public water system.

³**SED** – Sediment. **SW** – Surface Water.

Table A-7. List of metals laboratory methods for surface water samples by data provider

This listing is a compilation from available data. Sampled years in parenthesis. All years not necessarily used in analyses. Historic methods, at times, unspecified.

Provider	Surface Water – Metals laboratory methods				
	Aluminum (Al)	Antimony (Sb)	Arsenic (As)	Barium (Ba)	Beryllium (Be)
USEPA Region 6 (2015)	EPA 200.7	EPA 200.8	EPA 200.8	EPA 200.8	EPA 200.8
USEPA Region 8 (2015)	EPA 200.7	EPA 200.8	EPA 200.8	EPA 200.8	EPA 200.8
USEPA Region 9 (2015)	EPA 200.7	EPA 200.8	EPA 200.8	EPA 200.8	EPA 200.8
USEPA Follow-up (2015-2016)	EPA 200.7 EPA 200.8	EPA 200.8	EPA 200.8	EPA 200.8	EPA 200.8
Colorado DPHE (1968-2016)	EPA 200.7 Unspecified	NA	EPA 200.8 Unspecified	EPA 200.7	EPA 200.8 Unspecified
New Mexico ED (2001-2016)	EPA 200.7 EPA 200.8 Unspecified	EPA 200.8 Unspecified	EPA 200.8 Unspecified	EPA 200.7 EPA 200.8 Unspecified	EPA 200.8 Unspecified
Utah DEQ (1975-2016)	EPA 200.7 EPA 200.8 Unspecified	EPA 200.8	EPA 200.8 Unspecified	EPA 200.8 Unspecified	EPA 200.8
Navajo Nation (1999-2015)	EPA 200.7 EPA 200.8	EPA 200.7 EPA 200.8	EPA 200.7 EPA 200.8 SM 3114-C	EPA 200.7	EPA 200.7
Southern Ute Indian Tribe (1992-2016)	EPA 200.7 SU SOP	EPA 200.8	EPA 200.8 EPA 206.2_M SU SOP	EPA 200.8	EPA 200.8
Ute Mountain Ute Tribe (1996-2015)	EPA 200.7	EPA 200.8 EPA 200.9	EPA 200.8 EPA 200.9	SM 3111-B	NA
City of Farmington (2015-2016)	EPA 200.7	EPA 200.8	EPA 200.8	EPA 200.7 EPA 200.8	EPA 200.7 EPA 200.8
River Watch (1991-2016)	EPA 200.7	NA	EPA 200.7	NA	NA
Mountain Studies Institute (2016)	EPA 200.7	NA	EPA 200.8	NA	NA
SADIE (2011-2015)	EPA 200.7 EPA 200.8 EPA 6010	EPA 200.8	EPA 200.8 EPA 6020	EPA 200.8	EPA 200.7 EPA 6010
USEPA historic (1971-2000)	NA	Unspecified	Unspecified	NA	Unspecified
USGS MiniSipper (2015)	EPA 200.8	NA	NA	NA	NA
USGS GKM Database (2000-2015)	EPA 200.7 USGS I-1472-85 USGS I-1472-87 USGS I-1472-95 USGS I-2477-92 USGS I-4471-97 Unspecified	USGS I-2477-92 USGS I-4471-97 Unspecified	USGS I-2020-05 USGS I-2063-98 USGS I-2477-92 USGS I-4020-05 USGS I-4063-98 Unspecified	EPA 200.7 USGS I-1472-85 USGS I-1472-87 USGS I-1472-95 USGS I-2477-92 USGS I-4471-97 Unspecified	USGS I-2477-92 USGS I-4471-97 Unspecified
USGS Paper 1651 (1994-2002)	ICP-AES ICP/MS	ICP-AES ICP/MS	ICP-AES ICP/MS	ICP-AES ICP/MS	ICP-AES ICP/MS

Provider	Surface Water – Metals laboratory methods				
	Boron (B)	Cadmium (Cd)	Calcium (Ca)	Chromium (Cr)	Chromium (III)
USEPA Region 6 (2015)	NA	EPA 200.8	EPA 200.7	EPA 200.8	NA
USEPA Region 8 (2015)	NA	EPA 200.8	EPA 200.7	EPA 200.8	NA
USEPA Region 9 (2015)	NA	EPA 200.8	EPA 200.7	EPA 200.8	NA
USEPA Follow-up (2015-2016)	NA	EPA 200.8	EPA 200.7	EPA 200.8	NA
Colorado DPHE (1968-2016)	EPA 200.7 Unspecified	EPA 200.8 Unspecified	EPA 200.7	EPA 200.7 Unspecified	NA
New Mexico ED (2001-2016)	EPA 200.7 Unspecified	EPA 200.8 Unspecified	EPA 200.7 Unspecified	EPA 200.8 Unspecified	NA
Utah DEQ (1975-2016)	EPA 200.7 Unspecified	EPA 200.8 Unspecified	EPA 200.7 Unspecified	EPA 200.8 Unspecified	NA
Navajo Nation (1999-2015)	EPA 200.7	EPA 200.7 EPA 200.8 EPA 200.9	EPA 200.7	EPA 200.7 EPA 200.8	EPA 200.7 SM 3500-CR(D)
Southern Ute Indian Tribe (1992-2016)	NA	EPA 200.7 EPA 200.8 SU SOP	EPA 200.7	EPA 200.7 EPA 200.8 SU SOP	Calculation
Ute Mountain Ute Tribe (1996-2015)	EPA 200.7 EPA 200.9	EPA 200.7 EPA 200.8 EPA 200.9	EPA 200.7 SM 3500-CA (C) SM 3500-CA(D)	EPA 200.8	NA
City of Farmington (2015-2016)	NA	EPA 200.7 EPA 200.8	EPA 200.7	EPA 200.7 EPA 200.8	NA
River Watch (1991-2016)	NA	EPA 200.7	EPA 200.7	NA	NA
Mountain Studies Institute (2016)	NA	EPA 200.8	EPA 200.7	NA	NA
SADIE (2011-2015)	NA	EPA 200.8 EPA 6020	EPA 200.7 EPA 200.8 EPA 6010	EPA 200.7 EPA 200.8 EPA 6010	NA
USEPA historic (1971-2000)	NA	Unspecified	EPA 215.1	Unspecified	NA
USGS MiniSipper (2015)	NA	EPA 200.8	EPA 200.8	EPA 200.8	NA
USGS GKM Database (2000-2015)	NA	EPA 200.7 USGS I-2138-89 USGS I-2477-92 USGS I-4471-97 Unspecified	USGS I-1472-85 USGS I-1472-87 USGS I-1472-95 Unspecified	EPA 200.7 USGS I-1233-93 USGS I-2020-05 USGS I-2477-92 USGS I-3233-93 USGS I-4020-05 Unspecified	NA
USGS Paper 1651 (1994-2002)	ICP-AES	ICP-AES	ICP-AES ICP/MS	ICP-AES ICP/MS	NA

Provider	Surface Water – Metals laboratory methods				
	Chromium (VI)	Cobalt (Co)	Copper (Cu)	Iron (Fe)	Lead (Pb)
USEPA Region 6 (2015)	NA	EPA 200.8	EPA 200.8	EPA 200.7	EPA 200.8
USEPA Region 8 (2015)	NA	EPA 200.8	EPA 200.8	EPA 200.7	EPA 200.8
USEPA Region 9 (2015)	NA	EPA 200.8	EPA 200.8	EPA 200.7	EPA 200.8
USEPA Follow-up (2015-2016)	NA	EPA 200.8	EPA 200.8	EPA 200.7	EPA 200.8
Colorado DPHE (1968-2016)	Unspecified	EPA 200.7	EPA 200.7 EPA 200.8 Unspecified	EPA 200.7 Unspecified	EPA 200.8 Unspecified
New Mexico ED (2001-2016)	NA	EPA 200.8 Unspecified	EPA 200.8 Unspecified	EPA 200.7 Unspecified	EPA 200.8 Unspecified
Utah DEQ (1975-2016)	Unspecified	EPA 200.8	EPA 200.8 Unspecified	EPA 200.7 Unspecified	EPA 200.8 Unspecified
Navajo Nation (1999-2015)	SM 3500-CR(D)	EPA 200.7 EPA 200.8	EPA 200.7	EPA 200.7	EPA 200.7 EPA 200.8 EPA 200.9
Southern Ute Indian Tribe (1992-2016)	SM 3500-CR(D)	EPA 200.8	EPA 200.7 EPA 200.8 SU SOP	EPA 200.7 SU SOP	EPA 200.7 EPA 200.8 SU SOP
Ute Mountain Ute Tribe (1996-2015)	NA	NA	EPA 200.7 EPA 200.8 EPA 200.9	SM 3111-B EPA 200.7 EPA 200.9 EPA 6010B	EPA 200.7 EPA 200.8 EPA 200.9
City of Farmington (2015-2016)	NA	EPA 200.8	EPA 200.8	EPA 200.7	EPA 200.8
River Watch (1991-2016)	NA	NA	EPA 200.7	EPA 200.7	EPA 200.7
Mountain Studies Institute (2016)	NA	NA	EPA 200.8	EPA 200.7	EPA 200.8
SADIE (2011-2015)	NA	EPA 200.8	EPA 200.8 EPA 6020	EPA 200.7 EPA 6010	EPA 200.8 EPA 6020
USEPA historic (1971-2000)	NA	NA	Unspecified	Unspecified	Unspecified
USGS MiniSipper (2015)	NA	NA	EPA 200.8	NA	EPA 200.8
USGS GKM Database (2000-2015)	NA	USGS I-2020-05 USGS I-2477-92 USGS I-4020-05 Unspecified	EPA 200.7 USGS I-1472-85 USGS I-1472-87 USGS I-1472-95 USGS I-2020-05 USGS I-2274-89 USGS I-2477-92 USGS I-4020-05 USGS I-4471-97 Unspecified	EPA 200.7 USGS I-1472-85 USGS I-1472-87 USGS I-1472-95 USGS I-4471-97 Unspecified	EPA 200.7 USGS I-2403-89 USGS I-2477-92 USGS I-4471-97 Unspecified
USGS Paper 1651 (1994-2002)	NA	ICP-AES ICP/MS	ICP-AES ICP/MS	ICP-AES ICP/MS SpectroPhoto	ICP-AES ICP/MS GFAAS

Provider	Surface Water – Metals laboratory methods				
	Magnesium (Mg)	Manganese (Mn)	Mercury (Hg)	Molybdenum (Mo)	Nickel (Ni)
USEPA Region 6 (2015)	EPA 200.7	EPA 200.8	EPA 245.1	EPA 200.8	EPA 200.8
USEPA Region 8 (2015)	EPA 200.7	EPA 200.8	EPA 245.1	EPA 200.8	EPA 200.8
USEPA Region 9 (2015)	EPA 200.7	EPA 200.8	EPA 245.1	EPA 200.8	EPA 200.8
USEPA Follow-up (2015-2016)	EPA 200.7	EPA 200.8	EPA 245.1 EPA 1631E	EPA 200.8	EPA 200.8
Colorado DPHE (1968-2016)	EPA 200.7 Unspecified	EPA 200.7 EPA 200.8 Unspecified	EPA 200.8 EPA 245.1 Unspecified	EPA 200.7 Unspecified	EPA 200.7 Unspecified
New Mexico ED (2001-2016)	EPA 200.7 Unspecified	EPA 200.7 EPA 200.8 Unspecified	EPA 245.1 Unspecified	EPA 200.8 Unspecified	EPA 200.8 Unspecified
Utah DEQ (1975-2016)	EPA 200.7 Unspecified	EPA 200.8 Unspecified	EPA 245.1 EPA 200.8 Unspecified	EPA 200.8	EPA 200.8 Unspecified
Navajo Nation (1999-2015)	EPA 200.7	EPA 200.7	EPA 1631E EPA 245.1	EPA 200.7 EPA 200.8	EPA 200.7
Southern Ute Indian Tribe (1992-2016)	EPA 200.7	EPA 200.7 EPA 200.8 SU SOP	EPA 245.1 EPA 7470A SU SOP	EPA 200.8	EPA 200.7 EPA 200.8 SU SOP
Ute Mountain Ute Tribe (1996-2015)	EPA 200.7 SM 3111-B SM 3500-Mg(B)	EPA 200.7 EPA 200.8 SM 3111-B	EPA 245.1 EPA 245.2	EPA 200.8	EPA 200.8 EPA 200.9
City of Farmington (2015-2016)	EPA 200.7	EPA 200.7	EPA 245.1	EPA 200.8	EPA 200.8
River Watch (1991-2016)	EPA 200.7	EPA 200.7	NA	NA	NA
Mountain Studies Institute (2016)	EPA 200.7	EPA 200.8	EPA 245.1	NA	NA
SADIE (2011-2015)	EPA 200.7	EPA 200.7	NA	EPA 200.8	EPA 200.7
USEPA historic (1971-2000)	EPA 242.1	Unspecified	Unspecified	NA	Unspecified
USGS MiniSipper (2015)	EPA 200.8	EPA 200.8	NA	NA	NA
USGS GKM Database (2000-2015)	USGS I-1472-85 USGS I-1472-87 USGS I-1472-95 Unspecified	EPA 200.7 USGS I-1472-85 USGS I-1472-87 USGS I-1472-95 USGS I-2477-92 USGS I-4471-97 Unspecified	USGS I-2462-85 USGS I-2464-01 USGS I-3462-85 USGS I-4464-01 Unspecified	EPA 200.7 USGS I-2477-92 USGS I-4471-97 Unspecified	EPA 200.7 USGS I-1472-85 USGS I-1472-87 USGS I-1472-95 USGS I-2020-05 USGS I-2477-92 USGS I-4020-05 USGS I-4471-97 Unspecified
USGS Paper 1651 (1994-2002)	ICP-AES ICP/MS	ICP-AES ICP/MS	CVAAS ICP/MS	ICP-AES ICP/MS	ICP-AES ICP/MS

Provider	Surface Water – Metals laboratory methods				
	Potassium (K)	Selenium (Se)	Silver (Ag)	Sodium (Na)	Thallium (Tl)
USEPA Region 6 (2015)	EPA 200.7	EPA 200.8	EPA 200.8	EPA 200.7	EPA 200.8
USEPA Region 8 (2015)	EPA 200.7	EPA 200.8	EPA 200.8	EPA 200.7	EPA 200.8
USEPA Region 9 (2015)	EPA 200.7	EPA 200.8	EPA 200.8	EPA 200.7	EPA 200.8
USEPA Follow-up (2015-2016)	EPA 200.7	EPA 200.8	EPA 200.8	EPA 200.7	EPA 200.8
Colorado DPHE (1968-2016)	EPA 200.7 Unspecified	EPA 200.8 Unspecified	EPA 200.8 Unspecified	EPA 200.7 Unspecified	NA
New Mexico ED (2001-2016)	EPA 200.7 Unspecified	EPA 200.8 EPA 200.9 EPA 270.2 Unspecified	EPA 200.8 Unspecified	EPA 200.7 Unspecified	EPA 200.8 Unspecified
Utah DEQ (1975-2016)	EPA 200.7 Unspecified	EPA 200.8 SM 3114-C Unspecified	EPA 200.8 Unspecified	EPA 200.7 Unspecified	EPA 200.8
Navajo Nation (1999-2015)	EPA 200.7	EPA 200.7 EPA 200.8 SM 3114-C	EPA 200.7 EPA 200.8	EPA 200.7	EPA 200.7 EPA 200.8
Southern Ute Indian Tribe (1992-2016)	EPA 200.7	EPA 200.8 SM 3500-SE (C) SU SOP	EPA 200.7 EPA 200.8 SU SOP	EPA 200.7	EPA 200.8
Ute Mountain Ute Tribe (1996-2015)	EPA 200.7 SM 3500-K (D)	EPA 200.8 EPA 200.9	EPA 200.8 EPA 200.9	EPA 200.7 SM 3500-NA(D)	NA
City of Farmington (2015-2016)	EPA 200.7	EPA 200.8	EPA 200.8	EPA 200.7	EPA 200.8
River Watch (1991-2016)	EPA 200.7	EPA 200.7	NA	EPA 200.7	NA
Mountain Studies Institute (2016)	NA	EPA 200.8	NA	NA	NA
SADIE (2011-2015)	EPA 200.7 EPA 6010	EPA 200.8	EPA 200.8 EPA 6020	EPA 200.7 EPA 6010	EPA 200.8
USEPA historic (1971-2000)	EPA 258.1	EPA 270.2 Unspecified	Unspecified	EPA 273.1	Unspecified
USGS MiniSipper (2015)	NA	NA	NA	NA	NA
USGS GKM Database (2000-2015)	SM 3120 ICP USGS I-1630-85 Unspecified	USGS I-2020-05 USGS I-2477-92 USGS I-2668-98 USGS I-4020-05 USGS I-4471-97 USGS I-4668-98 Unspecified	USGS I-2477-92 USGS I-2724-89 USGS I-2725-93 USGS I-4471-97 Unspecified	USGS I-1472-85 USGS I-1472-87 USGS I-1472-95 Unspecified	USGS I-2477-92 USGS I-4471-97
USGS Paper 1651 (1994-2002)	FAAS ICP-AES ICP/MS	ICP-AES ICP/MS	ICP-AES ICP/MS	ICP-AES ICP/MS	ICP/MS

Provider	Surface Water – Metals laboratory methods			
	Uranium (U)	U-234/235/238	Vanadium (V)	Zinc (Zn)
USEPA Region 6 (2015)	NA	NA	EPA 200.8	EPA 200.8
USEPA Region 8 (2015)	NA	NA	EPA 200.8	EPA 200.8
USEPA Region 9 (2015)	NA	NA	EPA 200.8	EPA 200.8
USEPA Follow-up (2015-2016)	NA	NA	EPA 200.8	EPA 200.8
Colorado DPHE (1968-2016)	EPA 200.8 Unspecified	EPA 200.8	EPA 200.7	EPA 200.7 EPA 200.8 Unspecified
New Mexico ED (2001-2016)	EPA 200.8	EPA 200.8 Unspecified	EPA 200.8 Unspecified	EPA 200.8 Unspecified
Utah DEQ (1975-2016)	NA	NA	EPA 200.8	EPA 200.8 Unspecified
Navajo Nation (1999-2015)	EPA 200.8	NA	EPA 200.7	EPA 200.7 EPA 200.8
Southern Ute Indian Tribe (1992-2016)	NA	NA	EPA 200.8	EPA 200.7 EPA 200.8 SU SOP
Ute Mountain Ute Tribe (1996-2015)	NA	EPA 200.8	EPA 200.8 EPA 200.9	EPA 200.7 EPA 200.8 SM 3111-B
City of Farmington (2015-2016)	NA	NA	EPA 200.8	EPA 200.7
River Watch (1991-2016)	NA	NA	NA	EPA 200.7
Mountain Studies Institute (2016)	NA	NA	NA	EPA 200.8
SADIE (2011-2015)	NA	NA	EPA 200.8	EPA 200.7 EPA 200.8 EPA 6010
USEPA historic (1971-2000)	Unspecified	NA	NA	EPA 289.1 Unspecified
USGS MiniSipper (2015)	NA	NA	NA	EPA 200.8
USGS GKM Database (2000-2015)	NA	NA	EPA 200.7 USGS I-1472-85 USGS I-1472-87 USGS I-1472-95 USGS I-2020-05 USGS I-4020-05	EPA 200.7 USGS I-1472-85 USGS I-1472-87 USGS I-1472-95 USGS I-2020-05 USGS I-2477-92 USGS I-4020-05 USGS I-4471-97 Unspecified
USGS Paper 1651 (1994-2002)	ICP/MS	NA	ICP-AES ICP/MS	ICP-AES ICP/MS

Table A-8. List of metals laboratory methods for sediment samples by data provider

This listing is a compilation from available data. Sampled years in parenthesis. All years not necessarily used in analyses. Historic methods, at times, unspecified. Digestion methods listed if known.

Sediment – Metals laboratory methods							
Provider	Aluminum (Al)	Antimony (Sb)	Arsenic (As)	Barium (Ba)	Beryllium (Be)	Boron (B)	Cadmium (Cd)
USEPA Region 6 (2015)	EPA 6010C Digestion: EPA 3050B	EPA 6020A Digestion: EPA 3050B	EPA 6020A Digestion: EPA 3050B	EPA 6020A Digestion: EPA 3050B	EPA 6020A Digestion: EPA 3050B	NA	EPA 6020A Digestion: EPA 3050B
USEPA Region 8 (2015)	EPA 6010C Digestion: EPA 3050B	EPA 6020A Digestion: EPA 3050B	EPA 6020A Digestion: EPA 3050B	EPA 6020A Digestion: EPA 3050B	EPA 6020A Digestion: EPA 3050B	NA	EPA 6020A Digestion: EPA 3050B
USEPA Region 9 (2015)	EPA 6010C Digestion: EPA 3050B SOP DV-IP-0015	EPA 6020A Digestion: EPA 3050B SOP DV-IP-0015	NA	EPA 6020A Digestion: EPA 3050B SOP DV-IP-0015			
USEPA Follow-up (2015-2016)	EPA 6010C Digestion: EPA 3050B	EPA 6020A Digestion: EPA 3050B	EPA 6020A Digestion: EPA 3050B	EPA 6020A Digestion: EPA 3050B	EPA 6020A Digestion: EPA 3050B	NA	EPA 6020A Digestion: EPA 3050B
CDPHE (2015-2016)	EPA 200.7	NA	EPA 200.8	EPA 200.7	EPA 200.8	NA	EPA 200.8
NMED (2002-2016)	EPA 200.8 Digestion: SOP 41415	EPA 200.7	EPA 200.8 Digestion: SOP 41415				
Utah DEQ (2015-2016)	EPA 200.8 EPA 6010C	EPA 200.8 EPA 6020	EPA 200.8 EPA 6020	EPA 200.8 EPA 6020	EPA 200.8 EPA 6020	NA	EPA 200.8 EPA 6020
Navajo Nation (2015)	EPA 6010B	EPA 6010B	EPA 6010B				
SUIT (2016)	NA	NA	ICP	NA	NA	NA	ICP
UMUT	NA	NA	NA	NA	NA	NA	NA
City of Farmington	NA	NA	NA	NA	NA	NA	NA
River Watch	NA	NA	NA	NA	NA	NA	NA
MSI	NA	NA	NA	NA	NA	NA	NA
SADIE (2012-2014)	EPA 200.7 Digestion: EPA 200.2	EPA 200.8 Digestion: EPA 200.2	EPA 200.8 Digestion: EPA 200.2	EPA 200.8 Digestion: EPA 200.2	EPA 200.7 Digestion: EPA 200.2	NA	EPA 200.8 Digestion: EPA 200.2
USEPA historic (1981-1985)	NA	Unspecified	Unspecified	NA	Unspecified	NA	Unspecified
USGS GKM Database (1977-2000)	NA	NA	USGS I-6062-85 USGS I-6063-98 Unspecified	Unspecified	Unspecified	NA	USGS I-5020-05 USGS I-5135-85 Unspecified
USGS Paper 1651 (1994-2002)	ICP-AES	ICP-AES	ICP-AES	ICP-AES	ICP-AES	NA	ICP-AES

	Sediment – Metals laboratory methods						
Provider	Calcium (Ca)	Chromium (Cr)	Chromium (III)	Chromium (VI)	Cobalt (Co)	Copper (Cu)	Iron (Fe)
USEPA Region 6 (2015)	EPA 6010C Digestion: EPA 3050B	EPA 6020A Digestion: EPA 3050B	NA	NA	EPA 6020A Digestion: EPA 3050B	EPA 6020A Digestion: EPA 3050B	EPA 6010C Digestion: EPA 3050B
USEPA Region 8 (2015)	EPA 6010C Digestion: EPA 3050B	EPA 6020A Digestion: EPA 3050B	NA	NA	EPA 6020A Digestion: EPA 3050B	EPA 6020A Digestion: EPA 3050B	EPA 6010C Digestion: EPA 3050B
USEPA Region 9 (2015)	EPA 6010C Digestion: EPA 3050B SOP DV-IP-0015	EPA 6020A Digestion: EPA 3050B SOP DV-IP-0015	NA	NA	EPA 6020A Digestion: EPA 3050B SOP DV-IP-0015	EPA 6020A Digestion: EPA 3050B SOP DV-IP-0015	EPA 6010C Digestion: EPA 3050B SOP DV-IP-0015
USEPA Follow-up (2015-2016)	EPA 6010C Digestion: EPA 3050B	EPA 6020A Digestion: EPA 3050B	NA	NA	EPA 6020A Digestion: EPA 3050B	EPA 6020A Digestion: EPA 3050B	EPA 6010C Digestion: EPA 3050B
CDPHE (2015-2016)	NA	NA	NA	NA	EPA 200.7	EPA 200.7	EPA 200.7
NMED (2002-2016)	EPA 200.7	EPA 200.8 Digestion: SOP 41415	NA	NA	EPA 200.8 Digestion: SOP 41415	EPA 200.8 Digestion: SOP 41415	EPA 200.7 Digestion: SOP 41415
Utah DEQ (2015-2016)	EPA 200.7 EPA 6010C	EPA 6020	NA	NA	EPA 200.8 EPA 6020	EPA 200.8 EPA 6020	EPA 200.7 EPA 6010C
Navajo Nation (2015)	EPA 6010B	EPA 6010B	EPA 7196A EPA 7199	EPA 7196A EPA 7199	EPA 6010B	EPA 6010B	EPA 6010B
SUIT (2016)	NA	ICP	NA	NA	NA	ICP	NA
UMUT	NA	NA	NA	NA	NA	NA	NA
City of Farmington	NA	NA	NA	NA	NA	NA	NA
River Watch	NA	NA	NA	NA	NA	NA	NA
MSI	NA	NA	NA	NA	NA	NA	NA
SADIE (2012-2014)	EPA 200.7 Digestion: EPA 200.2	EPA 200.8 Digestion: EPA 200.2	NA	NA	EPA 200.8 Digestion: EPA 200.2	EPA 200.7 EPA 200.8 Digestion: EPA 200.2	EPA 200.7 Digestion: EPA 200.2
USEPA historic (1981-1985)	NA	Unspecified	NA	NA	NA	Unspecified	NA
USGS GKM Database (1977-2000)	NA	USGS I-5020-05 USGS I-5236-85 Unspecified	NA	NA	USGS I-5020-05 USGS I-5239-85 Unspecified	USGS I-5020-05 USGS I-5270-85 Unspecified	USGS I-5020-05 USGS I-5381-86 Unspecified
USGS Paper 1651 (1994-2002)	NA	ICP-AES	NA	NA	ICP-AES	ICP-AES	ICP-AES

	Sediment – Metals laboratory methods						
Provider	Lead (Pb)	Magnesium (Mg)	Manganese (Mn)	Mercury (Hg)	Molybdenum (Mo)	Nickel (Ni)	Potassium (K)
USEPA Region 6 (2015)	EPA 6020A Digestion: EPA 3050B	EPA 6010C Digestion: EPA 3050B	EPA 6020A Digestion: EPA 3050B	EPA 7471A	EPA 6020A Digestion: EPA 3050B	EPA 6020A Digestion: EPA 3050B	EPA 6010C Digestion: EPA 3050B
USEPA Region 8 (2015)	EPA 6020A Digestion: EPA 3050B	EPA 6010C Digestion: EPA 3050B	EPA 6020A Digestion: EPA 3050B	EPA 7471A	EPA 6020A Digestion: EPA 3050B	EPA 6020A Digestion: EPA 3050B	EPA 6010C Digestion: EPA 3050B
USEPA Region 9 (2015)	EPA 6020A Digestion: EPA 3050B SOP DV-IP-0015	EPA 6010C Digestion: EPA 3050B SOP DV-IP-0015	EPA 6020A Digestion: EPA 3050B SOP DV-IP-0015	EPA 7471A	EPA 6020A Digestion: EPA 3050B SOP DV-IP-0015	EPA 6020A Digestion: EPA 3050B SOP DV-IP-0015	EPA 6010C Digestion: EPA 3050B SOP DV-IP-0015
USEPA Follow-up (2015-2016)	EPA 6020A Digestion: EPA 3050B	EPA 6010C Digestion: EPA 3050B	EPA 6020A Digestion: EPA 3050B	EPA 7471A	EPA 6020A Digestion: EPA 3050B	EPA 6020A Digestion: EPA 3050B	EPA 6010C Digestion: EPA 3050B
CDPHE (2015-2016)	EPA 200.8	NA	EPA 200.7 EPA 200.8	NA	NA	EPA 200.7	NA
NMED (2002-2016)	EPA 200.8 Digestion: SOP 41415	EPA 200.7	EPA 200.7 EPA 200.8 Digestion: SOP 41415	EPA 245.5	EPA 200.8 Digestion: SOP 41415	EPA 200.8 Digestion: SOP 41415	NA
Utah DEQ (2015-2016)	EPA 200.8 EPA 6020	EPA 200.7 EPA 6010C	EPA 200.8 EPA 6020	EPA 7471B	EPA 200.8 EPA 6020	EPA 200.8 EPA 6020	EPA 200.7 EPA 6010C
Navajo Nation (2015)	EPA 6010B	EPA 6010B	EPA 6010B	EPA 7471A	EPA 6010B	EPA 6010B	EPA 6010B
SUIT (2016)	ICP	NA	NA	CVAAS	NA	ICP	NA
UMUT	NA	NA	NA	NA	NA	NA	NA
City of Farmington	NA	NA	NA	NA	NA	NA	NA
River Watch	NA	NA	NA	NA	NA	NA	NA
MSI	NA	NA	NA	NA	NA	NA	NA
SADIE (2012-2014)	EPA 200.7 EPA 200.8 Digestion: EPA 200.2	EPA 200.7 Digestion: EPA 200.2	EPA 200.7 Digestion: EPA 200.2	EPA 7473	EPA 200.8 Digestion: EPA 200.2	EPA 200.8 Digestion: EPA 200.2	EPA 200.7 Digestion: EPA 200.2
USEPA historic (1981-1985)	Unspecified	NA	NA	Unspecified	NA	Unspecified	NA
USGS GKM Database (1977-2000)	USGS I-5020-05 USGS I-5399-85 Unspecified	NA	USGS I-5020-05 USGS I-5454-85 Unspecified	USGS I-5462-85 Unspecified	Unspecified	Unspecified	Unspecified
USGS Paper 1651 (1994-2002)	ICP-AES	ICP-AES	ICP-AES	CVAAS	ICP-AES	ICP-AES	ICP-AES

	Sediment – Metals laboratory methods					
Provider	Selenium (Se)	Silver (Ag)	Sodium (Na)	Thallium (Tl)	Vanadium (V)	Zinc (Zn)
USEPA Region 6 (2015)	EPA 6020A Digestion: EPA 3050B	EPA 6020A Digestion: EPA 3050B	EPA 6010C Digestion: EPA 3050B	EPA 6020A Digestion: EPA 3050B)	EPA 6020A Digestion: EPA 3050B	EPA 6020A Digestion: EPA 3050B
USEPA Region 8 (2015)	EPA 6020A Digestion: EPA 3050B	EPA 6020A Digestion: EPA 3050B	EPA 6010C Digestion: EPA 3050B	EPA 6020A Digestion: EPA 3050B	EPA 6020A Digestion: EPA 3050B	EPA 6020A Digestion: EPA 3050B
USEPA Region 9 (2015)	EPA 6020A Digestion: EPA 3050B SOP DV-IP-0015)	EPA 6020A Digestion: EPA 3050B SOP DV-IP-0015	EPA 6010C Digestion: EPA 3050B SOP DV-IP-0015	EPA 6020A Digestion: EPA 3050B SOP DV-IP-0015	EPA 6020A Digestion: EPA 3050B SOP DV-IP-0015	EPA 6020A Digestion: EPA 3050B SOP DV-IP-0015
USEPA Follow-up (2015-2016)	EPA 6020A Digestion: EPA 3050B	EPA 6020A Digestion: EPA 3050B	EPA 6010C Digestion: EPA 3050B	EPA 6020A Digestion: EPA 3050B	EPA 6020A Digestion: EPA 3050B	EPA 6020A Digestion: EPA 3050B
CDPHE (2015-2016)	EPA 200.8	NA	NA	NA	NA	EPA 200.7
NMED (2002-2016)	EPA 200.8 EPA 270.2 Digestion: SOP 41415	EPA 200.8 Digestion: SOP 41415	NA	EPA 200.8 Digestion: SOP 41415	EPA 200.8 Digestion: SOP 41415	EPA 200.8 Digestion: SOP 41415
Utah DEQ (2015-2016)	EPA 200.8 EPA 6020	EPA 200.8 EPA 6020	EPA 200.7 EPA 6010C	EPA 200.8 EPA 6020	EPA 200.8 EPA 6020	EPA 200.8 EPA 6020
Navajo Nation (2015)	EPA 6010B	EPA 6010B	EPA 6010B	EPA 6010B	EPA 6010B	EPA 6010B
SUIT (2016)	NA	NA	NA	NA	NA	ICP
UMUT	NA	NA	NA	NA	NA	NA
City of Farmington	NA	NA	NA	NA	NA	NA
River Watch	NA	NA	NA	NA	NA	NA
MSI	NA	NA	NA	NA	NA	NA
SADIE (2012-2014)	EPA 200.8 Digestion: EPA 200.2	EPA 200.8 Digestion: EPA 200.2	EPA 200.7 Digestion: EPA 200.2	EPA 200.8 Digestion: EPA 200.2	EPA 200.8 Digestion: EPA 200.2	EPA 200.7 Digestion: EPA 200.2
USEPA historic (1981-1985)	Unspecified	Unspecified	NA	Unspecified	NA	Unspecified
USGS GKM Database (1977-2000)	Unspecified	NA	NA	NA	NA	USGS I-5020-05 USGS I-6900-85 Unspecified
USGS Paper 1651 (1994-2002)	HG-AAS	ICP-AES	ICP-AES	Passive Leach & ICP/MS	ICP-AES	ICP-AES

Table A-9. Analytical methodology for metal analyses. Includes methods used for historic samples.

Metal Analysis		
Method ID	Method Technology	
EPA 7473	AAS	atomic absorption spectrometry
USGS I-1630-85		
USGS I-2020-05	cICP-MS	collision/reaction cell inductively coupled plasma-mass spectrometry
USGS I-4020-05		
EPA 7196A	colorimetric	spectrophotometer or filter photometer
SM 3500-CR (D)		
SM 3500-SE (C)		spectrophotometer
EPA 245.1	CVAAS	cold vapor atomic absorption spectrometry
EPA 245.2		
EPA 7470A		
EPA 7471A		
EPA 7471B		
USGS I-2462-85		
USGS I-3462-85		
USGS I-5462-85		
EPA 1631E	CV-AFS	cold vapor-atomic fluorescence spectrometry
USGS I-2464-01		
USGS I-4464-01		
SM 3500-CA (D)	EDTA	titration by ethylenediaminetetraacetic acid or its salts
EPA 215.1	FLAAS	flame atomic absorption spectrometry
EPA 242.1		
EPA 258.1		
EPA 273.1		
EPA 289.1		
SM 3111-B		
SM 3500-Mg (B)		
USGS I-5135-85		
USGS I-5236-85		
USGS I-5239-85		
USGS I-5270-85		
USGS I-5381-86		
USGS I-5399-85		
USGS I-5454-85		
USGS I-6900-85		
SM 3500-K (D)	FP	flame photometry
SM 3500-NA(D)		
EPA 200.9	GFAAS	graphite furnace atomic absorption spectrometry
EPA 206.2_M		
EPA 270.2		

Metal Analysis		
Method ID	Method Technology	
USGS I-1233-93	GFAAS	graphite furnace atomic absorption spectrometry
USGS I-2063-98		
USGS I-2138-89		
USGS I-2274-89		
USGS I-2403-89		
USGS I-2668-98		
USGS I-2724-89		
USGS I-2725-93		
USGS I-3233-93		
USGS I-4063-98		
USGS I-4668-98		
USGS I-6063-98		
SM 3114-C	HG-AAS	hydride generation-atomic absorption spectrometry
EPA 7199	IC	ion chromatography
SM 3500-CA (C)	ICP	inductively coupled plasma
EPA 200.8	ICP/MS	inductively couple plasma/mass spectrometry
EPA 200.8/6020		
EPA 6020		
EPA 6020A		
USGS I-2477-92		
USGS I-4471-97		
USGS I-5020-05		
SM 3120 ICP	ICP-OES	inductively coupled plasma-optical emission spectrometry
USGS I-4471-97		
EPA 200.7	ICP-AES	inductively coupled plasma-atomic emission spectroscopy
EPA 200.7/6010		
EPA 6010B		
EPA 6010C		
USGS I-1472-85		
USGS I-1472-87		
USGS I-1472-95		
USGS I-4471-97		
USGS I-5020-05		
Unspecified	Passive Leach & ICP/MS	passive leach method and inductively couple plasma/mass spectrometry
USGS I-6062-85	QTFAAS	quartz tube furnace atomic absorption spectrometry
Unspecified	SpectroPhoto	hach portable spectrophotometry
EPA 200.2	Not Applicable	solid and aqueous sample preparation (acid digestion)
EPA 3050B		solid sample preparation (acid digestion)
SOP 41415		solid sample preparation (acid digestion)

Table A-10. List of laboratory methods for general analytes by data provider.

This listing is a compilation of selected analytes from available data. Includes methods used for historic samples. Methods, at times, unspecified. All analytes not necessarily used in analyses.

Provider	General Analytes					
	Alkalinity (as CaCO ₃) (total)	Alkalinity Phenolphthalein (total hydroxide + 1/2 carbonate)	Bicarbonate (as CaCO ₃)	Carbonate (as CaCO ₃)	Hydroxide (as CaCO ₃)	Hardness (as CaCO ₃) (total) (Ca+Mg)
USEPA	SM 2320B Unspecified	NA	NA	NA	NA	SM 2340B
Colorado DPHE	EPA 310.1 SM 2320 Unspecified	SM 2320	NA	NA	NA	Calculation EPA 200.7 SM 2340B Unspecified
New Mexico ED	EPA 310.1 SM 2320B Unspecified	NA	EPA 150.1 EPA 310.1 SM 2320B SM 4500H+B Unspecified	EPA 150.1 EPA 310.1 SM 2320B SM 4500H+B Unspecified	NA	EPA 200.7
Utah DEQ	SM 2320B	NA	SM 2320 SM 2320B Unspecified	SM 2320 SM 2320B Unspecified	SM 2320 SM 2320B Unspecified	EPA 200.7 SM 2340B Unspecified
Navajo Nation	SM 2320B	SM 2320B	SM 2320B	EPA 310.1 SM 2320B	EPA 310.1 SM 2320B	SM 2340B
Southern Ute Indian Tribe	SM 2320 SM 2320B SU SOP	NA	SM 2320 SM 2320B	SM 2320 SM 2320B	SM 2320 SM 2320B	SM 2340B SU SOP Unspecified
Ute Mountain Ute Tribe	SM 2320 SM 2320B	NA	SM 2320 SM 2320B	SM 2320 SM 2320B	SM 2320 SM 2320B	AOAC 973.52 SM 2340B SM 2340C
City of Farmington	NA	NA	NA	NA	NA	NA
River Watch	EPA 310.1	EPA 310.1	NA	NA	NA	EPA 130.2
Mountain Studies Institute	NA	NA	NA	NA	NA	SM 2340B
SADIE	EPA 310.1	NA	NA	NA	NA	SM 2340B
USGS MiniSipper	NA	NA	NA	NA	NA	SM 2340B
USGS GKM database	USGS NFM 6.6 Unspecified	NA	Hach digital titrator Unspecified	Hach digital titrator Unspecified	NA	Calculation
USGS Paper 1651	Incremental Titration	NA	Incremental Titration	NA	NA	NA

Provider	General Analytes					
	Cyanide (Total)	Cyanides amenable to chlorination (HCN & CN)	Bromide	Bromate	Chloride	Fluoride
USEPA	Unspecified	NA	NA	NA	EPA 300.0 Unspecified	EPA 300.0
Colorado DPHE	Unspecified	NA	EPA 300.1	EPA 300.1 Unspecified	EPA 300.0 EPA 300(A) Unspecified	SM 4500-F-E EPA 300.0 EPA 300(A) Unspecified
New Mexico ED	EPA 335.4 QuikChem Method 10-204-00-1X	NA	EPA 300.1	NA	EPA 300.0 EPA 300(A) Unspecified	EPA 340.2 SM 4500F-C Unspecified
Utah DEQ	EPA 335.4	NA	NA	NA	EPA 300.0 EPA 325.2 EPA 325.3 Unspecified	Unspecified
Navajo Nation	EPA 335.2 EPA 335.3 SM 4500-CN(E) SM 4500-CN(G)	SM 4500-CN(G)	EPA 300.0	NA	EPA 300.0	EPA 300.0
Southern Ute Indian Tribe	NA	NA	NA	NA	SM 4500-CL(E) EPA 325.2	NA
Ute Mountain Ute Tribe	NA	NA	NA	NA	SM 4500-CL(B) SM 4500-CL(C) EPA 300.0	SM 4500-F-C EPA 300.0
City of Farmington	EPA 335.4	NA	NA	NA	NA	NA
River Watch	NA	NA	NA	NA	EPA 325.1	NA
Mountain Studies Institute	NA	NA	NA	NA	NA	NA
SADIE	NA	NA	NA	NA	EPA 300.0	EPA 300.0
USGS MiniSipper	NA	NA	NA	NA	NA	NA
USGS GKM database	NA	NA	NA	NA	USGS I-2057-90	ion chromatography USGS I-1327-85 Unspecified
USGS Paper 1651	NA	NA	ICP-AES ICP/MS	NA	Ion Chromatography	Ion Chromatography

Provider	General Analytes					
	Sulfate	Nitrogen nitrate (Nitrate as N)	Nitrogen nitrite (Nitrite as N)	Nitrate/ Nitrite (as N)	Phosphorus (Phosphate-phosphorus) (Phosphate total as P)	Dissolved Organic Carbon
USEPA	EPA 300.0	EPA 300.0	NA	NA	Unspecified	5310-B EPA 415.2
Colorado DPHE	EPA 300.0 EPA 300(A) Unspecified	EPA 300.0 EPA 353.2 Unspecified	EPA 300.0 EPA 353.2 Unspecified	EPA 353.2 Unspecified	EPA 365.1 Unspecified	NA
New Mexico ED	EPA 300.0 EPA 300(A) Unspecified	NA	NA	EPA 353.2 Unspecified	EPA 365.1 EPA 365.4 Unspecified	NA
Utah DEQ	EPA 300.0 EPA 375.2 Unspecified	Unspecified	Unspecified	EPA 353.2 Unspecified	EPA 365.1 EPA 365.2 SM 4500PF Unspecified	Unspecified
Navajo Nation	EPA 300.0 EPA 9056	EPA 353.2	EPA 300.0 EPA 353.2	NA	EPA 300.0 EPA 365.3 SM 4500-P-E	NA
Southern Ute Indian Tribe	SM 4500-SO4(D) EPA 375.3	Unspecified	EPA 353.2	EPA 353.2 SU SOP	EPA 365.1 SU SOP	NA
Ute Mountain Ute Tribe	SM 4500-SO4(D) EPA 300.0	SM 4500-NO3(D)	NA	EPA 300.0 EPA 353.2 EPA 353.3	SM 4500-P-E EPA 365.2 EPA 365.3	NA
City of Farmington	NA	NA	NA	NA	NA	NA
River Watch	EPA 375.4	NA	NA	EPA 353.2	EPA 365.3	NA
Mountain Studies Institute	NA	NA	NA	NA	NA	NA
SADIE	EPA 300.0	NA	NA	EPA 300.0	NA	EPA 415.3
USGS MiniSipper	NA	NA	NA	NA	NA	NA
USGS GKM database	Turbidimetric analysis USGS I-2057-90 Unspecified	NA	NA	NA	NA	USGS O-1122-92
USGS Paper 1651	ICP/MS Ion Chromatography SpectroPhoto	Ion Chromatography	NA	NA	Ion Chromatography	NA

	General Analytes					
Provider	Organic Carbon (total)	Total Dissolved Solids (TDS)	Total Suspended Solids (TSS)	pH	Specific Conductance (SC, EC) (conductivity)	Temperature (air) (water) (sample) (undefined)
USEPA	5310-B 9060A	SM 2540C	SM 2540D	SM 4500H+B Horiba U53G Meter Probe/Sensor Unspecified	Horiba U53G Meter Probe/Sensor Unspecified	Horiba U53G Meter Probe/Sensor Unspecified
Colorado DPHE	NA	EPA 160.1	EPA 160.2 SM 2540D	EPA 150.1 SM 4500-H Unspecified	EPA 120.1 Unspecified	EPA 170.1 SM 2550 Unspecified
New Mexico ED	EPA 415.1	EPA 160.1 SM 2540C Unspecified	EPA 160.2 SM 2540D Unspecified	Sonde Unspecified	Sonde SM 2510B Unspecified	Sonde Unspecified
Utah DEQ	NA	SM 2540C	EPA 160.2 SM 2540D	EPA 150.1 SM 2320 SM 2320B SM 4500H+B Unspecified	EPA 120.1 SM 2510B Unspecified	NA
Navajo Nation	NA	Unspecified	SM 2540D	Unspecified	Unspecified	Unspecified
Southern Ute Indian Tribe	NA	EPA 160.1 SM 2540C Sonde SU SOP	EPA 160.2 SM 2540D SU SOP	EPA 150.1 Sonde SU SOP	SM 2510B EPA 120.1 Sonde SU SOP	Sonde SU SOP
Ute Mountain Ute Tribe	NA	EPA 160.1 SM 2540C	EPA 160.2 SM 2540D	SM 4500H	SM 2510	EPA 170.1 SM 2550 SM 4500-O-G
City of Farmington	NA	NA	NA	Unspecified	Unspecified	Unspecified
River Watch	NA	NA	EPA C-008-1	EPA 150.1	NA	EPA 170.1
Mountain Studies Institute	NA	NA	NA	NA	NA	NA
SADIE	NA	NA	NA	EPA 150.1	EPA 120.1	EPA 170.1
USGS MiniSipper	NA	NA	NA	Sonde	Hobo CT logger Sonde STIC	Hobo CT logger Sonde STIC
USGS GKM database	USGS O-3100-83	Calculation USGS I-1750-85	Unspecified	USGS NFM 6.4 USGS I-1586-77 USGS I-2587-85 Unspecified	USGS I-1780-77 USGS I-2781-85 Unspecified	thermometer Unspecified
USGS Paper 1651	NA	NA	NA	Field Methods probe	Probe	Probe

Provider	General Analytes					
	Dissolved Oxygen (DO)	Dissolved oxygen saturation	RDO (RDO % SAT)	ODO (ODOsat)	Oxidation reduction potential (ORP)	Salinity
USEPA	Horiba U53G Meter Probe/Sensor Unspecified	Unspecified	NA	NA	Horiba U53G Meter Probe/Sensor Unspecified	Unspecified
Colorado DPHE	EPA 360.1 EPA 1002-8-2009 Unspecified	Unspecified	Unspecified	NA	NA	NA
New Mexico ED	Sonde Unspecified	Unspecified	NA	Sonde	NA	Unspecified
Utah DEQ	NA	NA	NA	NA	NA	NA
Navajo Nation	Unspecified	Unspecified	NA	NA	NA	Unspecified
Southern Ute Indian Tribe	SU SOP	NA	NA	Sonde	NA	NA
Ute Mountain Ute Tribe	SM 4500-O-G EPA 360.1	SM 4500-O-G	NA	NA	SM 2580	NA
City of Farmington	Unspecified	NA	NA	NA	NA	NA
River Watch	EPA 360.2	EPA 360.2	NA	NA	NA	NA
Mountain Studies Institute	NA	NA	NA	NA	NA	NA
SADIE	EPA 360.1	NA	NA	NA	NA	NA
USGS MiniSipper	Sonde	Sonde	NA	NA	NA	Sonde
USGS GKM database	ASTM D888-05 SM 4500-O G Unspecified	Calculation Unspecified	NA	NA	NA	NA
USGS Paper 1651	DO meter	NA	NA	NA	NA	NA

	General Analytes		
Provider	Turbidity	Percent Moisture (Sediments)	Flow (flow intermittency)
USEPA	Probe/Sensor Unspecified	NA	Sontek Flowtracker
Colorado DPHE	Unspecified	NA	Unspecified
New Mexico ED	Sonde	NA	Unspecified
Utah DEQ	EPA 180.1 Field turbidity Unspecified	PMOIST	USGS FLOW
Navajo Nation	Unspecified	NA	Unspecified
Southern Ute Indian Tribe	NA	NA	SU SOP
Ute Mountain Ute Tribe	NA	NA	ASTM D3858
City of Farmington	Unspecified	NA	Unspecified
River Watch	NA	NA	ASTM D3858
Mountain Studies Institute	NA	NA	NA
SADIE	NA	NA	SOP 722 FLDM-720
USGS MiniSipper	NA	NA	STIC USGS gage
USGS GKM database	EPA 180.1 Unspecified	NA	NA
USGS Paper 1651	NA	NA	NA

Table A-11. Links to quality assurance documentation from data providers

	Data Provider	Resource	Link
Federal	US EPA Region 6	<i>Interim Final Quality Assurance Sampling Plan Water and Sediment Sampling and Monitoring for Gold King Mine Spill Farmington, San Juan County, New Mexico.</i> USEPA R6. August 13, 2015.	https://www.epa.gov/sites/production/files/2015-09/documents/r6_king_mine_gasp_rev_1.pdf
	US EPA Region 8	<i>Sampling and Analysis Plan/Quality Assurance Project Plan For Gold King Mine Release Silverton, San Juan County, Colorado.</i> USEPA R8. September 2015.	https://www.epa.gov/sites/production/files/2015-09/documents/0001-1508-04_gkm_sap-qapp_rev1_091115.pdf
	US EPA Region 9	<i>Sampling and Analysis Plan/Quality Assurance Project Plan for Gold King Mine ER EPA Region 9 Operations Farmington, San Juan County, New Mexico.</i> USEPA R9. September 1, 2015.	https://www.epa.gov/sites/production/files/2015-09/documents/r9-gkm-sap-qapp-20150901.pdf
	US EPA	<i>Post-Gold King Mine Release Incident: Conceptual Monitoring Plan for Surface Water, Sediments, and Biology.</i> USEPA. March 2016.	https://www.epa.gov/sites/production/files/2016-03/documents/post-gkm-final-conceptual-monitoring-plan_2016_03_24_16.pdf
		Webpage: EPA ERT Standard Operating Procedures	https://www.epaosc.org/site/site_profile.aspx?site_id=2107
	USGS	National Field Manual for the Collection of Water-Quality Data. USGS. October 2015.	http://water.usgs.gov/owq/FieldManual/compiled/NFM_complete.pdf
		Webpage: Water-Resources Techniques, Methods, and Modeling	http://water.usgs.gov/techniques.html
Webpage: USGS Quality Assurance for Water-Quality Activities		http://water.usgs.gov/owq/quality.html	
States	Colorado	<i>Statewide Water Quality Management Plan.</i> Colorado Department of Public Health and Environment, Water Quality Control Division. 2011.	https://www.colorado.gov/pacific/cdphe/statewide-water-quality-management-plan
		<i>Sampling Analysis Plan (SAP) for River and Stream Water Quality Monitoring – FY 2015.</i> Colorado Department of Public Health and Environment.	https://www.colorado.gov/pacific/sites/default/files/FY15%20Water%20Chemistry%20SAP%20-%20Final.pdf

	Data Provider	Resource	Link
States	Colorado	<i>Standard Operating Procedures for the Planning of and Field Procedures for Conducting Monitoring Activity.</i> Colorado Department of Public Health and Environment. March 2010.	https://www.colorado.gov/pacific/sites/default/files/WQ_nonpoint_source-SOP-Water-Quality-Monitoring-Activities-030110.pdf
		<i>Sampling Analysis Plan (SAP) for Water Quality Monitoring in the Upper Animas River, Long-Term Monitoring Plan 2016-2017.</i> Colorado Department of Public Health and Environment.	https://www.colorado.gov/pacific/sites/default/files/WQ_Animas_Sample-Analysis-Plan-Revised-10-18-16.pdf
	New Mexico	<i>Quality Assurance Project Plan for Water Quality Management Programs.</i> Surface Water Quality Bureau New Mexico Environment Department. 2016.	https://www.env.nm.gov/swqb/QAPP/2016QAPPFinal_Complete_withAppendices_Approval_Signatures.pdf
		Webpage: Surface Water Quality Bureau - Monitoring & Assessment - Standards Operating Procedures	https://www.env.nm.gov/swqb/SOP/
		<i>Quality Assurance Project Plan Gold King Mine Spill Long-Term Monitoring Plan New Mexico Animas and San Juan River Sediment Assessment Sampling and Analysis.</i> New Mexico Environment Department. September 2016.	https://www.env.nm.gov/wp-content/uploads/2016/06/GKM_PXRF_QAPP_FINAL_Rev0.pdf
	Utah	<i>Quality Assurance Program Plan for Environmental Data Operations.</i> Utah Division of Water Quality. 2014.	http://www.deq.utah.gov/Compliance/monitoring/water/docs/2014/05May/DWQ_QAPP_5.1.14_Rev0.pdf
		Webpage: Utah Division of Water Quality - Quality Assurance Program Plan and Standard Operating Procedures	http://www.deq.utah.gov/Compliance/monitoring/water/qaqc.htm
		<i>Utah's Long-term Monitoring and Assessment Plan for the San Juan River and Lake Powell, Utah.</i> Utah Department of Environmental Quality, Division of Water Quality. March 2016.	http://www.deq.utah.gov/Topics/Water/goldkingmine/docs/2016/03March/Long-Term-Monitoring-Strategy-Outline-FINAL.pdf
	Tribes	Navajo Nation	<i>Quality Assurance Plan (QAP) for Surface Water Quality Data Collection.</i> Navajo Nation Environmental Protection Agency. June 2012.
<i>Quality Assurance Project Plan (QAPP) for Sediment Quality Data Collection.</i> Navajo Nation Environmental Protection Agency. August 2016.			

	Data Provider	Resource	Link
Tribes	Southern Ute Indian Tribe	EPA-approved Sample Analysis Plans (SAP) and Quality Assurance Project Plans (QAPP)	Specific link not found. General link provided. https://www.southernute-nsn.gov/
	Ute Mountain Ute Tribe	<i>Ute Mountain Ute Indian Tribe Water Pollution Prevention Program Quality Assurance Project Plan for the Monitoring of Surface and Ground Waters</i> . Revision No. 6, March 2007	Specific link not found. General link provided. http://www.utemountainutetribe.com/
NGOs	Mountain Studies Institute	<i>Animas River Water Quality at Rotary Park, Durango, Colorado Gold King Mine Release Monitoring</i> . Mountain Studies Institute. March 2016.	http://static1.squarespace.com/static/53bc5871e4b095b6a42949b4/t/57085018555986f2415aae75/1460162712812/EPA_RotaryPark_WQReport_20160407.pdf
		<i>Sampling and Analysis Plan/Quality Assurance Project Plan for Gold King Mine Release Silverton, San Juan County, Colorado</i> . USEPA R8. September 2015.	https://www.epa.gov/sites/production/files/2015-09/documents/0001-1508-04_gkm_sap-qapp_rev1_091115.pdf
	The Rivers of Colorado Water Watch Network (River Watch)	<i>Colorado River Watch Water Quality Sampling Manual</i> . Version 8.14. July 2014. (Chapter 1. Introduction)	https://drive.google.com/file/d/0B4xbDjUDjTxuWllpMERQYXFaRuk/view
		<i>Quality Assurance and Quality Control Plan</i> (Chapter 5. QAQC)	https://drive.google.com/file/d/0B4xbDjUDjTxubk9wANDJOGkyWkE/view

[This page intentionally left blank.]

Appendix B.
Surface Water Modeling Using
the Water Quality Analysis Simulation Program (WASP)

Contents

Contents	2
1. Introduction.....	3
2. The Water Quality Analysis Simulation (WASP) Model.....	3
3. Model Set Up.....	4
3.1. WASP Segmentation	4
3.2. Overall Conceptual Model.....	5
3.3. Model Parameterization and Calibration	6
3.3.1. Flow	7
3.3.2. Discharge Coefficients.....	8
3.3.3. Velocity Calibration.....	10
3.3.4. Particle Settling Rate	11
3.3.5. Partitioning	12
3.3.6. Dispersion	14
3.3.7. Resuspension	14
4. Simulation Scenarios	14
4.1. Plume Movement Scenario.....	14
4.2. Total and Dissolved Individual Metals Scenario	15
4.3. Year Following Gold King Mine Release	15
5. Scenario Results.....	16
5.1. Plume Movement.....	16
5.2. Total and Dissolved Individual Metals Scenario	18
5.3. Year Following Gold King Mine Release	19
6. Numerical Dispersion	21
6.1. Numerical Dispersion in WASP.....	21
6.2. Time Step Sensitivity.....	21
6.3. Negative Dispersion.....	22
7. Settling Velocity Sensitivity	23
8. References.....	24

1. Introduction

As part of the Gold King Mine analysis, EPA developed a mechanistic model to simulate the fate and transport of the metals released from the Gold King Mine as they traversed the Animas and San Juan Rivers. This Appendix serves to present the details of this modeling effort.

EPA used WASP7 (Water quality Analysis Simulation Program, version 7) to develop a mechanistic, differential mass model simulating metal concentrations in surface water and underlying sediments. EPA constructed the WASP Gold King Mine Model (GKM model) using the Simple Toxicant (TOXI) module within WASP7. The model was constructed to address a set of key questions:

- What were the characteristics of the plume as it moved downstream?
 - How long did it take for the peak plume concentration to reach a certain location?
 - How long did it take for the plume to pass a certain location?
 - How far downstream could the plume be detected compared to model simulation predictions?
- How were metal concentrations affected during and after the plume?
 - What were the peak total concentrations and individual metal (As, Cu, Pb, and Zn) concentrations as the plume traveled downstream?
 - What were the metal concentrations (total and dissolved) at certain locations over time?
- What was the fate of GKM generated metals in the river system including concentrations in the streambed?
- Did metals concentrations in sediment increase relative to background?
- What are the long term impacts of the GKM release?
 - What are the concentrations in the sediments compared to background concentrations?
 - What are the concentrations in the surface water during low, middle, and high flow periods, such as those that would occur during snowmelt?

Process-based mathematical models are valuable tools for system understanding and informing decisions. Measurement data often are sparse and cannot be extrapolated to investigate the environmental impacts of different policy options. As stated in a recent National Research Council report (National Research Council, 2007), environmental models are critical to the regulatory decision-making process, because the spatial and temporal scales linking environmental controls and environmental quality generally do not allow an observational approach to understand the relationship between economic activity and environmental quality. Environmental models are useful for understanding key research needs and prioritizing future data collection efforts.

We use WASP in this analysis to work concurrently with the empirical analysis. Both monitoring and modeling have their own strengths and weaknesses. By using them side-by-side, each can inform the other and improve our overall understanding of the system. A process-based model also lets us evaluate how well the conceptual model and its processes are representing the system. By applying WASP, we also are able to simulate concentrations over space and over time for the duration of the simulation, thereby helping to fill in the spaces between sample times and sample locations.

2. The Water Quality Analysis Simulation (WASP) Model

The Water Quality Analysis Simulation Program (WASP) is a dynamic and spatially resolved mechanistic, differential mass balance fate and transport modeling framework for environmental contaminants in surface waters and sediments. WASP7 is an enhancement of the original WASP developed in the 1980s (Di Toro et al., 1983; Connolly and Winfield, 1984; Ambrose, R.B. et al., 1988). Since then, WASP has undergone many improvements and enhancements, resulting in WASP version 7.52 released November

15, 2013. WASP7 is a modeling framework, which allows the user to construct the model design appropriate for the system of interest, in one, two, or three dimensions. WASP7 is designed to simulate conventional pollutants, organic chemicals, metals, mercury, pathogens, temperature, and salinity. WASP7 allows for the time varying processes of advection, dispersion, point and diffuse mass loading, boundary conditions, and boundary exchange. WASP can be linked to hydrodynamic and sediment transport models, or the user can use the algorithms within the WASP framework. WASP is one of the most widely used water quality models in the USA and throughout the world. WASP has been applied in the development of Total Maximum Daily Loads (TMDLs) (e.g., US EPA, 2001; US EPA 2004); simulation of nutrients in Tampa Bay, FL (Wang et al., 1999); and development of remediation strategies for mercury in the Sudbury River, MA (Knights 2010a, 2010b). The WASP TOXI module within WASP allows the user to assign kinetic processes to the contaminant of interest. These processes include: decay, sorption, oxidation, reduction, photo-reactions, biodegradation, hydrolysis, and volatilization. WASP7 is available for download at: <http://www.epa.gov/exposure-assessment-models/water-quality-analysis-simulation-program-wasp>.

WASP is a modeling framework, which allows the user to construct a site-specific surface water quality model. The model domain consists of WASP segments, which can be surface water or sediments. The user builds the model specific to the model domain of interest and decides which processes will be included. Developing the model requires a balance between complexity to capture the appropriate governing processes and simplicity. Increased complexity causes increased uncertainty, requires more parameters to describe the increased number of processes, and increases time and effort to implement the model.

3. Model Set Up

3.1. WASP Segmentation

EPA used the National Hydrography Dataset Plus (NHDPlus) dataset to delineate the WASP segmentation for the Gold King Mine WASP model. We used BASINS 4.1 (Better Assessment Science Integrating point & Non-point Sources, USEPA, 2015) to download shapefiles. These were clipped to the HUC8 layer covering the Animas and San Juan watersheds (UTNMCO SanJuanHUC8.shp). Stream characteristics were pulled from NHDPlus data. Using the WASPBuilder tool, a segment of the nhdflowline.shp file was selected near the point where the San Juan River empties into Lake Powell. The tool was used to automatically select segments upstream with a stream order of 3 or greater. Edits were made to this selection by hand to include/remove segments until the boundaries were continuous for the extent of the model domain (i.e., from where the Gold King Mine flowed into Cement Creek, the Animas River from Cement Creek to the San Juan, and the San Juan from the Navajo Dam release to Lake Powell). The team removed any braiding within the system to maintain a non-branching, one-dimensional stream network appropriate for use of the kinematic wave flow routing hydrodynamics module within WASP.

The GKM WASP model domain included three upstream boundaries: Cement Creek, Animas River, and the San Juan River. The portion of Cement Creek started at USGS flow gage 09358550, which is near the end of Cement Creek before it reaches the Animas River. The portion of the Animas River simulated was just upstream of the confluence with Cement Creek, at USGS gage 09358000. The portion of the San Juan River consisted of upstream of the confluence with the Animas River, from USGS gage 09355500.

The segments were divided into lengths with approximately equal travel time, as defined by a function of length and slope, to minimize numerical dispersion and provide model stability, using the WASPBuilder tool to create the original wif (WASP7 input file). The model domain, with the location of USGS flow gages and model boundaries are presented in Figure B-1. Gold King Mine Model Domain, Segmentation, and Flow

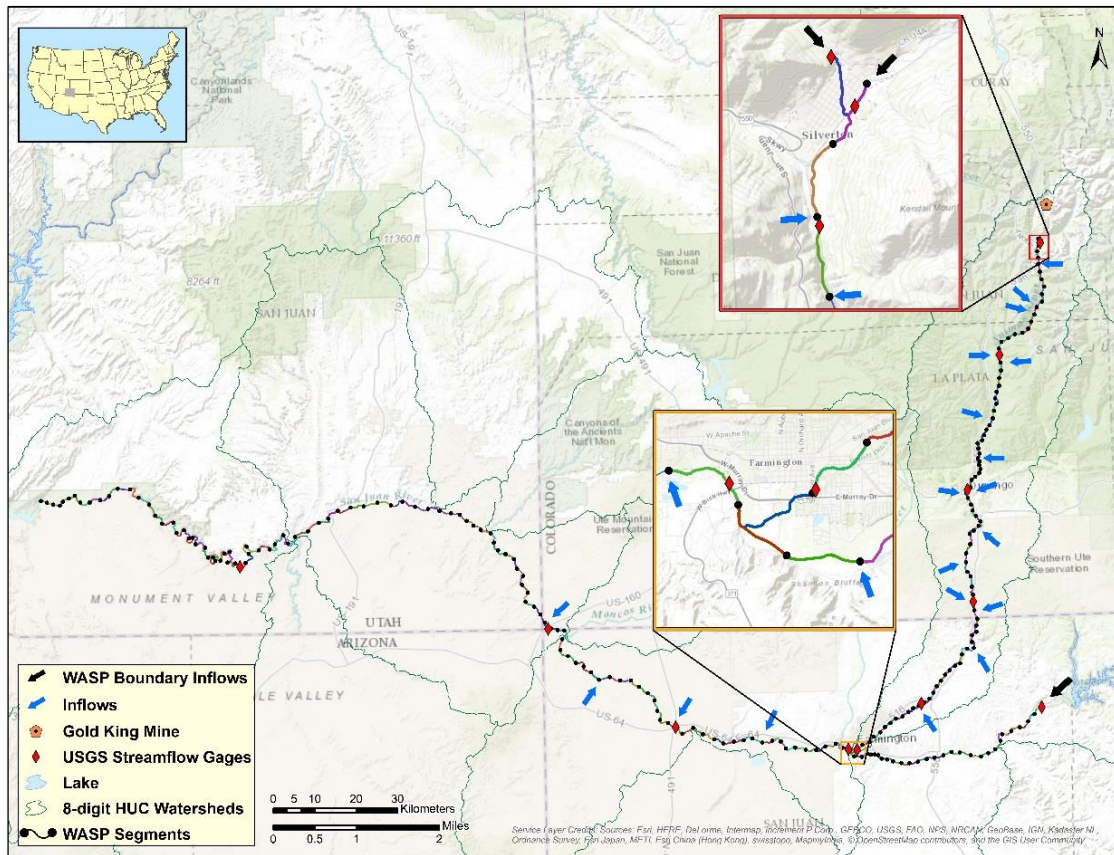


Figure B-1. Gold King Mine Model Domain, Segmentation, and Flow

The GKM Model is a one-dimensional surface water segment of linked surface water segments. Underneath each surface water segment is a single sediment layer segment. The GKM Model consists of 458 WASP segments, 229 surface water segments, 229 sediment layer segments, with an average length of 2,447 m, ranging from 922 m to 4,655 m. The details on the WASP segments are provided in the WASP Appendix Annex, Table R-1.

3.2. Overall Conceptual Model

WASP considers each segment as a continually stirred tank reactor (CSTR). The concentration is uniform throughout the given segment. Figure B-2 presents the conceptual model for the GKM Model. The governing processes for each segment have advection (i.e., flow) of water into and out of each water column segment. Dissolved and suspended particles travel into and out of the water column segment via advection. In each water column segment, an individual metal can partition to the solid phase or desorb back to the aqueous phase. Because of our inability to differentiate between precipitation of metals, the formation of solid phase compounds, or sorption, we use a lump parameter to describe the relationship between dissolved and particulate metals. Particulate metals can settle to the sediment layer. In the sediment layer, particulate metals can resuspend into the water column. Dissolved metals can diffuse between the water column and pore water in the sediments. As particulates accumulate in the sediment layer, then can also be buried and lost from the system. The parameterization of these processes are detailed in the following sections.

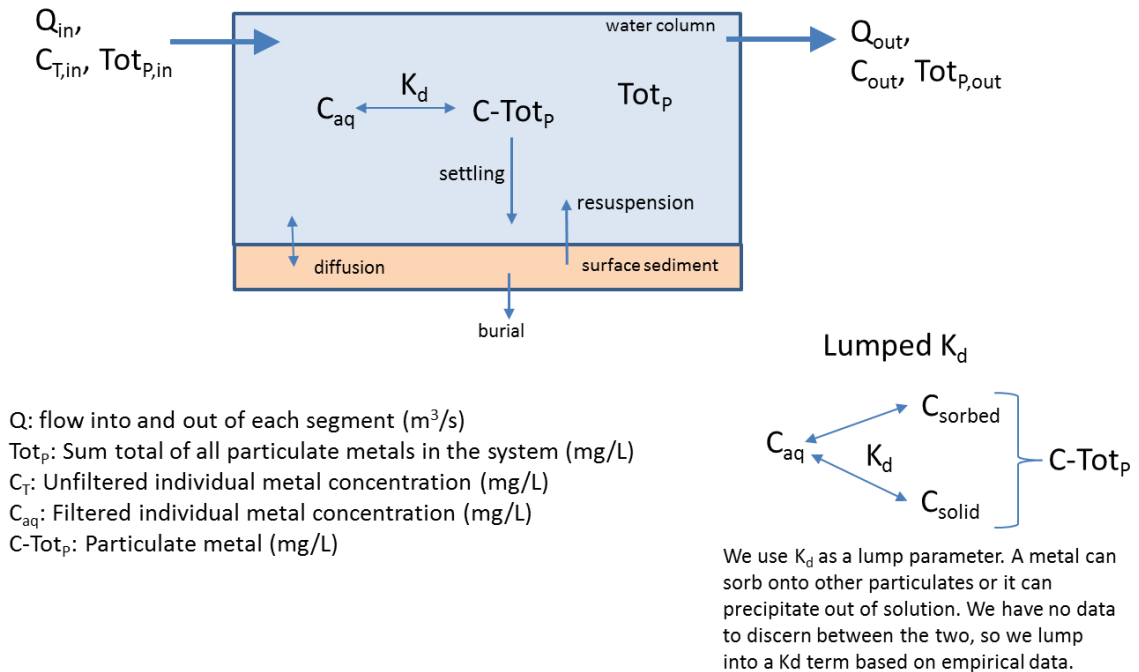


Figure B-2 Gold King Mine Conceptual Model

3.3. Model Parameterization and Calibration

The construction of the GKM model required the use of many parameters. These parameters came from different sources, including Geographic Information System (GIS) layers for the development of the model domain. Throughout the construction of the model, we use the word “parameterize” when we determine and use a specific value or set of values for a given parameter. We use the word “calibrate” when we manually adjust the value for a parameter to adjust simulated output to match observed values. We specifically calibrate the GKM model for velocity. We parameterize the model for settling velocity and partitioning by using empirically estimated data using regression relationships. Table B-1 presents the different types of data used, the type of variables associated with those data types, and the sources for those data.

Table B-1. WASP Variables and Their Sources

Input	Variables	Source
Stream Description	Segment Length, Width, Depth, Volume, Slope	BASINS, NHDPlus
Hydraulic Geometry	Velocity Exponent, Depth Exponent	USGS Gage Cross-section, Regression
Bottom Roughness	Manning’s Roughness	Calibrated
Flow, Snow Melt Conditions	Daily Streamflow	USGS Gages
GKM Release Load	Cement Creek Boundary Concentration	Empirical Data
Settling Rates	Settling Velocity	Empirical Data
Partition Coefficients	Partition coefficients	Empirical Data

3.3.1. Flow

The first part of model parameterization is establishing flow hydrodynamics. WASP is a modeling framework where the user defines the connectivity between segments as part of the input file. The connection between the segments were defined by having flow paths throughout the system, starting from the three upstream boundaries and flowing to the end of the domain or into the next flow path: the three main flow paths are Cement Creek (from GKM to the Animas River), Animas River (upstream of Cement Creek to San Juan), and the San Juan River (Navajo Dam to Lake Powell). Observed gage data were used to provide input flows over time using daily time steps for flow at the three upstream stations. The only difference is that a 15-minute time step was used for the duration of the GKM release at Cement Creek, because the flow varied over short timeframes. We did not have information for flows coming in via tributaries along the stretch of the modeled region. We also did not have information on withdrawals from the rivers, such as for irrigation. To account for changes of flows going downstream, we used the gages along the stretch of river and added or subtracted flows at these locations. We subtracted the upstream gage from a downstream gage and added that value to that location, whether it was a positive or negative value. Upon running the simulation, we compared observed flows to simulated flows to make sure they matched. To smooth out the flows through the system, we have distributed flows coming into the model between each USGS gage along the river. Table B-2 shows USGS gages used in the model and how the incoming flows are distributed. Figure B-1 shows a spatial representation.

Table B-2. Summary Table for GKM Boundary Conditions and Streamflow Inputs. The following tables are the inputs to GKM WASP model simulated from 1/1/2011 – 12/31/2011 at USGS gage stations along system. Inputs are based on observed daily data from each gage.

USGS Site Name	USGS Site Number	WASP Boundary	Segment Number	River Distance from GKM [km]	Segment Inputs – (%)
Animas River at Silverton, CO	9358000	Yes	1	-	1-(100)
Cement Creek at Silverton, CO	9358550	Yes	2	12.7	2-(100)
Animas River Below Silverton, CO	9359020	No	5	16.0	4, 5-(50)
Animas River at TTR Above Tacoma, CO	9359500	No	21	47.5	6, 11, 13, 21-(25)
Animas River at Durango, CO	9361500	No	46	94.2	22,30, 38, 46-(25)
Animas River Near Cedar Hill, NM	9363500	No	62	128.9	47, 52, 57, 62-(25)
Animas River Below Aztec, NM	9364010	No	81	166.8	63, 69, 81-(25)
Animas River at Farmington, NM	9364500	No	92	188.4	-
San Juan River at Farmington, NM	9365000	No	122	193.5	118-(75), 122-(25)
San Juan River at Shiprock, NM	9368000	No	140	244.1	131, 140-(50)
San Juan River at Four Corners, CO	9371010	No	160	298.1	150, 160-(50)
San Juan River Near Bluff, UT	9379500	No	199	421.4	-
San Juan River Near Archuleta, NM	9355500	Yes	93	-	93-(100)

The simulated flows at each gage were compared to the observed flows at each gage. Given that the flows are effectively driven by the gages, the flows should match up closely. We present them here solely for confirmation and completeness.

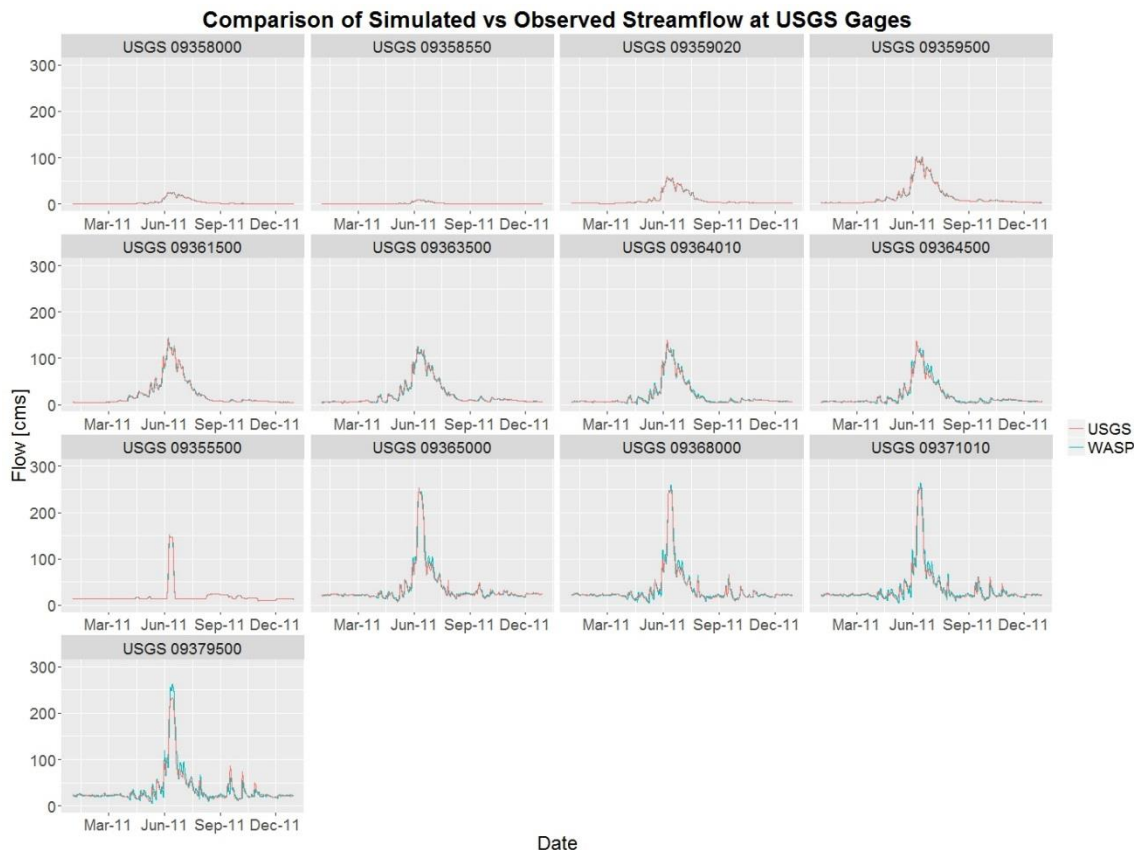


Figure B-3. Comparison of Simulated versus Observed Streamflow

3.3.2. Discharge Coefficients

EPA used WASP7’s kinematic wave formulation for hydrodynamics, which is a module within WASP7. The kinematic wave is based on the continuity and momentum equations and Manning’s equation (Leopold and Maddock, 1953). The kinematic wave formulation simulates the movement of water in a one-dimensional river network, simulating the velocity, depth, width, and flow in each river segment. The kinematic wave formulation accounts for changes in flow so that water depth increases with increased flow, thereby moving waves of water along the river network. EPA calibrated the velocity of the river by adjusting the Manning’s roughness of the bottom of the river and by adjusting the velocity exponent. The hydraulic geometry of each segment is related to flow, Q , by:

$$U = aQ^b \quad U \text{ is mean velocity, m/s (EQN B-1)}$$

$$H = cQ^f \quad H \text{ is mean depth, m (EQN B-2)}$$

$$B = kQ^m \quad B \text{ is mean width, m (EQN B-3)}$$

where $a, b, c, f, k,$ and m are empirical coefficients or exponents. By taking the logarithm of these equations, one can perform a regression to predict the values for the exponents. EPA used cross-sectional data at the USGS gages to plot velocity, depth, and width versus flow on a log-log scale (Figure B-4). The slope of the regression line for velocity and depth provide the exponents used in WASP. Table B-3 shows the regression model equations for each USGS gage. The final parameters used in the GKM Model are included in the Annex Table R-1.

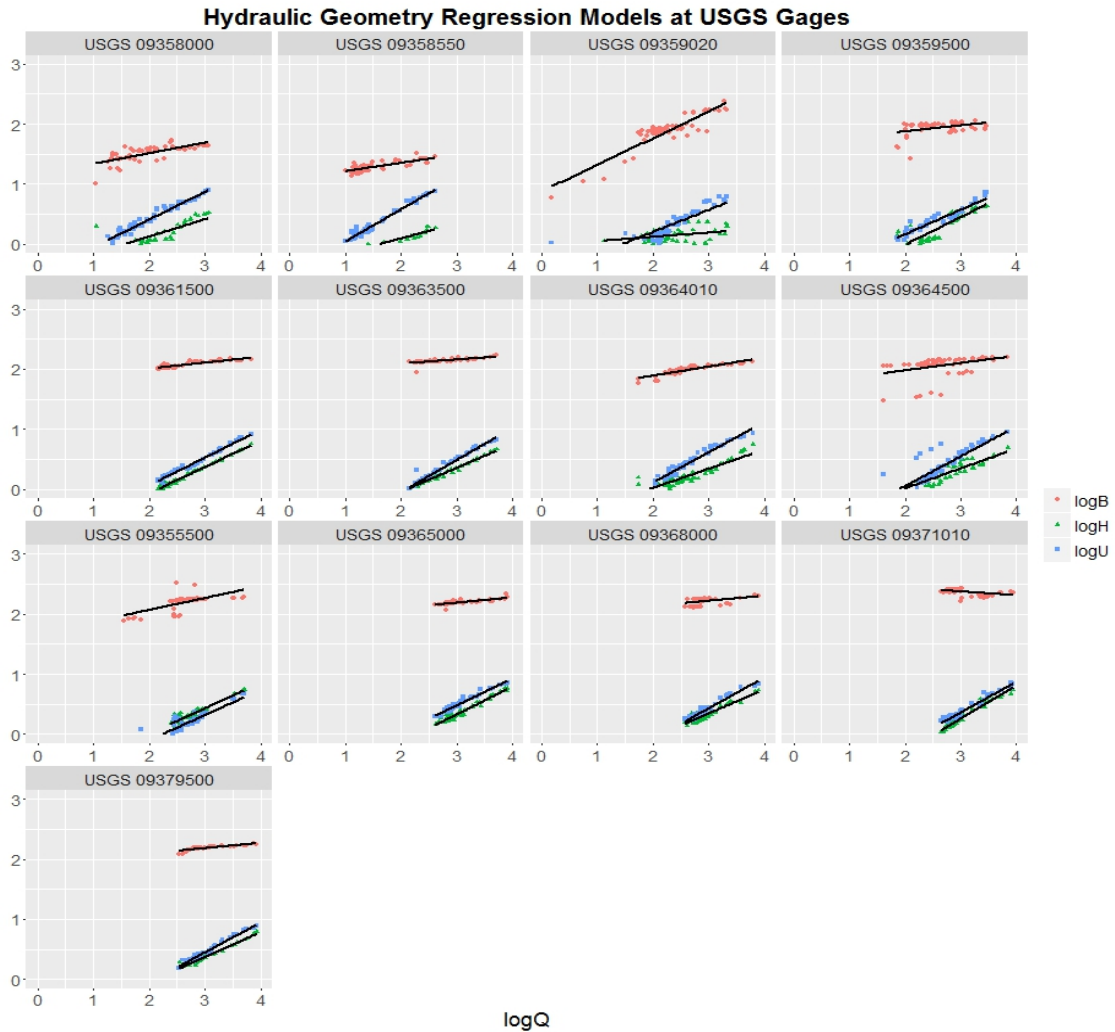


Figure B-4. Hydraulic Geometry Regression Models

Table B-3. Regression Model Equations for Hydraulic Geometry Coefficients

Station	Log B (Width)	Log H (Depth)	Log U (Velocity)
USGS 09358000	$0.178x + 1.1542$	$0.3466x - 0.6091$	$0.4755x - 0.5454$
USGS 09358550	$0.138x + 1.075$	$0.3201x - 0.5724$	$0.5416x - 0.5018$
USGS 09359020	$0.4512x + 0.8693$	$0.174x - 0.296$	$0.3748x - 0.5732$
USGS 09359500	$0.1078x + 1.6499$	$0.4844x - 0.9988$	$0.408x - 0.6517$
USGS 09361500	$0.0977x + 1.8127$	$0.4383x - 0.946$	$0.4639x - 0.8665$
USGS 09363500	$0.0652x + 1.9613$	$0.3972x - 0.8371$	$0.5379x - 1.1241$

Station	Log B (Width)	Log H (Depth)	Log U (Velocity)
USGS 09364010	$0.1589x + 1.5677$	$0.2875x - 0.538$	$0.6368x - 1.2258$
USGS 09364500	$0.1138x + 1.7462$	$0.3293x - 0.6482$	$0.5569x - 1.0981$
USGS 09355500	$0.0398x + 2.1311$	$0.4556x - 0.939$	$0.504x - 1.1904$
USGS 09365000	$0.0783x + 1.9573$	$0.462x - 1.0571$	$0.46x - 0.9009$
USGS 09368000	$0.085x + 1.9635$	$0.4025x - 0.8589$	$0.5128x - 1.1055$
USGS 09371010	$0.2473x + 1.6208$	$0.2035x - 0.3559$	$0.5507x - 1.2704$
USGS 09379500	$0.0885x + 1.9176$	$0.4141x - 0.8728$	$0.4973x - 1.0442$

3.3.3. Velocity Calibration

Simulated velocities were calibrated to USGS observed data by adjusting the Manning’s roughness coefficient, n , and the velocity exponent. Using a series of cross-sectional observations for each gage site, EPA researchers were able to adjust this value in the model to match the observed velocities within ± 0.1 of the average residual, except USGS 09355500 matched at 0.3. The year 2011 was selected as the calibration period because it was the most recent, complete set of streamflow data at every site. For this study, EPA used 11 gages with continuous observed streamflow to drive the model. The final bottom roughness values are presented in the Annex Table R-1.

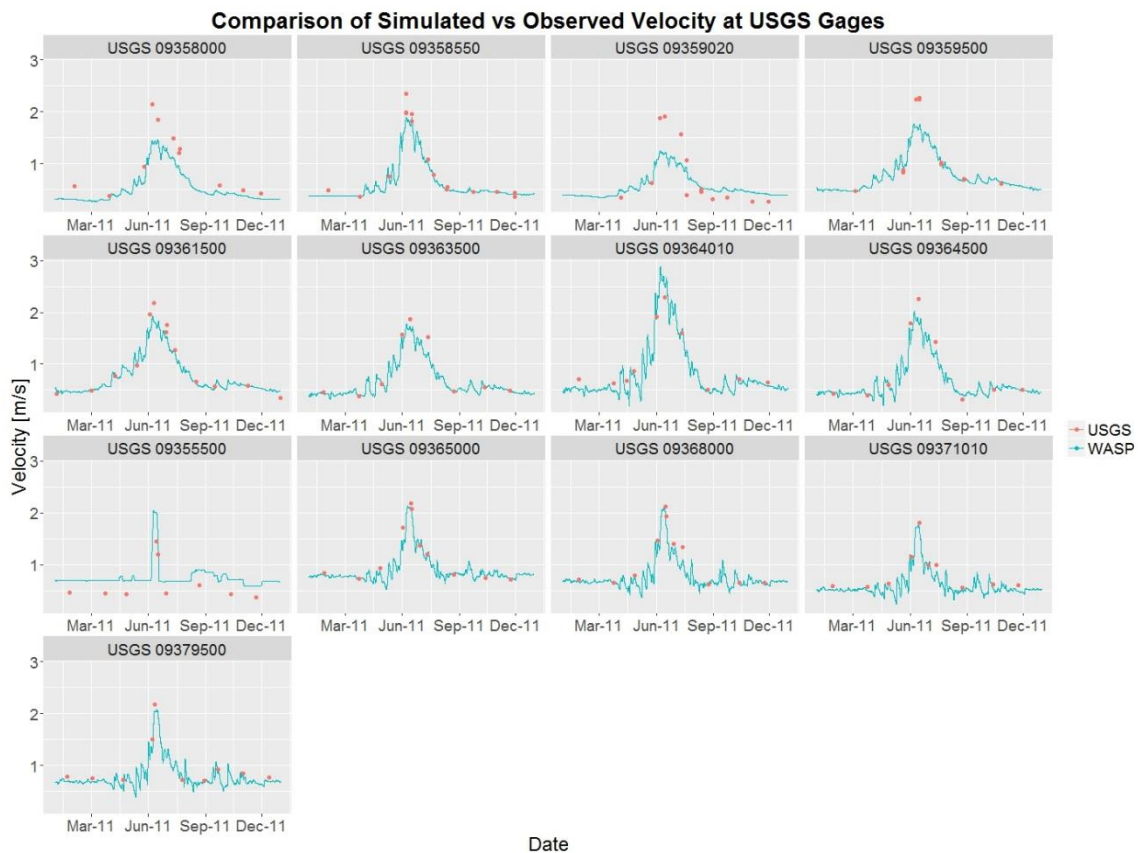


Figure B-5. Comparison of Simulated versus Observed Velocity

3.3.4. Particle Settling Rate

Particulate settling rate was calculated by using the empirically estimated total metal mass (not including Ca, K, Mg, and Na) as it traveled downstream (see Figure B-6).

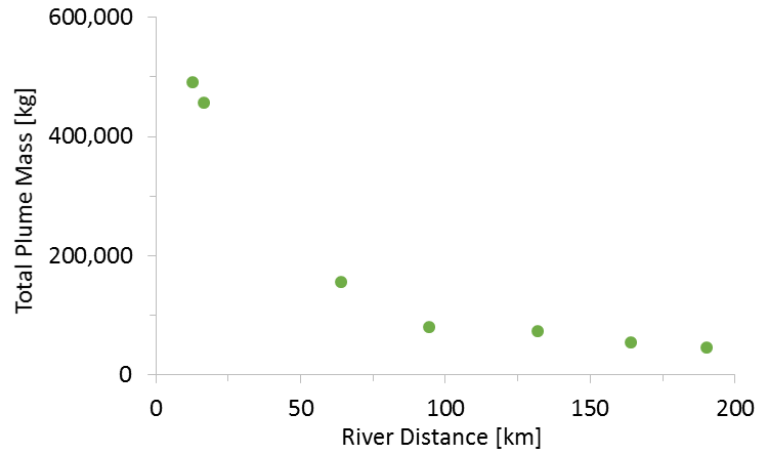


Figure B-6. Empirically-estimated Total Mass over Distance

The assumption is that the only loss process is via settling of metals. By knowing how far the plume travels and the stream velocity, the team could calculate the time of travel. Then knowing the fraction of mass lost over this time, the team could calculate the average settling velocity. After setting up the WASP model, it was first run with no settling to determine travel times and stream velocities. Using the plume travel times, the team could then use the combination of empirically estimated plume mass along with the simulated stream velocity and time of travel to estimate the settling velocity at each location. This is represented by Figure B-7 and mathematically in equations B-4 and B-5.

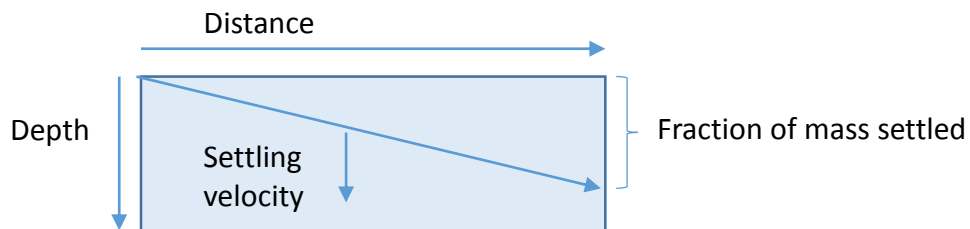


Figure B-7. Conceptual Diagram for Estimating Settling Rate

$$Time\ of\ Travel = \frac{Distance}{Stream\ Velocity} \quad (EQN\ B-4)$$

$$Settling\ Velocity = Fraction\ of\ Mass\ Settled \frac{Depth}{Travel\ Time} \quad (EQN\ B-5)$$

The estimated settling velocities for different distances along with their effective particle size are presented in Table B-4.

Table B-4. Empirically estimated Total Mass at Different Locations used to Estimate Settling Velocity. Losses in total mass at sample sites along the GKM release are used along with WASP segment stream velocity and average depth to calculate average settling velocities.

Location	River Distance [km]	Total Mass - Cations [kg]	Mass Fraction Dropped	Avg Depth [m]	Stream Velocity [m/s]	Time to Travel [s]	Settling Velocity [m/d]	Particle Diameter Size [mm]
Cement Creek	12.5	490,404	-	-	-	-	-	-
Animas at Silverton	16.4	457,124	0.07	2.1	0.59	6,585	1.85	0.0048
Animas at Baker's Bridge	64	155,396	0.66	2.8	0.88	54,087	2.97	0.0061
Animas at Durango	94.2	79,760	0.49	3.5	0.44	68,621	2.12	0.0051
NAR6	132	72,828	0.09	2.5	0.78	48,630	0.38	0.0022
Animas at Aztec	164.1	54,657	0.25	2.4	0.86	37,526	1.40	0.0042
Animas at Farmington	190.2	45,360	0.17	2.6	0.85	30,545	1.26	0.0040

Settling velocities for each WASP segment are presented in Annex Table R-2. Given that it is unclear when the change in settling velocity happened moving downstream, the assumption is that the settling velocity was centered around the location for which it was calculated (e.g., at 12.5 km, 16.4 km, 64 km). For a sensitivity analysis, the team did one run with the settling velocity changing immediately right after a location, and another run with settling velocity staying the same until it reached a known location.

3.3.5. Partitioning

A lumped parameter is used to account for the distribution between dissolved metals and total metals. There was no information on metal speciation, which would be required to add additional detail on this process. The only data available were total metals and dissolved metals. The processes governing the distribution between phases was unclear (i.e., whether non-dissolved metals were metal precipitates or metals sorbed to the other particulate metals in the system). To account for this an effective partition coefficient, K_d , was applied. Because the system was changing as the plume traveled downstream, the estimated K_d is incorporated as a function of distance. The assumption was that K_d changed as it traveled down the Animas River. Once the plume reached the San Juan River, the assumption applied was that the K_d had reached its final value. The K_d was then held constant along the San Juan River (after $x = 200$ km). The K_d is defined as

$$K_d = \frac{Me_T / Tot_T}{Me_{diss}} \quad (\text{EQN B-6})$$

Where Me_T is the total concentration (unfiltered) of the metal (mg/L), Tot_T is the total concentration of all other metals (kg/L), and Me_{diss} is the dissolved (filtered) concentration of the metal (mg/L). This was used for all metals of interest.

A regression was used to develop a relationship for K_d versus distance.

The values used to estimate K_d are presented in Table B-5. The regressions are presented in Figure B-8. The incorporation of partition coefficients into WASP per segment are presented in the Annex, Table R-9.

Table B-5. Empirically estimated Metal Concentrations at Different Distances

River Km	Total [mg/L]					Dissolved [mg/L]			
	Total Metals [mg/L]	As	Cu	Pb	Zn	As	Cu	Pb	Zn
12.5	39683.0	29.052	129.551	631.870	155.320	0.297	70.827	0.955	172.200
16.4	11582.9	8.475	37.538	182.836	45.937	0.004	6.755	0.243	19.259
64	521.0	0.338	1.474	7.204	3.088	0.001	0.221	0.002	1.989
94.2	217.8	0.137	0.652	2.915	1.451	0.001	0.009	0.000	0.275
132	103.1	0.061	0.265	1.298	0.739	0.000	0.002	0.003	0.011
164.1	63.6	0.037	0.161	0.788	0.487	0.001	0.002	0.000	0.004
190.2	44.9	0.026	0.112	0.632	0.359	0.001	0.003	0.000	0.004

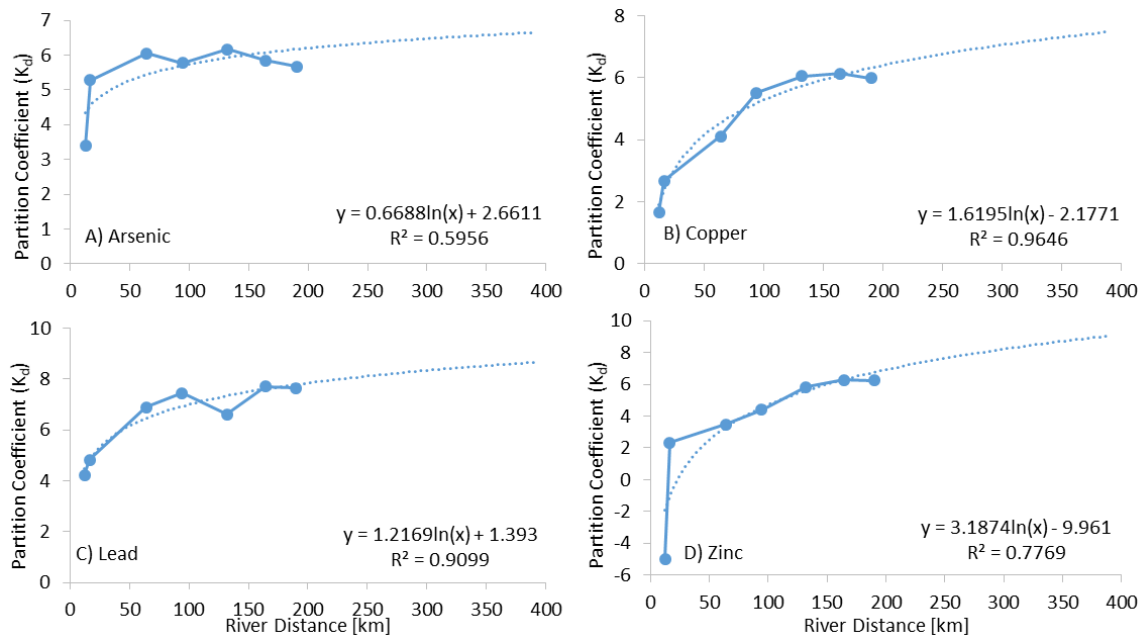


Figure B-8. Partition coefficient regressions for arsenic, copper, lead, and zinc

3.3.6. Dispersion

Mechanical dispersion was included into the model to account for interactions between the water column and surface benthic layers. A dispersion coefficient of 1×10^{-4} was used for every segment pair in the model. Figure B-9 shows the conceptual diagram for dispersion. Based on Fick's First Law, the exchange is calculated using the formula:

$$E = -\frac{E_{12} \times A_{12}}{L_{12}} (C_2 - C_1)$$

Where

- A_{12} = area of segment
- $C_{1,2}$ = midpoint of segment depth
- L_{12} = distance between midpoint
- E_{12} = Dispersion coefficient

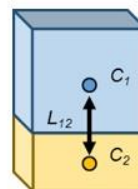


Figure B-9. Conceptual Diagram for Estimating Dispersion

The values used in the GKM Model are presented in the Annex, Table R-3.

3.3.7. Resuspension

Resuspension is simulated in WASP as a constant velocity, using a value of 0.00001 m/d for all segments. The way that resuspension is structured, the resuspension velocity is a constant independent of the velocity of the river above the sediment layer. Therefore, the movement of mass from the sediment layer (i.e., mass per time) is defined as the resuspension velocity (i.e., length per time) multiplied by the concentration in the sediment (i.e., mass per volume) multiplied by the cross-sectional area of the sediment layer segment interfacing the water column segment (i.e., area). Therefore, as the velocity of the stream increases, the water column concentration would decrease as the mass flux remains constant.

4. Simulation Scenarios

Once the GKM model was constructed, a series of simulations were performed to answer different questions. These simulations used the same underlying GKM model, with some adjustments depending on the type of simulation running and the questions of interest. The boundary concentrations, initial conditions, time period, and flow regime all depended on the simulation and are presented in the specific simulation scenario.

4.1. Plume Movement Scenario

In this scenario, the entire movement of plume was simulated. The goal of this scenario was to estimate how long it took for the plume to reach specific locations and how long the plume lasted there. This scenario simulated total metals without the four major cations (i.e., Ca, K, Mg, and Na).

The processes incorporated in the system include advection with the flow of the water, vertical dispersion, and settling and resuspension of the metals. There were two simulations performed using two different boundary conditions at the San Juan River upstream boundary. The first case was a simulation with only the Gold King Mine release into Cement Creek. This simulation was designed to investigate solely the change in total metals concentration in the Animas and San Juan Rivers. The second case used a boundary concentration at the San Juan River, using observed data to represent the background conditions. This case was designed to simulate the concentrations of metals from the release combined with the background

concentrations. Because of the total metal concentrations, this case provided a better simulation to compare with observed concentrations in the San Juan River. Details on the Plume Movement Scenario are presented in Table B- 6.

Table B- 6. Plume Movement Scenario

Initial Conditions	Zero concentration everywhere: sediments, water
Boundary Conditions	1) Incoming flow of total metals based on empirical estimates at Cement Creek boundary 2) San Juan background concentrations based on observations at San Juan River upstream boundary
Time Period	March 16, 2015 to Nov 16, 2015
Flow Regime	March 16, 2015 to Nov 16, 2015 (See Annex, Table R-5)

4.2. Total and Dissolved Individual Metals Scenario

This scenario was designed to simulate the movement of each individual metal along with the total metals in the system. In this scenario, there were four simulations, one for each metal. The goal of this scenario was to see how the total and dissolved concentrations of each metal changed over time and over the length of the river domain. The use of WASP in this context provides exposure concentrations for the duration of the plume throughout the length of the model domain. Details on this scenario are presented in Table B-7.

Table B-7. Total and Dissolved Individual Metals (As, Cu, Pb, Zn)

Initial Conditions	Zero concentration everywhere: sediments, water
Boundary Conditions	Incoming concentration at Cement Creek boundary: total metals, total individual metals based on empirical estimates
Time Period	March 16, 2015 to Nov 16, 2015
Flow Regime	March 16, 2015 to Nov 16, 2015 (See Annex, Table R-5)

4.3. Year Following Gold King Mine Release

This scenario investigated the conditions after the plume had passed and what the long-term effects would be in the Animas and San Juan Rivers. To that end, the simulation was for a hypothetical year following the release at the Gold King Mine. This scenario simulated November 16, 2015 to December 31, 2016 by using the final concentrations in the sediment from the GKM Model Plume simulation as the initial conditions for this scenario. The model used flow data from 2010 to 2011 flow data, because it is the last complete hydrologic record available. This year was a typical year, with high flow periods during snowmelt and lower flow during the other months. The goal of this work was to see how the high flows and low flows would affect sediment and water column concentrations over time. This work also presents the total and individual sediment concentrations after the plume has passed and for the year after. Details on this scenario are presented in Table B-8.

Table B-8. Year Following Gold King Mine Release

Initial Conditions	Metal concentrations in the sediments based on the final day of the plume simulations: Nov 16, 2015.
Boundary Conditions	Boundary conditions set to zero
Time Period	Nov 16, 2015 to Dec 31, 2016
Flow Regime	Nov 16, 2010 to Dec 31, 2011 (See Annex, Table R-6)

5. Scenario Results

5.1. Plume Movement

WASP was run to simulate total metal concentrations as it traversed the system. The total metal concentrations for the entirety of the plume are presented in Figure B-10, which presents the concentration for a given river distance over time. The plume is seen to have high concentrations immediately (i.e., at 12.7 km). The concentration drops and spreads as it moves downstream. The effect of numerical dispersion and drag forces is evidenced in that the plume takes longer and longer to pass a given location. The shape of the plume is not quite a normal curve, as the leading edge rises quicker (Figure B-10, the left side of the curve) than the tail (Figure B-10, the right side of the curve), which takes longer to recede.

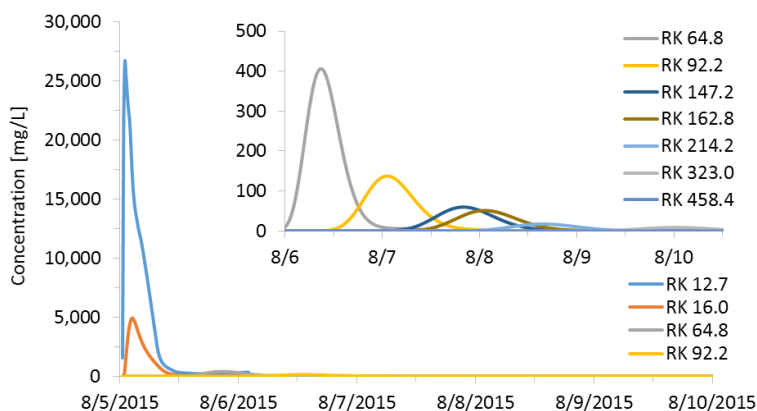


Figure B-10. Total metal concentrations over time for specific river distances.

As the plume travels downstream, the peak concentration decreases appreciably. This is due mostly by dilution. Settling and dispersion further decrease the peak concentration. Figure B-11 plots the peak concentration relative to the source as a percentage to demonstrate this change over distance.

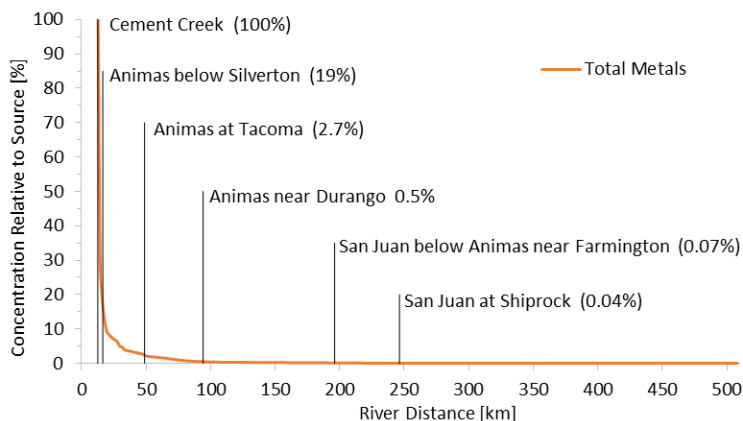


Figure B-11. Decrease in peak concentration as the plume travels downstream

Peak total metal concentrations decreased traveling downstream. Figure B-12 shows the simulated peak total metal concentrations plus observed concentrations. The two lines represent two different cases, one with no metals coming in from San Juan and the other with background metals concentrations in the San Juan, based on observations. The observed data show peak total metal concentrations from the empirical analysis (A) and observed data as the plume passed from August 5 to 11, 2015 (B). As shown in the observed data (B), it was difficult to precisely capture the plume peak concentration with the observed results. The WASP modeling helps fill in the spaces between observations with simulated data. The WASP simulation adds in understanding the shape of the curve and does well at capturing the decreasing peak and observed data over the length of the Animas River. Once the San Juan River is reached, the observed concentrations and empirical analysis predicted peak concentrations jump in concentration. This is due to the high concentrations coming in from the San Juan River (i.e., background, upstream concentrations). This jump cannot be caused by the Gold King Mine release. It is therefore difficult for the empirical analysis to distinguish the Gold King Mine concentrations from the background concentrations.

The observed concentrations (B) are higher than the empirically based concentrations (A). The WASP simulation helps in sorting out the peak concentrations that would be caused by the Gold King Mine release from the observed concentrations. In (A) the empirically estimated peak concentrations fall between the two lines. In (B) the observed concentrations are right up against the top line with San Juan background. WASP helps to elucidate the decreasing concentrations of the Gold King Mine and how it falls in line with the background concentrations.

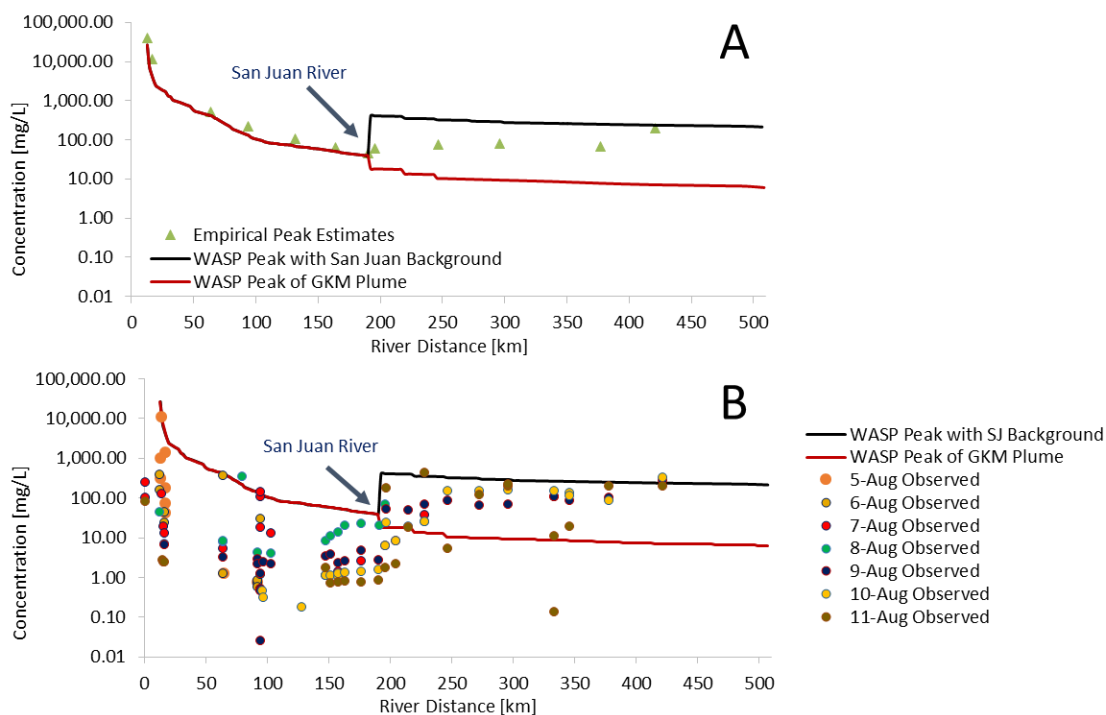


Figure B-12. Simulated Peak concentrations of total metals. The boundary condition at the San Juan was simulated with no metals (lower, red line) and background particulate metals (upper, black line). A) empirical analysis estimated peak concentrations. B) observed concentrations from August 5 to 11, 2015.

5.2. Total and Dissolved Individual Metals Scenario

Total concentration and dissolved concentration of four individual metals (i.e., arsenic, copper, lead, and zinc) were simulated for the Gold King Mine. The simulated peak concentrations are presented in Figure B-13. Along with the WASP simulated results, the empirically calculated peak concentrations are presented. The WASP simulated total metals and empirically estimated peak concentrations match up quite well. For the metals simulated, the total peak concentrations drop rapidly in the upstream section after the plume enters the Animas River. Concentrations drop less quickly over the remainder of the Animas. Upon reaching the San Juan River, the concentrations remain relatively steady, with a slow decline. The dissolved concentrations are different for the metals. Arsenic and lead drop quickly and the ratio of dissolved to total is small, showing that much of the arsenic and lead are present in particulate/colloidal form early on. This matches with their relationship to pH, where arsenic and lead would be the first metals to form solids. Zinc and copper are almost completely dissolved in the upstream reaches of the Animas River. The dissolved and total concentrations are almost the same, suggesting that there is a low concentration of particulate/colloidal zinc and copper. Going downstream, the pH starts to increase, resulting in a change from dissolved to particulate/colloidal form. As the dissolved line separates from the total line, more and more particulate/colloidal is formed. For copper, this starts happening quickly. For zinc, the dissolved and total line stay together until approximately 50km downstream. Then the zinc dissolved line moves farther from the total line, suggesting that more particulate is formed. The formation of particulate is important, since it is the particulate form that will settle to the streambed. The dissolved form will advect downstream. This would suggest that zinc would not settle to the streambed until farther downstream, while arsenic and lead will start settling immediately.

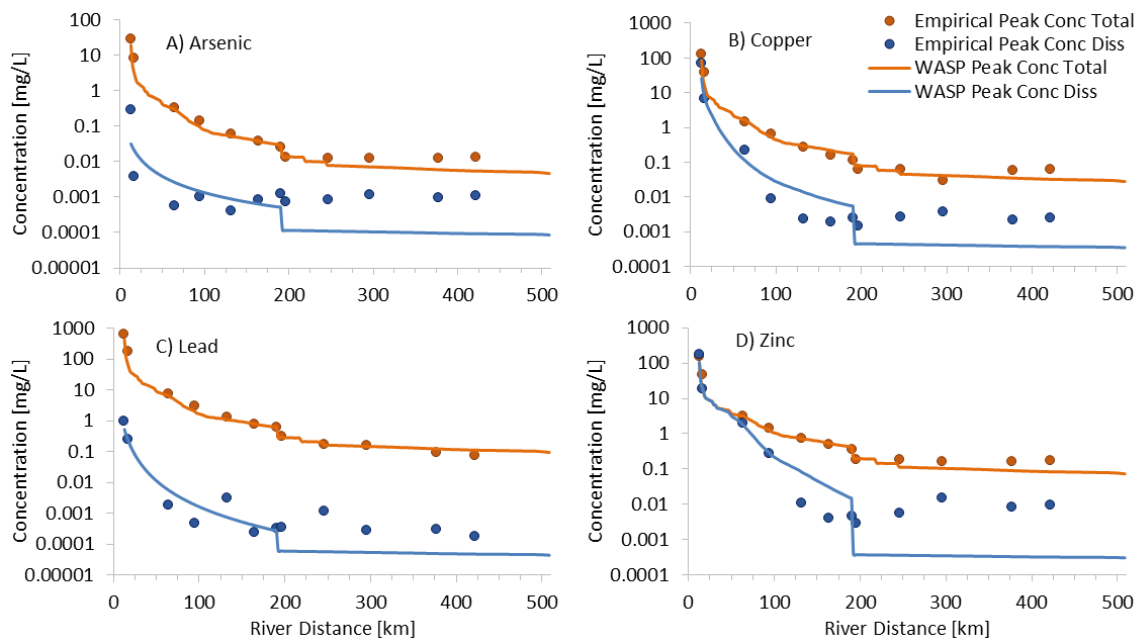


Figure B-13. Total and Dissolved Simulated and Observed Peak Concentrations for Four Select Metals. Concentrations of (A) arsenic, (B) copper, (C) lead, and (D) zinc are plotted on a log scale. Both peak total (unfiltered) concentrations and dissolved (filtered) concentrations are plotted on a log-scale. Empirically estimated peak concentrations are plotted for both as well.

5.3. Year Following Gold King Mine Release

Figure B-14 shows the concentrations in the water column and the sediment for the year following the Gold King Mine release. The sediment concentrations did not noticeably change over the course of the year. The water column concentrations were higher during the low flow period than the high flow period. This is due to the construct of the WASP model, where flux back to the water column is defined as a steady rate, independent of flow. Therefore, when there is less water over the sediment, the water column concentration is higher. The sediments show zones of higher deposition versus lower. Zones where there is a drop in sediment concentration suggests that less metals settled there. The steady decrease over distance shows that, generally, the impact of the release on the sediments decreased traveling downstream.

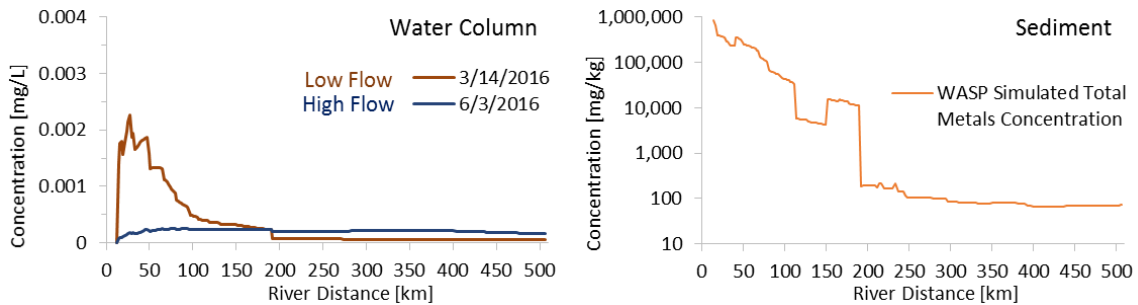


Figure B-14. Total metal concentrations in the water column and the sediment the year following the Gold King Mine release.

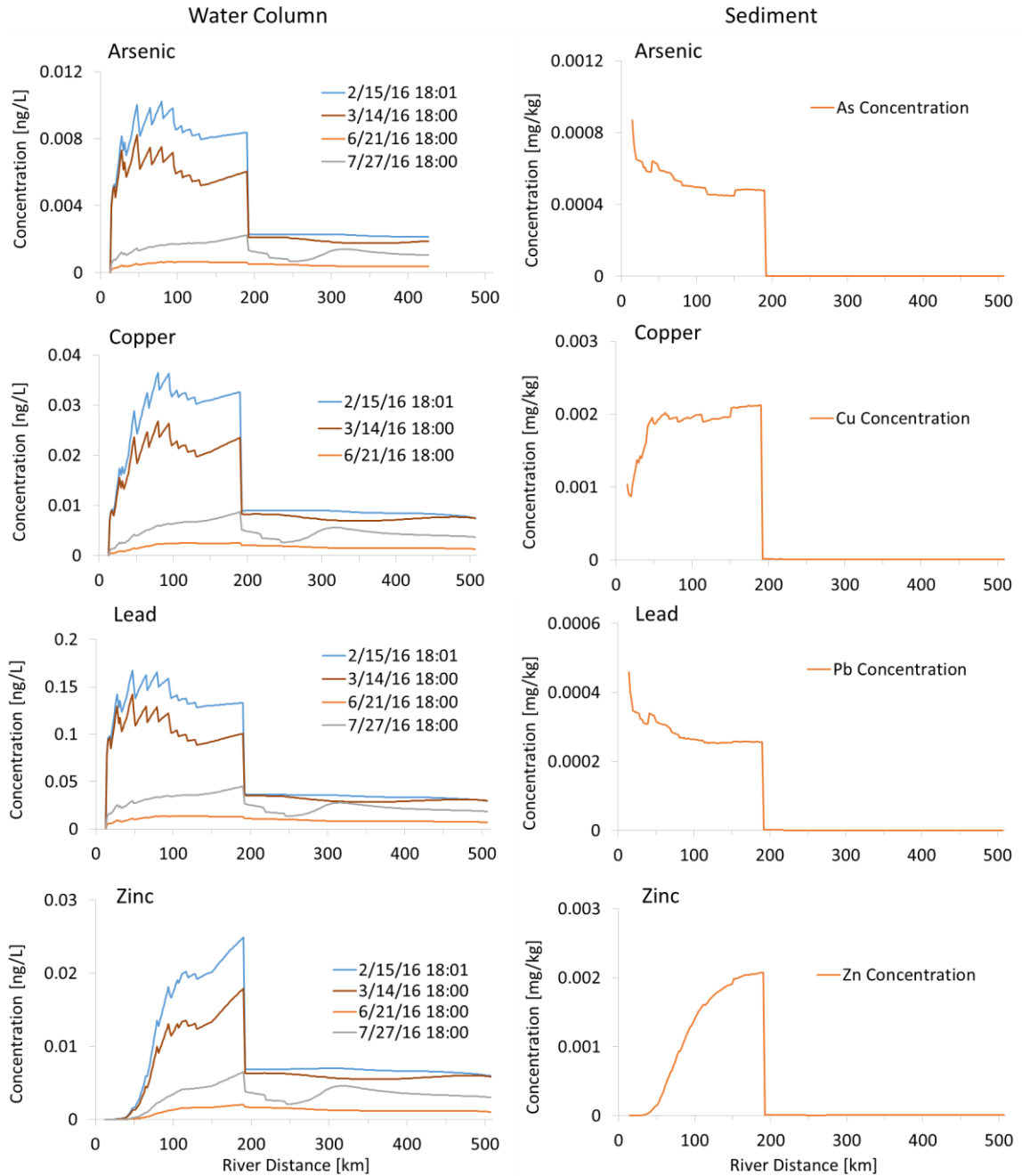


Figure B-15. Individual metals in water column and sediments. Water Columns for different times and flows.

Figure B-15 shows the following year after the Gold King Mine simulated results for individual metals (i.e., arsenic, copper, lead, zinc) in the water column and the sediment. As would be expected from the surface water simulations during the release, arsenic and lead are seen to fall to sediment early and in large amounts, due to their forming particulate/colloids immediately. The sediment concentrations decrease moving downstream. Copper follows a different pattern, as it is dissolved far upstream. It, however, becomes particulate/colloidal and the settles to the sediment layer rather uniformly as it traverses the

Animas River. Zinc stays dissolved longer, and starts to settle slower. The effect is that zinc concentrations in the sediment are simulated to increase as it travels down the Animas River.

The accumulation in the sediments is reflected in the water column results. Again, lower flows result in higher concentrations. What is different about the water column, however, is when a metal is resuspended in the water column, it then travels downstream, so concentrations may increase moving downstream, even though concentrations in the sediment below may decrease. So, arsenic, copper, and most of lead are seen to increase in water column concentration as one goes downstream. This is particularly seen in the San Juan River. Metals move from the sediments to the water column, then when the Animas River enters the San Juan, there is the dilution of mixing, but the simulated concentrations stay non-zero, and is effectively transported down the San Juan River.

6. Numerical Dispersion

Numerical dispersion is a phenomenon that occurs when solving differential equations using numerical methods. The effect is caused by having the assumption that a segment is a well-mixed container and using time steps and/or segment lengths that do not follow exactly the characteristic equation. WASP is designed to have adjusting time steps to reduce numerical instability. The time step is chosen based on the smallest segment and the velocity in that segment. The simulated hydrodynamics therefore controls the time step. Rivers and streams typically have longitudinal dispersion, due to hydrologic and morphologic properties that affect mixing processes. For large rivers, these values typically range between 10^4 and 10^6 cm^2/s (Schnoor, 1996).

6.1. Numerical Dispersion in WASP

To investigate how much numerical dispersion was being introduced, the EPA team calculated how much the plume was spreading, by using the simulated width of the plume for different times. The width of the plume (99.7% of the plume mass) spreads as $2 \cdot (2Dt)^{0.5}$ (Domenico and Schwartz, 1990), where D is dispersion [cm^2/s] and t is time [s]. Through rearrangement, one can calculate the effective dispersion, which is what WASP is introducing. Using two points, at 0.52 days, the plume spread 13.7 km, and at 2.48 days, the plume spread 76.5 km, resulting in D of 5.8×10^5 and 3.8×10^6 cm^2/s , respectively. These values are on the higher side of the range of typical river values but reasonable. This suggests that WASP is introducing numerical dispersion that one might expect to find in typical rivers. The presence of the advective front in the Gold King Mine, then, may be due to a mechanism that the WASP model is not incorporating. This may feasibly be due to the nature of the effective chemical reactor, with the solute front, followed by the acid peak (pH drop), followed by the trailing suspended particulates. It is also possible that the observations have some error, and those data are not fully capturing the full dispersion of the plume in the system.

6.2. Time Step Sensitivity

One of the factors governing numerical dispersion is the time step. The EPA team investigated increasing the minimum time step that WASP was allowed to take. For the model simulations in this report, the minimum time step was 0.0001 days. For this sensitivity, three minimum time steps were used: 0.005, 0.008, and 0.004 days. Any minimum time steps larger than 0.004 days resulted in WASP crashing (i.e., became numerically unstable). Results are presented in Figure B-16. As can be seen in the plume concentrations, the expected effect was observed. As time step was decreased, the peak concentration increased for a given snapshot in time resulted. The width of the plume becomes smaller by restricting the time step.

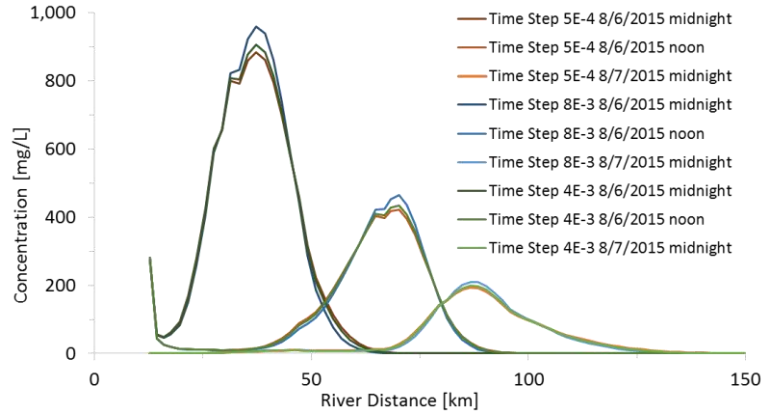


Figure B-16. Plume concentrations versus distance for different times using different time steps.

6.3. Negative Dispersion

One method of addressing numerical dispersion in numerical modeling techniques is by introducing negative dispersion. This is typically applied when there is a strong advective front, which numerically will generally be dispersed, since it is mathematically difficult to maintain such a strong advective front. Here, the model was run using an applied longitudinal dispersion of $-0.016 \text{ m}^2/\text{s}$ ($-160 \text{ m}^2/\text{s}$). The effect of introducing negative dispersion is that any concentration gradient will reverse the direction of dispersion (i.e., effectively trying to pull the concentration towards the center rather than diffusing outwards). This was the highest negative dispersion that could be used in the model without it crashing. The effect was as expected: the plume peak concentration was increased and the width was decreased. It still was unable to fully capture the sharpness of the sonde data. However, it should also be noted that Sonde data is for specific conductivity, which represents dissolved ionic species. The WASP plume captures both dissolved and suspended particulate data. Results are presented in Figure B-17.

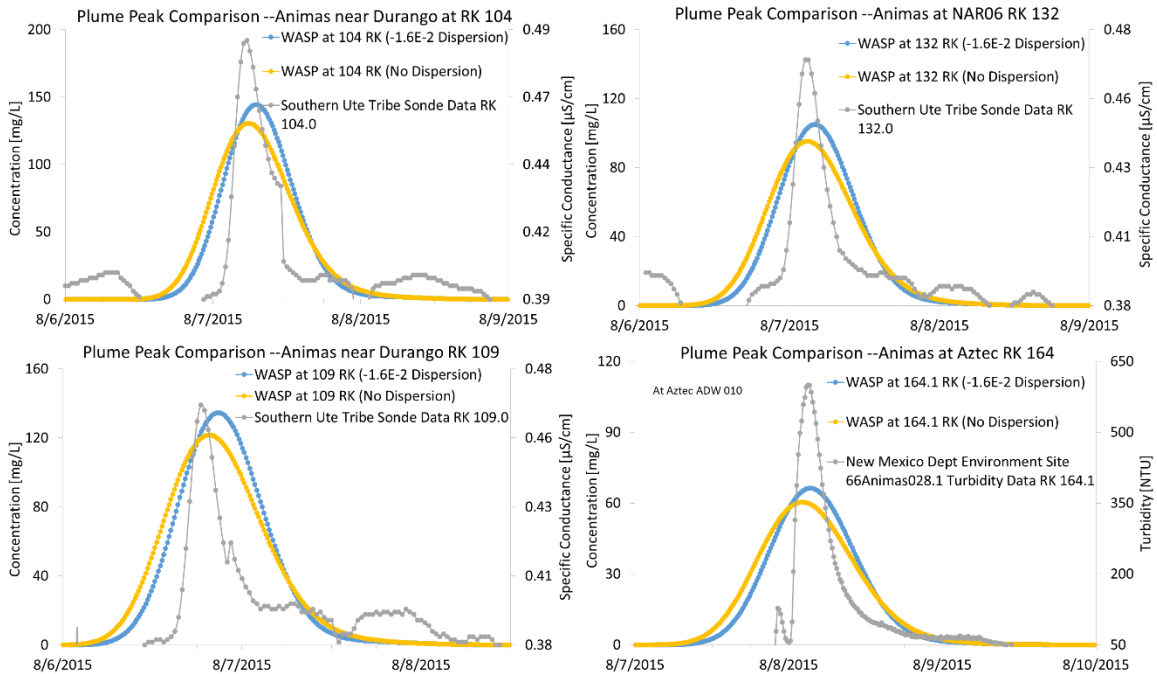


Figure B-17. Comparison of original WASP output, introduction of negative dispersion, and observed data at four locations.

7. Settling Velocity Sensitivity

It is uncertain how the estimated settling velocity changed as it moved downstream. The model in this study used a centered approach, having the settling velocity change half-way between locations where the plume mass was empirically estimated. To investigate sensitivity of the results, two different schemes were used for implementing the estimated settling velocities: an upper bound (i.e., the settling velocity changes to next value immediately after a given location) and a lower bound (i.e., the settling velocity changes at the next location and remains constant until right before the next location). This resulted in some variability in upper reaches of the Animas River as demonstrated in Figure B-17.

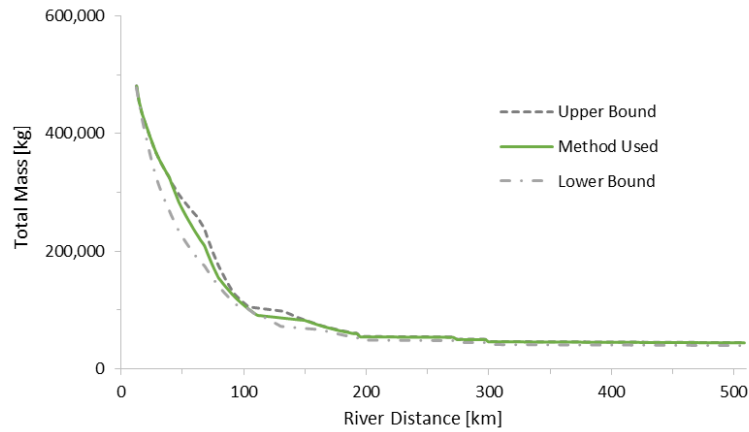


Figure B-18. GKM Model simulated total mass of plume for every segment, including sensitivity of the implementation of settling velocity.

8. References

- Ambrose, R. B., Wool, T. A., Connolly, J. P., Schanz, R. W. (1988). WASP. 4, A hydrodynamic and water quality model, Rep. No. EPA/600/3-87/03. 9, USEPA, Athens, GA.
- Connolly, J. P., Winfield, R. P. (1984). A user's guide for WASTOX, a framework for modeling the fate of toxic chemicals in aquatic environments. Environmental Research Laboratory, Office of Research and Development, US Environmental Protection Agency.
- DiToro, D. M., Fitzpatrick, J. J., Thomann, R. V. (1983). Water quality analysis simulation program (WASP) and model verification program (MVP)-documentation. US Environmental Protection Agency, Duluth, MN. EPA-600/3-81-004.
- Domenico, P.A., Schwartz, F.W. 1990. Physical and Chemical Hydrogeology. J Wiley & Sons. New York.
- Knights, C. D. 2010. Modeling Mercury Transport and Transformation along the Sudbury River, with Implications for Regulatory Action. Volume 1. Mercury Fate and Transport. U.S. Environmental Protection Agency. Office of Research and Development. National Exposure Research Laboratory. Ecosystems Research Division. Athens, GA
- Knights, C. D. 2010. Modeling Mercury Transport and Transformation along the Sudbury River, with Implications for Regulatory Action. Volume 2. Evaluating the Effectiveness of Different Remedial Alternatives to Reduce Mercury Concentrations in Fish. U.S. Environmental Protection Agency. Office of Research and Development. National Exposure Research Laboratory. Ecosystems Research Division. Athens, GA.
- Leopold, Luna B and Maddock, Thomas, Jr. 1953. The Hydraulic Geometry of Stream Channels and Some Physiographic Implications. Geological Survey Professional Paper 252. United States Government Printing Office, Washington.
- National Research Council. 2007. Models in Environmental Regulatory Decision Making. National Academies Press, Washington, DC.
- Schnoor, J.L. 1996. Environmental Modeling: Fate and Transport of Pollutants in Water, Air, and Soil. J Wiley & Sons. New York.
- U.S. Environmental Protection Agency. 2001. Total maximum daily load (TMDL) for total mercury in fish tissue residue in the middle and lower Savannah River watershed. Region 4, Athens, GA.
- U.S. Environmental Protection Agency. 2004. Total maximum daily load (TMDL) development for total mercury in fish tissue residue in the Canoochee River (Canoochee Watershed). Region 4, Athens, GA.
- Wang, P. F., Martin, J., & Morrison, G. (1999). Water quality and eutrophication in Tampa Bay, Florida. Estuarine, Coastal and Shelf Science, 49(1), 1-20.

Appendix C.

**Geochemical Considerations
Regarding the Gold King Mine Release**

Contents

Abstract.....	3
Background.....	4
Summary of sampling and analyses used in this report.....	10
Characterization of the release volume and chemistry	11
Assessment of the fate of solutes in the release waters as they enter the Animas River	16
Analytical considerations.....	33
References.....	34

Abstract

On August 5, 2015, starting at ~11:00 a.m., a dammed drift entry to the Gold King Mine (GKM), near Silverton, CO, was breached, releasing a minepool of acidic mine drainage (AMD) estimated to be roughly 11.4 million liters. Using sample data, estimated release volume and very conservative assumptions, the dominant solutes in the release waters that migrated to the Animas River were SO_4^- (≤ 138000 kg), Ca (≤ 31100 kg), Al (≤ 6550 kg), and Fe (≤ 3530 kg). Acidity load was calculated to be ≤ 54000 kg CaCO_3 . The higher loadings for trace elements included Zn (1790 kg) and Cu (730 kg), with other trace elements present at lower loadings Co (14 kg), Pb (12 kg), Cd (7.2 kg) and Ni (6.2 kg).

These release waters cascaded downslope to Cement Creek, entraining and suspending large quantities of spoil, soil and sediments. Based on the data available, e.g., apparent increases in Al and Ca, substantial amounts of soluble salt solids and minerals likely were suspended and partially dissolved in the turbulent flow of the waters as they cascaded to Cement Creek or perhaps flooded stream valleys to suspend overbank sediments. Depending on the mineralogy, dissolution of these salts likely would have affected pH as quickly as the salts dissolved.

The Cement Creek watershed is mapped as containing roughly 100 mines, with four mines alone reported to have been discharging 2,300 to 3,000 liters/minute (L/m) of untreated AMD. Consequently, Cement Creek is severely degraded, having low pHs and high metals content. Given the low pHs typical of Cement Creek, few chemical changes likely occurred in the release waters during the short residence time in Cement Creek, mainly ranging from 2 to 17 hrs.

Both upstream and downstream of Cement Creek, the Animas River is buffered at moderately alkaline pHs by bedrock including carbonate and chlorite minerals. When the acidic release waters flowed from Cement Creek into the Animas, starting at ~1:00 p.m.: i) pH in the mixing waters increased quickly, dramatically accelerating the rate of Fe oxidation; ii) major AMD solutes, including Fe, Al, and Mn, quickly precipitated as incipient oxide solids and minerals, perhaps including transitory mineral phases; iii) freshly precipitated and/or suspended soluble salt mineral phases, that had been near equilibrium with solutes, dissolved, and reprecipitated as oxides in the case of Al and Fe; and iv) trace metals would have sorbed and/or entered solid solution with the Al and Fe oxides.

Based on hydrograph data in Cement Creek near the confluence with the Animas, effectively all of the release waters flowed into the Animas over a 17.25-hour period. For flow rates and alkalinities likely present in the Animas at the time of the release, the calculated acidity load could have been neutralized by roughly two days of Animas flow at most, and probably less. Calculations for calcite saturation suggest that the release acidity was effectively neutralized by about 150 km downstream from GKM in the Animas River.

Neutralization of the GKM acidity generated colloidal solids as reaction products including amorphous and short-range-ordered $\text{Fe}(\text{OH})_3$, $\text{Al}(\text{OH})_3$ and Mn oxyhydroxides, resulting in yellow coloration in the Animas River. These colloids scavenged the dissolved trace metals in the release waters. Data for lower Animas River show that dissolved metal concentrations were low, $\mu\text{g/L}$ levels and less. Calculations of sorption equilibration of these trace metals, including Zn, Cu and Pb, on $\text{Fe}(\text{OH})_3$ surfaces yield modeled concentrations that are consistent with observation, supporting that partitioning to the freshly precipitated colloids was a dominant mechanism that decreased dissolved concentrations of these trace elements in the lower Animas River.

When investigating AMD and mine outflows, geochemical assessments can be more specific if pH is measured at the time of sample collection, dissolved Fe^{2+} , Fe^{3+} , Al^{3+} , Mn^{2+} and SO_4^- are measured, and acidity is determined by titration. Selective extraction of sediments, perhaps including oxalate and/or dithionite extractions, might aid interpretation of solids formed by reactions of AMD in the environment.

Background

The setting: Gold King Mine (GKM) is located north of Silverton Colorado (Figure C-1), in the southern reaches of the Colorado Mineral Belt. The oldest rock in the region includes late Precambrian (i.e., >540 million years ago) sedimentary, metamorphic and igneous rocks (Luedke and Burbank 1999). During a series of regional volcanic eruptions that took place during the late Paleogene (i.e., 28-23 million years ago), magma intruded into a northeasterly striking shear zone, altering preexisting rock, leaving rich metalliferous sulfide ores and associated hydrothermal enrichments (Luedke and Burbank 1999). The ores are mainly vein-type

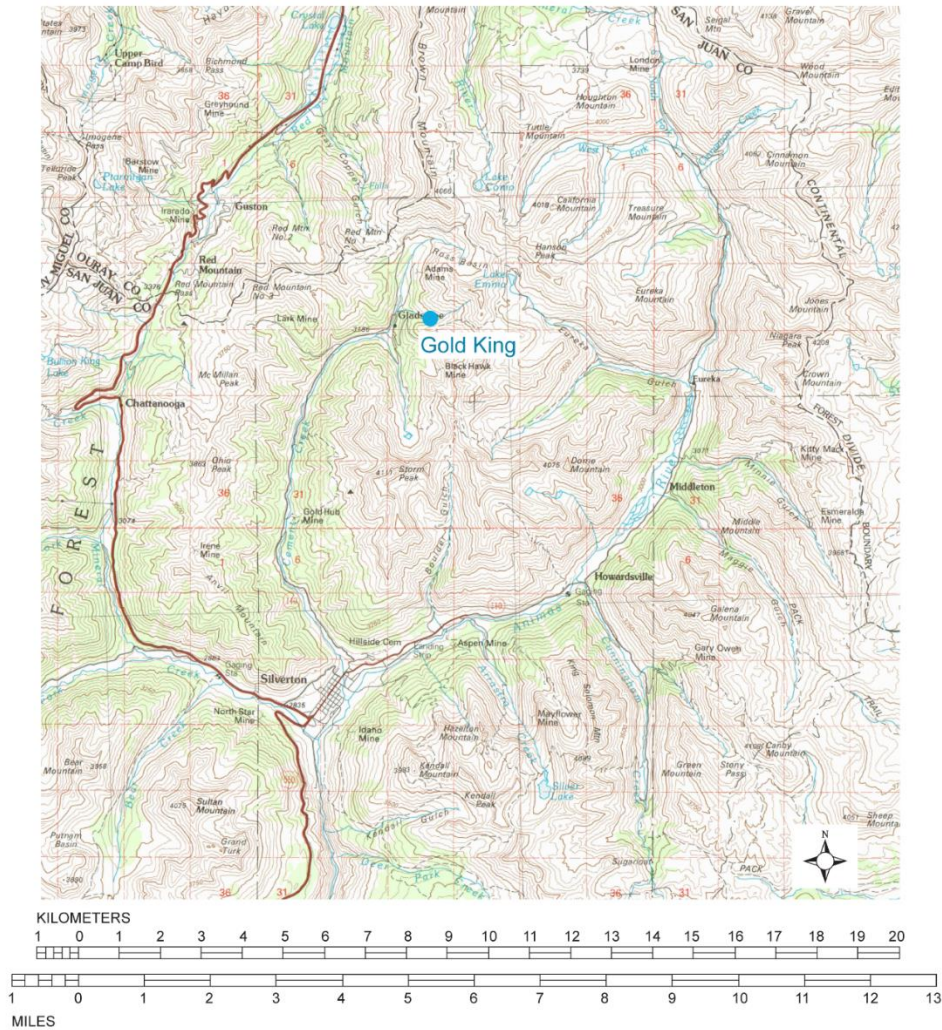


Figure C-1. Location of Gold King Mine, north of Silverton, in the Cement Creek watershed. Image from USGS, 30x60 Silverton, Colorado Quad (U.S.G.S. 1982). Water flow is north to south. Animas River flows NNE to SSW, with Silverton situated on its western bank. Cement Creek flows from north of Gold King Mine to its confluence with the Animas just north of Silverton. Mineral Creek flows from the west to its confluence with the Animas just south of Silverton.

deposits but extensive volumes of rock are pyritized around the vein zones. In present day, mineralized relict calderas remain, including the Silverton caldera (Figure C-2), just north and west of the town of Silverton, and in which GKM is situated (Yager and Bove 2002).

These sulfide deposits largely were composed of iron (e.g., pyrite), copper (chalcopyrite), lead, zinc, mercury and arsenic (Luedke and Burbank 1999). Notably, gold and silver also were present at anomalous concentrations. With these and other elements present at economic scales the region has been subject to extensive mining for more than a century and today the region is riddled with abandoned mines. These abandoned mines have been generating acid and metals for a century, and regional streams have been extensively contaminated.

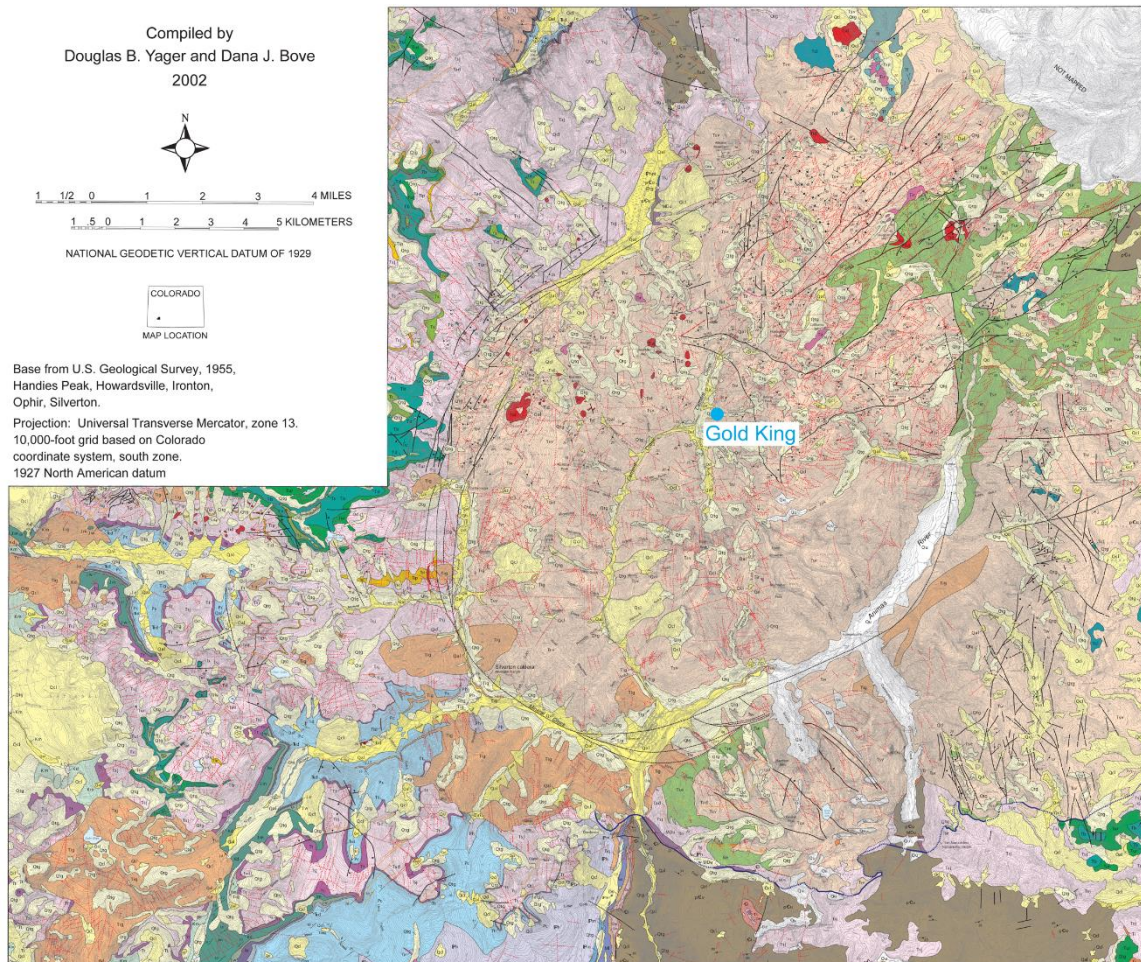


Figure C-2. Geologic map of the area surrounding Gold King Mine. Mapping units are lost in this image because it is reduced from the original scale. However, the outline of Silverton Caldera in which Gold King Mine is situated is clearly visible, bounded by the Animas River to the east, Mineral Creek to the south, and outlined by sub-parallel sets of faults and vein structures (black lines) to the west and northwest. This view shows that Cement Creek drains the highly mineralized Silverton Caldera exclusively. Original map is by Yager and Bove (Yager and Bove 2002). The volcanic release from this caldera was 75 km^3 , a volume much in excess of the 1980 release from Mt. St. Helens of 0.5 km^3 , for comparison (Doug Yager, USGS, personal communication to John Washington, USEPA, May 10, 2016).

The GKM is situated adjacent to Cement Creek (Figure C-1). Cement Creek flows into the Upper Animas River roughly 14 km downstream of GKM (Figure C-1). In turn, the Animas River flows into the San Juan

River 192 km downstream of GKM. The chemistry of Cement Creek is severely impacted with low pHs and high metals from several decades of uncontrolled mining discharges and naturally acidic waters (Schemel and Cox 2005). Today, the Cement Creek watershed is mapped as containing roughly 100 independent mines (US-Mining 2016), and considerably more than 100 when all mine openings and prospects are mapped (Church et al. 2007).

Until EPA started treating flow from the GKM after the August 2015 release, four mines alone (GKM, Sunnyside with its American Tunnel, Red & Bonita, and Mogul; Figure C-3) had been reported as releasing 600 to 800 gallons per minute (2,300-3,000 L/min.) of untreated acidic mine drainage (AMD) into Cement Creek (Olivarius-Mcallister 2013). Much of the recent discharge from these four mines is thought to result from installation of bulkheads in the American Tunnel in 1996 and 1997 which blocked free flow from Sunnyside Mine, raising regional ground water to discharge at other locations by the early 2000s (Gobla and Gemperline 2015). The spatial relationship and potential hydraulic connection of GKM with the American Tunnel is depicted in Figure C-4.

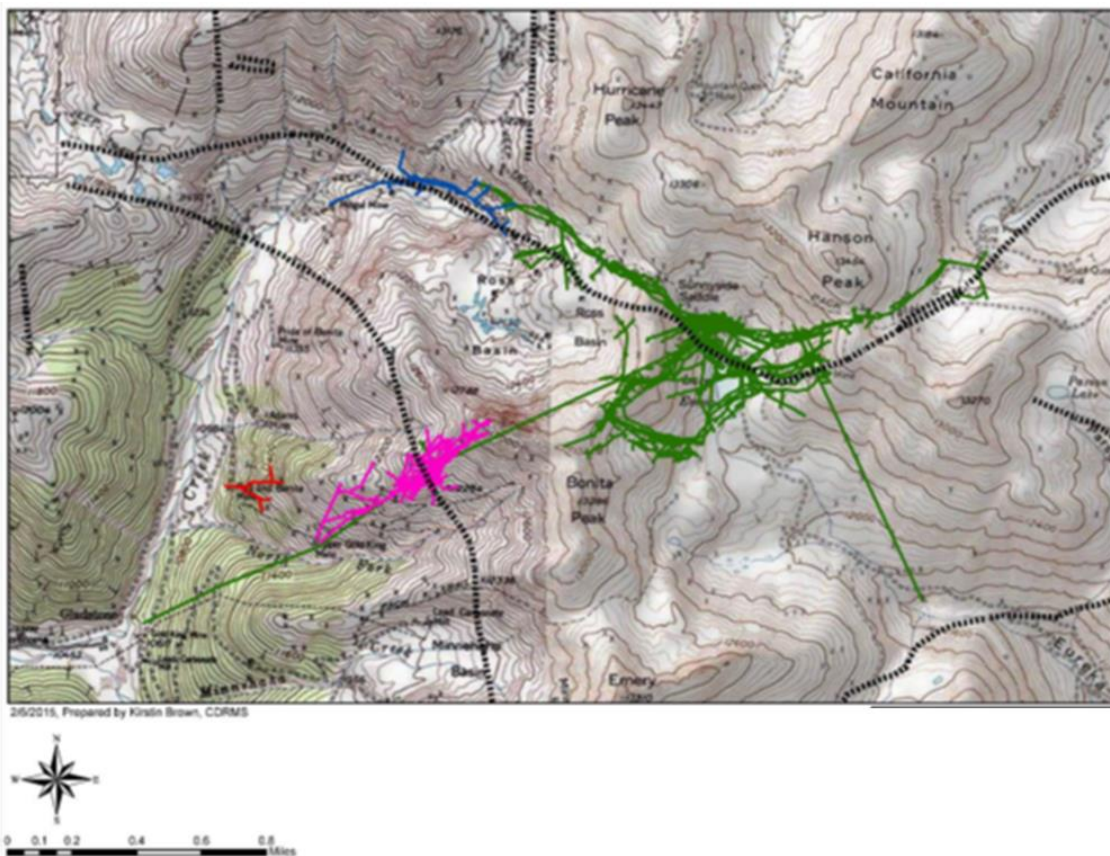


Figure C-3. Map depicting footprints for Gold King Mine (pink), Red and Bonita Mine (red), Mogul and Grand Mogul Mines (blue), and Sunnyside Mine (green) with the American Tunnel (also green) extending westerly under Gold King to emerge near Gladstone. Map is from Gobla and Gemperline (Gobla and Gemperline 2015).

In stark contrast to Cement Creek, the Animas River is buffered by calcareous rock and maintains moderately alkaline pHs over the reach between Cement Creek and the San Juan River. These moderately alkaline, well-buffered pHs help to suppress dissolved-metal concentrations in the Animas and its waters discharging into the San Juan (Schemel and Cox 2005).

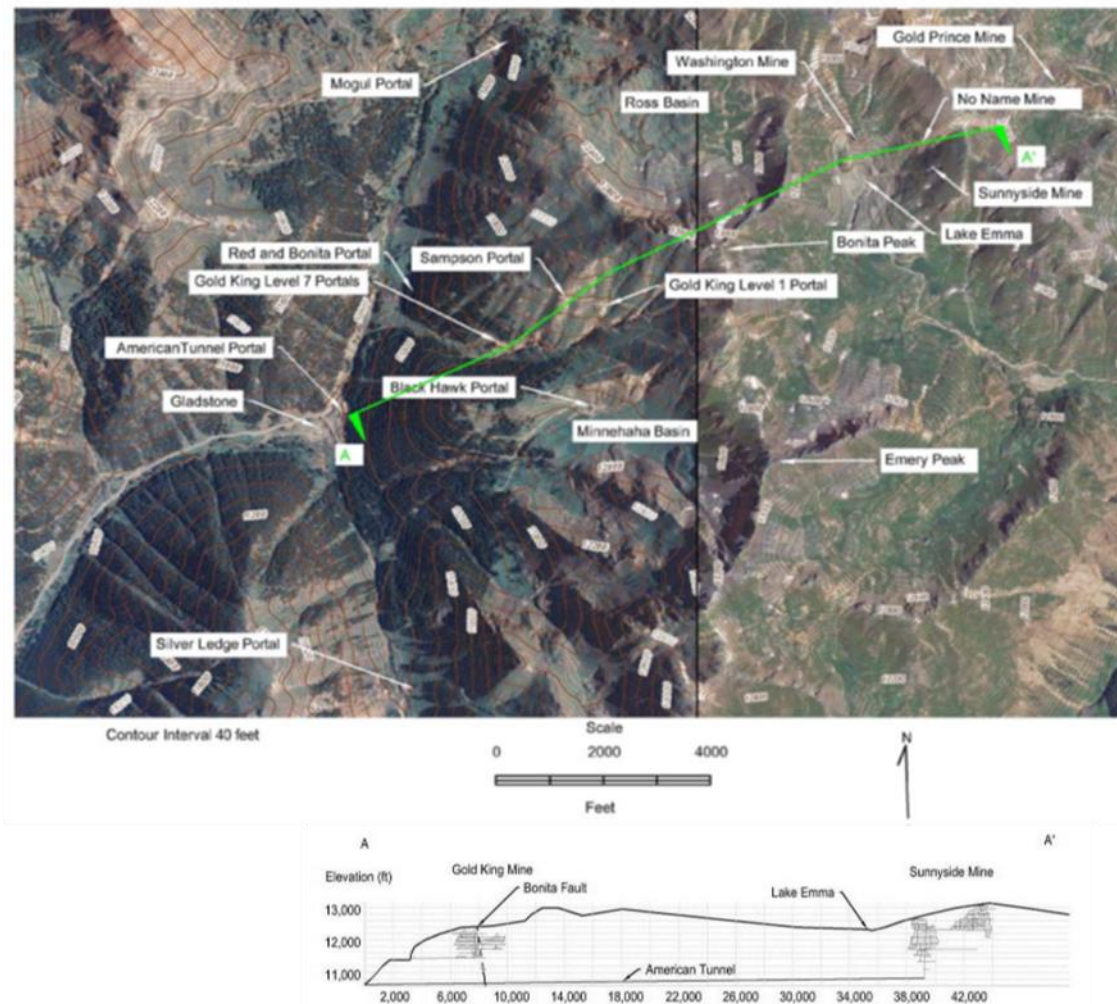
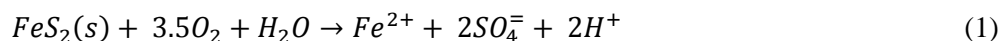
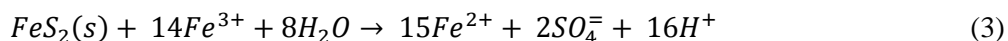
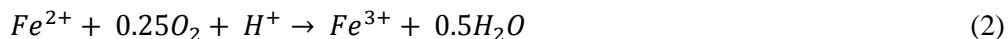


Figure C-4. Aerial trace and profile of a cross-section through Sunnyside and Gold King mines. This profile illustrates that Sunnyside Mine can drain through the American Tunnel, under Gold King Mine. The Bonita fault bisects Gold King Mine and the American Tunnel, likely fostering hydraulic connectivity between the mines. Lake Emma, located west of Sunnyside Mine on the cross-section, is reported to have failed and drained into the Sunnyside complex in 1978. Images are from Goble and Gemperline (Goble and Gemperline 2015).

Concerns with mine releases: Mine releases and abandoned mine outflows present two general areas of concern: i) acidity and acid generation, and ii) mobilization of trace and toxic metals.

Acid Generation: Mining voids act as drains for overlying and adjacent land, dropping the groundwater table. When the water table drops, sulfide-rich overburden and mining wastes that previously had been submerged in groundwater containing ~10 ppm O₂ or less, are exposed to air containing up to 21% (i.e., 208,000 ppm) O₂. These sulfide-mineral ores are highly reduced (i.e., electron rich) and, when exposed to oxygen, the minerals oxidize (i.e., yield electrons) and dissolve according to the following reactions, using pyrite (FeS₂) as an example (Rose and Cravotta 1998):





Reactions 1 and 3 of these oxidation and dissolution reactions generate acid, i.e., H^+ . When the dissolved metallic products of Reactions 1 through 3 are exposed to oxidizing and moderate-pH conditions, either through time or via migration of the metal-bearing waters, the major metals precipitate as authigenic (formed in place) amorphous solids and mineral phases.

When mine discharges occur in low flows, or by diffuse groundwater discharge, often the dominant part of these authigenic solids are stable crystalline-oxide minerals (e.g., hematite and goethite for iron minerals), minerals that occur abundantly in pristine soils and sediments as well as areas affected by AMD. In contrast, when large volumes of AMD are introduced suddenly into the environment as with a release, the relatively slow crystallization processes that are required to form stable crystalline minerals do not have time to take place and incipient amorphous to short-range-ordered crystalline phases are the dominant solids to form (Figure C-5). Over days to years, depending on chemical conditions, these incipient solids recrystallize to stable mineral phases (Figure C-5). The stoichiometry for these intermediate amorphous and mineral phases can be given as:



The incipient solids formed in Reactions 4-6 are prominent after large releases of AMD, being visible as yellow (and perhaps red, white or black) staining in rivers of moderate pHs. The stains arising from large AMD releases commonly are called “yellowboy”.

Each of these precipitation reactions, Reactions 4-6, generate additional acid, augmenting acidity generated by oxidation, Reactions 1 and 3. All these acid-generating reactions can take place after migrating in water over considerable distances from the source, so that pH actually can decrease as the waters flow away from a mine source. Iron and manganese are multivalent, and these metals often are present in their reduced, more soluble divalent state. Numerous minerals can form from higher-valence oxidized iron and manganese species, which can cause precipitation of these metals to proceed dominantly after these cations are oxidized. Manganese oxidation, in particular, can proceed slowly, even more so than iron (Skousen et al. 1998). Also, the mineralogy of the manganese oxide minerals varies as a sensitive function of numerous variables, so the stoichiometry of the acid production for manganese precipitation can be variable.

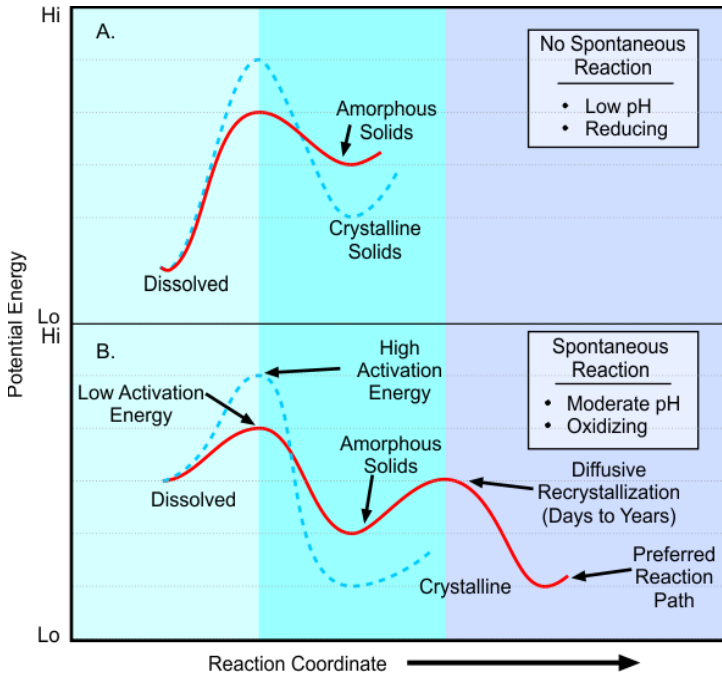


Figure C-5. Potential energy (for which low energy is relatively stable) vs reaction progress. Under conditions expected in a deep subsurface minepool, metals largely are stable in the dissolved state (A). When mine waters are released to common surficial conditions (moderate pHs and oxidizing), Fe, Al and Mn generally nucleate and precipitate to form amorphous or short-ranged ordered oxide minerals (e.g., ferrihydrite, gibbsite, birnessite) that are prominent in AMD releases as “yellowboy,” but these solids slowly recrystallize to more stable crystalline phases (e.g., hematite, goethite, and ordered gibbsite and birnessite).

Importantly, Reactions 4-6 commonly occur during periods of low-mine discharge as well as after releases. However, when mine flow is slow and/or diffuse, the rate at which these incipient phases are generated is counterbalanced by recrystallization to form more stable minerals which tend to become entrained in, and/or adhered to, streambed sediments. As a result, under low-flow conditions, these intermediate phases often can be observed only over limited areas. During periods of slow AMD releases, the prominent “yellowboy” commonly is not visible over long reaches of streams; nevertheless, the stable secondary mineral products of AMD oxidation and neutralization are ubiquitously distributed over long reaches of streams downgradient of long-term mine releases. These stable solids commonly are visible in streambeds and soils as red to yellowish brown (Fe), white (Al) and black (Mn) stains.

As a consequence of all the above, the acidity of AMD often is composed dominantly of the free acidity of H^+ , as well as Fe, Al and Mn, and AMD acidity is estimated reasonably well by the equation (Rose and Cravotta 1998):

$$Acidity = 50 \left\{ \frac{3[Fe^{3+}] + 2[Fe^{2+}]}{55.85} + \frac{3[Al^{3+}]}{26.98} + \frac{2[Mn^{2+}]}{54.94} + 10^{(3-pH)} \right\} \quad (7)$$

where acidity has units of mg $CaCO_3/L$, the metals are mg/L and pH is in standard units. If pH exceeds the first hydrolysis constant for Fe^{3+} , $pH \sim 2.2$, Equation 7 requires modification for hydrolysis. In addition to this calculated value, acidity also can be measured by a titration after addition of H_2O_2 to oxidize Fe and

Mn; this procedure is described in EPA Method 305.1. Calculated and measured acidities commonly agree reasonably well but can be discrepant if other metals are present at levels sufficient to add acidity upon precipitation. In order to assess the impact and fate of AMD in the environment with quantitative resolution, it is necessary to calculate or measure the value of acidity.

Trace-metal mobilization: AMD usually is elevated in numerous metals, often including some combination of Zn, Cd, Cu, Pb, As, Hg, Ni, Co, Mo, W, As, Se, Ag and Au among others. When these metals are present at elevated concentrations in, or adjacent to, mineralized zones, they can be mobilized as acid conditions are generated by sulfide dissolution and/or oxide-mineral precipitation.

As AMD waters are neutralized in the environment, the mobility of most of these trace metals decreases dramatically. Under moderate-pH, oxidizing conditions, the dissolved concentrations of these metals tend to be limited by specific and electrostatic sorption to authigenic Fe, Al and Mn oxide solids, both the incipient and stable mineral phases (Rose 1979). Secondary sinks under these conditions include electrostatic sorption to aluminosilicate clays and chelation with natural organic matter.

Summary of sampling and analyses used in this report

The GKM release occurred on August 5, 2015, flowing from the mine breach into nearby Cement Creek. Interpretations in this report regarding the impact and fate of this release are based on samples collected by EPA and other government entities, and include: i) roughly 500 water-sampling events, ranging from the mine to 550 km downstream, well into the San Juan River, and from the time of the release until 28 days after the release; ii) water samples analyses for up to 60 dissolved and total chemical properties; iii) roughly 320 sediment samples, ranging from the 12.5 to 640 km downstream, well into the San Juan River, and from the time of the release until more than 27 days after the release; and iv) sediment samples extractions by EPA Method 3050B, a hot concentrated-acid extraction that dissolves most metals in the primary and authigenic mineral phases.

In this manuscript, data reported as “dissolved” are the fraction remaining in water samples after the water has been passed through a 0.45- μm filter. Incipient solids such as $\text{Fe}(\text{OH})_3$ precipitate as amorphous to poorly ordered ferrihydrite. Typical single-grain ferrihydrite diameters are 3 to 7 nm (Schwertmann and Taylor 1989). Under most environmental conditions, these particles tend to aggregate into clusters of 2 μm (Schwertmann and Taylor 1989) to 50 μm (Anthony et al. 1997), with this aggregation being favored by dissolved anions neutralizing the positive surface charges of these colloids at low to moderate pHs. When these particles aggregate, they will tend to be excluded from the dissolved fraction, being retained on the filter in their aggregates. However, the magnitude of the GKM release, and the vigor of the oxidation-precipitation reaction at the Cement Creek – Animas River confluence suggested by the kinetic calculations described below (oxidation half-lives as low as seconds), might well have exceeded the capacity of the environmental system to yield stable colloidal aggregates. If so, colloidal precipitates in the upper Animas might have remained single-grained or unusually fine-grained aggregates capable of passing a 0.45- μm filter, and thereby being included in the “dissolved” fraction. This unusual outcome of high supersaturation SIs being calculated with respect to an incipient $\text{Fe}(\text{OH})_3$ solid phase has been described by Nordstrom (2011). Nordstrom attributed this unusual outcome to a combination of detection-limit artifacts and perhaps incipient ferric colloids being able to pass through filters. Calculations depicted below suggest that this possible artifact was not overwhelming in the few samples collected from the lower Animas that detectable dissolved Fe.

The general quality of the collected data can be assessed for those samples having an exhaustive suite of analytes, particularly including sulfate for mine drainage investigations. In this study, 233 samples out of >3,000 had sulfate analyses. In Appendix F, these 233 samples were subjected to tests for quality and

completeness of the analytical suite by three methods: i) comparison of sum of analytes, total dissolved solids and total dissolved solids estimated from the field measures of specific conductance and temperature; ii) ratios of dissolved to total analytes; and iii) cation-anion charge balance. These efforts suggest support that the general quality of these data are high (Appendix F).

Characterization of the release volume and chemistry

The timing and volume of the mine release have been estimated by staff the EPA team using data from a stream gage on Cement Creek, roughly 12.5 km downstream of the mine and designated herein as location “CC48” (Figure C-6). Based on interpretation of these data, excess water from the mine release flowed past CC48 from roughly 12:45 p.m. until 6:00 a.m., a period of 17.25 hours. Based on the data from CC48, the volume of the release was 11,420,000 liters.

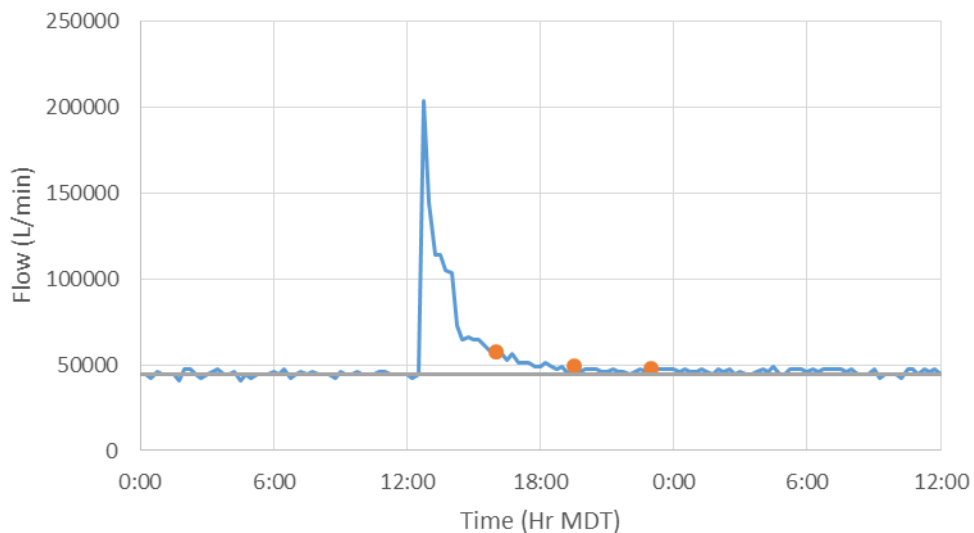


Figure C-6. Hydrograph at gage CC48 on Cement Creek, for August 5, 2015. The horizontal line is the average of the flow values prior to arrival of the mine release waters. The orange points designate when a sample was collected from nearby 14th St Bridge or at CC48 for chemical analysis.

The best estimates of the composition of the mine release centrally are from three sampling events (with some additional data from later samples): i) water samples collected from the mine opening (designated as location CC06) on August 15, ten days after the release; ii) water samples collected from where Gold King discharge flows from a tributary into Cement Creek (GKM13), 0.9 km from the mine opening, ten days after the release on August 15; and iii) water samples collected from the “14th Street Bridge” (designated CC 14th St Bridge), ~13 km down Cement Creek from GKM, on August 5 at 4:00 p.m. (roughly three hours after maximum flow at sample point CC48 one kilometer upstream from the 14th Street Bridge; Figure C-6). Both total and dissolved analytes are reported for these samples (Table C-1). Total analytes include the dissolved portion plus suspended material, the large majority of which is stable natural mineral grains that are denser than water and can be expected to settle out of the water column as flow velocity decreases. Dissolved analytes are the more mobile fraction and, therefore, the fate of the dissolved fraction generally is of greater concern. The fate of dissolved constituents can be interpreted with standard geochemical approaches. This geochemical report

Table C-1. Samples useful for characterizing release-water composition.

Study Location		CC06		GKM13		CC 14th St Bridge	
Site Location		Discharge		Cement Creek		Cement Creek	
Sample Date		8/15/2015		8/15/2015		8/5/2015	
Sample Time		9:00		10:45		16:00	
Distance from source (km)		0		0.87		13.46	
		Dissolved	Total	Dissolved	Total	Dissolved	Total
pH	(SU)	2.93	2.93	3.19	3.19		
Aluminum	(mg/l)	34	33	28	26	91.9	945
Antimony	(mg/l)	0.0037	0.00062	0.0015	0.0004	0	0.321
Arsenic	(mg/l)	0.044	0.0055	0.016	0.0012	0	8.23
Barium	(mg/l)	0.0086	0.0087	0.0085	0.009	0	9.73
Beryllium	(mg/l)	0.011	0.011	0.009	0.0086	0.0348	0.135
Cadmium	(mg/l)	0.082	0.085	0.08	0.084	0.0983	0.165
Calcium	(mg/l)	370	380	350	360	461	454
Chromium	(mg/l)	0.0055	0.003	0.0033	0.001	0	0.706
Cobalt	(mg/l)	0.11	0.11	0.1	0.1	0.204	0.384
Copper	(mg/l)	4.6	4.6	3.9	3.8	10.4	36.7
Iron	(mg/l)	150	120	96	70	49.5	9930
Lead	(mg/l)	0.042	0.029	0.024	0.011	0.15	179
Magnesium	(mg/l)	27	27	26	28	36.5	279
Manganese	(mg/l)	36	36	31	32	37.1	78
Mercury	(mg/l)	0.00008	0.00008	0.00008	0.00008		0.0192
Molybdenum	(mg/l)	0.0042	0.00077	0.0014	0.00045	0	2.01
Nickel	(mg/l)	0.069	0.072	0.068	0.07	0.0915	0.276
Potassium	(mg/l)	2.4	2.5	2.2	2.2	6.63	212
Selenium	(mg/l)	0.0047	0.0033	0.0038	0.0032	0	0
Silver	(mg/l)	0.0001	0.0001	0.0001	0.0001	0	1.11
Sodium	(mg/l)	5.3	5.2	52	54	4.96	23.4
Thallium	(mg/l)	0.00029	0.00029	0.00023	0.00023	0	0
Vanadium	(mg/l)	0.038	0.0025	0.014	0.0003	0	5.47
Zinc	(mg/l)	20	20	18	18	26.8	44
Sulfate	(mg/l)	1600	1600	1400	1400		
Chloride	(mg/l)	0.36	0.36	1.2	1.2		
Fluoride	(mg/l)	10	10	8.9	8.9		
Nitrate as N	(mg/l)	0.023	0.023	0.025	0.025		

focuses on the dissolved chemical data and generally will not address the suspended fraction except as it relates to the dissolved fraction through precipitation, sorption or dissolution reactions.

The completeness and internal consistence of these samples, both within and between samples, can be assessed with cation-anion charge balances (Figure C-7). Trace species having multiple oxidation states

represented in Figure C-7 were assigned a valence, and charge for oxyanions, based on professional judgement because equilibrium cannot be assumed for polyvalent trace elements. The charge balances for CC06 and GKM13 are 0.986 and 1.043, respectively, indicating good internal consistence between cations and anions, and suggesting that i) all major cations and anions are represented in these analyses and ii) judged trace speciation was qualitatively reasonable.

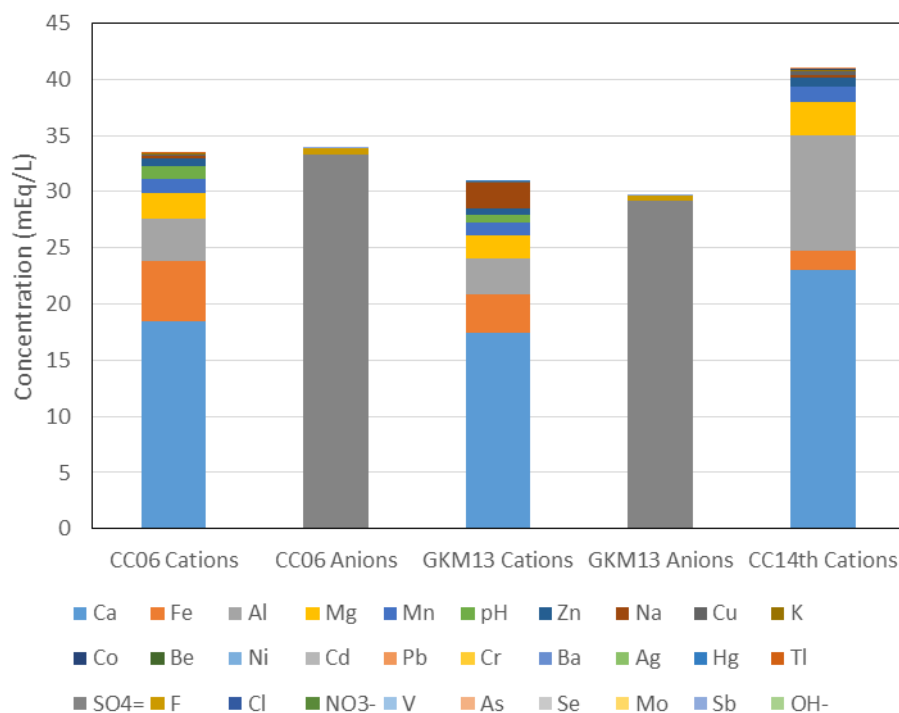


Figure C-7. Cation/anion balance for water samples from CC06, GKM13, and CC14th Street Bridge. Cation/anion for CC06 is 0.986 and for GKM13 is 1.043, close to the ideal balance of 1.000. Anions and pH were not analyzed for the CC14th St sample. The valence of Fe was not analyzed. However, at pH~3, the dominant species of ferrous Fe is Fe²⁺ and of ferric Fe is as FeOH²⁺ (neglecting SO₄⁻), so Fe is represented here as having 2+ charge.

For the purposes of estimating the composition of the August 5 release, also noteworthy on Figure C-7 is that the August 5 sample drawn from the release waters mixed with Cement Creek (CC 14th St Bridge), has a higher total concentration of cations than do the August 15, post-release waters collected near the mine, i.e., CC06 and GKM13. The most prominent differences of CC 14th St Bridge from the other two samples is that Ca and Al are more concentrated and Fe is less concentrated (Figure C-7). These observations suggest that i) the original release waters differed from water flowing from GKM on August 15, and/or ii) that release waters entrained solutes as the waters flowed from the mine and down Cement Creek toward the Animas River. Later in this report, it is argued that most of the remediation of the release waters occurred in the Animas River. Within this context, the “release source” is best thought of as what flowed from Cement Creek into the Animas River. As such, the CC 14th St sample offers unique insight to the quality of the actual release waters. Unfortunately, this sample also was diluted substantially by Cement Creek (Figure C-6). The EPA team estimated the undiluted quality of the release waters from this sample using:

$$Q_t c_t = Q_r c_r + Q_c c_c \quad (8)$$

where Q is flow rate (L/min), c is concentration (mg/L), subscript t stands for total (i.e., the composite value of the August 5 sample), subscript r stands for release water (i.e., the value ultimately desired), and subscript c stands for creek (i.e., the value estimated for the Creek in the absence of the mine-water release). Background flow was estimated from USGS gage readings recording before the release waters arrived at the gage and background solute concentrations were estimated from samples collected in Cement Creek days after the release waters had left Cement Creek.

Having solved for the estimated concentrations of the release waters using Equation 8 (solving for c_r), in the interest of generating a conservative estimate of the source, the highest reported value of i) the estimate of c_r using CC14th St data and Equation 8, ii) CC06 data and iii) GKM13 data. Looking at quality of mining-degraded watersheds, Nordstrom (2011) noted that initial flushes of water leaving watersheds after precipitation events were highly enriched in mining-related solutes. Considering this effect, and in the interest of generating a conservative estimate of the source term, the concentrations were doubled for the first 30 minutes of the release event to arrive at very conservative upper-limit estimates of the release. These conservative estimates of the source term for the waters released from Cement Creek to the Animas River on August 5, 2015 are summarized in Table C-2.

The CC 14th St Bridge sample did not include a measured pH. In the interest of remaining conservative, the team assumed the pH of CC 14th was the same as that measured in GKM sample CC06, pH=2.9 (Table C-1). The CC 14th sample also did not report a value for SO_4^- . Referring to Figure C-7, the anions in samples CC06 and GKM13 are comprised almost entirely of SO_4^- . Based on this observation, the team estimated SO_4^- for CC14th and for the release waters by charge balance with the cations (Table C-2). Then they used Equation 7 to estimate acidity of these source waters (Table C-2).

These estimates of the release-water composition as it entered Animas River (Table C-2) are very conservative and likely to overestimate actual composition. Because of dilution, and neutralization by salts and other minerals, pH likely was higher than the assumed 2.9, and the solubility of numerous minerals is highly sensitive to pH in this range. Even in the unlikely case that pH in the Creek was 2.9, assuming a water temperature of 8 °C in Cement Creek, calculations performed in Geochemist's Workbench (Bethke 1998) indicate the Peak Concentration estimated in Table C-2 is supersaturated with gypsum ($\text{CaSO}_4 \cdot 2\text{H}_2\text{O}$) as well as other minerals. Calculation of this supersaturated condition supports the notion that these estimates of release water composition (Table C-2) are, indeed, conservative and likely to overstate the concentrations of at least some solutes.

The fate of iron in surficial settings depends on its valence state which was not determined in these samples. In "The Setting" subsection above, it was argued that much of the discharge waters arose from deep pools of regionally interconnected mines that had been sealed from the atmosphere by bulkheads. This sealed state and the large scales of the mine pools suggests that O_2 was in short supply. In addition, reaction of Fe^{3+} with pyrite (Reaction 3) proceeds strongly to the right, yielding Fe^{2+} and SO_4^- , with an equilibrium constant of $\log K \sim 99$ (Bethke 1998). And numerous kinetic studies have shown that, at acidic pHs, oxidation of pyrite by Fe^{3+} (Reaction 3) proceeds much more quickly than it does with O_2 (Reaction 1) (Rose and Cravotta 1998). Based on expected paucity of O_2 in the mine waters and propensity for pyrite oxidation to proceed exhaustively and quickly by Fe^{3+} , the oxidation state of Fe in the source waters at GKM likely was dominantly ferrous, Fe^{2+} .

Table C-2. Conservative estimate of composition of release waters that flowed from Cement Creek into the Animas River.

Analyte	Dissolved Concentration					Dissolved Load			
	Unit	Peak Flow at 12:45 PM	Plume + Bkgnd Mean	Creek Bkgnd	Plume Mean	Unit	Plume + Bkgnd	Bkgnd During Plume	Plume Only
Aluminum	mg/l	619	113	7.60	542	kg	6541	352.6	6188
Antimony	mg/l	0.015	0.003	0.000	0.015	kg	0.194	0.019	0.176
Arsenic	mg/l	0.301	0.051	0.005	0.238	kg	2.95	0.237	2.71
Barium	mg/l	0.069	0.025	0.015	0.067	kg	1.46	0.696	0.769
Beryllium	mg/l	0.231	0.042	0.002	0.205	kg	2.42	0.077	2.35
Cadmium	mg/l	0.674	0.125	0.010	0.594	kg	7.23	0.447	6.78
Calcium	mg/l	2438	537	177	2003	kg	31073	8195	22878
Chromium	mg/l	0.006	0.004	0.001	0.014	kg	0.207	0.046	0.161
Cobalt	mg/l	1.26	0.24	0.03	1.11	kg	13.9	1.24	12.6
Copper	mg/l	70.92	12.6	0.40	62.4	kg	731	18.56	712.6
Iron	mg/l	268	61	13.3	255	kg	3528	619	2910
Lead	mg/l	1.03	0.20	0.02	0.93	kg	11.8	1.14	10.61
Magnesium	mg/l	197	43	9.93	175	kg	2462	461	2001
Manganese	mg/l	206	41	5.80	185	kg	2385	269	2116
Mercury	mg/l	0.000	0.000	0.000	0.000	kg	0.004	0.004	0.000
Molybdenum	mg/l	0.025	0.006	0.000	0.028	kg	0.345	0.023	0.322
Nickel	mg/l	0.55	0.11	0.02	0.46	kg	6.15	0.88	5.27
Potassium	mg/l	40.6	8.0	1.77	33.3	kg	462	82.0	380
Selenium	mg/l	0.034	0.007	0.001	0.034	kg	0.415	0.027	0.388
Silver	mg/l	0.017	0.004	0.000	0.017	kg	0.204	0.005	0.200
Sodium	mg/l	18.0	5.9	4.40	12.0	kg	341	204	137
Thallium	mg/l	0.016	0.003	0.000	0.017	kg	0.202	0.009	0.194
Vanadium	mg/l	0.064	0.014	0.003	0.058	kg	0.800	0.138	0.662
Zinc	mg/l	157	31	3.00	145	kg	1790	139	1651
Sulfate	mg/l	11240	2386	613	9588	kg	137949	28449	109500
pH	SU	2.90	2.90	2.90	2.90	kg	73.4	58.9	14.5
Acidity	mgCaCO ₃ /l	4598	931	152	4097	kg CaCO ₃	53822	7031	46791

Explanation: For all parameters except sulfate, pH and acidity: “Peak” and “Bkgnd” concentrations were estimated in the empirical analysis; “Plume + Bkgnd” load estimated in the empirical analysis; “Bkgnd during plume” load estimated from “Bkgnd” concentration times bkgnd flow estimate of 46.4 ML; “Plume Only” load estimated by difference of “Plume + Bkgnd” – “Bkgnd;” “Plume Mean” concentration estimated by “Plume Only” load divided by estimated plume volume of 11.42 ML.

Table C-3. Abiotic Fe²⁺ oxidation half-life at P_{O₂} = 0.2 atm. Calculated as a function of pH, using kinetic data of Singer and Stumm (1970)

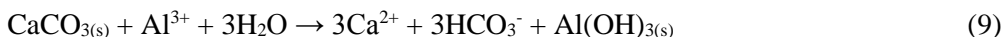
pH (su)	T _{1/2}
0	65.89 years
1	65.89 years
2	65.84 years
3	61.01 years
4	7.32 years
5	30.05 days
6	7.22 hours
7	4.33 minutes
8	2.60 seconds
9	0.03 seconds

Explanation: In Cement Creek, pH probably ranged from 2 to 4 (red field), so abiotic Fe²⁺-oxidation half-life likely was years to decades, effectively yielding no ferric Fe during the hours-long transit from Gold King Mine down Cement Creek to the Animas River. In the Animas River, pH likely dominantly ranged from 6 to 8 (green field), so abiotic Fe²⁺ oxidation half-life likely was seconds to hours, and probably mostly in the seconds to minutes range shortly after the release waters mixed with the Animas water. Consequently, Fe²⁺ in the release waters likely oxidized to Fe³⁺ quickly in the Animas River.

The abiotic oxidation of Fe²⁺ under oxidizing, acidic conditions is quite slow (Washington et al. 2004), with a half-life of roughly seven years at pH 4 and roughly 60 years at pH 3 and less (Table C-3; Annex C1) (Singer and Stumm 1970). Microbes can accelerate Fe²⁺ oxidation rate (Rose and Cravotta 1998), and probably Fe-oxidizing bacteria were entrained in the disaggregated spoil at the GKM opening that was eroded during the breach event (Youtube 2015) and carried as suspended load down Cement Creek. Nevertheless, it seems likely that most of the dissolved Fe in the release waters remained reduced during the hours-long transit down Cement Creek. Consequently, the chemical composition of the release waters likely changed little during the short time it took to flow down Cement Creek, other than perhaps alternately dissolving and precipitating Ca²⁺, and perhaps other, SO₄⁻ salts as the release waters flowed over normally dry lands above the Creek banks.

Assessment of the fate of solutes in the release waters as they enter the Animas River

In contrast to Cement Creek, the Animas River is buffered by calcareous bedrock above the confluence with Cement Creek (Desborough and Yager 2000, Schemel and Cox 2005). Immediately upstream of Cement Creek, the Animas drains the Silverton Volcanics that are chiefly composed of volcanoclastic sediments, including calcite which often is “pervasive and disseminated throughout the groundmass and within microveinlets,” and, “where not intensely altered,” “has the ability to buffer acidic waters” (Yager and Bove 2002). The Silverton Volcanics also include chlorite (Yager and Bove 2002), which can enhance alkalinity as well (Desborough and Yager 2000). Buffering capacity likely is enhanced still more about one kilometer downstream of Silverton where the Animas transects numerous pre-Tertiary sedimentary beds including numerous lithologic units of limestone and calcareous shale (Yager and Bove 2002). The alkalinity of these waters is important for its potential to neutralize the acidity of the Gold King release. For example, for acidity generated from Al³⁺ (Reaction 6):



Given this geologic setting, and using the data collected for this study, saturation indices (SIs) were calculated, using thermodynamic data reported in Parizek et al. (1971), for calcite (CaCO_3) and dolomite ($\text{CaMg}(\text{CO}_3)_2$) downstream of the GKM including Cement Creek, the Animas River and into the San Juan River (Figure C-8A and C-8B; Annex C2). Negative SI values indicate that water is undersaturated with a mineral phase, values of near zero indicate the water roughly is in equilibrium with mineral, and positive SI values suggest the mineral should precipitate from solution. The SIs are generated from thermodynamic data and need to account for the deviation of the real aqueous solution from an ideal thermodynamic condition using activity coefficients (γ). Activity coefficients require knowledge of the ionic strength (I) of the solution. The value of I, is calculated using the concentrations of all major solutes. So calculation of mineral SIs requires a complete suite of major-chemical analytes. However, many of the samples in this study include data only for selected species, major and toxic metals for example. Consequently, to accommodate this dataset, I was calculated for those samples that were subjected to analysis for all major analytes. Speciation of these analytes (e.g., Al^{3+} vs $\text{Al}(\text{OH})_2^+$) was estimated based on judgement of conditions including reported pH, inferred $[\text{O}_2]$ and similar geochemical parameters. Then for these samples, γ was calculated using the Extended Debye-Huckel Equation (Stumm and Morgan 1981). Samples having an incomplete suite of analytes were assigned values of γ from geographically nearby samples having similar geochemical characteristics. With all samples/analytes having calculated or estimated values for γ , SI values were calculated. Consistent with calculation of I, calculation of γ included correction for impact of pH on speciation and assessment for complexation by major solutes (e.g., SO_4^-). For these calculations, it was assumed that the river waters equilibrated with atmospheric CO_2 , $\log P_{\text{CO}_2} = -3.40$ (atmospheres units). For samples not having reported values of pH, pH was assigned values of nearby samples having similar reported geochemical analytical profiles. Figures C-8A and C-8B indicate that the Animas was variably undersaturated with respect to calcite and dolomite immediately downstream of Cement Creek at the time the samples were collected for about 100 km (suggesting the presence of acidity), but that Animas remained roughly saturated with these alkaline minerals for most samples >150 km (suggesting neutralization of acidity in these locations). Additional data for the Animas upstream of its confluence with Cement Creek indicate moderately alkaline conditions as well (data not shown), so the only Animas data indicating pronounced undersaturation with calcite is for samples collected at the confluence with Cement Creek and downstream of this location as far as ~150 km from GKM, collected during the time of the release. Taken altogether, these observations suggest that the acidity of the release water was effectively neutralized at roughly 150 km downstream from the GKM.

Acidity-Alkalinity Balance of the release waters at the Cement-Animas confluence: Table C-2 reports a maximum estimated load of acidity in the mine release as ~54,000 kg as CaCO_3 . Based on interpretation of data from the gage in Cement Creek near the confluence with the Animas, the acidity load flowed into the Animas over a period of roughly 17.25 hours on August 5.

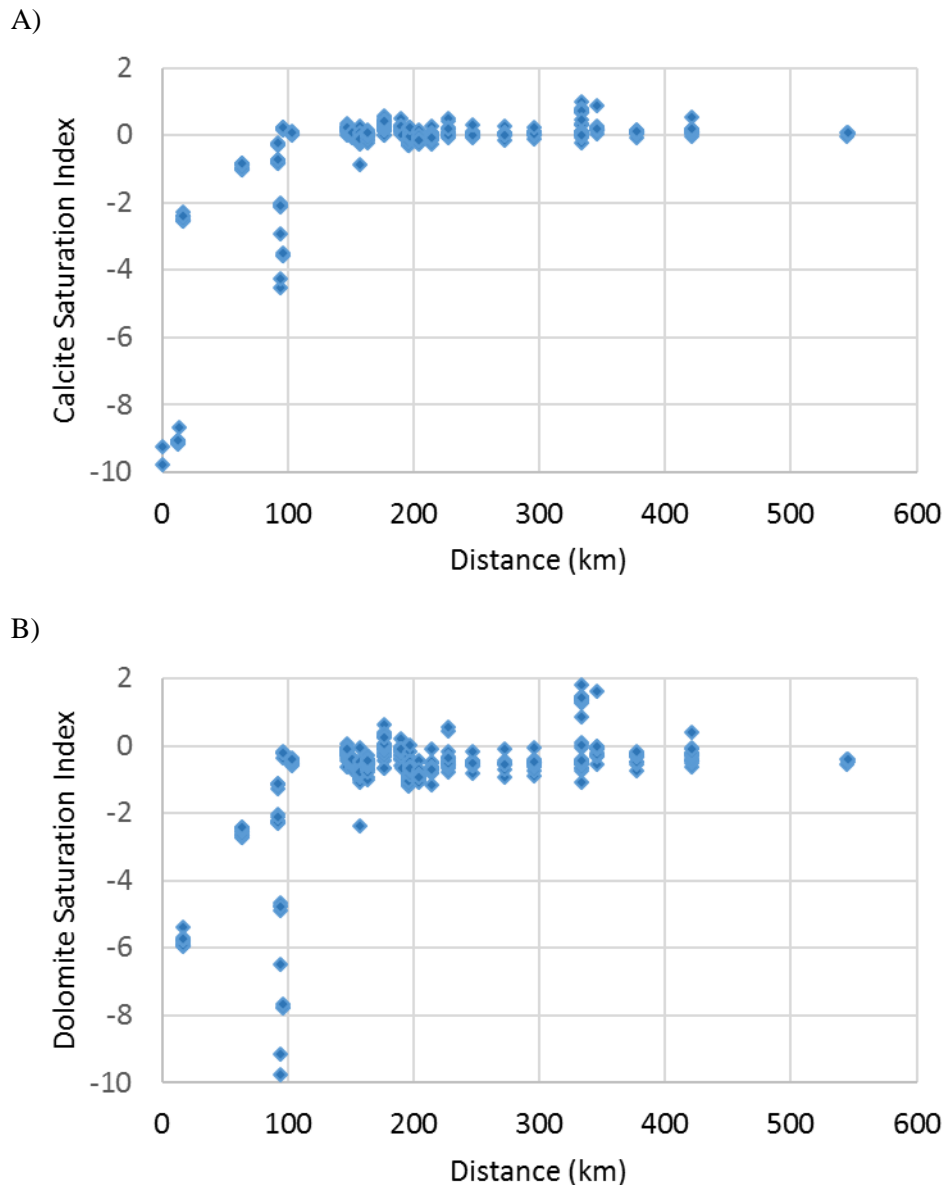


Figure C-8. Saturation Indices (SIs) for calcite (A) and dolomite (B) vs distance from Gold King Mine. An SI of zero indicates saturation with the mineral phase. Negative SI values indicates that the water is undersaturated with the mineral.

According to data from a gage in the Animas River upstream of Cement Creek, on August 5, flow in the Animas at the confluence with Cement Creek was about 115 ft³/sec (11.7M liters/hr). Alkalinity has been measured in water samples collected by EPA from the Animas River upstream of Cement Creek, falling in the range of 30 mg CaCO₃/l. As the Animas flows downstream, alkalinity ascends to about 90 mg CaCO₃/l, consistent with expectations for waters draining carbonate bedrock. For these values of flow and alkalinity in the Animas, the 54,000 kg load of acidity in the release could be neutralized with about 50 to 150 hours of Animas flow without any additional dissolution of carbonate bedrock, roughly three to nine times the time increment of the release from Cement Creek to the Animas. The actual time to neutralize the release waters in the Animas likely was substantially shorter because, i) the acidity load of the release could well have been much less than the estimates in Table C-2 in that these estimates were arrived at with

very conservative assumptions, ii) carbonaceous bed sediments or bedrock likely added alkalinity in the acidic release waters as they migrated down the Animas, and iii) downstream tributary inflow might have augmented alkalinity as well.

Accelerated oxidation of Fe in the Animas River: Whereas abiotic oxidation Fe^{2+} half-life is on the order of years to decades at $\text{pH} \leq 4$, at the moderately alkaline pH values observed in the Animas, the oxidation half-life falls to seconds to hours. Using the kinetic data supplied by Singer and Stumm (1970), the ferrous oxidation half-life falls to 7 hours at pH 6, 4 minutes at pH 7 and 3 seconds at pH 8 (Table C-3). This generation of Fe^{3+} through oxidation of Fe^{2+} will foster precipitation of amorphous and micro-crystalline ferric-oxide phases (Reaction 4).

Taken altogether, the combined factors of (i) the saturation indices for calcite suggesting near-saturation for all distances downstream of 150 km (Figure C-8), (ii) the capacity of the Animas to neutralize the release load of acidity with <150 hours of flow, and (iii) the accelerated rate of Fe^{2+} oxidation at moderately alkaline pHs (Table C-3), constitute compelling evidence that essentially all of the release acidity was neutralized in the Animas River within about 100-150 km of stream distance from GKM.

Precipitation of incipient oxyhydroxide colloidal solids which dyed the Animas River yellow: The neutralization of mine release waters that took place in the Animas entailed precipitation of Fe^{3+} , Al^{3+} and Mn^{4+} incipient oxide phases of the type shown in Reactions 4-6. The progress of these precipitation reactions has been modeled thermodynamically (Table C-4) using Geochemist's Workbench (Bethke 1998) and the results are depicted in Figures C-9 to C-12. Geochemist's Workbench is well-known commercial software that enables the qualified user to model thermodynamic equilibrium of water, having user-specified properties, with mineral phases, also specified by the user. This modeling can be done toward different objectives, e.g., calculation of equilibrium constants, modeling of reaction progress, and generation of a variety of equilibrium diagrams. In Figures C-9 to C-12, Cement Creek waters were reacted with sufficient calcite masses to just saturate the system, mimicking the alkaline state of the Animas as reflected in Figure C-8. The reactions were modeled at 11 °C, in equilibrium with 0.208 atmospheres of O_2 and $10^{-3.4}$ atmospheres of CO_2 . Silica was modeled as being in approximate equilibrium with quartz. Minerals that were excluded from precipitating in this modeling included: i) primary minerals that typically do not form authigenically in sediments and soils, ii) secondary minerals that commonly form by recrystallization from incipient mineral phases, and iii) crystalline minerals composed of low-level trace elements that more likely were entrained as impurities in dominant mineral phases.

Figure C-9 depicts "Peak Flow" (Table C-2) concentrations entering the Animas. This figure should include the most complex suite of minerals that might have precipitated during the event. Figure C-10 depicts the "Plume + Background Mean" (Table C-2) concentrations entering the Animas; these values are the mean estimated concentrations of solutes emitted from Cement Creek during the plume, representing complete mixing of the entire volume of plume and creek waters during the release period. Comparison of Figures C-9 and C-10 suggests that no unique minerals precipitated solely during release of the most concentrated water. Using the mineral masses depicted in Figure C-10, Figure C-11 provides estimates of minerals modeled as precipitating from the plume waters in the Animas River. Figure C-12 depicts "Creek Background" (Table C-2) water reacting with Animas alkalinity. Comparison of Figures C-10 and C-12 suggests that most mineral species that potentially precipitated during the plume also potentially precipitate from Cement Creek waters as they enter the Animas under normal-flow conditions at other times as well. The only minerals that modeling suggests might have precipitated during plume release but not during the depicted "background" flow (Figure C-12) include gypsum ($\text{CaSO}_4 \cdot 2\text{H}_2\text{O}$), alunite ($\text{KAl}_3(\text{SO}_4)_2(\text{OH})_6$), smithsonite (ZnCO_3), and tenorite (CuO). Alunite is an endmember mineral in the isostructural alunite-jarosite ($\text{KFe}_3(\text{SO}_4)_2(\text{OH})_6$) family, having a complex set of solid solutions

Table C-4. Properties assumed in thermodynamic reaction-progress modeling of plume waters flowing into the Animas River

Parameter	Assignment
Temperature	11 °C
O ₂ Fugacity	0.2 atmospheres, fixed
CO ₂ Fugacity	10 ^{-3.4} atmospheres, fixed
Assumed [Si]	2.8 mg/L, ~equilibrium with quartz
Charge Balance	SO ₄ ⁼
Activity Model	Extended Debye-Huckel
Thermodynamic Database	
GWB Release 4.0.2 Oct94 dataset, based on the Wolery et al., Lawrence Livermore Laboratory dataset dat0.3245r46 with additions for gibbsite log K from Nordstrom et al. (1984):	
Gibbsite crystallinity	Log K
Fully crystalline (2-5 μm)	8.11
Micro-crystalline (2-20 weeks)	9.35
Amorphous (freshly precipitated)	10.8
Suppressed Minerals (minerals not used in modeling because they are stable, as opposed to freshly precipitated, or do not form in sedimentary settings)	
Hematite	CuCr ₂ O ₄
Goethite	NiFe ₂ O ₄
Pyrolusite	Co(FeO ₂) ₂
Ba ₃ (AsO ₄) _{2(c)}	Co ₃ O ₄
CuFeO _{2(c)}	Co ₂ SiO ₄
Cu ₃ (AsO ₄) _{2(c)}	Ferrite (Cu, Zn, Mg, Ca)

in the cation sites (K⁺, Na⁺, H₃O⁺) (Brophy and Sheridan 1965), and (Al³⁺, Fe³⁺, Cu²⁺, and Zn²⁺) (Scott 1987), so any alunite-jarosite minerals associated with the plume waters, probably were solid solutions, albeit near end-member. And the isostructural jarosite potentially can precipitate during background-type flows (Figure C-12). Whether alunite-jarosite minerals, or other Al and Fe³⁺ hydroxysulfate minerals, actually precipitated in the Animas during this event is uncertain and dealt with in more detail in the next section. Whether smithsonite and tenorite actually precipitated is uncertain as well; considering the trace-level concentrations of Zn²⁺ and Cu²⁺ in the presence of more dominant precipitating mineral phases, most of these metals could have been entrained as impurities in other minerals.

A number of minerals depicted in Figures C-9 to C-12 likely are transitory and unstable in the Animas River. This is evident for the alunite-jarosite group in that the masses of these minerals dissolve at 60% to 90% of reaction completion. This is because, as acidity is neutralized by limestone alkalinity, Al^{3+} and Fe^{3+} activity is regulated to progressively lower levels by precipitation of amorphous $\text{Al}(\text{OH})_3$ and $\text{Fe}(\text{OH})_3$; as Al^{3+} and Fe^{3+} activity drops the ion-activity products (IAPs) for the alunite-jarosite minerals fall below saturation. Effectively, alunite and jarosite (or any hydroxysulfate salts) are replaced by the relatively more stable $\text{Al}(\text{OH})_3$ and $\text{Fe}(\text{OH})_3$. Figures C-9 and C-10 depict gypsum ($\text{CaSO}_4 \cdot 2\text{H}_2\text{O}$), dolomite ($\text{CaMg}(\text{CO}_3)_2$), barite, smithsonite and tenorite as being stable (because they remain at reactions' completion). However, as the plume migrated down the Animas, SO_4^- activity likely dissipated with a resulting dissolution of gypsum, leaving Ca^{2+} activity to be controlled by its normal constraint in the lower Animas, calcite (Figure C-8).

Likewise, dolomite might well have dissolved if it became undersaturated in the lower Animas (Figure C-8). If smithsonite and/or tenorite precipitated, these minerals might well have redissolved as well because Zn and Cu likely are controlled to relatively lower activities by sorption on ferric and aluminum hydroxides as described two sections below.

It is noteworthy, that the Gold King discharge event is not unique in acting as a potential source of Al and Fe^{3+} hydroxysulfate minerals to the Animas River from Cement Creek. In fact, modeling of reaction progress for Cement Creek background waters with Animas alkalinity suggests precipitation of transitory jarosite phases (Figure C-12).

Based on the "Plume + Background" data (Figure C-10), gypsum comprised the largest load among the unstable minerals in the plume. For the calculated discharge from Cement Creek during plume release of 11.42 ML, roughly 9,300 kg of gypsum was carried by, or precipitated from, the plume waters as they mixed with the Animas (Figure C-11). Lesser amounts of other unstable minerals (e.g., Al and Fe^{3+} hydroxysulfates) might have precipitated as well. These minerals would have entrained trace metals as impurities in addition to the major solutes, Zn and Cu described above. When these minerals redissolved, the impurities would have entered solution too. The concentrations of these trace impurities then would be subject to the same long-term fate as Zn and Cu, scavenging by stable hydroxide minerals as described two sections below.

Of the remaining minerals depicted in Figures C-9 to C-12, gibbsite ($\text{Al}(\text{OH})_3$), ferrihydrite ($\text{Fe}(\text{OH})_3$) and birnessite (MnO_2) should remain as solids in the Animas, their stability supported by the alkaline pHs of the carbonate-buffered waters. Over time, these solids likely will recrystallize to still-more stable forms such as long-range ordered gibbsite, goethite (FeOOH) and/or hematite (Fe_2O_3). Using the modeling depicted in Figure C-10, and the calculated 11.42 ML discharge volume, roughly 3,700 kg of gibbsite and 1,300 kg of ferrihydrite precipitated in the Animas during the Gold King discharge event (Figure C-11). Based on thermodynamic principles, and not kinetic, Figures C-9 to C-12 depict birnessite as precipitating before ferrihydrite. Manganese oxidation/precipitation kinetics are slow, however, and Mn likely precipitated only well after ferrihydrite precipitation had initiated (Skousen et al. 1998). Also, Mn mineralogy is complex, the actual precipitating mineral species being sensitive to a number of variables. Birnessite is common among these mineral species and a suitable representative of Mn chemistry, but the actual mineralogy might differ. Using birnessite as a proxy for authigenic Mn minerals, roughly 800 kg of Mn minerals precipitated in the Animas during the discharge event.

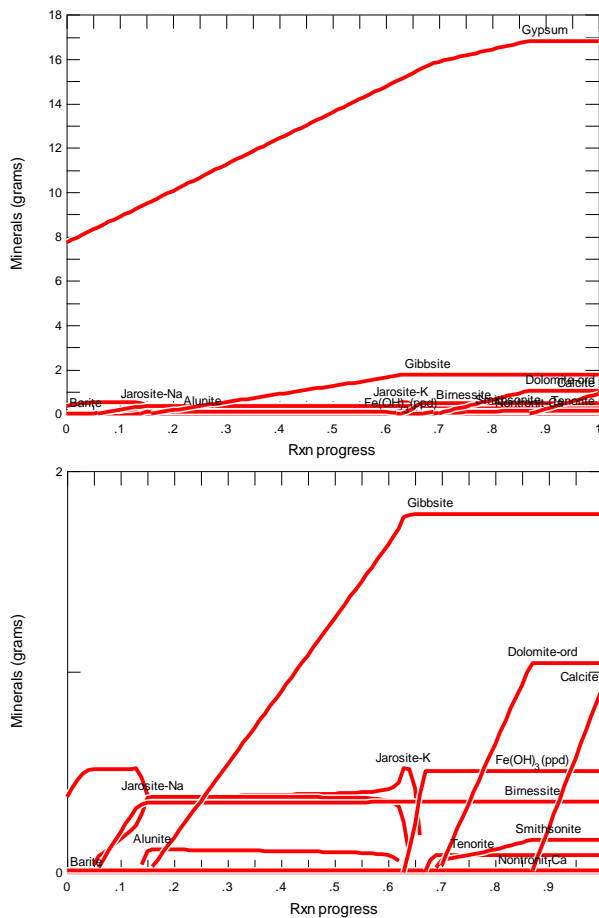


Figure C-9. Simulation of the reaction of “Peak Concentration” release waters (Table C-2) flowing from Cement Creek with Animas River alkalinity: 9A depicts gypsum to be supersaturated initially, consistent with the conservative assumption of disregarding solubility constraints to estimate release water composition; 9B expands the y axis to show detail of the less-massive phases and indicates that Na-jarosite and barite were supersaturated initially as well. To perform this titration simulation, a mass of calcite (CaCO_3) is chosen such that one kilogram of Peak Concentration release water (Table C-2) is saturated with calcite at reaction’s end, consistent with the chemistry of the Animas at ≥ 150 km downstream from Gold King (Figure C-8). Shown here, at reaction’s end gibbsite ($\text{Al}(\text{OH})_3$), ferrihydrite ($\text{Fe}(\text{OH})_3$), birnessite (MnO_2), gypsum ($\text{CaSO}_4 \cdot 2\text{H}_2\text{O}$) and dolomite ($\text{CaMg}(\text{CO}_3)_2$) are expected to have precipitated from solution. The saturated state of the Animas River with gypsum likely was short-lived and, after the sulfate-rich release waters migrated downstream, any gypsum that precipitated would have redissolved. Similarly, dolomite might have dissolved after $[\text{Mg}^{2+}]$ decreased. For these temporary phases, it is likely that they would have entrained trace metals within the lattice as impurities and, as they dissolve, the trace metals would have entered solution. These trace metals then would be scavenged by the hydroxide minerals as they migrated down the Animas as described in the text.

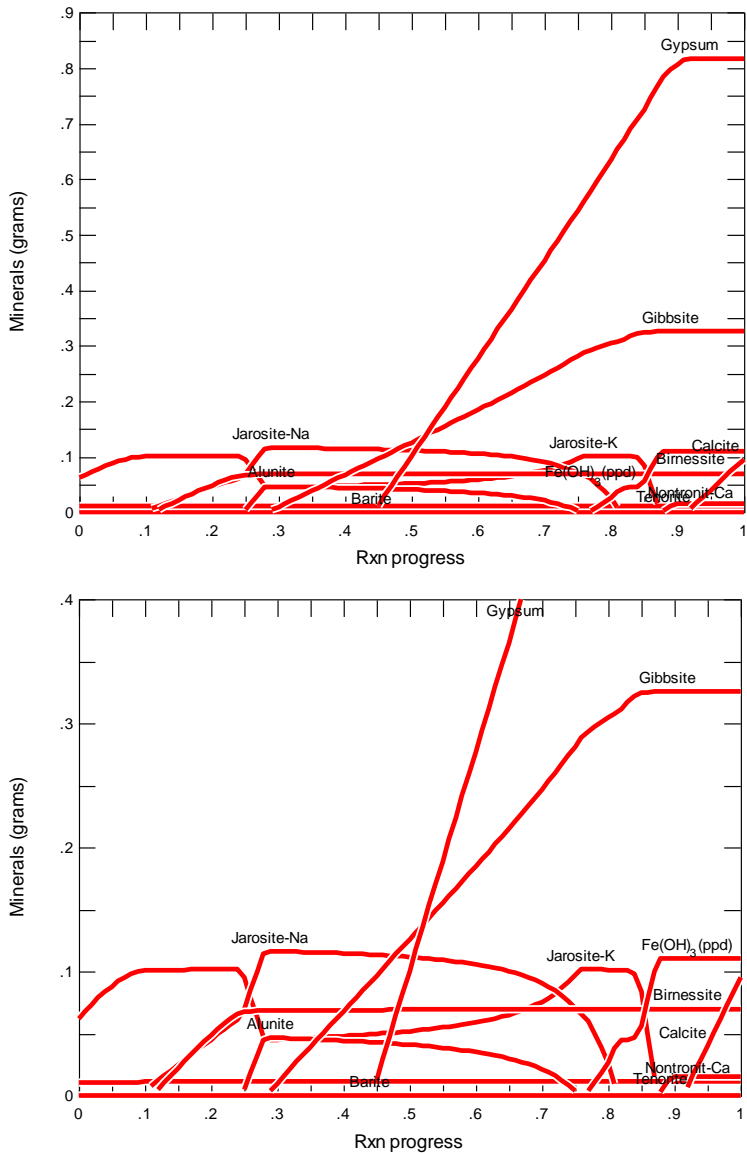


Figure C-10. Simulation of reaction of Plume + Background Mean concentrations with Animas alkalinity. Both graphs depict the same reaction scheme, but with the y axis expanded on the lower to show detail. The masses of minerals precipitated from one kg of solution (plotted on the y axis), along with the calculated discharge of 11.42 ML, can be used to estimate masses of minerals precipitated from the waters released during plume discharge from Cement Creek (Figure C-11).

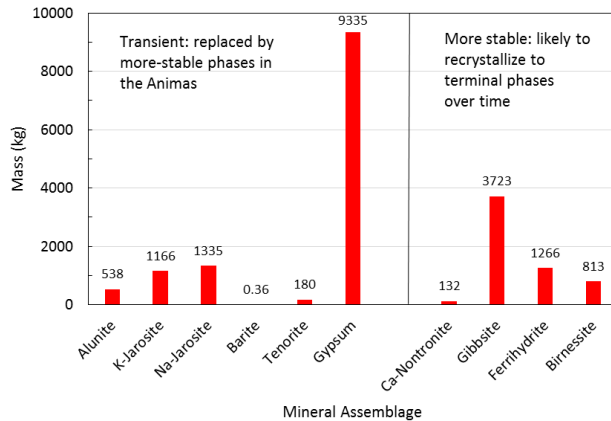


Figure C-11. Masses of minerals precipitated from the release waters (and Cement Creek water flowing with release waters) as these waters intermingled and reacted with Animas River water as estimated from thermodynamic modeling of titration of “Plume + Background Mean” water with calcite alkalinity that is present in the Animas (Figure C-10). Cations initially in alunite and jarosite likely will ultimately enter the more stable gibbsite and ferrihydrite phases, respectively. Whether low trace levels of Ba and Cu will form discrete mineral phases such as barite and tenorite, respectively, or sorb to and isomorphically substitute directly in more-stable mineral phases is uncertain, but ultimately these ions likely will be bound to more stable minerals and their aqueous concentrations maintained at low levels as suggested by modeling described later in this report. Gypsum, likely will be unstable in the low-SO₄⁻ waters of the Animas; comprised of Ca²⁺ and SO₄⁻, these innocuous ions will migrate downstream. Nontronite (Ca_{0.165}Fe₂Al_{0.33}Si_{3.67}O₁₀(OH)₂) is a commonly occurring smectite clay mineral. Gibbsite, ferrihydrite and birnessite are commonly occurring oxyhydroxide minerals and likely will recrystallize to similar, but still more stable, phases over time, as elaborated upon later. The modeled masses of metals bound in the four “more stable” minerals are Fe = 700 kg, Al = 1290 kg, and Mn = 510 kg.

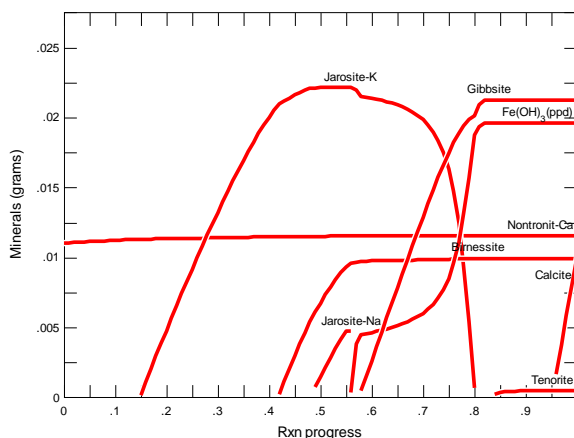


Figure C-12. Simulation of the reaction of Cement Creek Background Mean solutes with Animas alkalinity. It is noteworthy that this thermodynamic modeling suggests jarosite precipitates from solution for Cement Creek background waters alone. Like with the plume waters, however, jarosite is replaced by more stable hydroxide mineral phases.

Downstream chemistry data can be used to evaluate the modeling predictions for the stable minerals described above and in Figures C-9 to C-12. Using thermodynamic data reported in Geochemist's Workbench (Bethke 1998), for samples having detectable Al^{3+} the SIs for gibbsite ($\text{Al}(\text{OH})_3$) are plotted as a function of distance from GKM in Figure C-13. The small positive SI values shown for gibbsite in Figure C-13 indicate the waters are saturated with respect to gibbsite and strongly support that gibbsite colloids were suspended in these water samples, just as predicted by the modeling shown in Figures C-9 to C-12. This equilibrium of Al with $\text{Al}(\text{OH})_3$ in circumneutral waters also has been reported for mine waters by Nordstrom (2011) and many others.

Using thermodynamic data from Geochemist's Workbench (Bethke 1998) and assuming the oxidation state of dissolved Fe to be ferric as justified by kinetic principles (Table C-3), the SIs for ferrihydrite are plotted in Figure C-14 for those Animas samples having detectable levels of dissolved Fe. Figure C-14 indicates saturation with respect to ferrihydrite, also consistent with the modeling depicted in Figures C-9 to C-12.

It is noteworthy that the near-equilibrium calculated for $\text{Al}(\text{OH})_3$ and $\text{Fe}(\text{OH})_3$ in the lower Animas (Figures C-13 and C-14) strongly suggests that, even if Al and/or Fe^{3+} transitory hydroxysulfate minerals were transported to, or formed in, the Cement-Animas confluence, either: i) these hydroxysulfate minerals dissolved and were fully replaced by the more stable hydroxides; or ii) dissolution of these hydroxysulfate phases is slow relative to the precipitation of the relatively stable hydroxide phases. In either case, these hydroxide minerals evidently were effective constraints on solution chemistry in the post-event water samples drawn from the lower Animas.

Mineralogy of Al and Fe^{3+} hydroxysulfates as related to plume discharge into the Animas: As noted above, modelling based solely on thermodynamics suggests that alunite-jarosite type minerals might have precipitated during plume release (Figures C-9 & C-10), and even during normal "background" discharge of Cement Creek (Figure C-12). In fact, it seems doubtful that alunite or jarosite precipitated in the Animas at the confluence with Cement Creek, either during plume discharge or at other times.

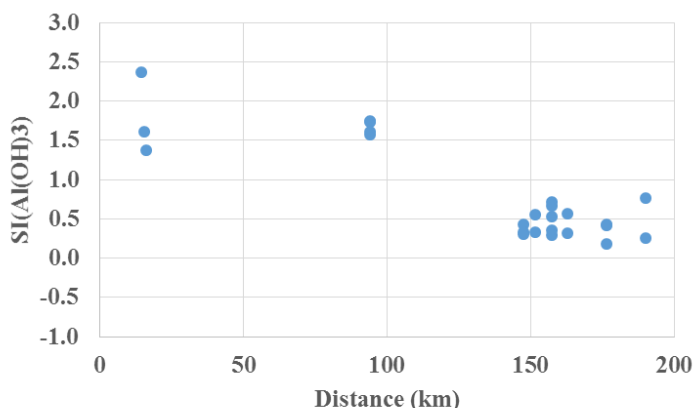


Figure C-13. Saturation indices (SIs) with respect to gibbsite ($\text{Al}(\text{OH})_3$) vs distance from Gold King Mine. The positive SI values suggest saturation with the mineral gibbsite limited the dissolved concentration of aluminum. Many additional samples were analyzed for aluminum (as reflected in the large number of sample points depicted in Figure C-8), but aluminum fell below the reporting limit in these other samples. Few sulfate data are available for the southern Animas but, using the mean of the available SO_4^- data and thermodynamic data from Geochemist's Workbench, the saturation index for alunite indicates gross undersaturation (SI alunite ~ -18).

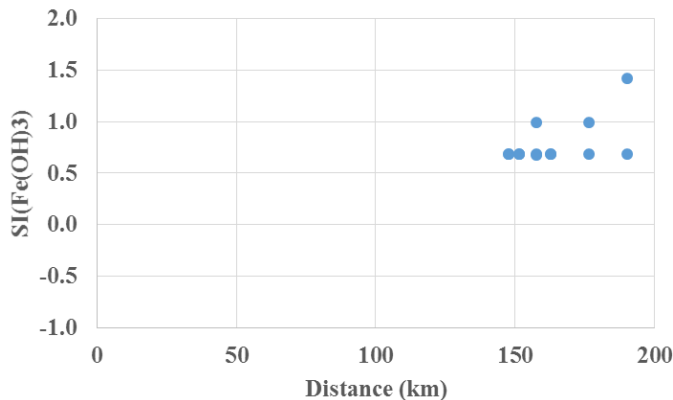


Figure C-14. Saturation indices (SIs) with respect to ferrihydrite ($\text{Fe}(\text{OH})_3$) vs distance from Gold King Mine. These data indicate saturation with respect to ferrihydrite. With most of these SI values falling at about 1.0 and less, these data suggest that reported values for “dissolved Fe” were not overwhelmed by single-grain incipient precipitates passing through the $0.45 \mu\text{m}$ filters employed in this study -- at least for the down-river values shown in this figure. Many additional samples were analyzed for iron (as reflected in the large number of sample points depicted in Figure C-8), but iron fell below the reporting limit in these other samples. Few sulfate data are available for the southern Animas but, using the mean of the available SO_4^- data and thermodynamic data from Geochemist’s Workbench, the saturation index for K-jarosite indicates gross undersaturation (SI jarosite ~ -9).

Addressing alunite and Al hydroxysulfate minerals, according to Bigham and Nordstrom, “for pH values much less than 5.0, dissolved Al behaves as a conservative constituent” (Bigham and Nordstrom 2000). Measurements of pH taken in Cement Creek at Silverton on August 12 and 14, 2015, seven and nine days after the release, were pH = 3.63 and 3.60, so Al hydroxysulfate precipitation was unlikely in Cement Creek. When pH is increased to >5.0 , precipitation kinetics seem to favor formation of hydrobasaluminite ($\text{Al}_4(\text{SO}_4)(\text{OH})_{10} \cdot 10\text{H}_2\text{O}$) and basaluminite ($\text{Al}_4(\text{SO}_4)(\text{OH})_{10} \cdot 4\text{H}_2\text{O}$) because these minerals are found more commonly in low-temperature mixing zones while alunite is dominantly observed in acidic hypersaline lakes and zones of hydrothermal alteration (Bigham and Nordstrom 2000). The aluminite minerals are metastable with respect to alunite and gibbsite (Bigham and Nordstrom 2000). Based on the presence of gibbsite and absence of alunite at reactions’ completion in Figures C-9 to C-12, any aluminite minerals that might have precipitated during admixing of plume and Animas waters would be expected to recrystallize to gibbsite. Bolstering this inference, Figures C-9 to C-12 depict modeling of closed geochemical systems, wherein SO_4^- is not lost to surroundings; considering that SO_4^- was diluted in the open system of the Animas River, gibbsite would be expected to be even more stable relative to alunite than depicted in these figures. All of this reasoning is strongly supported by the observation that the lower Animas was near equilibrium with gibbsite during the few sampling events when Al was at detectable levels (Figure C-13).

Addressing jarosite and Fe^{3+} hydroxysulfate minerals, remembering the arguments presented earlier, that Fe dominantly was in reduced form in GKM water, and Fe oxidation in Cement Creek probably was slow relative to its residence time in Cement Creek, it is unlikely that ferric hydroxysulfate minerals would have formed to any considerable extent in Cement Creek.

However, even if there was some ferric Fe, i) infrequent detection of jarosite in all but the most acidic settings, ii) common observation of supersaturation with jarosite in less acidic settings, and iii) the typically well-ordered lattice of jarosite, all suggest that kinetic barriers might impede jarosite under all but the most acidic environmental conditions (Bigham and Nordstrom 2000). In contrast, schwertmannite ($\text{Fe}_8\text{O}_8(\text{OH})_6\text{SO}_4$) commonly is observed in waters having $2 < \text{pH} < 4$ (Bigham and Nordstrom 2000). Based

on experimental and observational evidence, Bigham and coworkers have proposed that jarosite tends to form in the range $1.5 < \text{pH} < 2.5$, schwertmannite in the range $2.5 < \text{pH} < 5.5$, and ferrihydrite is favored at $\text{pH} > 5.5$ (Bigham et al. 1996, Bigham et al. 1996). So if some Fe was present in ferric oxidation state in GKM, considering that Cement Creek pHs (3.60-3.63 at Silverton) fall in the range for the formation of schwertmannite over jarosite, schwertmannite would be more likely to form in Cement Creek than jarosite. When the plume waters mixed with the more voluminous alkaline waters of the Animas, pH likely ascended to > 5.5 and under these conditions, ferrihydrite would be favored over jarosite. Schwertmannite is metastable and, even if it did form in the Animas, it likely recrystallized to ferrihydrite or a stable oxide phase like goethite or hematite.

One possibility that cannot be dismissed is that alunite-jarosite-type minerals were present in the spoil or stream banks that were eroded by the plume. If these minerals were suspended in the plume surge, it remains possible that these minerals could have been carried in suspension to the Animas River. It is noteworthy, however, that there are large documented occurrences of jarosite in the Animas watershed. One such occurrence is mapped in the Mineral Creek watershed, whose confluence with the Animas is downstream of Cement Creek. Here, Yager et al. (2000) mapped a major alteration zone on the flanks of Mount Moly in the Mineral Creek watershed as “quartz-sericite-pyrite (Q-S-P) altered host rock, with jarosite- and goethite-stained surfaces.”

Trace element sorption in the incipient solid/mineral phases and long-term occlusion in crystalline oxides: Unlike aluminosilicate clays, which have substantial permanent surface charges, oxide solids dominantly have surface charges that vary with pH and ionic strength (I); at low pH values charge is positive, at high pH values charge is negative, and there is a pH (unique to each oxide solid) at which the surface has a “zero point of charge” (ZPC). The ZPC for ferrihydrite is about 7.9-8.2 (Dzombak and Morel 1990), for goethite it is about 9.0-9.7 (Sverjensky 1994), for hematite about 8.5 (Sverjensky 1994), and for gibbsite about 8.0-9.2 (Hsu 1989) (Table C-5). As a consequence of this variable surface charge, the affinity of these solids for sorbing most cationic metals at low pH values, like those in Cement Creek, is very low. In contrast, at circum-neutral pH values like those in the Animas River, trace metals are scavenged by Fe, Al and Mn oxide solids (Benjamin and Leckie 1981).

Superimposed on this surface-charge effect, trace metals have an intrinsic affinity for oxide solids as well, and this affinity varies among the oxide solids. For example, Cu and Zn have been reported to have greater affinities for Al oxides than for Fe oxides, but Pb sorbs to Fe oxides more so than Al oxides (Coston et al. 1995, Karthikeyan et al. 1997). For freshly precipitated amorphous to short-range ordered $\text{Fe}(\text{OH})_3$, similar to the colloids precipitated in the Animas River, at low concentrations of sorbing metals, Benjamin and Leckie have reported relative affinities in the order $\text{Pb} > \text{Cu} > \text{Zn} > \text{Cd}$ (Benjamin and Leckie 1981). This ordering is consistent with that reported by Ford et al. for freshly precipitated $\text{Fe}(\text{OH})_3$ of $\text{Pb} > \text{Ni} > \text{Mn} = \text{Cd}$ (Ford et al. 1997).

Table C-5. Typical particle size, diagenetic times and zero point of charge for selected Al and Fe oxides under surficial conditions

Mineralization Phase	Size	Formation Time	Time	Zero Point of	ZPC	
	Size Range (1)	Reference	Scale (6)	Reference	Charge	Reference
Aluminum Oxide						
amorphous Al(OH) ₃ nucleation	<100 nm	2	≤24 hours	4	8.0-9.2	11
amorphous Al(OH) ₃ flocs/aggregates	2 μm - 2 mm	3 & 4	seconds to hours		8.0-9.2	11
microcrystalline gibbsite aggregates	2 μm - 2 mm	3 & 4	2 to 20 weeks	4	8.0-9.2	11
crystalline gibbsite aggregates	2 μm - 2 mm	3 & 4	~2 years	4	8.0-9.2	11
kaolinitic clay aggregates	2 μm - 2 mm	3 & 4	years to millenia	7		
Ferric Oxide						
amorphous Fe(OH) ₃ nucleation	2 - 7 nm	5	seconds to hours	8	7.9 - 8.2	12
2-line ferrihydrite flocs/aggregates	2 μm - 2 mm	3	seconds to hours		7.9 - 8.2	12
6-line ferrihydrite aggregates	2 μm - 2 mm	3	≥1 - 3 year	9	7.9 - 8.2	12
goethite or hematite aggregates	2 μm - 2 mm	3	≥1 - 3 year	9 & 10	9.0-9.7 or 8.5	13

Explanation

- 1) Single grain for incipient nucleation, aggregates for later phases, as is their habit
- 2) Hsu, 1989, p. 340
- 3) Schwertmann & Taylor, 1989, p. 417; given common, extensive co-substitution of Al & Fe in oxides
- 4) Nordstrom et al., 1984, p. 35
- 5) Schwertmann & Taylor, 1989, p. 392; Cornell and Schwertmann, 2003, p. 78
- 6) Formation time scale is under a variety of laboratory idealized surficial conditions. Actual times can vary drastically.
- 7) Langmuir, 1997, p. 252
- 8) Cornell & Schwertmann, 2003, p. 207
- 9) Cornell & Schwertmann, 2003, p. 207; Kukkadapu, et al., 2003
- 10) Cornell & Schwertmann, 2003, p. 207; Kukkadapu, et al., 2003; Schwertmann & Cornell, 2000, p. 110
- 11) Hsu, 1989
- 12) Dzombak & Morel, 1990
- 13) Sverjensky, 1994

While partitioning of trace metals on oxide solids is complex, research has converged toward an internally consistent modeling approach to account for both the intrinsic affinity and electrostatic components of the phenomenon. Particularly relevant for the Gold King release, Dzombak and Morel (Dzombak and Morel 1990) have consolidated numerous studies on the sorption of metals on amorphous Fe oxide over a range of pH values and trace-metal concentrations as described by:

$$K_e = \frac{\{(SOMe^+)(H^+)\}}{\{(SOH)(Me^{2+})\}} \exp\left(\frac{-zF\Psi_o}{RT}\right) \quad (10)$$

where K_e is a sorption constant, $(SOMe^+)$ is the activity of metal Me^{2+} on the oxide solid surface (molar), (SOH) is the activity of protonated surface species (molar), (Me^{2+}) is the trace metal activity in bulk solution (molar), z is the elementary electrostatic charge of the ion (2 in this example), Ψ_o is the difference in electrostatic potential between the sorption layer and the bulk liquid, a function of deviation of pH from ZPC (V), F is the Faraday Constant (96,485 J/(V mol)), R is the Universal Gas Constant (8.314 J/(K mol)) and T is temperature (K). The equilibrium concentration of metals can be determined by manipulating

Equation 10 and transposing (Me) and K_e (Annex C3). Values for the chemical component of Equation 10 necessary to estimate dissolved concentrations of As, Cu, Pb and Zn in sorptive equilibrium with specified concentrations of ferrihydrite, are summarized from Dzombak and Morel (1990) in Bethke (1998). Values for the electrostatic component of Equation 10 can be determined from graphs and tables reported in Dzombak and Morel. Using total concentration data for four locations in the lower Animas and variables quantitated with Equation 10, dissolved concentrations of As, Cu, Pb and Zn are estimated and compared to observed dissolved concentrations in Table C-5. Looking at the “Modeled/Peak Dissolved Ratios” in Table C-6, the modeled dissolved cations agree with the observed values at all four river locations as they should considering that dissolved values are used to solve for sorption site density in Equation 10 (Annex C3). In contrast, this model predicts higher concentrations of the oxyanion AsO_4^- than are reported for these river locations. This probably is due at least partially to having modeled sorption on only one of three As-sorption sites. Some of the deviation might also be due to As binding to Al-oxide colloids, or another phase. Fortunately, the observed values of dissolved As are very low (Table C-6), even less than the low values predicted by this sorption-modeling effort.

Mineral recrystallization to more stable phases and the long-term occlusion of trace elements: As oxide solids age, they undergo crystallization to more thermodynamically stable forms (Figure C-5), a process commonly called Ostwald ripening (Steeffel and van Cappellen 1990). For Fe oxide solids, freshly precipitated amorphous $\text{Fe}(\text{OH})_3$ will order itself to short-range ordered $\text{Fe}(\text{OH})_3$, then to longer-range order to form the mineral ferrihydrite ($\text{Fe}(\text{OH})_3$), and then to still more stable mineral phases such as goethite and hematite (Figure C-15). Likewise, as freshly precipitated Al oxides age, they undergo recrystallization from amorphous \rightarrow microcrystalline \rightarrow crystalline gibbsite (Figure C-16). As these Fe and Al minerals age and recrystallize to more stable phases, they equilibrate with progressively lower solution activities (Nordstrom et al. 1984). These aged mineral phases are widely distributed in soils and sediments, in contaminated and pristine settings alike, throughout the environment.

Typical times for recrystallization and growth of selected authigenic Al and Fe oxides, as well as typical particle sizes, have been culled from the literature (Nordstrom et al. 1984, Hsu 1989, Schwertmann and Taylor 1989, Langmuir 1997, Schwertmann and Cornell 2000, Cornell and Schwertmann 2003, Kukkadapu et al. 2003) and summarized in Table C-5. Particle sizes listed in Table C-5 start with single-grain for incipient nucleation and then flocs/aggregates, as this is the habit for these minerals (Hsu 1989, Schwertmann and Taylor 1989). Particle density of these minerals will fall in the range of 3.9 g/cm^3 (Schwertmann and Taylor 1989). The aggregates listed in Table C-5 might have considerably lower bulk densities than this value for the amorphous phases but will approach the particle density value as aging occurs and mineral grains inter-grow and become progressively more intimately inter-connected.

The rate at which these colloids floc, sorb and settle from the water column will not be a function solely of density and particle size, but also surface charge and concentrations of counter-ions in solution. Surface charge is a function of pH; the further pH is from the zero-point-of-charge (ZPC), the greater the surface charge. Oxide minerals of Al and Fe generally have ZPCs of 8 and higher (Table C-5). For an upper Animas pH of ~ 6.5 to ~ 7.5 then, these colloids would have been mildly positively charged and relatively high concentrations of divalent SO_4^{2-} would have enhanced flocculation, aggregation and settling. In the lower Animas, pH generally is ~ 8.3 , decreasing surface charge on these colloids. Coupled with possibly lower SO_4^{2-} in the lower Animas due to dilution and higher concentrations of monovalent HCO_3^- from carbonate dissolution, colloid flocculation might have been less effective in the lower Animas, perhaps fostering suspended transport in the water column.

Table C-6. Estimation of dissolved metal concentrations in equilibrium with Fe(OH)₃ solids at the pH of the Animas River and Comparison with Estimated Peak Values (including background) at Four River Locations

Site		Durango	NAR	Aztec	Farmington
Distance from GKM (km)		95	132	163	190
Date/Time of Plume Peak		8/7/15 2:00 AM	8/7/15 2:30 PM	8/8/15 3:00 AM	8/8/15 10:45 AM
Peak Total Concentrations (mg/l)	Fe	226.27	76.40	33.76	17.36
	As	0.11	0.06	0.03	0.02
	Cu	0.47	0.23	0.12	0.08
	Pb	3.14	1.41	0.54	0.39
	Zn	1.18	0.54	0.42	0.31
Peak Dissolved Concentrations (mg/l)	Fe	2.2770	0.4500	0.0449	0.0199
	As	0.0008	0.0004	0.0006	0.0009
	Cu	0.0071	0.0023	0.0013	0.0019
	Pb	0.0004	0.0031	0.0002	0.0002
	Zn	0.1399	0.0110	0.0028	0.0033
	pH (SU)	7.42	8.00	7.90	8.11
Log K _e	As	-9.68	-10.40	-10.25	-10.58
	Cu	-3.34	-2.96	-3.04	-2.93
	Pb	-5.10	-4.72	-4.80	-4.69
	Zn	-1.44	-1.06	-1.14	-1.03
Modeled Dissolved Concentrations (mg/l)	As	0.1050	0.0577	0.0260	0.0193
	Cu	0.0071	0.0023	0.0013	0.0019
	Pb	0.0004	0.0031	0.0002	0.0002
	Zn	0.1400	0.0110	0.0028	0.0033
Modeled/Peak Dissolved Ratio	As	127.29	144.26	44.77	21.71
	Cu	1.00	1.00	1.00	1.00
	Pb	1.00	1.00	1.00	1.00
	Zn	1.00	1.00	1.00	1.00

Explanation: At four Animas River locations, for which calculations indicate Gold King acidity had been neutralized, total concentrations of Fe, As, Cu, Pb and Zn, and pH, are used as input to estimate dissolved concentrations of As, Cu, Pb and Zn invoking electrostatic and chemical equilibrium with suspended colloidal Fe(OH)₃. Observed dissolved values are used to solve for sorption site density in this model (see Annex C3).

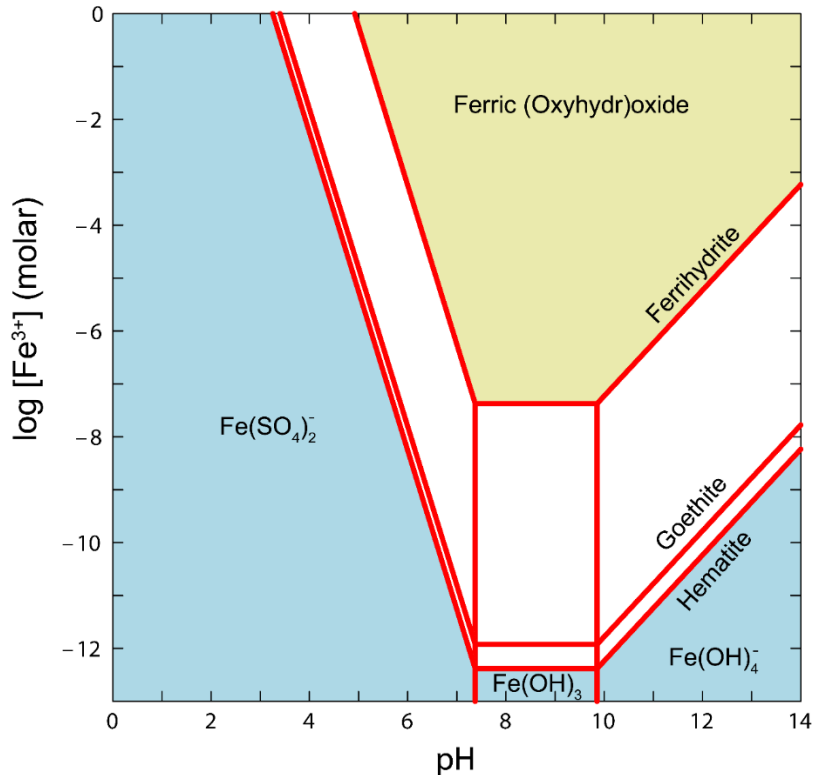


Figure C-15. Stability fields of ferric oxide minerals as a function of $[\text{Fe}^{3+}]$ and pH, with $[\text{SO}_4^-] = 90$ mg/l, similar to conditions expected in the upper Animas. Generally, as waters become supersaturated with mineral phases, say by an increase in pH, less thermodynamically stable mineral phases will precipitate first, e.g., amorphous $\text{Fe}(\text{OH})_3$ or stoichiometric ferrihydrite. Over time these incipient mineral phases recrystallize to more stable forms, e.g., goethite or hematite as shown here. As these minerals recrystallize to more stable forms, they equilibrate with progressively lower solution activities. Thermodynamic data as reported in Geochemist's Workbench (Bethke 1998).

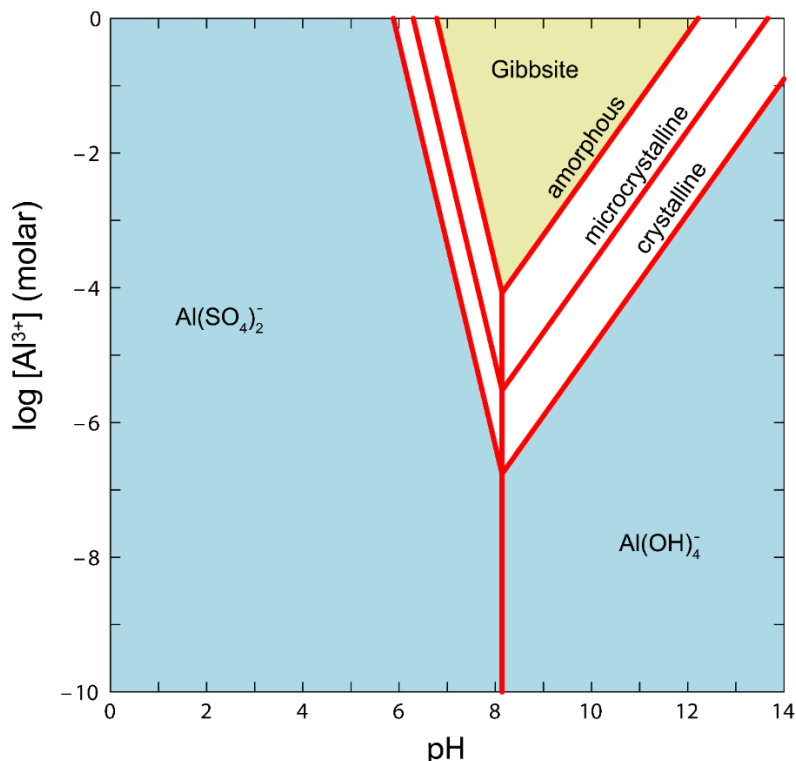


Figure C-16. Stability fields of aluminum oxide minerals as a function of $[Al^{3+}]$ and pH, with $[SO_4^-] = 90$ mg/l, similar to conditions expected in the upper Animas. Generally, as waters become supersaturated with mineral phases, say by an increase in pH, less thermodynamically stable mineral phases will precipitate first, e.g., amorphous $Al(OH)_3$. Over time these incipient mineral phases recrystallize to more stable forms, e.g., microcrystalline and crystalline gibbsite. As these minerals recrystallize to more stable forms, they equilibrate with progressively lower solution activities. Thermodynamic data for Al as reported in Nordstrom et al. (Nordstrom et al. 1984) with additional data from Geochemist's Workbench (Bethke 1998).

As incipient mineral solids age to stable crystalline minerals, progressively larger fractions of trace metals in these minerals become bound nonreversibly or hysterically (Ford et al. 1997). As these solids crystallize and recrystallize, their relative affinities for metals changes but overall the reversibility of metal binding continues to diminish (Coughlin and Stone 1995). For example, Ford et al. noted that, as the $Fe(OH)_3$ aged, affinity of the solid for Mn and Ni increased, but the affinity for Pb and Cd decreased (Ford et al. 1997). And the relative affinities of thermodynamically stable minerals for sorbing metals varies from that of $Fe(OH)_3$ as well. For example, Forbes et al. (1976) reported relative affinities for goethite as $Cu > Pb > Zn > Co > Cd$ which is consistent with that reported by Coughlin and Stone (1995), $Cu > Pb > Ni = Co > Mn$. As a result of this long-term recrystallization to more stable thermodynamic minerals, and concomitant hysteric binding of trace metals, the long-term fate of much of the released trace metals is to be bound in the lattices of stable Fe and Al oxide minerals.

Placing the release in context of long-term releases from Gold King and similar mines: Over the long term, all mines discharge water at the same rate that they are recharged. The minimum rate of recharge to a mine generally is determined by the (i) regional groundwater recharge rate, (ii) area of the mine, and (iii) depth of the mine. Sometimes, nearby mines might divert recharge away from a neighboring mine that otherwise would enter the mine or increase recharge to the mine, effectively decreasing or increasing the mine's footprint. And sometimes, if a mine approaches a surface water body, excess water might leak into

the mine. Barring complicating factors, however, recharge to mines can be reasonably estimated from information on precipitation-recharge rate, mine area and mine depth alone.

For abandoned mines, often the largest part of discharge commonly is not visible as discrete surface flow, instead winnowing its way to the surface at numerous small stream-bank weeps and as diffuse stream-bottom discharge. According to the owner of GKM, at one time the main discrete discharge from GKM was 7 gallons per minute (gpm) (Castillo 2015). The owner reports that, when hydrologic practices changed in an adjacent mine (e.g., installing bulkheads in the American Tunnel), the main discrete discharge from GKM increased to 250 gpm (950 liters/minute) (Castillo 2015). A rate of 250 gpm roughly equates to 1.4 million liters per day, roughly 12% of the estimated August 5 release volume of 11 million liters. So at the recent rate of discharge, the volume of the GKM release was being released from GKM every eight days.

Put in this context, given normal variability of environmental systems, the contamination released by the GKM breach was not fated to be vaulted away for centuries, but would have been expected to have residence times in the mine of days or weeks before discharge to Cement Creek.

Analytical considerations

- 1) When characterizing mining discharges, always measure pH (in the field) and dissolved Fe^{2+} , Fe^{3+} , Al^{3+} and Mn^{2+} . The dissolved metals should be sampled using a 0.2 μm filter in the field. These data allow acidity to be calculated. Acidity characterizes the AMD capacity to maintain acidic pH values, conditions under which toxic-metal mobility is high. Knowledge of iron valence not only is necessary for calculating acidity, but also affects rates at which acidity releases free H^+ , thereby dropping pH. Also knowledge of Fe valence allows calculation of the potential for precipitation or dissolution of ferric and ferrous minerals.
- 2) When characterizing mining discharges, measure SO_4^- so that ionic strength, activity coefficients and complexation can be calculated easily.
- 3) When there is an AMD release, and knowledge of the fate of the release metals is desired, collect samples of the streambed upgradient for background and downgradient to below where the AMD staining (e.g., “yellowboy”) is evident. Consider running two selective extractions on these sediment samples: i) oxalate extraction to characterize incipient oxide solids and the AMD metals in this phase; and ii) dithionite extraction to characterize the pre-existing authigenic oxide minerals, and their metals, as a reference to gauge the magnitude by which release metals exceed the pre-existing state of the streambed.
- 4) When characterizing mining discharges, measure acidity in the water phase with a heated pre-oxidation step followed by titration with a base. For example, EPA Method 305.1 is intended for this purpose.

References

- Anthony, J. W., R. A. Bideaux, K. W. Bladh, Nichols and M.C. (1997). Handbook of Mineralogy Volume III. Chantilly, VA, Mineralogical Society of America.
- Benjamin, M. M. and J. O. Leckie (1981). "Multiple-site adsorption of Cd, Cu, Zn, and Pb on amorphous iron oxyhydroxide." *Journal of Colloid and Interface Science* **79**: 209-221.
- Bethke, C. M. (1998). *The Geochemist's Workbench, Release 3.0*. Urbana-Champaign, IL, U. Illinois.
- Bigham, J. M. and D. K. Nordstrom (2000). "Iron and aluminum hydroxysulfates from acid sulfate waters." *Reviews in Mineralogy and Geochemistry* **40**: 351-403.
- Bigham, J. M., U. Schwertmann and G. Pfab (1996). "Influence of pH on mineral speciation in a bioreactor simulating acid mine drainage." *Applied Geochemistry* **11**: 845-849.
- Bigham, J. M., U. Schwertmann, S. J. Traina, R. L. Winland and M. Wolf (1996). "Schwertmannite and the chemical modeling of iron in acid sulfate waters." *Geochimica et Cosmochimica Acta* **60**: 2111-2121.
- Brophy, G. P. and M. F. Sheridan (1965). "Sulfate Studies IV: the jarosite-natrojarosite-hydronium jarosite solid solution series." *The American Mineralogist* **50**: 1595-1607.
- Castillo, M. (2015). Gold King Mine Owner: 'I foresaw disaster' before spill. CNN website: <http://www.cnn.com/2015/08/13/us/colorado-epa-animas-river-spill-owner/index.html>.
- Church, S. E., P. von Guerard and S. E. Finger (2007). Integrated investigation of environmental effects of historical mining in the Animas River watershed, San Juan County, Colorado. E5. Mine inventory and compilation of mine-adit chemistry data. , US Geological Survey.
- Cornell, R. M. and U. Schwertmann (2003). *The Iron Oxides*. Darmstadt, Germany, Wiley-VCH.
- Coston, J. A., C. C. Fuller and J. A. Davis (1995). "Pb and Zn adsorption by a natural aluminum- and iron-bearing surface coating on an aquifer sand." *Geochimica et Cosmochimica Acta* **59**: 3535-3547.
- Coughlin, B. R. and A. T. Stone (1995). "Nonreversible adsorption of divalent metal ions (Mn, Co, Ni, Cu, and Pb) onto goethite: effects of acidification, Fe addition, and picolinic acid addition." *Environmental Science & Technology* **29**: 2445-2455.
- Desborough, G. A. and D. B. Yager (2000). Acid-neutralizing potential of igneous bedrocks in the Animas River headwaters, San Juan County, Colorado. U. S. G. Survey.
- Dzombak, D. A. and F. M. M. Morel (1990). *Surface Complex Modeling: Hydrous Ferric Oxide*. New York, NY, John Wiley & Sons.
- Forbes, E. A., A. M. Posner and J. P. Quirk (1976). "The specific adsorption of divalent Cd, Co, Cu, Pb, and Zn on goethite." *Journal of Soil Science* **27**: 154-166.
- Ford, R. G., P. M. Bertsch and K. J. Farley (1997). "Changes in transition and heavy metal partitioning during hydrous iron oxide aging." *Environmental Science & Technology* **31**: 2028-2033.

- Gobla, M. J. and C. M. Gemperline (2015). Technical evaluation of the Gold King Mine incident. Reclamation: Managing Water in the West. Denver, CO, U.S. Department of the Interior, Bureau of Reclamation: 64.
- Hem, J. D. (1989). Study and Interpretation of the Chemical Characteristics of Natural Water. Washington, D.C., U.S. Geological Survey.
- Hsu, P. H. (1989). Chapter 7 Aluminum oxides and hydroxides. Minerals in Soil Environments. J. B. Dixon and S. B. Weed. Madison, WI, Soil Science Society of America: 331-378.
- Karthikeyan, K. G., H. A. Elliott and F. S. Cannon (1997). "Adsorption and coprecipitation of copper with the hydrous oxides of iron and aluminum." Environmental Science & Technology **31**: 2721-2725.
- Kukkadapu, R. K., J. M. Zachara, J. K. Fredrickson, S. C. Smith, A. C. Dohnalkova and C. K. Russell (2003). "Transformation of 2-line ferrihydrite to 6-line ferrihydrite under oxic and anoxic conditions." American Mineralogist **88**: 1903-1914.
- Langmuir, D. (1997). Aqueous Environmental Geochemistry. Upper Saddle River, NJ, Prentice Hall.
- Lindsay, W. L. (1979). Chemical equilibria in soils. New York, NY, John Wiley & Sons.
- Luedke, R. G. and W. S. Burbank (1999). Geologic map of the Silverton and Howardsville quadrangles, southwestern Colorado. U. S. G. Survey.
- Nordstrom, D. K. (2011). "Hydrogeochemical processes governing the origin, transport and fate of major and trace elements from mine wastes and mineralized rock to surface waters." Applied Geochemistry **26**: 1777-1791.
- Nordstrom, D. K., S. D. Valentine, J. W. Ball, L. N. Plummer and B. F. Jones (1984). Partial compilation and revision of basic data in the WATEQ programs. Water-Resources Investigation Report 84-4186. Menlo Park, CA, U.S. Geological Survey: 43.
- Olivarius-McAllister, C. (2013). A legacy that won't die. The Durango Herald. <http://www.durangoherald.com/article/20130803/NEWS01/130809830/-1/mining/A-legacy-that-won't-die-&template=minegart>.
- Parizek, R. R., W. B. White and D. Langmuir (1971). Hydrogeology and geochemistry of folded and faulted rocks of the central Appalachian type and related land use problems. University Park, PA, Penn State University.
- Rose, A. W. and C. A. I. Cravotta (1998). Geochemistry of Coal Mine Drainage. Coal Mine Drainage Prediction and Pollution Prevention. Harrisburg, Pennsylvania, Pennsylvania Department of Environmental Protection: 1-1 to 1-22.
- Rose, A. W., Hawkes, Herbert E., Webb, John S. (1979). Geochemistry in Mineral Exploration, 2nd Edition. New York, NY USA, Academic Press.
- Schemel, L. E. and M. H. Cox (2005). Descriptions of the Animas River-Cement Creek Confluence and Mixing Zone near Silverton, Colorado, during the Late Summers of 1996 and 1997, U.S. Geological Survey.
- Schwertmann, U. and R. M. Cornell (2000). Iron Oxides in the Laboratory. New York, NY, Wiley-VCH.

- Schwertmann, U. and R. M. Taylor (1989). Chapter 8 Iron oxides. Minerals in Soil Environments. J. B. Dixon and S. B. Weed. Madison, WI, Soil Science Society of America: 380-438.
- Scott, K. M. (1987). "Solid solution in, and classification of, gossan-derived members of the alunite-jarosite family, northwest Queensland, Australia." The American Mineralogist **72**: 178-187.
- Singer, P. C. and W. Stumm (1970). "Acidic mine drainage: The rate-determining step." Science **167**: 1121-1123.
- Skousen, J., A. W. Rose, G. Geidel, J. Foreman, R. Evans and W. Hellier (1998). A Handbook of Technologies for Avoidance and Remediation of Acid Mine Drainage. Morgantown, WV, The National Mine Land Reclamation Center, West Virginia University: 131.
- Steeffel, C. I. and P. V. van Cappellen (1990). "A new kinetic approach to modeling water-rock interaction: the role of nucleation, precursors, and Ostwald ripening." Geochimica Et Cosmochimica Acta **54**(10): 2657-2677.
- Stumm, W. and W. W. Morgan (1981). Aquatic Chemistry. New York, NY, Wiley-Interscience.
- Sverjensky, D. A. (1994). "Zero-point-of-charge prediction from crystal chemistry and solvation theory." Geochimica Et Cosmochimica Acta **58**: 3123-3129.
- U.S.G.S. (1982). 1:100000-scale metric topographic map of Silverton, CO. 30x60 Minute Series. Reston, VA, U.S. Geological Survey.
- US-Mining. (2016). "San Juan County, CO Mines. <http://www.us-mining.com/colorado/san-juan-county>."
- Washington, J. W., D. M. Endale, L. P. Samarkina and K. E. Chappell (2004). "Kinetic control of oxidation state at thermodynamically buffered potentials in subsurface waters." Geochimica Et Cosmochimica Acta **68**: 4831-4842.
- Yager, B. B. and D. J. Bove (2002). Generalized geologic map of part of the upper Animas River watershed and vicinity, Silverton, Colorado, U.S. Geological Survey.
- Yager, D. B., A. M. Mast, P. L. Verplanck, D. J. Bove, W. G. Wright and P. L. Hagerman (2000). Natural Versus Mining-Related Water Quality Degradation to Tributaries Draining Mount Moly, Silverton, Colorado. Fifth International Conference on Acid Rock Drainage (ICARD2000), Denver, CO, Society for Mining, Metallurgy, and Exploration, Inc.
- Youtube. (2015). "EPA releases Gold King Mine blowout footage: <https://www.youtube.com/watch?v=ZBIR05tDCbI>."

Annex C1: Fe²⁺ oxidation kinetics of Singer and Stumm

Singer and Stumm (1970) report the abiotic oxidation of Fe²⁺ in water by dissolved O₂ to proceed at a rate according to:

$$\frac{-d[Fe^{2+}]}{dt} = k[Fe^{2+}][O_2][OH^-]^2 + k'[Fe^{2+}][O_2] \quad (1)$$

Rearranging:

$$\frac{d[Fe^{2+}]}{[Fe^{2+}]} = -\{k[O_2][OH^-]^2 + k'[O_2]\}dt \quad (2)$$

Integrating:

$$\int \frac{d[Fe^{2+}]}{[Fe^{2+}]} = -\{k[O_2][OH^-]^2 + k'[O_2]\} \int dt \quad (3)$$

$$\ln \frac{[Fe^{2+}]_t}{[Fe^{2+}]_0} = -[O_2]\{k[OH^-]^2 + k'\}\Delta t \quad (4)$$

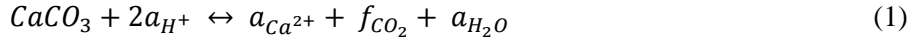
Rearranging and solving for half-life:

$$T_{1/2} = \frac{\ln 2}{[O_2]\{k[OH^-]^2 + k'\}} \quad (5)$$

Singer and Stumm (1970) report values of k and k', [OH⁻] is specified by designating pH, and [O₂] is taken as in equilibrium with the atmosphere, 0.208 atmospheres.

Annex C2: Reactions and equations for calculating calcite and dolomite saturation

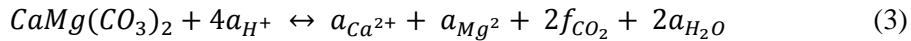
For calcite reacting with water:



where CaCO_3 is calcite, a is activity and f is fugacity. Measures of pH are measures of H^+ activity, $a_{\text{H}^+} = -\log(\text{pH})$. Activity of other solutes is calculated from concentration by multiplying concentration by the activity coefficient γ . The value of γ is calculated from the extended Debye-Huckel equation (Stumm and Morgan 1981). Likewise f is calculated from partial pressure multiplying partial pressure by the fugacity coefficient; for these calculations, the fugacity coefficient is taken as unity. In these calculations P_{CO_2} is taken as $10^{-3.4}$ atmospheres, the August 2015 monthly mean CO_2 partial pressure recorded at the NOAA, Mauna Loa, HI observatory (<http://www.esrl.noaa.gov/gmd/ccgg/trends/>). Using the thermodynamic data reported in Parizek et al. (1971), $\log K$ for Reaction 1 is -9.86. Then the saturation index for calcite, SI_{calcite} is:

$$SI_{\text{calcite}} = \log \left\{ \frac{a_{\text{Ca}^{2+}} f_{\text{CO}_2}}{a_{\text{H}^+}^2 10^{9.86}} \right\} \quad (2)$$

By analogy with calcite, the governing equations for dolomite saturation are:



where $\text{CaMg}(\text{CO}_3)_2$ is dolomite and $\log K = -19.71$. Then:

$$SI_{\text{dolomite}} = \log \left\{ \frac{a_{\text{Ca}^{2+}} a_{\text{Mg}^{2+}} 2f_{\text{CO}_2}^2}{a_{\text{H}^+}^4 10^{19.71}} \right\} \quad (4)$$

Annex C3: Solving for dissolved metals in equilibrium with Fe(OH)₃ colloids

Using Zn²⁺ at Durango as an example:

$$\text{Log } K_{strong} + \frac{zF\Psi}{RT} = \text{Log } K_{app} = -0.96 \quad (1)$$

$$K_{app} = 10^{-0.96} = \frac{a_{Zn^{2+}[>FeOH]}}{a_{H^+[>FeOZn^+]}} \quad (2)$$

The variables $a_{Zn^{2+}}$ and a_{H^+} are measured.

Assuming sorbing metals do not interfere with one another,

$$[>FeTot] = [>FeOH] + [>FeOZn^+] \quad (3)$$

Where [>FeTot] represents the total concentration of potential sorption sites for Zn²⁺, both unoccupied and occupied. Dzombak and Morel offer a method to calculate [>FeTot] from values of total Zn concentration in water samples. Rearranging Eqtn 3 and substituting into Eqtn 2:

$$K_{app} = 10^{-0.96} = \frac{a_{Zn^{2+}[>FeOH]}}{a_{H^+}([>FeTot]-[>FeOH])} \quad (4)$$

$$[>FeOH] = \frac{10^{-0.96} a_{H^+} ([>FeTot] - [>FeOH])}{a_{Zn^{2+}}} \quad (5)$$

$$[>FeOH] + \frac{10^{-0.96} a_{H^+} [>FeOH]}{a_{Zn^{2+}}} = \frac{10^{-0.96} a_{H^+} [>FeTot]}{a_{Zn^{2+}}} \quad (6)$$

$$[>FeOH] \left\{ 1 + \frac{10^{-0.96} a_{H^+}}{a_{Zn^{2+}}} \right\} = \frac{10^{-0.96} a_{H^+} [>FeTot]}{a_{Zn^{2+}}} \quad (7)$$

$$[>FeOH] = \frac{10^{-0.96} a_{H^+} [>FeTot]}{a_{Zn^{2+}} + (10^{-0.96}) a_{H^+}} \quad (8)$$

Then [>FeOZn⁺] can be determined by substituting Eqtn 8 into Eqtn 3 and rearranging.

[This page intentionally left blank.]

Appendix D.

Groundwater Data and Methods

Contents

Overview.....	3
Background: Groundwater-surface water interactions in the Animas River floodplain deposits.....	5
A Water Flow Balance Investigation for the Upper Animas River.....	6
High Resolution Water Levels Investigation for the Lower Animas River	8
Groundwater Modeling Approach	9
GFLOW Groundwater Model	10
GMS-MODFLOW	12
AnAqSim Groundwater Model	12
Stepwise Progressive Approach	13
Dupuit-Forchheimer Flow	14
Single Homogeneous Aquifer with Horizontal Base	15
Steady-state flow	18
Groundwater Levels and Calibration.....	19
Lower Animas River Groundwater Models.....	19
Lower Animas River GFLOW Model Setup.....	19
Lower Animas River GFLOW Model Calibration.....	21
Scenario 1. GFLOW regional model for January 2016 hydrologic condition.....	23
Scenario 2. GFLOW regional model of the August 2015 hydrologic period	25
Scenario 3. GFLOW Regional model of the August-October 2015 Hydrologic Period	28
Local Scale GFLOW Model for a Lower Animas River Floodplain Community Well	29
Mid Animas River Groundwater Models.....	31
Mid Animas River GFLOW Model Setup	34
Mid Animas River GFLOW Model Calibration	34
Scenario 1. GFLOW Regional Model for the Aug-Dec, 1947-1955 Historical Time Period	34
Scenario 2. GFLOW regional model for the August – October 2015 hydrologic period.....	37
Local scale GFLOW model for a mid-Animas River floodplain community well	37
Consideration of Uncertainty in the Groundwater Modeling	38
Mid Animas: Exploration of the steady-state modeling assumption.....	38
Analytical solution.....	38
Modeling of Transient Flow	40
Mid Animas: Exploration of Fully Three-Dimensional Flow vs. Dupuit-Forchheimer Flow	42
Mid Animas: Exploration of local scale aquifer heterogeneities and anisotropy	45
Mid Animas: Sensitivity Analysis of Breakthrough Times of a Conservative Solute to a Pumping Well.....	49
Empirical Evidence.....	49
Mid Animas River Floodplain Community Wells	49
Lower Animas River Floodplain Community Wells.....	51
Summary	52
References.....	53

Overview

A groundwater analysis was conducted to investigate the potential for impact of the Gold King Mine (GKM) surface water release on downstream floodplain water supply wells. The accidental release of about 3 million gallons of acid mine drainage to Cement Creek above Silverton, Colorado, on August 5, 2015, resulted in a plume of dissolved and colloidal metals that flowed downstream to enter the Animas River near Silverton, Colorado, and joined with the San Juan River in New Mexico, continuing on through Utah before reaching the Lake Powell reservoir around August 12. At any point along the river, the measurable dissolved plume flowed past within 48 hours. The legacy of deposited colloidal and particulate metals remained in the bed sediment. There are hundreds of active pumping wells located in the floodplain deposits of these rivers, including community wells, and private irrigation and household wells. This investigation was limited to the wells in the Animas River floodplain of Colorado and New Mexico (See Figure D-1).

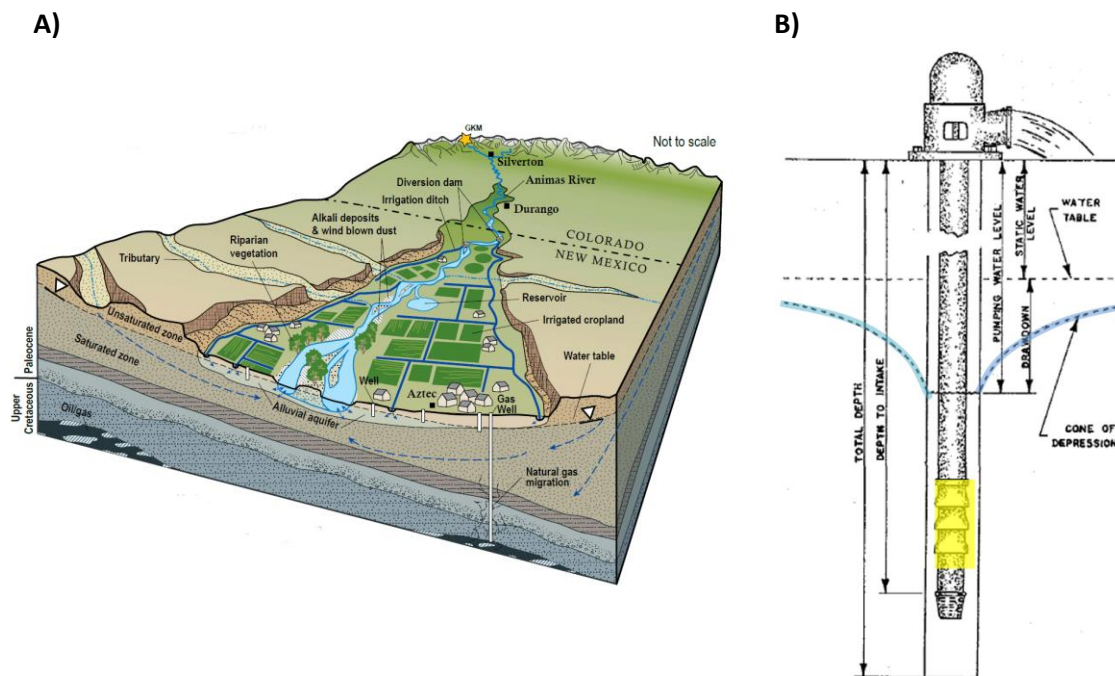


Figure D-1. A conceptual graphic of the floodplain aquifer of the Animas River and presence of water supply wells and irrigation ditches. A) The groundwater flow lines indicate that on a regional basis the river is gaining water from groundwater, but on a local basis, perhaps under the influence of pumping wells, the reach may switch to a losing condition. The New Mexico Bureau of Geology and Mineral Resources has a dedicated aquifer monitoring program. A synoptic survey of river and well water levels was conducted in August 2015, and January and March of 2016. After Timmons et al. (2016). B) A zoom-in engineering drawing of a typical community water supply well, showing influence of pumping from the screened interval on the water table resulting in a local cone of depression. After WestWater Associates (2010).

The definitive question the groundwater investigation addresses is: “Could drinking water or irrigation wells drawing from river alluvium become impacted from the chemicals associated with the GKM release?” (USEPA, 2016, pg. 70). This question may be broken up into three interrelated questions:

- a) Which wells, if any, receive some of their water from the river?

It is assumed that most of the time the Animas River is “gaining” water from the surrounding groundwater aquifer as it flows from Silverton, Colorado to Farmington, New Mexico, meaning that the floodplain is draining groundwater to the river. Under this scenario, dissolved contaminants present in the river flow would travel downstream and not enter subsurface groundwater and have an exposure pathway to the floodplain water supply wells.

It would surprise few to find out that a high pumping well screened in the shallow permeable alluvium and located adjacent to the river receives some of its water directly from the river, even if that stretch of river is understood to be a gaining reach. But how far away would the well need to be to stop sourcing from river water? And at what pumping rate would the well not be able to locally reverse the regional groundwater gradient toward the river, and thus stop sourcing from river water? Are there scenarios in location and time where the Animas River loses water to the floodplain aquifer, and thus bring the exposure pathway into play? And what happens with well-to-groundwater interactions if the river reach is “losing” water to the aquifer? Does this bring low volume private pumping wells into play?

- b) What are the travel times of water from the river to the sourcing wells?
- c) What is the dilution in the sourcing well of possible contaminants received from the river?

In contrast to the highly visible and publically tracked surface water plume associated with the GKM release, the subsurface is hidden and, for this event, the empirical data are limited. The groundwater assessment is open to multiple lines of evidence, including insights gained from physics-based computer simulations that conform to field observations. Question [a] can be answered with capture zone analyses for the various wells. Question [b] can be answered by use of forward particle tracking starting at the river and ending in the well. Question [c] can be answered by tracing particles backward in time from the well, using a uniform distribution of particles around the well, and then comparing the number of path lines that reach the river to those that do not.

This Appendix details the data requirements and methodology for the capture zone analysis and particle tracking. First, the foundations of the geology for the study region are described, including the nature of the flood plain deposits that make up the alluvial aquifer of the Animas River. Second, a discussion is presented about the basis for computational model selection and the approach taken for this study. Third, the results of the capture zone and particle tracking investigations for the lower and mid Animas River water supply wells are presented.

The Appendix closes with an investigation of empirical evidence of river-to-well communication and possible GKM plume capture. Of the several community wells investigated, there was a single community pumping well located in the mid Animas River floodplain and only 35m from the river that had observed dissolved metals concentrations with the characteristics of a breakthrough of a river plume moving through the aquifer to the well within a plausible time window. The signal was not definitive since there were other dissolved metals that did not indicate a breakthrough. In other words, the hypothesis that this well experienced a river-to-well plume could not be rejected. Note the raw well water concentrations of the

dissolved metals (i.e, pre-treatment and distribution) were significantly below human health advisory levels.

As a caveat, this study was limited to an investigation of the potential for impact. An investigation of the significance of impact would require a more detailed human exposure and drinking water risk assessment. For example, only assessment of raw well water was considered, and not the water quality post treatment and distribution (i.e., water at the tap). The analysis was limited to publically available data; no site-specific data were collected by the authors of this Report. And the groundwater assessment was limited to the dissolved constituents of the GKM plume and did not consider the deposited metals in the sediment, which could be a long-term source.

Background: Groundwater-surface water interactions in the Animas River floodplain deposits

The Animas River of Colorado and New Mexico is in dynamic communication with the permeable floodplain deposits, which contains a shallow aquifer that in some locations supports public community wells and private irrigation and household wells, among other water uses. See Figure D-2. The aquifers of interest are the “ribbon” floodplain deposits of the Animas River as it moves through the igneous/metamorphic rocks of the upper watershed, the sedimentary/sandstone-dominated middle area, and the shale-dominated lower area. The different geology has influence on the floodplain geomorphology and the shallow groundwater quality.

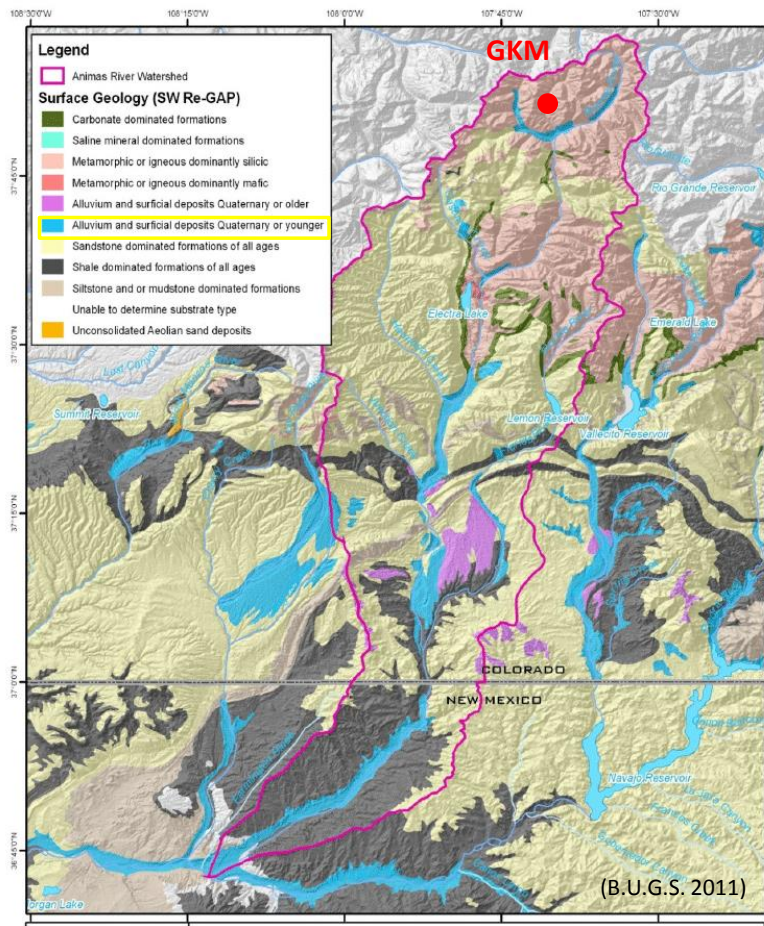


Figure D-2. Surficial geology of the Animas River watershed. The aqua blue designates the alluvial floodplain deposits. (B.U.G.S., 2011). Gold King Mine is in the far northern headwaters of the watershed. Broadly, the Animas River runs over three distinct geology zones: (1) the upper Animas and igneous/metamorphic rocks; (2) the mid Animas and the sandstones; and (3) the lower Animas and the shales. These distinct geology zones have influence on stream geomorphology and floodplain deposit water quality.

The Animas River floodplain of Colorado and New Mexico and the aquifer beneath is tapped by a large number of water supply wells and irrigation ditches. While the river is predominately a gaining stream on a regional basis, there are some times and locations where a river reach may be losing water to the shallow groundwater system (Timmons et al., 2016). This Appendix will examine multiple lines of evidence for groundwater-surface water interactions, including a water flow balance investigation, and a high resolution water elevation investigation.

A Water Flow Balance Investigation for the Upper Animas River

The Animas River discharge reflects the annual cycle of late spring to early summer snowmelt runoff, with subsequent decreases in discharge, interrupted by infrequent rain events. This is demonstrated for the upper Animas River near Silverton, Colorado (See Figures D-3 and D-4A). The cluster of U. S. Geological Survey (USGS) streamflow gages near Silverton allows a flow balance analysis to be conducted:

$$Q_{A@S} + Q_{C@S} + Q_{M@S} + Q_{GW} = Q_{Abs} \tag{1}$$

or

$$Q_{GW} = Q_{Abs} - Q_{A@S} - Q_{C@S} - Q_{M@S} \tag{2}$$

where USGS gages include the Animas River below Silverton (Q_{Abs}), Animas River at Silverton ($Q_{A@S}$), Cement Creek at Silverton ($Q_{C@S}$), Mineral Creek at Silverton ($Q_{M@S}$). The difference between the sum of the cumulative tributary stream flows upstream and the measured streamflow downstream is inferred to be made up of contributing diffuse groundwater inflow (Q_{GW}) along the Animas River between the upgradient and downgradient stations. The Animas River around Silverton is understood to be a gaining stream much of the time, with groundwater draining toward the river, with some episodic exceptions during high river stage, such as annually during late-spring early-summer snowmelt, or during high rain events, as shown in Figure D-4B.

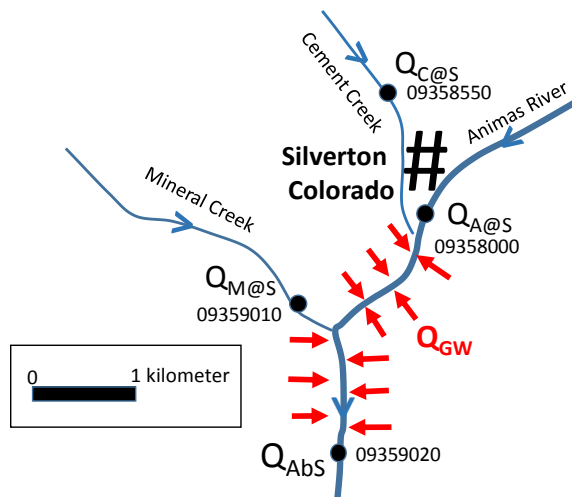
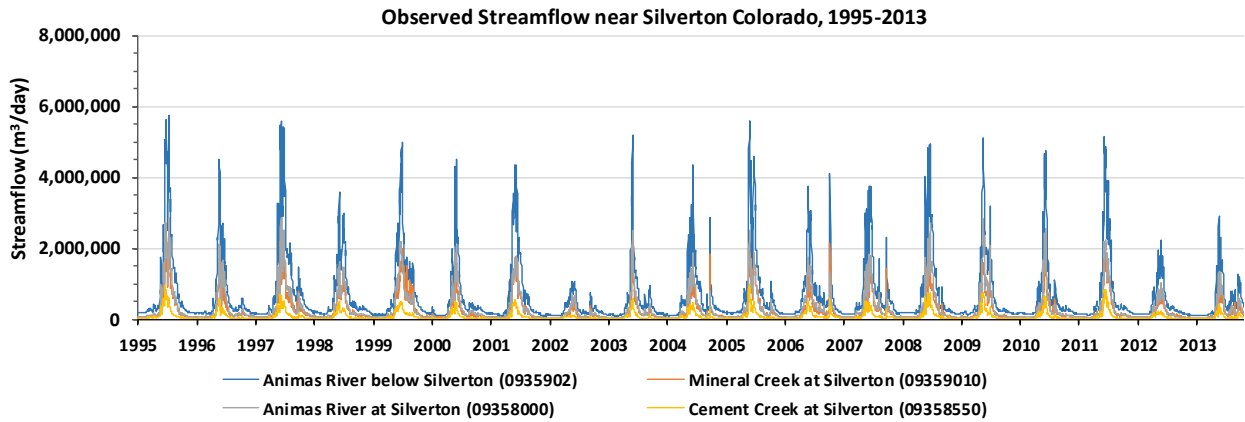


Figure D-3. Conceptual representation of the Upper Animas River discharges measured by the US Geological Survey and diffuse groundwater discharge near Silverton, Colorado. USGS gages include Animas River below Silverton (Q_{Abs}), Animas River at Silverton ($Q_{A@S}$), Cement Creek at Silverton ($Q_{C@S}$), Mineral Creek at Silverton ($Q_{M@S}$). The inferred averaged groundwater contribution to the outlet flow (Q_{GW}) includes diffuse subsurface flows and discrete spring flows as shown in red.

A)



B)

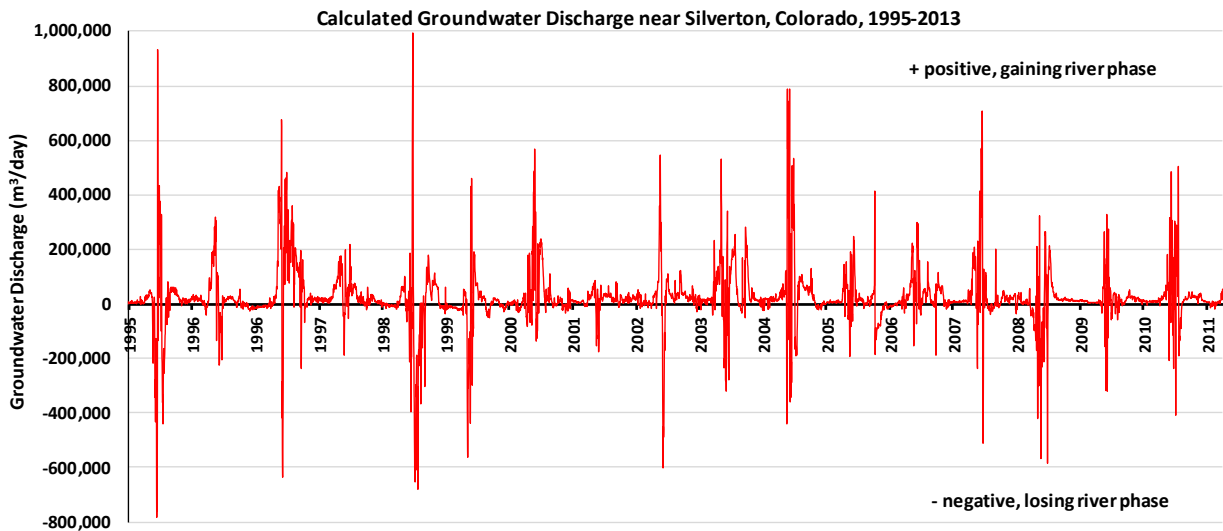


Figure D-4. Streamflow analysis of the upper Animas River near Silverton, Colorado, 1995-2013. A) Streamflow hydrographs of measured discharge in cubic meters per day of the Animas River and tributaries near Silverton, Colorado. B) Inferred groundwater inflows along the section of the Animas River around Silverton, Colorado. The positive inflow implies that the Animas River is gaining groundwater. The negative exceptions suggest the river losing flow to the alluvial groundwater system.

Church *et al.* (2007, Chapter E9, pg. 488) applied a tracer-dilution method in the Cement Creek watershed and suggest that up to 21% of streamflow can be related to diffuse subsurface flow discharging to the stream; the rest comes from discrete mine effluent, springs, and tributaries.

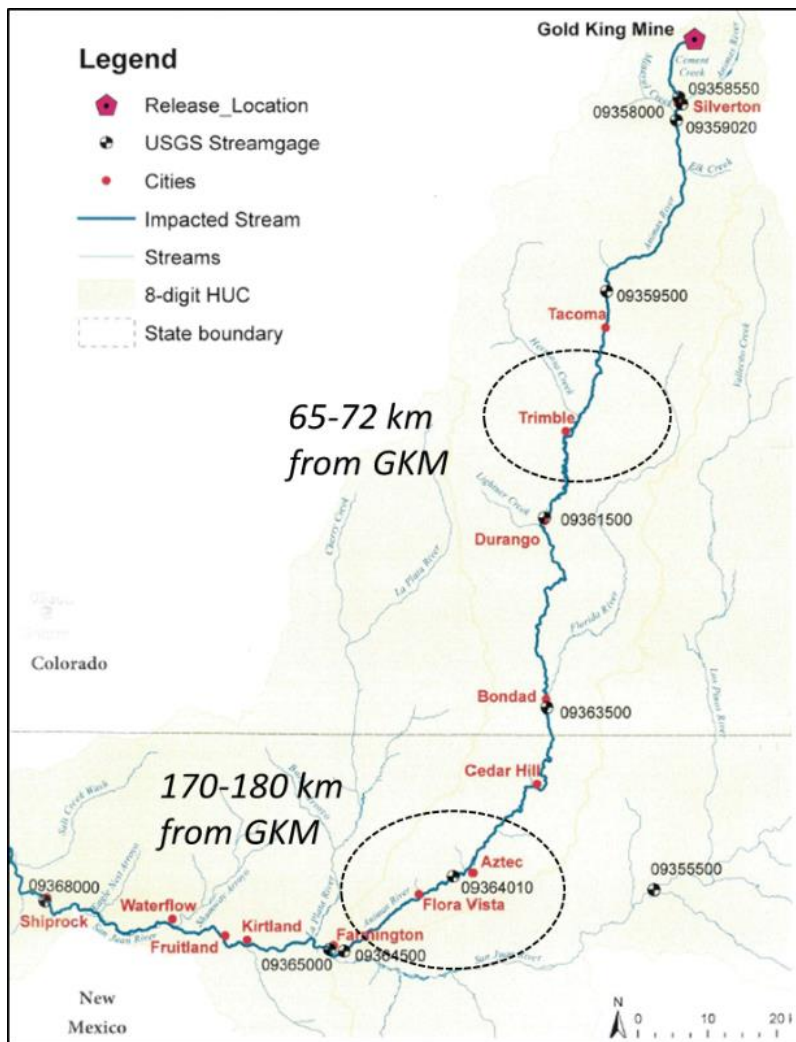


Figure D-6. The mid Animas and lower Animas River clusters of community and private wells selected for groundwater modeling analyses. (1) the mid Animas River area between Tacoma and Durango, Colorado, 65-72 km downstream of the GKM release site; and (2) the lower Animas River area between Aztec and Farmington, New Mexico, 170-180 km downstream of GKM.

Groundwater Modeling Approach

The groundwater impact investigation used a step-wise and progressive computational modeling approach incorporating hand calculation, empirical and spreadsheet analyses, and mechanistic groundwater simulations using analytic element and finite difference methods.

Analytic element modeling is especially well suited for the progression from simple to more complex representations of the geohydrologic system in order to test understanding. A suite of simple models with few measurable parameters is often preferred over a multi-parameter model that could better fit the data, at least for groundwater flow problems (Kelson et al. 2002). Simple models are used within a deterministic approach in this GKM investigation; a stochastic approach would require more field data than are available. The theoretical foundations of the analytic element method are documented in Strack and Haitjema (1981a, 1981b) and Strack (1989). The practical application of the analytic element method is covered in Haitjema

(1995). A community of practice web page includes a survey of analytic element models (www.analyticelements.org).

While especially suitable for groundwater flow modeling at different scales, analytic element modeling does have some limitations. For instance, both transient flow and three-dimensional flow are only partially available. While an analytic element model can represent macro-scale heterogeneities (e.g., the difference in hydraulic conductivity associated with alluvium and hard-rock aquifers) in a piece-wise manner, the models do not currently represent gradually varying aquifer properties. Numerical methods for computational groundwater simulation, including finite element and finite difference methods, are better positioned for more complex conceptual model representation (e.g., transient flow, fully 3D flow, spatially discretized aquifer properties). Fitts (2012) offers a review and comparison of analytic element and numerical modeling techniques in the context of groundwater geology applications, including subsurface solute and contaminant transport. What follows is a discussion of the specific computational models selected for this study.

GFLOW Groundwater Model

The analytic element computer program GFLOW (v.2.2.2) was used in this project to solve for regional and steady groundwater flow in single-layer aquifers (Haitjema 1995). GFLOW is well documented and accepted within the groundwater modeling community (Hunt 2006; Yager and Neville 2002), particularly when applied to shallow groundwater flow systems involving groundwater/surface water interactions (Johnson and Mifflin 2006; Juckem 2009) and for recharge estimation (Dripps et al. 2006). The mathematical foundation of the model includes equations that express the physics of steady advective groundwater flow within a continuum; continuity of flow and Darcy's law are satisfied at the mathematical elementary volume.

GFLOW solves the regional steady-state groundwater flow equations using the analytic element method (Haitjema 1995; Strack 1989) based on the principle of superposition of elements where line-sink elements represent streams, point-sink elements represent wells, line-doublet polygon elements represent discontinuities of aquifer properties (e.g., hydraulic conductivity, base elevation, and no-flow boundaries), and area elements represent aquifer recharge. The model domain is unbounded making solutions flexible in scale, from regional to local, and vice versa. Boundary conditions corresponding with physical features are superimposed, putting more detailed representations in the nearfield and coarser representations in the far field. The separated influences of these elements on the regional flow field are shown in Figure D-7.

The areas of interest for GFLOW models in this project ranged in scale from full "ground watershed" aligned with the surface watershed down to an individual pumping well. Theoretically, analytic element solutions are spatially infinite, and good modeling practice typically represents both a far field, with coarse representation of elements and geohydrologic features, and a near field at higher resolution.

In GFLOW, to create a bounded flow solution assigned to a topographically defined surface watershed, a closed string of no-flow line elements is placed on the perimeter of the surface watershed. Even though the static no-flow boundary is an artificial one (i.e., not actually occurring in the natural system), the setup is justified in geohydrologic systems where the shape of the shallow water table tends to follow the shape of the surface topography, permitting the assumption that groundwater fluxes in and out of this boundary are insignificant. Also, the base of the single-layer aquifers is assumed to be horizontal and to constitute a no-flow boundary and, indeed, it is assumed that deep leakage is minimal. GFLOW can represent flow in the aquifer as either unconfined or confined, or both. The bounded solution setup simplifies the calibration of a water balance associated with a surface watershed in the mountain terrain.

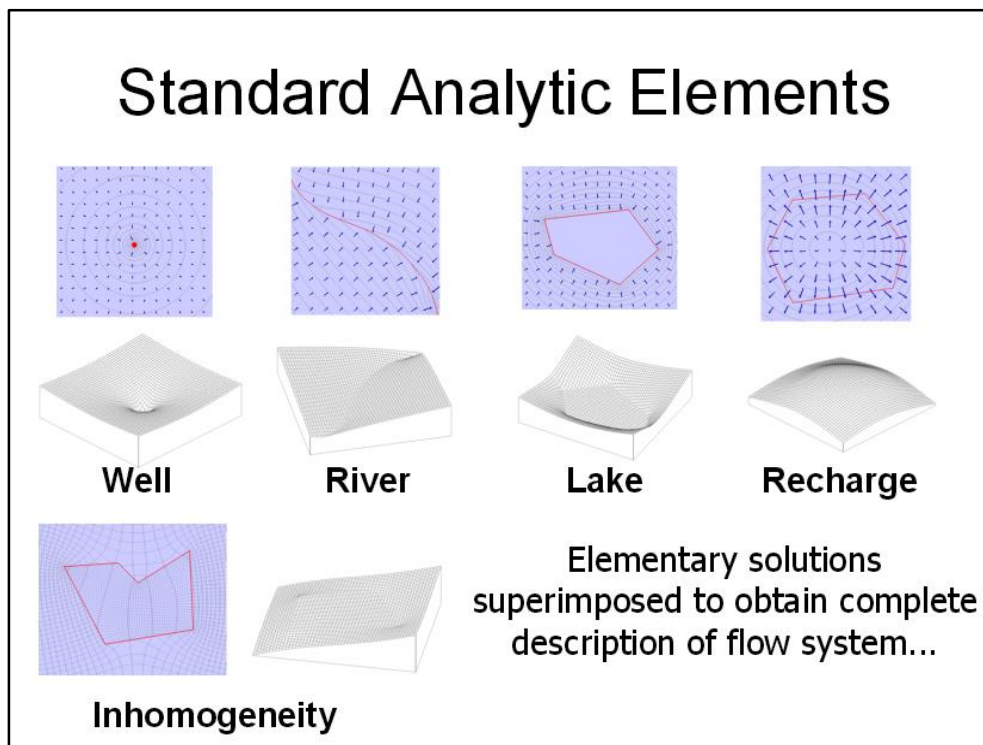


Figure D-7. Analytic elements: elementary mathematical points, lines, and polygons and associated landscape features. The suite of standard analytic elements available for superposition in the model domain to create a site specific model. The influence of the element on the hydraulic head contours and gridded water table surface and the velocity vectors is shown (Source: Craig 2014).

Shallow groundwater flow systems are often intimately linked with surface drainage. The perennial stream network is understood to be flowing year round. In contrast, the ephemeral stream network is dry most of the year, only flowing during intense rainfall events and contributing to rapid surface runoff. The intermittent stream network is understood to be supported by shallow drainage of the unsaturated soil horizon. For a stream to be flowing when it has not rained for many days, the source of the river water is subsurface groundwater drainage, also called baseflow. The distinction on the landscape of perennial, intermittent, and ephemeral flow is dynamic and dependent on antecedent soil moisture conditions.

An output of the GFLOW regional groundwater model is a continuous surface representing piezometric head, or groundwater flow potential. This surface of heads is the same as the water table surface for unconfined aquifers such as in the Animas River alluvium. The model-predicted elevation of the water table depends on the aquifer recharge rate and the aquifer transmissivity (i.e., hydraulic conductivity times aquifer thickness). Assuming a constant transmissivity, the higher the recharge rate, the higher the model-predicted elevation of the water table. Conversely, assuming a higher recharge rate, the higher the aquifer transmissivity, the lower the model-predicted water table will be. Once the recharge rate is known after conducting baseflow analysis, the model can be calibrated to “fit” the observed water table elevations at points by varying the aquifer transmissivity, and monitoring the model-predicted water table at monitoring wells where the water table elevation is measured.

In summary, the two calibration targets, baseflow at the watershed outlet and observed elevations of the water table in unconfined aquifers, allow for the parameterization of the average recharge and transmissivity of the regional steady state aquifer flow system equations in the GFLOW model.

GMS-MODFLOW

Sometimes, conceptual complexity, particularly at the local scale, suggests numerical modeling techniques. The USGS MODFLOW model is the most widely used groundwater flow model in the world. MODFLOW uses the finite difference numerical solution technique, with grid-based rows and columns, cells, multi-layer aquifer, non-horizontal base elevations, hydraulic conductivity, porosity and storativity can vary by cell (Harbaugh 2005; See Figure D-8). MODFLOW has undergone 30 years of development and quality testing by USGS.

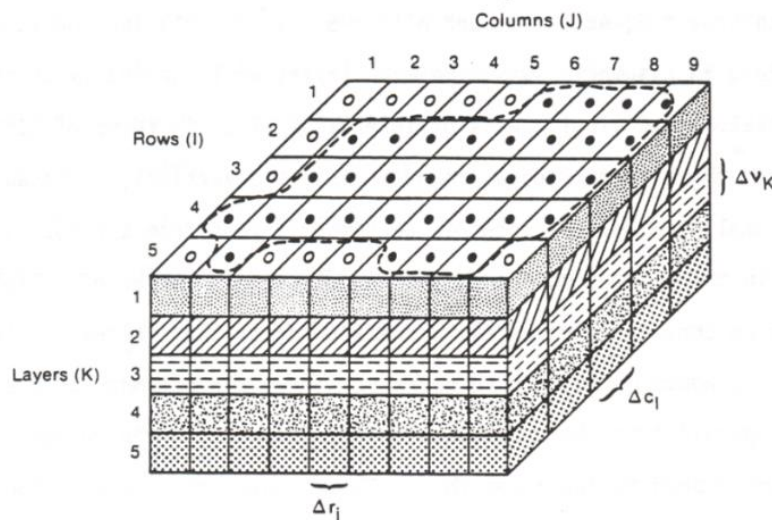


Figure D-8. The finite difference solution in MODFLOW solves for groundwater flow between cells as defined by rows, columns, and layers. The aquifer boundary (often a no-flow boundary) is shown as a dashed outline.

For this project, the EPA team used the MODFLOW-NWT and MODPATH (particle tracking) solvers within the Groundwater Modeling System (Aquaveo, GMS v 10.1). GMS includes standard MODFLOW example run files to confirm proper model installation. In addition to facilitating a standard cell-based interface to the MODFLOW finite difference grid, GMS includes a geohydrological conceptual design environment much like GFLOW.

AnAqSim Groundwater Model

The AnAqSim (release 3, 29 Sept 2016; www.fittsgeosolutions.com) groundwater modeling system invokes hybrid semi-analytic and numerical solution techniques. It uses subdomain analytic element models as described in Fitts (2010), which gives it strong capabilities with respect to heterogeneity and anisotropy. It also employs high-order line elements, spatially variable area sinks, and finite-difference time steps to allow multi-level aquifer systems and wide-ranging transient flow simulations.

AnAqSim uses one separate two-dimensional model for each subdomain. In each subdomain model, the resistance to vertical flow is neglected and the head is independent of elevation within the subdomain (Dupuit assumption). Resistance to vertical flow and three-dimensional flow are modeled by using multiple levels with vertical leakage between levels. The simplest model would be one level (i.e., two-dimensional), and only one subdomain (i.e., homogeneous). A plan view of such a simple model is shown in Figure D-9.

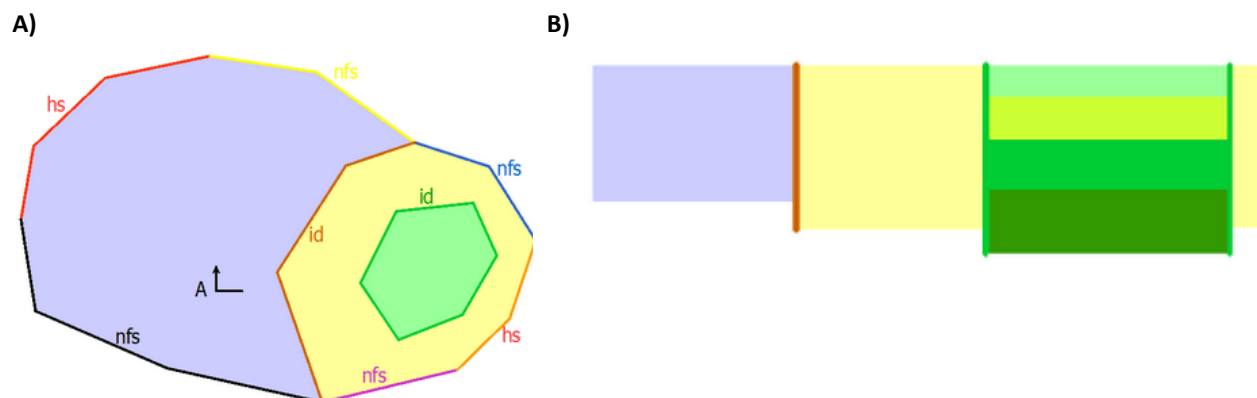


Figure D-9. Simple hypothetical AnAqSim model. A) Plan view showing domains and boundaries (head specified (hs), normal flux specified (nfs); internal domain (id). B) Cross-sectional view A-A' showing layers within domains.

Stepwise Progressive Approach

The stepwise and progressive groundwater modeling approach is not new (Sullivan et al., 2015, Appendix C; also <http://www.haitjema.com>). Ward et al. (1987) applied what they called a telescopic mesh refinement (TMR) computational groundwater modeling approach to the Chem-Dyne hazardous waste site in southwestern Ohio. They used three different finite differences numerical computer models for the three different scales at which they were modeling. Conditions on the grid boundary of the local scale were obtained from the regional-scale modeling results, while, similarly, the conditions on the grid boundary of the site scale were obtained from the local-scale modeling results. In contrast, the analytic element method for computational groundwater modeling allows these different scales to be treated within the same model by locally refining the input data, thus avoiding transfer of conditions along artificial boundaries from one model into the other. The step-wise progressive groundwater modeling approach taken for this study starts with regional scale analytic element modeling with GFLOW and progresses to local scale finite difference modeling with MODFLOW and local scale hybrid modeling with AnAqSim, as understanding and data justify.

The step-wise progressive groundwater modeling approach puts the emphasis on testing conceptual understanding, and less focus on site-specific prediction. The modeling steps for this study included: (1) building the regional scale model including the far-field hydrogeologic boundary conditions; (2) testing the model performance with field observations of streamflow and water levels in wells as part of the calibration/harmonization process; (3) zooming down within the regional model to include local refinement of the conceptual model around the pumping well, such as aquifer heterogeneities, three-dimensional flow, transient responses; (4) another round of testing the model performance with field observations, such as pumping test data; and (5) repeating the modeling process by returning insights to the regional scale, and so on. Ideally, the modeling stops when the degree of hydrogeological and numerical complexity is sufficient that adding more detail does not change the essence of the model simulation, and impact the answer to the study questions.

The GFLOW model was used for the initial regional-scale and local-scale modeling of steady state flow. The regional models provide initial boundary conditions for local scale transient and full 3D modeling using MODFLOW, and local scale aquifer heterogeneity, including anisotropy, using AnAqSim (See Table D-1). The implications of the various levels of complexity are discussed in the next sections.

Table D-1. Conceptual Complexity and Groundwater Model Selection

	Spatial Scale	Conceptual Complexity	GFLOW	MODFLOW	AnAqSim
	Regional	Single layer infinite aquifer (piecewise homogeneous properties, horizontal base elevations, point sinks for wells, line-sinks for rivers, area elements for zoned recharge and aquifer properties), Dupuit Forchheimer assumption (neglect resistance to vertical flow; hydraulic heads constant with depth, horizontal 2D flow), Non-time variant (steady state) stress and flow	☑		
	Local	Extracted constant head outer boundary condition from regional model, time-variant (transient) stress and flow		☑	
	Local	Extracted constant head outer boundary condition from regional model, three dimensional flow		☑	
	Local	Extracted constant head outer boundary condition from regional model heterogeneous internal domains, anisotropy of hydraulic conductivity			☑
	Both	Particle tracking (reverse – capture zones; forward – breakthrough response)	☑	☑	☑

Dupuit-Forchheimer Flow

The analytic element models used in this project fall in the class of codes that solve “two-dimensional flow in the horizontal plane,” at least that is how these types of models are routinely referenced (USEPA, 2016, pg.71). This is misleading terminology. GFLOW is a *Dupuit-Forchheimer model* (DF model), which is a model in which resistance to vertical flow is being ignored, thus not vertical flow itself (Strack, 1984). While the underlying partial differential equation in GFLOW involves only the horizontal coordinates (x and y), flow into the vertical direction can and is being approximated using conservation of mass considerations. Consequently, path lines in GFLOW are being traced in three dimensions.

The DF models offer a better approximation to actual three-dimensional flow systems in aquifers that are rather thin when compared to their lateral extent. In practice, this translates into groundwater flow systems in which the distances *L* between boundary conditions (e.g., distance of the well from the river) is larger than five times the aquifer thickness. This is for isotropic aquifers. In case the aquifer is anisotropic, with a lower vertical hydraulic conductivity than the horizontal conductivity, the following criterion may be used (Haitjema 2006):

$$L \geq 5H \sqrt{k_h/k_v} \tag{3}$$

Where H is the aquifer thickness, k_v is the vertical hydraulic conductivity, and k_h is the horizontal conductivity. For example, consider a well which is 35 horizontal meters from the river with a well screen that is about 25 meters below river. If $K_h/K_v = 10$ (Note: ratios of 5 to 50 are common), the vertical distance in an equivalent isotropic medium would be about 80 meters vertical distance (i.e., scale the vertical axis by the square root of K_h/K_v to make an equivalent isotropic medium). In this case, the vertical resistance between river and well screen would likely be greater than the horizontal resistance. Neglecting the vertical resistance in the GFLOW model overestimates the communication between well and river, and underestimates the travel time for flow from river to well (USEPA, 2016, pg. 81). The condition in the displayed formula above is not meant for wells that are relatively close to the Animas River, and unfortunately these are the wells of most interest (most likely to receive river water).

What is the consequence of violating the Dupuit-Forchheimer (DF) criterion for wells near the river? In reality the well-river interaction is influenced by possible bottom resistance to flow between the river and the aquifer, as well as resistance to vertical flow inside the aquifer. Neither is included in the model presented, although bottom resistance could have been applied. By not including any of these resistances, the flow potential for drawing water from the river that flows into the well is *overestimated*. In other words, the model as constructed is *conservative* with respect to the objectives of this study (USEPA, 2016, pg 81). Computer simulations of capture zones including full 3D flow from MODFLOW are compared to DF capture zones using GFLOW later in this Appendix.

Single Homogeneous Aquifer with Horizontal Base

GFLOW represents the alluvium near the Animas River as a single homogenous aquifer, which means that it lumps the various depositional layers in the alluvium into a single homogenous layer. Furthermore, it assumes a horizontal aquifer base below which no flow is considered. The question is how these simplifications affect the modeling results. Specifically, what effect does this simplification have on the potential well-river interaction? (U.S. EPA, 2016, pg. 73)

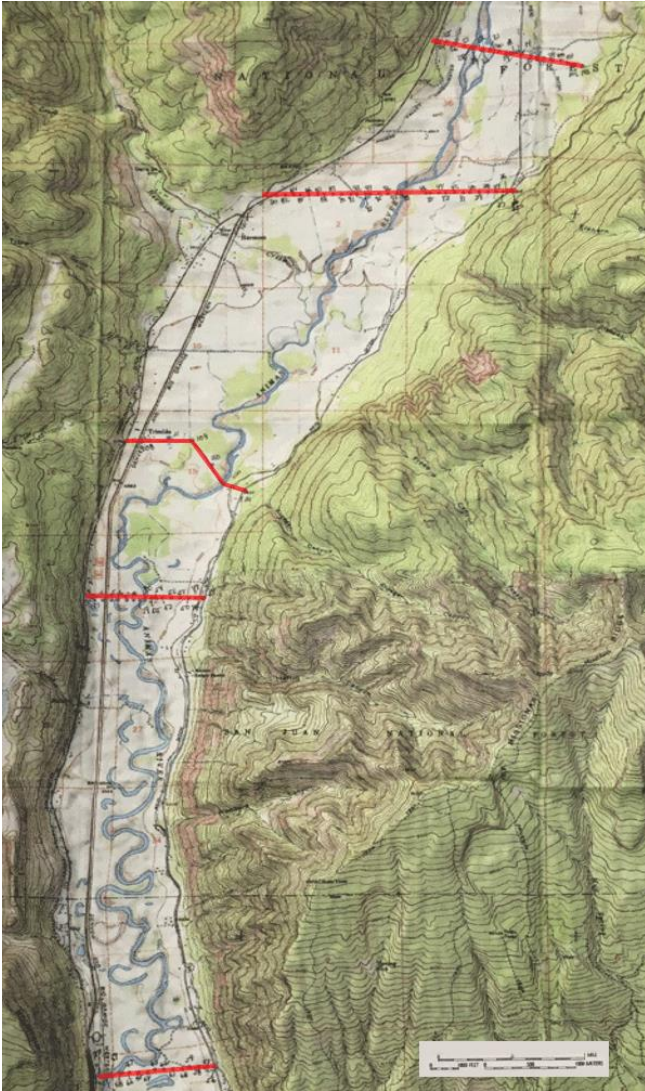
There is not much known about the alluvial aquifer in terms of spatial heterogeneity and depth. The actual aquifer base at a specific location is unknown, but a geophysical survey gives some insight.

The Animas Water Company invested in a geophysical/gravimetric survey of the floodplain aquifer of the mid Animas River watershed near Hermosa, getting estimates of the base of the aquifer in five survey lines (or cross-sections). The permeable deposits are much deeper (i.e., 600 to 1000 feet) than the current depth of the community wells in this area (i.e., approximately 100 feet; See Figure D-10).

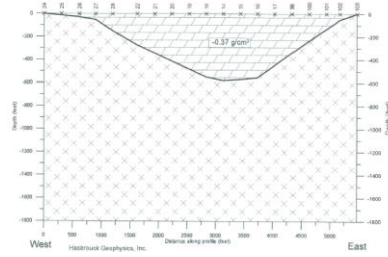
The geophysical survey offered depths based on a two-layer model and three-layer model. The selection of the depths associated with the two-layer model most likely lead to an underestimation of the aquifer thickness. This does not affect the flow regime much since the range of transmissivity in the model does not depend on this assumption because it has been constrained by pump test data. Assuming for a moment that the transmissivity is accurate, or reasonable, an underestimation of the aquifer thickness will result in an overestimation of the hydraulic conductivity, since the product of the two is the known transmissivity. So while the discharge rates in the aquifer, including the flow component from the river if present, are not affected (See Question [a]), the specific discharges and associated average groundwater flow velocities are. An underestimation of the aquifer thickness will result in an underestimation of the groundwater travel times (question [b]). This is *conservative* in view of the model objective since actual arrival of contaminants may be later than predicted by the model.

The actual aquifer heterogeneity offers the potential for preferential pathways from the river to the well. The USGS conducted a detailed study in the upper Animas River watershed near Eureka, Colorado, and a trench study revealed some of the complexity of the stratigraphy and gravel deposits (See Figure D-11).

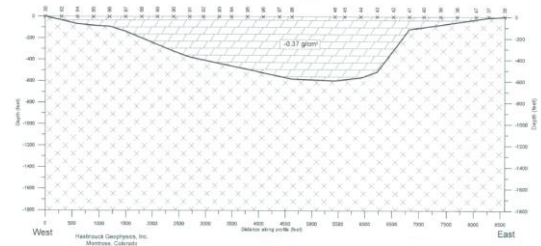
A)



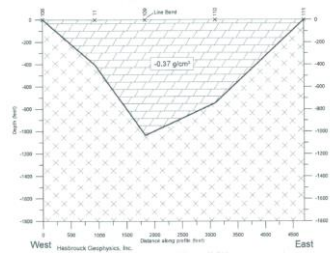
B)



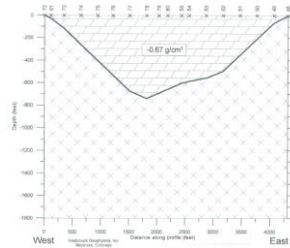
C)



D)



E)



F)

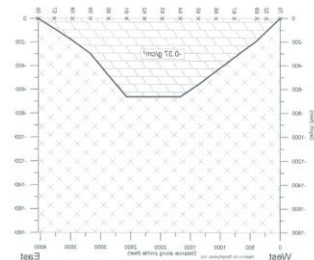


Figure D-10. Geophysics modeling of the shallow floodplain aquifer base elevation based on a gravity survey. (a) map of the five gravity survey lines; (b) line 1 gravity and depth profile – 2-layer model; (c) line 2; (d) line 5; (e) line 3; and (f) line 4. The model suggests the depth of the aquifer ranges from 600 ft to 1000 ft. Data source: Hasbrouk Geophysics, 2003.

A)



B)

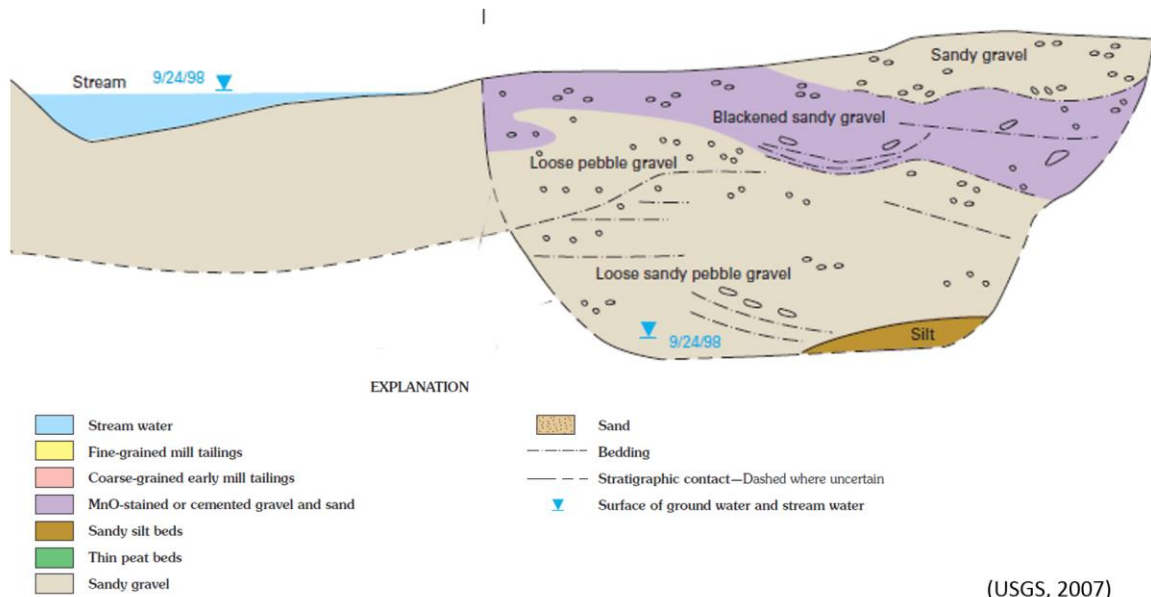


Figure D-11. Animas River in floodplain near Eureka above Silverton, Colorado. A) Google Earth image showing the braided dry channels and the location of the geologic cross section. B) Generalized geologic cross section of the shallow floodplain deposits of the Animas River above Silverton (Vincent, Elliott, 2007). The shallow stratifications include pebble and sandy gravels.

The GFLOW model assumes a homogeneous aquifer that lacks preferential flow. Consequently, the assumption of homogeneity is not conservative in view of the model objectives. Preferential pathways would shorten the travel times from the river to the well (See Question [b]). While a multi-layer model could be able to capture this effect to some degree, such as AnAqSim, data on aquifer stratification near the study wells or between the wells and the river are absent.

Preferential flow may well outweigh the effect of the aquifer thickness on the groundwater velocities. This will enter into the discussions regarding the empirical evidence of river-to-well communication at the end of this appendix.

Steady-state flow

The GFLOW simulates steady state flow, ignoring water that may go into storage or is released from storage due to temporal changes in the water table (i.e., unconfined flow) or head (i.e., confined flow). For the purpose of capture zone delineation in the context of wellhead protection, a steady state model is considered adequate (USEPA, 2016, pg 75). In fact, producing capture zones that change over time seems impractical for the purpose of managing wellhead protection areas. However, replacing the actual transient flow system by a steady state, one raises the question what the steady state model actually represents. Haitjema (1995, 2006), using a study by Townley (1995), presents a dimensionless response time, τ :

$$\tau = \frac{SL^2}{4TP} \quad (4)$$

where S [-] is the aquifer storage coefficient, L [m] the distance between head specified boundaries, T [m²/day] the aquifer transmissivity (i.e., the product of aquifer thickness and hydraulic conductivity), and P [days] the period of a periodic forcing function. When considering seasonal variations in flow in the alluvial aquifer, the definition of L can be more conveniently defined as the distance between the river and the valley boundary (e.g., rock outcrop). Haitjema (2006) offers the following rules of thumb:

- $\tau < 0.1$ treat transient flow in the aquifer as successive steady state.
- $0.1 \leq \tau \leq 1$ transient flow cannot be meaningfully represented by a steady state model.
- $\tau > 1$ represent transient flow by a steady state model using average boundary conditions.

These guidelines are approximate in that values just below 0.1 or just above 1 are to be considered transitional from the aquifer responding relatively quickly or slowly to transient forcing, respectively.

A periodicity of $P=365$ days is appropriate to assess the response of the flow system to seasonal variations in recharge (e.g., inflow into the aquifer near the rock outcrop) and seasonal variations in river stages; it is not suitable to assess the response of the flow system to short term variations in pumping and short-term variations in river stage (e.g., storm surges). For that purpose, a periodicity of $P=1$ day would be a better choice. This reduction in the value of P would further increase the value of τ indicating that the aquifer responds rather slowly to storm events and pumping variations. This will be explored in testing against mid Animas River data later in this appendix.

Groundwater Levels and Calibration

In this study, the groundwater flow model GFLOW is being calibrated using observed potentiometric heads (e.g., confined flow rock areas) or water table elevations (e.g., unconfined flow alluvium). In addition, base flows in the Animas River are also included as calibration targets. Calibration leads to the determination of most likely hydrogeological parameters such as hydraulic conductivities, aquifer recharge due to precipitation, and perhaps stream bottom resistances (USEPA, 2016, pg. 78). In the Animas River of New Mexico, high-resolution synoptic surveys of static water levels were available. In the Animas River of Colorado, the EPA team used the static water levels reported in well driller's logs.

Currently, hydraulic gradients toward the Animas River are generated in the model by defining head specified boundaries away from the river. The water released by these head-specified boundaries presumably comes from the surrounding mountains. A common approach in modeling flow in alluvial valleys is to apply so-called "mountain range recharge" along the valley boundaries at the bottom of the surrounding mountains. In GFLOW, this could be done using discharge-specified line-sinks along the base of the mountains or boundary of the alluvium. Since there were not data to support the mountain range recharge, the contribution was estimated using observed baseflow increases along the Animas River.

Lower Animas River Groundwater Models

A pumping well located in proximity to the river has the possibility of reversing the background hydraulic gradient and capturing water from the river, depending on proximity and pumping rates. Groundwater flow modeling was used to investigate pumping scenarios consistent with observed conditions. The lower Animas River regional groundwater modeling will be presented first because of the existence of a high-resolution topographic data set (i.e., digital elevation model, DEM) and a series of synoptic surveys of the well water levels and river water levels from August 2015 and into 2016.

Lower Animas River GFLOW Model Setup

The regional groundwater model solves the hydrological water balance between the USGS gages at Aztec and Farmington. The DEM is used to define the outer boundary of the catchment (See Figure D-12).

The surficial geology of the lower Animas River watershed for the study region is mapped in Figure D-13. A sampling of community wells was extracted from the New Mexico Water Rights Reporting System (NMWRRS) for the Animas River floodplain between Aztec and Farmington (RK 170-180), and the data reported in Table D-2.

The layout of analytic elements used in the GFLOW representation of the lower Animas River are shown in Figure D-14. The base of the single-layer aquifer is assumed to be horizontal and to constitute a no-flow boundary. The GFLOW model represents the outer boundary as a no-flow boundary, that is, no solution occurs outside of this boundary. GFLOW also uses a polygon to distribute area recharge over the catchment only. Another analytic element polygon encloses the floodplain alluvium and associates a higher hydraulic conductivity than the outer rock domain. The perennial stream network defines an internal boundary condition. The nominated stream locations from USGS topographic maps or digital elevation models (DEM) were translated into GFLOW line-sink representations of streams. Head at a location on the landscape is understood to be the elevation at which water saturates an open pipe piezometer driven into the aquifer. The strength (i.e., inflow/outflow per unit length) of the line-sink is determined in the analytic element solution by maintaining a specified head in the center of the line-sink element. A combination of methods was used to estimate the land surface elevation at select locations on the base map: (1) labeling elevations where elevation contour lines from the USGS map crossed the stream channel; and/or (2) linear interpolation along the line-sink. The line-sinks were then manually superimposed on the base map, ensuring that vertices at the end of line-sink strings corresponded with points of known head/elevation from

the USGS sources. The head at the center of each of the line-sink strings is calculated through linear interpolation. Wells are represented with point elements. A piece-wise representation of the hydraulic conductivity (k) property is achieved with the polygonal representation of the higher- k unconsolidated floodplain deposits.

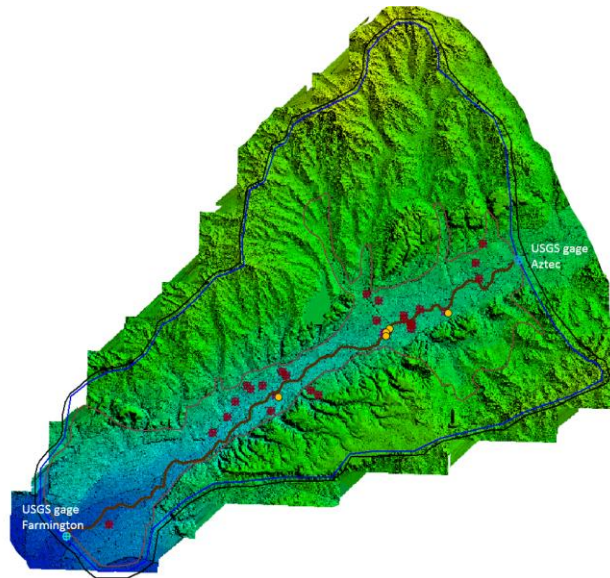


Figure D-12. Community wells (orange) and private wells (red) for the Lower Animas River floodplain study area. The catchment draining between the USGS gages at Aztec and Farmington was delineated as guided by the LiDAR DEM. Data source: New Mexico Resource Geographic Information System (<http://rgis.unm.edu/>)

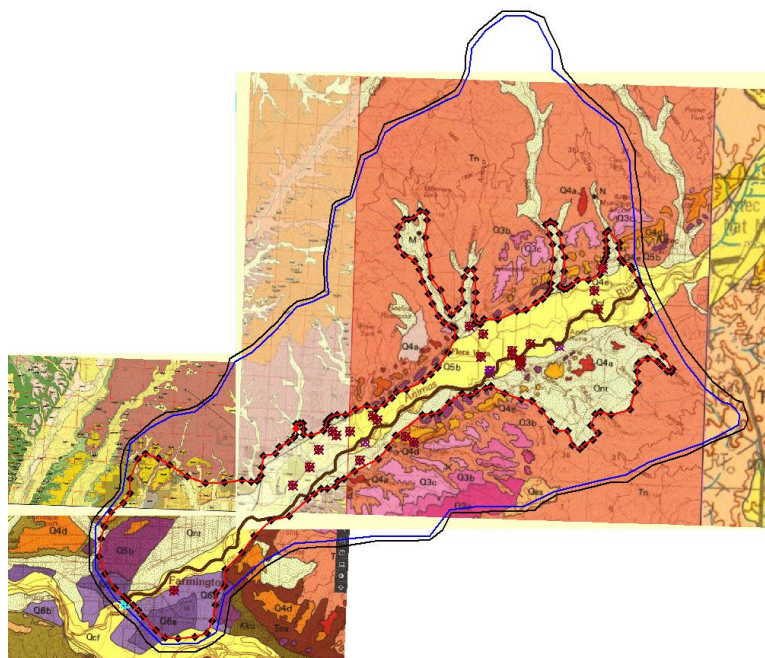


Figure D-13. Lower Animas River geology. The interpreted boundary of the alluvial aquifer is delineated. Data: USGS national geologic model database.

Table D-2. Lower Animas River floodplain, community well data, New Mexico

Identification*	Total Depth (Ft)	Static Water Level (Ft bgs ^{&})	Pumped Water Elevation (Ft bgs)	Well Yield (gpm) Observed, Estimated	Average Annual Well Diversion Right (Acre-ft)
76m174km	21	6	NA	150	62.9
21m174km	23	7	NA	150	62.9
101m174km	21	7	NA	150	62.9
90m179km	25	NA	NA	1,000	1,935
18m171km	NA	NA	NA	125	1.36

*An ID was assigned to the community wells incorporating distance from river (in meters) and downstream distance from GKM (in kilometers) in the name.

[&] Feet below ground surface

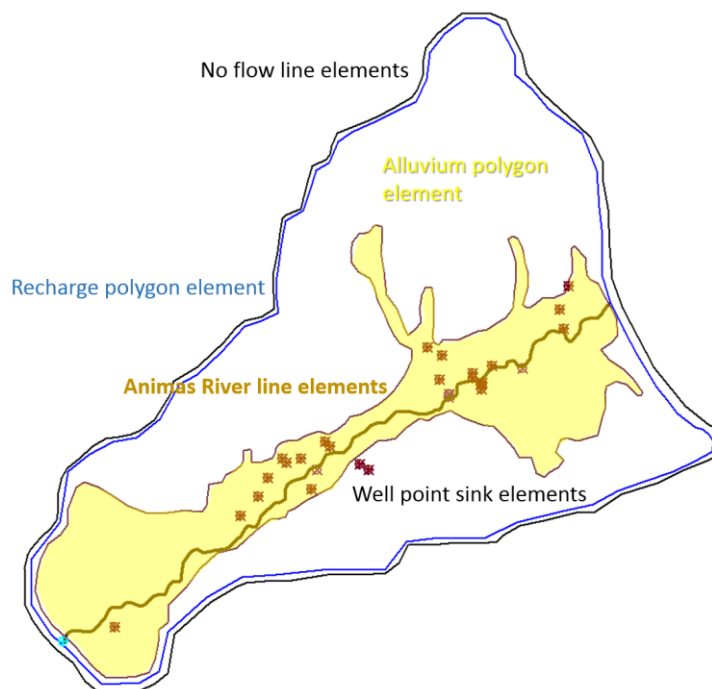


Figure D-14. Layout of GFLOW analytic elements for the Lower Animas model.

Lower Animas River GFLOW Model Calibration

The areal recharge was distributed over the catchment between the USGS gages in order to satisfy the water balance of August 2015. The observed stream flows are shown in Table D-3. USGS gage data for Farmington was provisional at the time of analysis, so estimated based on historical observations at two gages.

Table D-3. Observed stream flows and statistics in the lower Animas River of New Mexico.

USGS Gage Name	USGS Gage Number	Discharge average 8/12-8/15/2016 (cfs)	Discharge on 1/14/2016 (cfs)	Discharge average August-October, 2015 (cfs)	Discharge average August-October, 2003-2015 (cfs)
Animas River below Aztec NM	09364010	654.7	229	365	428
Animas River Farmington NM	09369500	684.3	240 estimated*	360	438

* $Q_{farm}/Q_{aztec} = 1.049$ based on 2003-2016 data for January.

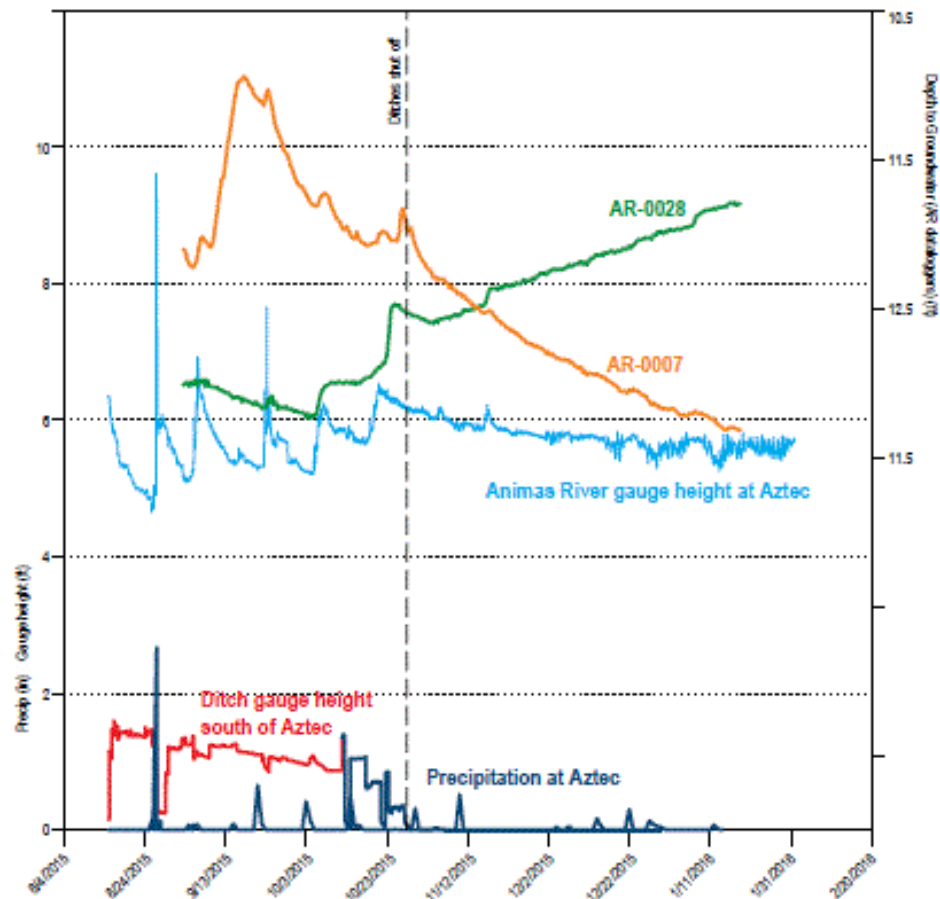


Figure D-15. Hydrographs from Aztec area including a well with continuous data recorder plotted with influences from precipitation and Animas River stage and ditch gage height. Well AR-0007 is located on the south side of Aztec, is 32 ft deep, and is located on the east side of the river. (modified from Timmons et al., 2016).

The NMBRMR conducted a synoptic survey of water levels in private wells during the period August 2015, January and March 2016 (Timmons et al., 2016). They also monitored continuous precipitation and Animas River and irrigation ditch stages at select locations (See Figure D-15). As would be expected, the Animas River stage elevation responds very quickly to precipitation events. The alluvial well in this location has a more muted and delayed response to the precipitation/river stage signal. An approximate five-day delay in the signal from river stage to well response is expected based on observations at an alluvial well. Also, the influence of the irrigation ditches is apparent. Once the irrigation ditch is drained for the winter, the water levels in the alluvial well drop to the baseflow levels. A significant observation is the sensitivity of aquifer water levels to the operation of the irrigation ditches which are important sources of water for the irrigated cropland in the growing season.

Scenario 1. GFLOW regional model for January 2016 hydrologic condition

The GFLOW model was calibrated first for areal recharge over the catchment area, and second for hydraulic conductivity of the rock and alluvium. The January 2016 period was used for calibration since during this baseflow period the irrigation ditches were not involved in the water balance (i.e., the start-simple-and-add-complexity strategy). The EPA team used the synoptic survey of water levels conducted by Timmons et al. (2016). The regional recharge over the study area was calibrated to satisfy the regional water balance at the Farmington USGS gage (See Figure D-16). The water balance means input – output = change storage = zero (i.e., or $Q_{\text{farm}} = Q_{\text{aztec}} + N_{\text{study area}} * \text{study area} - Q_{\text{wells}}$). The river flows Q_{farm} and Q_{aztec} are known from USGS gage data. An average pumping rate for the private domestic water wells was assumed to be 400 gallons per day, recognizing that this is an overestimate of consumptive use given that there will be an expected return flow to the aquifer via septic discharge. The study area is calculated using GIS and the USGS DEM and an estimate of the catchment boundary. The water fluxes of rock \leftrightarrow alluvium and alluvium \leftrightarrow river are computed internally to the GFLOW model. The model is calibrated to match the Q_{farm} at the outlet by varying the net recharge, including lumped ET loss, over the study area ($N_{\text{study area}}$). The result was a recharge over the catchment area of $N=1.556E-4$ m/d.

The GFLOW map of hydraulic head contours are shown in Figure D-17 (a). The resulting manual calibration of the hydraulic conductivity that minimized the residual error was $k_{\text{rock}} = 0.035$ m/d and $k_{\text{alluv}} = 2.2$ m/d. The calibration statistics for the wells located in the alluvial floodplain are shown in Figure D-17 (b). The GFLOW model parameters are summarized in Table D-4.

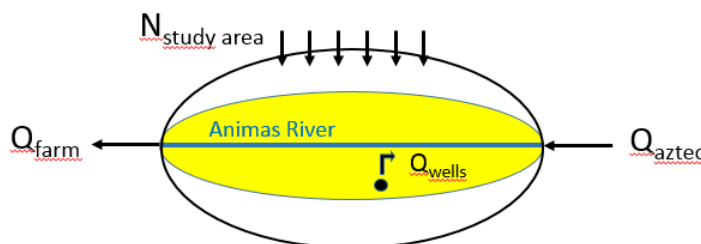
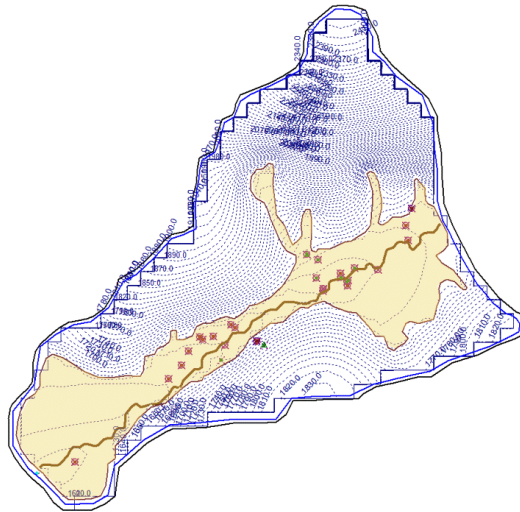


Figure D-16. Conceptual diagram of water balance used in the GFLOW model for the lower Animas River without ditch diversions.

Table D-4. Summary of Lower Animas GFLOW parameters for January 2016 model calibration.

Parameter	Model Value
Alluvium porosity (n) [-]	0.2
Alluvium base elevation [m]	1600
Alluvium thickness [m]	100
Alluvium hydraulic conductivity [m/d]	2.2
Rock porosity (n) [-]	0.2
Rock base elevation [m]	1600
Rock thickness [m]	100
Rock hydraulic conductivity [m/d]	0.35
Areal recharge (N) (m/d)	1.556E-4
Net flow Farmington (Q _{farm}) [m ³ /d]	587,178.1

A)



B)

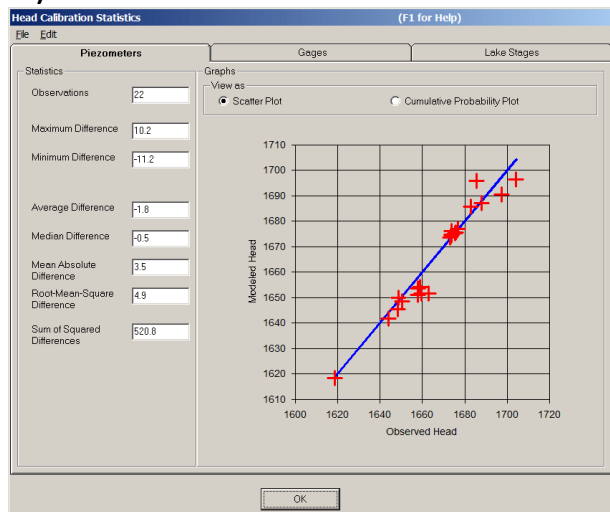


Figure D-17. GFLOW calibration for lower Animas River regional groundwater model for January 2016 flow conditions. The model areal recharge satisfying water balance was $N = 1.556E-4$ m/d. Static water levels were measured at wells and entered into the GFLOW model as test points. Calibration minimizes the residual error or difference between the observed water levels and the model predicted water levels. A) resulting calibrated model and regional hydraulic head contours; B) calibration statistics for the test points located in the alluvium, alluvium hydraulic conductivity $k_{alluv} = 2.2$ m/d. Thus, at any specific alluvium well the model is on average low by 1.8 m.

Scenario 2. GFLOW regional model of the August 2015 hydrologic period

During the August 2015 period, the time of the GKM release and plume transport, the irrigation ditches would be expected to be in full operation in the Lower Animas River area. A GFLOW model was constructed to include the irrigation ditches as constant head linesinks. The location of the ditches in Farmington are shown in Figure D-18. The elevation of the water levels in the ditches was estimated using the LiDAR DEM. The layout of linesink representation of the ditches in the GFLOW model is shown in Figure D-19.

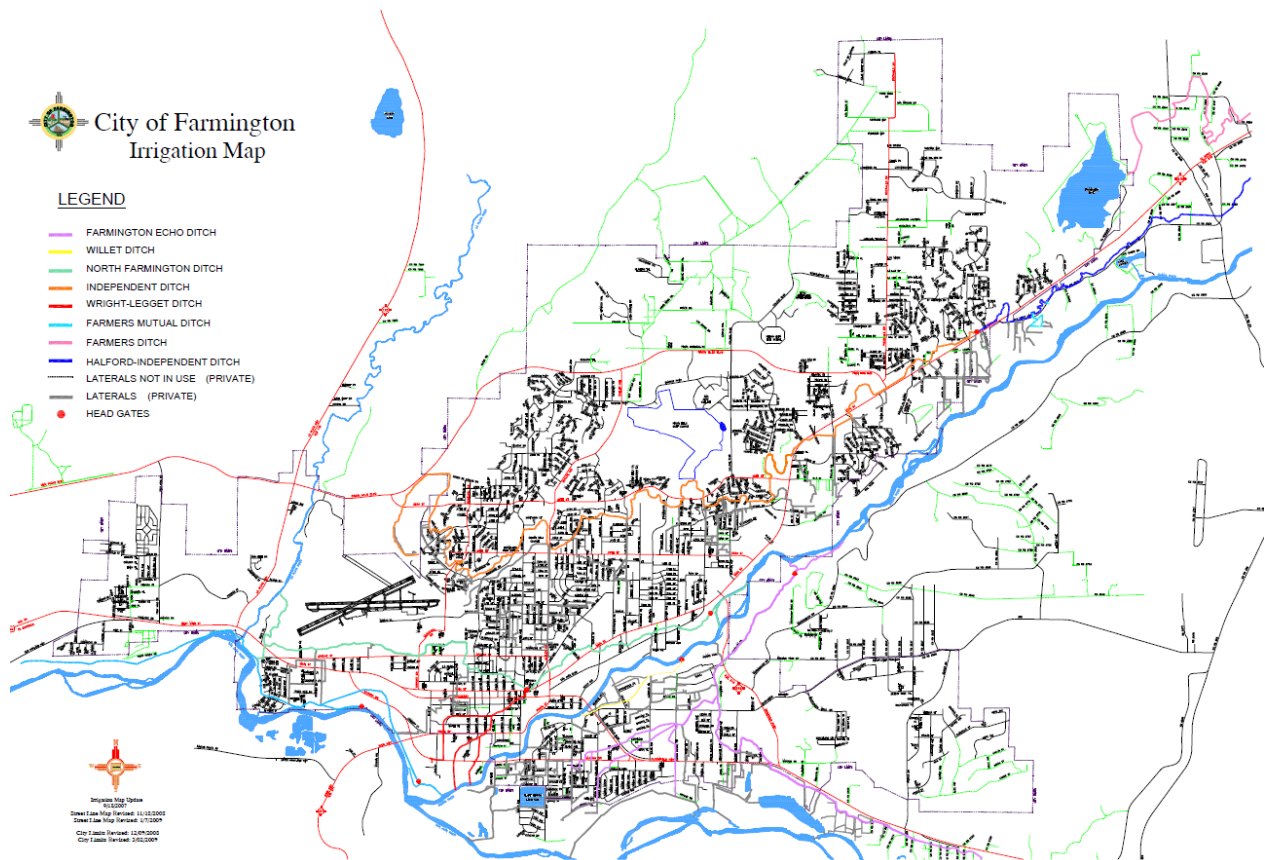


Figure D-18. City of Farmington, NM, irrigation ditch map. The streets are shown as black lines; the irrigation ditches are shown in colors (city map, updated 2009).

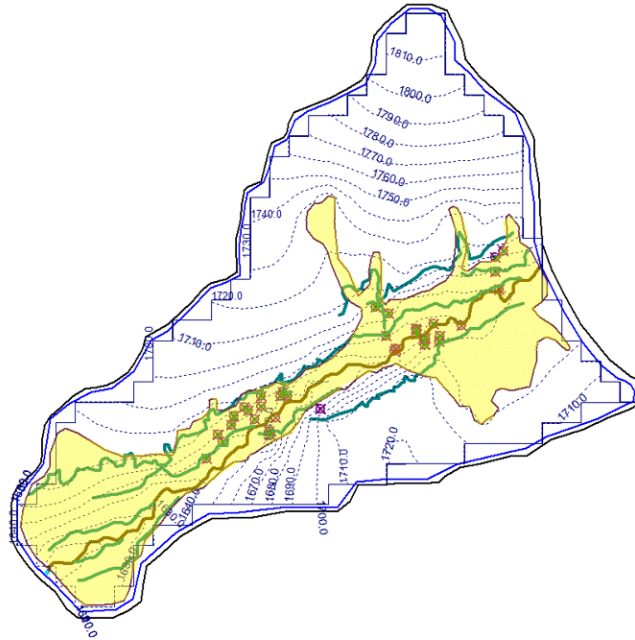
The NMBGMR provided a synoptic survey of private water well elevations for the dates, 8/17 – 8/20/2015. A five-day delay from Animas River stage to well response is expected. Therefore, Animas River discharge was averaged for dates 8/12-8/15/2016, see Table D-3 for the water flows.

The GFLOW solution that satisfies the steady water balance for the August 2015 time period, and which minimizes the residual error between model calculated hydraulic head and observed water levels in the water supply wells is shown in Figure D-20. The only parameter changed from the previous Scenario 1 was the net flow at Farmington 1,548,682.3 m^3/d as a calibration target. The areal recharge that minimized the model difference in predicted flow at the catchment outlet at Farmington was $N=0.215e-4 m/d$.



Figure D-19. GFLOW layout of elements including line-sink representation of irrigation ditches in the lower Animas River study area. The elevation of the water levels maintained by the ditches informed by the high-resolution LiDAR elevation data.

A)



B)

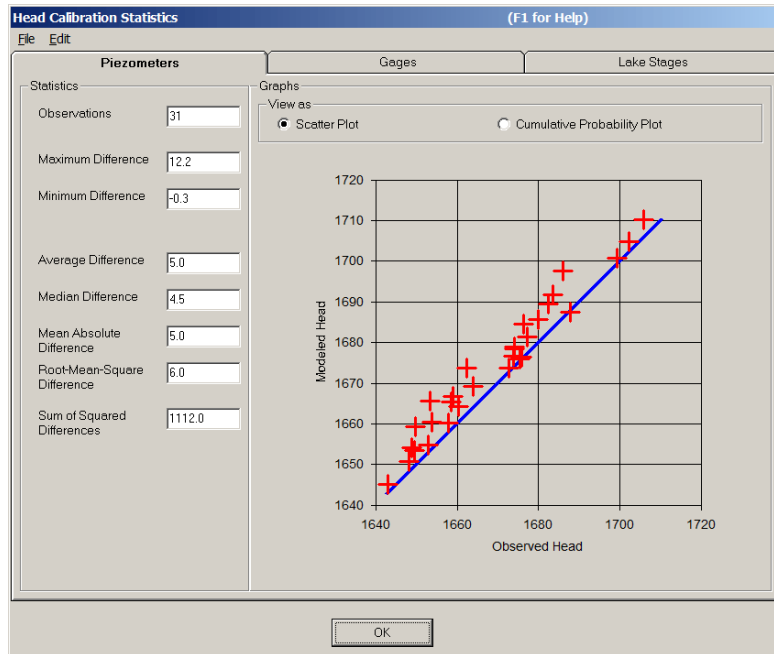


Figure D-20. GFLOW regional groundwater model lower Animas River for August 2015 time-period, including irrigation ditches. The effective recharge over the catchment area $N=0.215e-4$ m/d minimized model predicted error at the outlet at Farmington. The average head difference error went up to plus 5m.

Scenario 3. GFLOW Regional model of the August-October 2015 Hydrologic Period

The water balance for the lower Animas River study area can be refined to include the observed major diversions from the Animas River to the irrigation ditches. These data are collected by the New Mexico Office of the State Engineer, Interstate Stream Commission, and publically available on the Real-Time Water Measurement Information System webpage (<http://meas.ose.state.nm.us/>). The sum of the diversions for the August to October 2015 time-period is summarized in Table D-5.

Table D-5. Irrigation ditch diversions (New Mexico Office of the State Engineer)

Ditch Name	Diversions Aug-Oct 2015 (m ³ /d)
Kello-Blancett	21,166.3
Halford-Independent	40,105.1
Ranchmans-Terrell	7,358.2
Farmington Echo	69,476.7
North Farmington/Wright-Leggett	11,649.0
Sum total	149,755.3

The Scenario 2 GFLOW model was adjusted to represent the August-October 2015 water balance, including the influence of ditch diversion and pumping well extraction. With reference to the conceptual diagram of the water balance of Figure D-21, the study area Animas River inflows at Aztec, NM was estimated as the measured flow (from Table D-2, 428 cfs or 894,142.6 m³/d) minus the total diversions (149,755.3 m³/d) or $Q_{aztec} = 744,387.3 \text{ m}^3/\text{d}$. The observed average flow at Farmington, NM is $Q_{farm} = 880,128.6 \text{ m}^3/\text{d}$. The estimated pumping rates included those of the community wells (i.e., reported average diversions) and estimated for the private wells (i.e., 400 gallons per day; Note this is a high estimate since it does not include return flow via septic fields). The water fluxes of rock ↔ alluvium and alluvium ↔ river/ditches are computed internal to the GFLOW model. The GFLOW manual calibration varied the net recharge (i.e., lumps the ET losses and return flows) over the floodplain alluvium deposits until the residual error (i.e., model observed minus model simulated flow at the Farmington outlet, Q_{farm}) was minimized, resulting in model recharge over the alluvium $N_{alluv} = 0.0053 \text{ m}/\text{d}$. The results of the calibration are presented in Figure D-22. The 90-day capture zones of the wells are too small to be seen at this scale. The model suggests only the 21m-174km community well pumping at a maximum rate of 817.6 m³/d sources from the river.

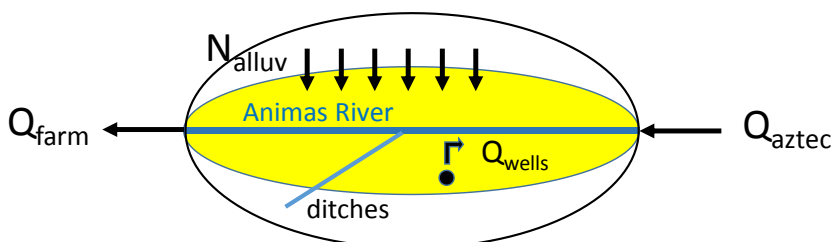


Figure D- 21. Conceptual diagram of water balance used in the GFLOW model for the lower Animas River including the influence of irrigation ditch diversions.

Local Scale GFLOW Model for a Lower Animas River Floodplain Community Well

The calibrated regional GFLOW model for the averaged hydro period August-October 2015 provides the basis for the evaluation of floodplain water supply well sourcing from the lower Animas River, where an example community well (i.e., 21m174km) is used to explore local scale capture zone delineation and solute breakthrough.

While the GFLOW model predicted the 21m174km community well could source from the Animas River, the first arrival of the plume was predicted to take over 90 days, with significant dilution predicted. The aquifer would take almost two years to flush under these conditions (See Figure D-23).

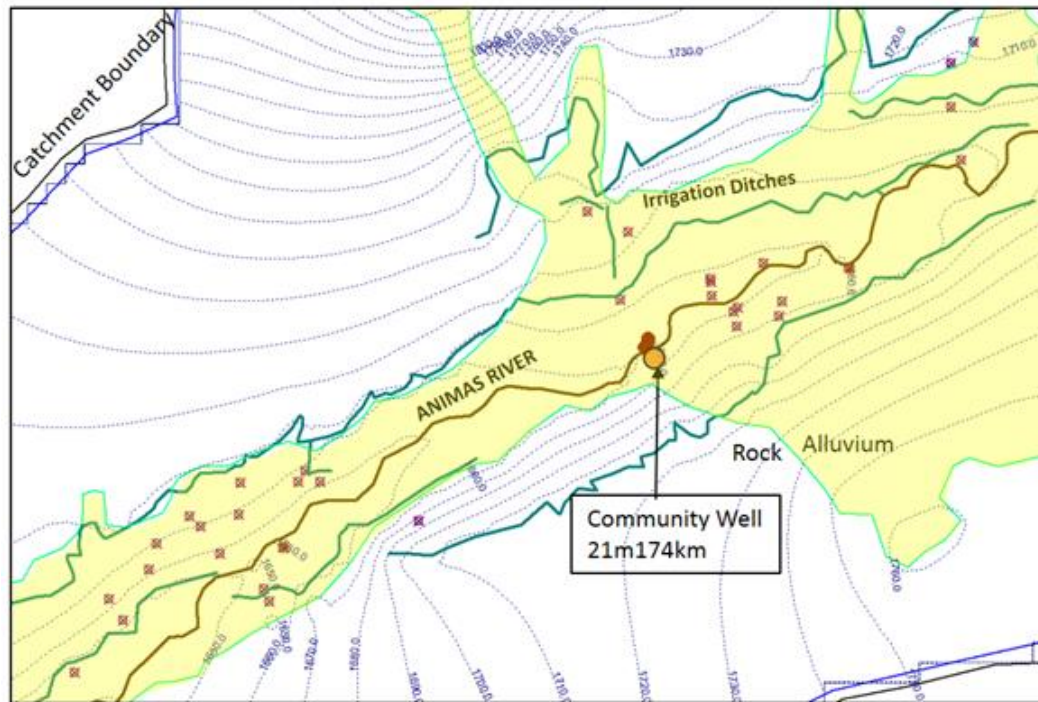


Figure D-22. GFLOW model of groundwater-surface water interactions in the lower Animas River floodplain between Aztec and Farmington, New Mexico (RK 170-180) for the averaging period August – October 2015.

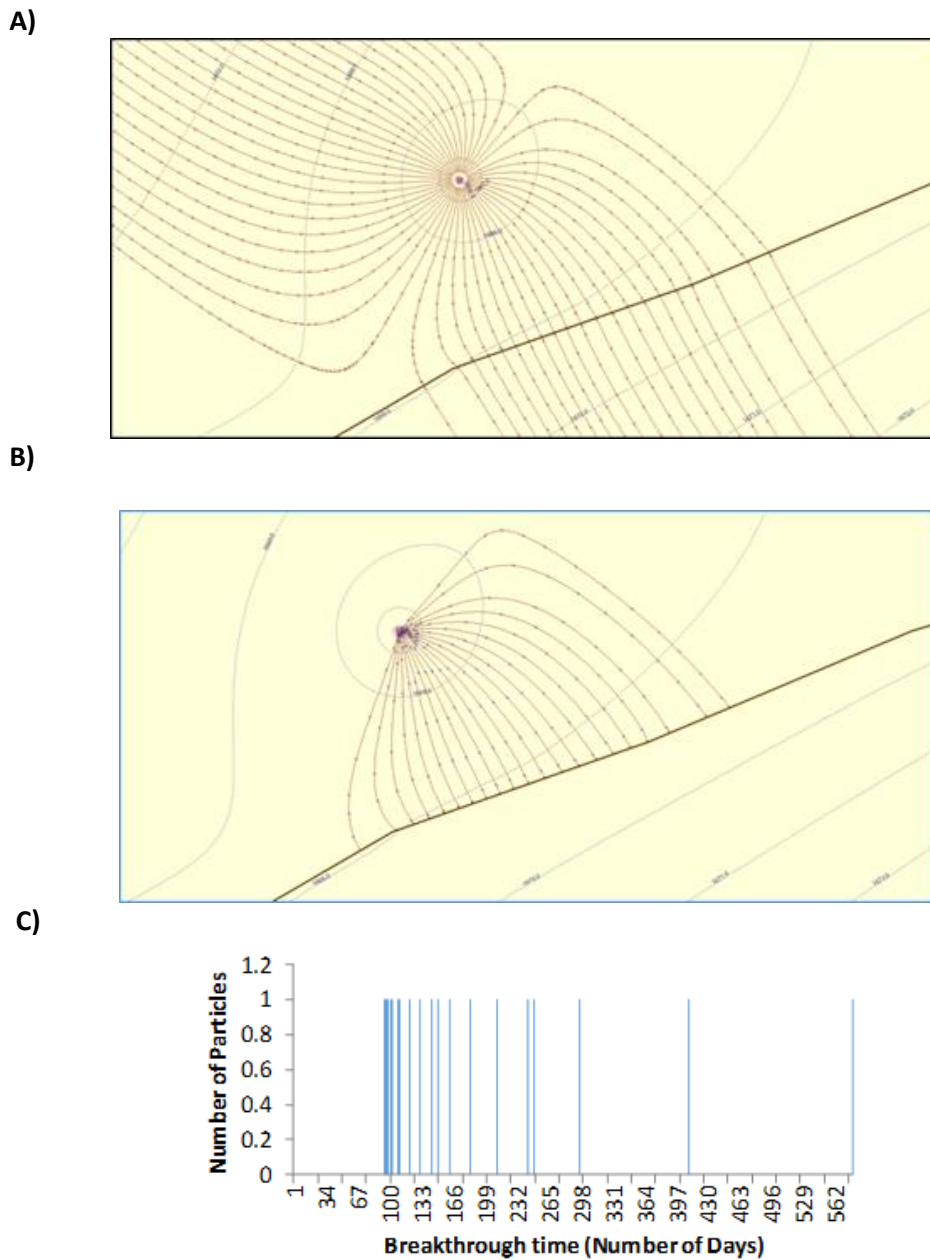


Figure D-23. GFLOW capture zone and solute breakthrough histogram for lower Animas community well. Community well (21m-174km), high pumping ($Q_w=817.6 \text{ m}^3/\text{d}$) and low porosity ($n=0.25$). A) capture zone delineation with 48 reverse streamlines; B) particle tracking with 21 forward pathlines; C) predicted time of arrival breakthrough (days) are reported in a histogram, with a particle arriving in 94 days. Breakthrough time with same pumping but higher porosity ($n=0.35$) has a particle arriving in 131 days. Suggested peak river concentration is diluted to about 2% ($1/48$). Flushing of the aquifer in about 565 days. Note that advective transport is steady (time invariant pumping and hydrology) and does not account for dispersion, sorption, or decay of solute.

Mid Animas River Groundwater Models

A second cluster of community wells was the focus of the mid Animas River floodplain groundwater modeling (RK 65-72). The floodplain also supports a large number of private/domestic wells (See Figure D-24).

Five community wells located in the mid Animas River floodplain of Colorado were identified by EPA Region 8. The initial modeling focused on the northern cluster of wells around Hermosa, CO. The sanitation department wells were not selected for modeling. The straight-line distance of each community well from the river ranges from 35 m to 1,000 m. The location of the nearest river shoreline was defined using the latest Google Earth imagery. The wells are approximately 66-71 km downstream of the GKM release point. The name of each community well combines the distance from the river, in meters, and the distance downstream from the GKM release, in kilometers (See Figure D-25).

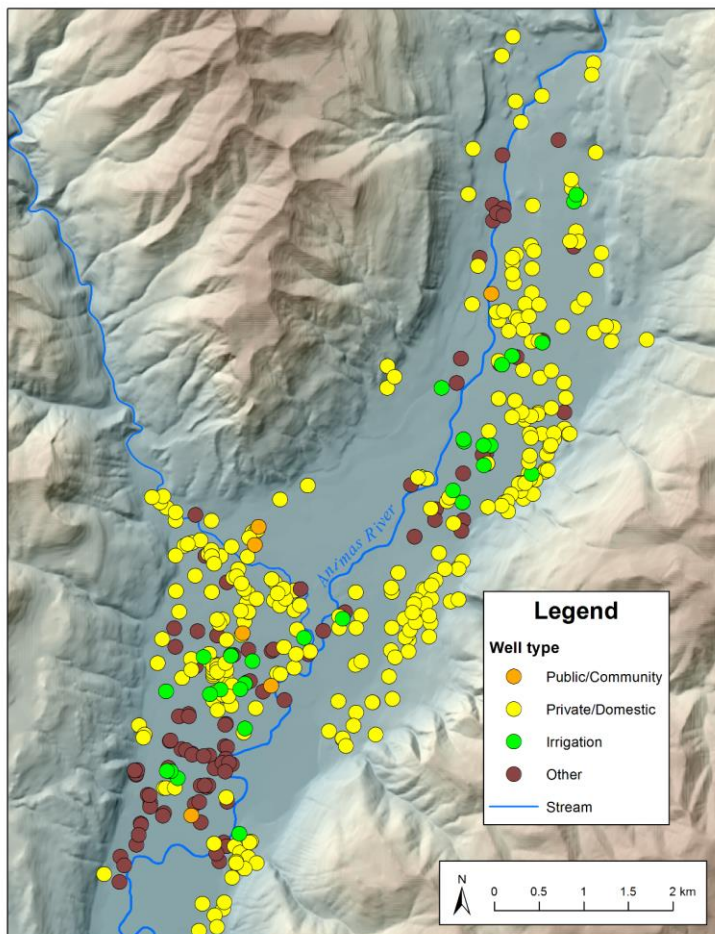


Figure D-24. Water supply wells of the floodplain of the mid Animas River. The background is the topographic DEM and the hydrography of the USGS Hermosa Quad. Well data are available from the Colorado DWR well permit search database. The community wells are represented by the orange circles.

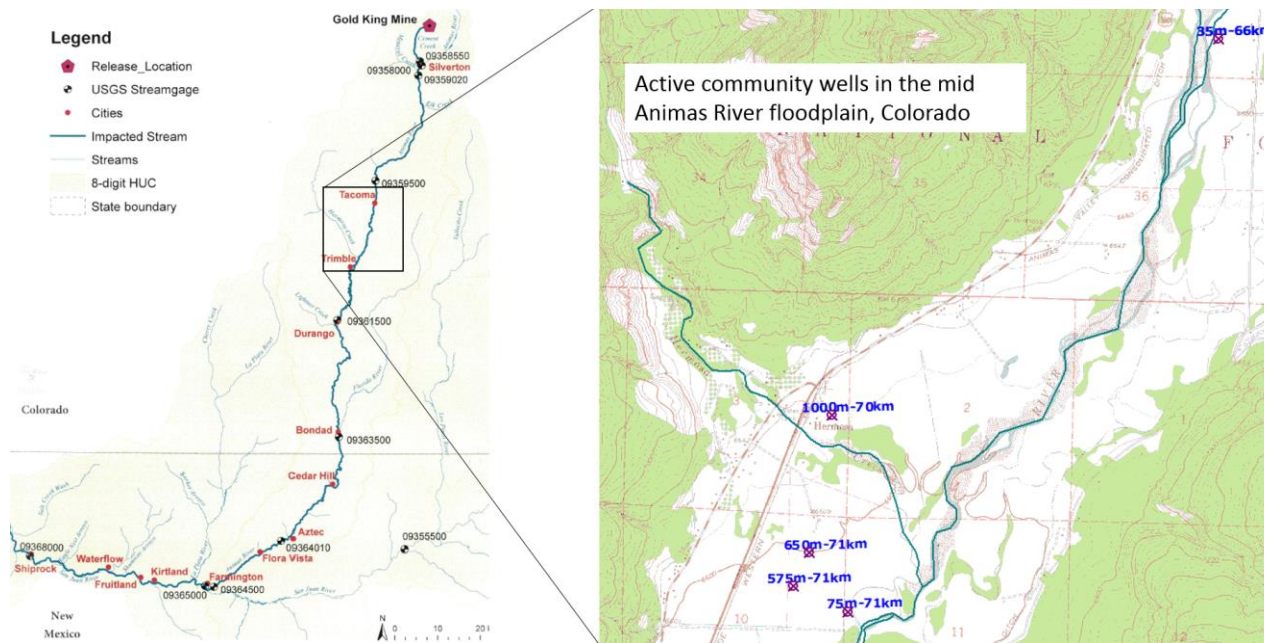


Figure D-25. Selected community wells for investigation located in the mid Animas River floodplain near Hermosa between Tacoma and Trimble, Colorado. Basemap: USGS 7.5 minute topographic DRG (digital raster graphic).

Basic information regarding the wells is reported in the Colorado Department of Water Resources Well Permit online database (www.dwr.state.co.us/WellPermitSearch). The (x, y) location of the wells are georeferenced to electronic base maps in the UTM Zone 13 NAD83 projection and attempted confirmation with Google Earth imagery. The sustained yield and water level drawdown are reported in the driller’s log. An ID was assigned to the community wells incorporating distance from river, in meters, and downstream distance from GKM in kilometers, in the name (See Table D-6).

Table D-6. Community well data (source: Colorado Div Water Resources, Well Permit Search, CDNR CDSS)

Identification*	Total Depth (Ft)	Screened Intervals (Ft bgs ^{&})	Static Water Level (Ft bgs)	Pumped Water Elevation (Ft bgs)	Well Yield (gpm) Observed, Estimated	Average Annual Well Diversions (Acre-ft, Years)
35m66km	100	70-95	22.5	25.0	480 (580)	56.4 (1996-2014)
75m71km	87	45-85	10.5	13.5	445 (600)	145.74 (1997-2014)
575m71km	210	NA	18.2	19.3	100 (450)	139.38 (2009-2014)
650m71km	120	50-60,70-95,105-115	24	28.75	400 (600)	162.65 (1998-2014)
1000m70km	100	72.75-100	31.2	35.2	425 (425)	NA

*An ID was assigned to the community wells incorporating distance from river (in meters) and downstream distance from GKM (in kilometers) in the name.

[&]Ft bgs is Feet Below Ground Surface

Table D-7. USGS streamflow data at gaging stations in mid Animas River area.

USGS Gage Name	USGS Gage Number	Discharge on 8/1/2015 (m ³ /d)	Discharge Averaged 2015, Aug-Oct (m ³ /d)	Discharge Historical, 1947-1955, Aug-Dec (m ³ /d)
Animas River Tall Timbers Resort, CO	09359500	1,350,510	739,318	521,194
Animas River Durango, CO	09361500	1,313,811	898,984	776,519

The regional GFLOW model solves the Animas River water balance for the area draining between USGS Tall Timbers Resort, CO and USGS Durango, CO for different time periods, as shown in Table D-7. The catchment between the two USGS gages of the study area and the boundary of the Animas River floodplain is defined using the USGS digital topographic map and the USGS Hermosa, CO quad geology map (Figure D-26).

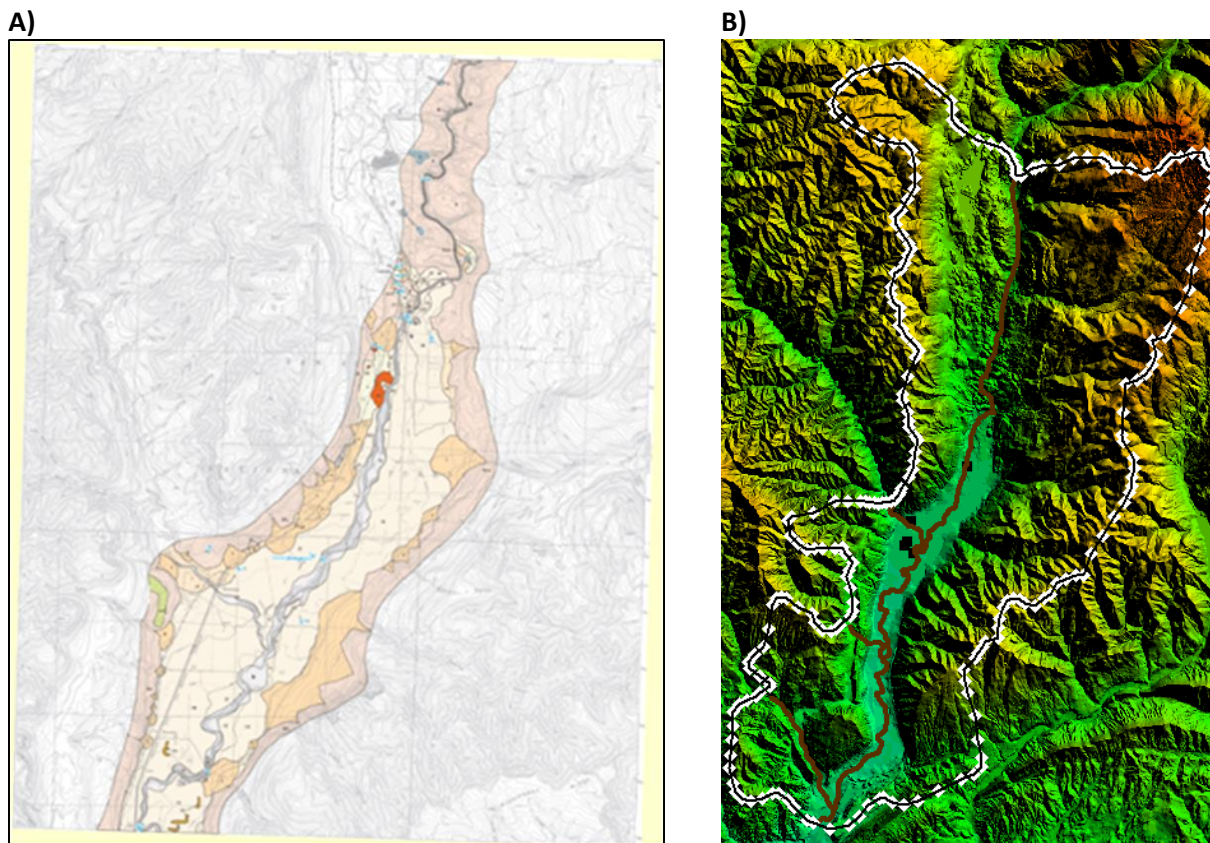


Figure D-26. Mid Animas River geology and digital elevation. A) USGS surface geology map Hermosa, Colorado quad, showing the alluvial floodplain deposits surrounded by rock (Blair, Yager, 2002). B) USGS NED 10-m resolution and the topographically defined catchment between USGS gage stations at Tall Timbers Resort and Durango, Colorado. The alluvial floodplain shows up in light blue-green.

Mid Animas River GFLOW Model Setup

The layout of GFLOW analytic elements for the mid Animas River floodplain groundwater model is shown in Figure D-27. A no-flow boundary is maintained at the catchment boundary or drainage area between the USGS gage on the Animas River at Tall Timbers resort, and the USGS gage on the Animas River near Duragno. The aquifer base elevation is considered no-flow in the GFLOW model. The gravimetric estimate of aquifer thickness occurred at each of the scan lines (Hasboux Geophysics, Inc., 2003; Figure D-10). These were used to parameterize a stepping base representation in the GFLOW model.

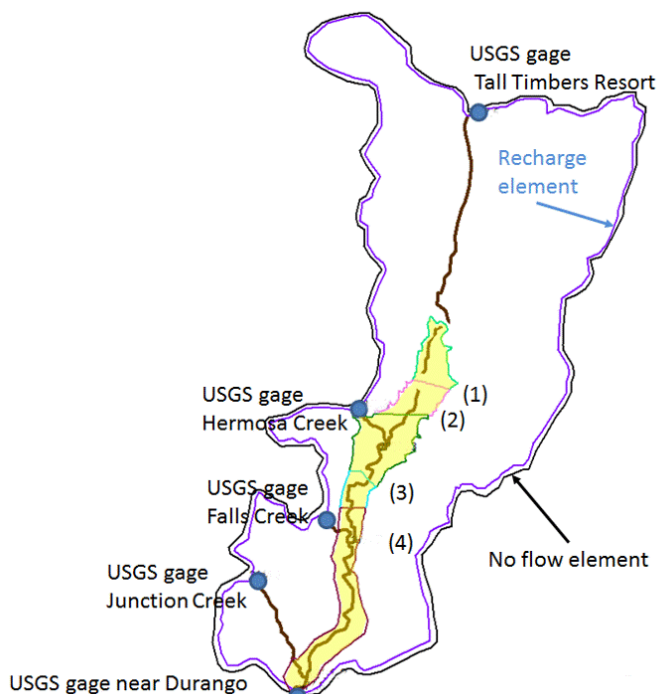


Figure D-27. GFLOW layout of analytic elements for the mid Animas River floodplain groundwater model. A no-flow boundary is maintained at the catchment boundary or drainage area between the USGS gage on the Animas River at Tall Timbers resort, and the USGS gage on the Animas River near Duragno. The aquifer base elevation is considered no-flow in the GFLOW model. The gravimetric estimate of aquifer thickness occurred at each of the scan lines. These were used to parameterize a stepping base representation in the GFLOW model.

Mid Animas River GFLOW Model Calibration

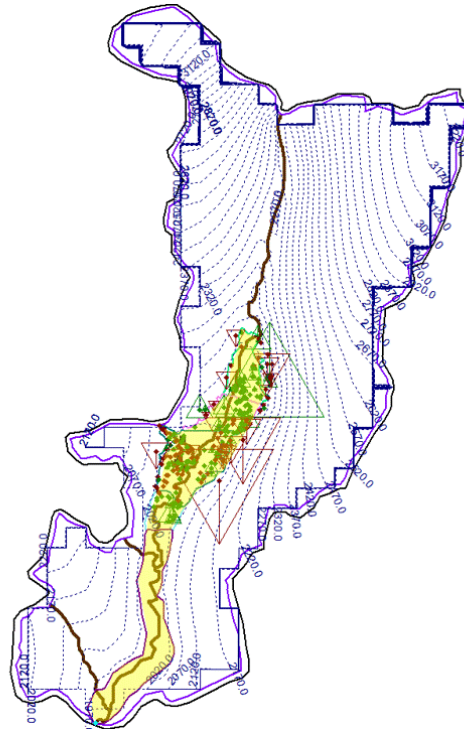
Scenario 1. GFLOW Regional Model for the Aug-Dec, 1947-1955 Historical Time Period

The August-December historical record from 1947-1955 of daily stream flows at the USGS gages at Tall Timber Resort and Durango were used to estimate the average area recharge on the catchment draining between these two stations. Model calibration for exiting average stream flows provides the estimate for average areal recharge ($N = 0.000463 \text{ m/d} = 6.6 \text{ in/yr}$). Model calibration minimizing the difference between model calculated hydraulic heads and observed water levels in wells was used to estimate hydraulic conductivity of the rocks and floodplain deposits. Unlike in the lower Animas River floodplain, the team did not have the synoptic survey of water levels in wells. We used the static water levels reported in the well driller's logs. This had impact on the model error (See Figure D-28 (a), (b), (c)).

Table D-8. Summary of Mid Animas GFLOW parameters for Aug-Dec, 1947-1955 model calibration.

Parameter	Model Value
Alluvium porosity (n) [-]	0.2
Alluvium 1 base elevation [m]	1915.1
Alluvium 1 thickness [m]	92
Alluvium 1 hydraulic conductivity [m/d]	60
Alluvium 2 base elevation [m]	1897.1
Alluvium 2 thickness [m]	92
Alluvium 2 hydraulic conductivity [m/d]	60
Alluvium 3 base elevation [m]	1755.2
Alluvium 3 thickness [m]	92
Alluvium 3 hydraulic conductivity [m/d]	60
Alluvium 4 base elevation [m]	1875.1
Alluvium 4 thickness [m]	92
Alluvium 4 hydraulic conductivity [m/d]	60
Alluvium 5 base elevation [m]	1808.1
Alluvium 5 thickness [m]	92
Alluvium 5 hydraulic conductivity [m/d]	60
Rock porosity (n) [-]	0.2
Rock base elevation [m]	1977
Rock thickness [m]	92
Rock hydraulic conductivity [m/d]	0.2
Areal recharge (N) (m/d)	4.63E-4
Net flow Durango ($Q_{durango}$) [m ³ /d]	776,518.6

A)



B)

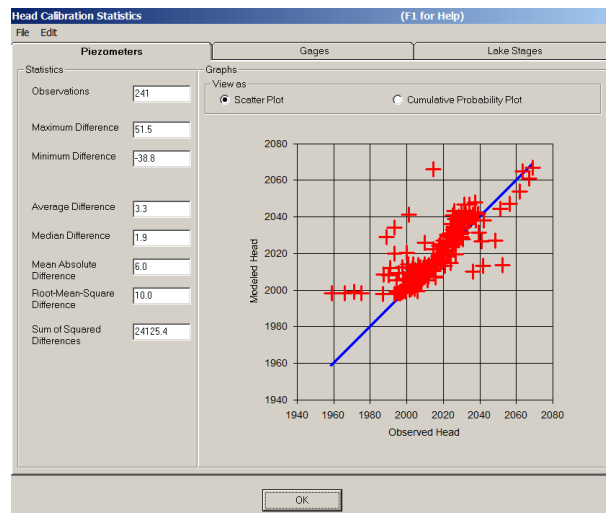


Figure D-28. GFLOW mid Animas River floodplain regional groundwater model calibration results. The model used the water balance areal recharge of $N = 0.000463 \text{ m/d} = 6.6 \text{ in/yr}$. The result of the calibration suggested the hydraulic conductivity of the rock, $k_{\text{rock}} = 0.2 \text{ m/d}$, and of the floodplain alluvium $k_{\text{alluv}} = 60 \text{ m/d}$. (a) plot of head contours in the mid Animas River and showing test points of observed static water levels (historical). The triangles indicate the magnitude of the residual error (model – observed) and direction of triangle signifies sign of residual, positive tip of triangle up, negative tip of triangle down. (b) plot of model predicted heads vs the observed heads for the floodplain test points (avg error +3.3 m).

Scenario 2. GFLOW regional model for the August – October 2015 hydrologic period

Building on the previous result, the GFLOW model was adapted for the August –October 2015 mid Animas River water balance. The flow of the mid Animas River groundwater model was input at the USGS gage location at Tall Timbers resort, and the areal recharge over the study area was solved for such that the model predicted outflow in the Animas River outlet at Durango matched the observed, using data from **Table D-7**. The resulting areal recharge was $N=4.377E-4$ m/d.

Local scale GFLOW model for a mid-Animas River floodplain community well

The GFLOW model was used to zoom into the mid Animas River floodplain near Baker’s Bridge (RK 65-72) showing groundwater-surface water interactions for the averaging period August-October 2015 (See Figure D-29). The GFLOW model suggests that only three private wells in the mid Animas River area directly source river water, with distances of the wells from the river ranging from 10-123 m. There were many other wells within 123 m of the river that the model suggested do not source river water. Therefore, distance from the river alone is not predictive of well sourcing from the river. Geomorphology and the location of losing sections of the river are factors. The model suggests that the Baker’s Bridge area where the Animas River leaves the mountain pass and enters the floodplain valley has groundwater seeping into the aquifer and a potential “hyporheic” zone.

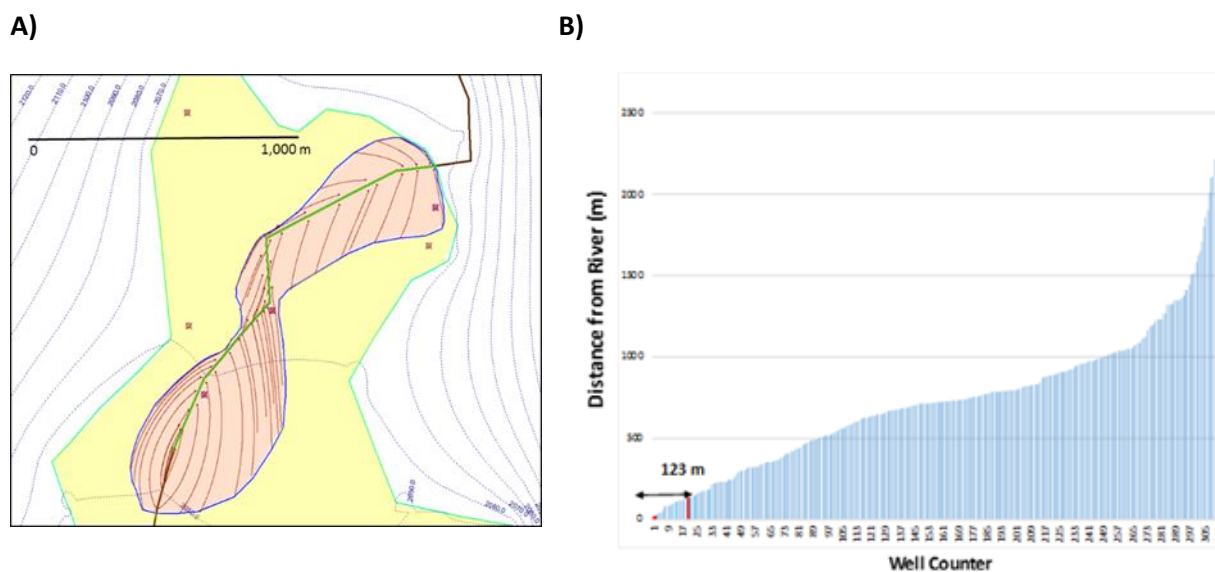


Figure D-29. GFLOW model of the mid Animas River floodplain near Baker’s Bridge (RK 65-72) showing groundwater-surface water interactions for the averaging period August-October 2015. A) Hydraulic head contours (m) are shown as dotted lines and the river flow is north to south. The gaining sections of the river are colored black; the losing sections shown in green. Forward particle traces are shown in red, with residence time limited to 90 days’ time-of-travel. Note there are three private domestic pumping wells located inside the “hyporheic” zone colored light red. B) The bar graph shows the distances of wells from the river of over 300 wells. Distances ranged from 10m to over 2,000 m.

The calibrated regional mid Animas River GFLOW model for the August–October 2015 hydro period was used to evaluate the local scale capture zones and particle tracking solute transport for the mid Animas River floodplain community well 35m66km (Figure D-30). The combination of parameters (i.e., low recharge, high alluvium hydraulic conductivity, high well pumping rate, low alluvium porosity) creates the earliest breakthrough of 25 days. Full sensitivity analysis on area recharge, hydraulic conductivity of aquifer material, and pumping rate of well is described in a later section. Note that advective transport is steady (time invariant pumping and hydrology) and does not account for dispersion, sorption, or decay of solute.

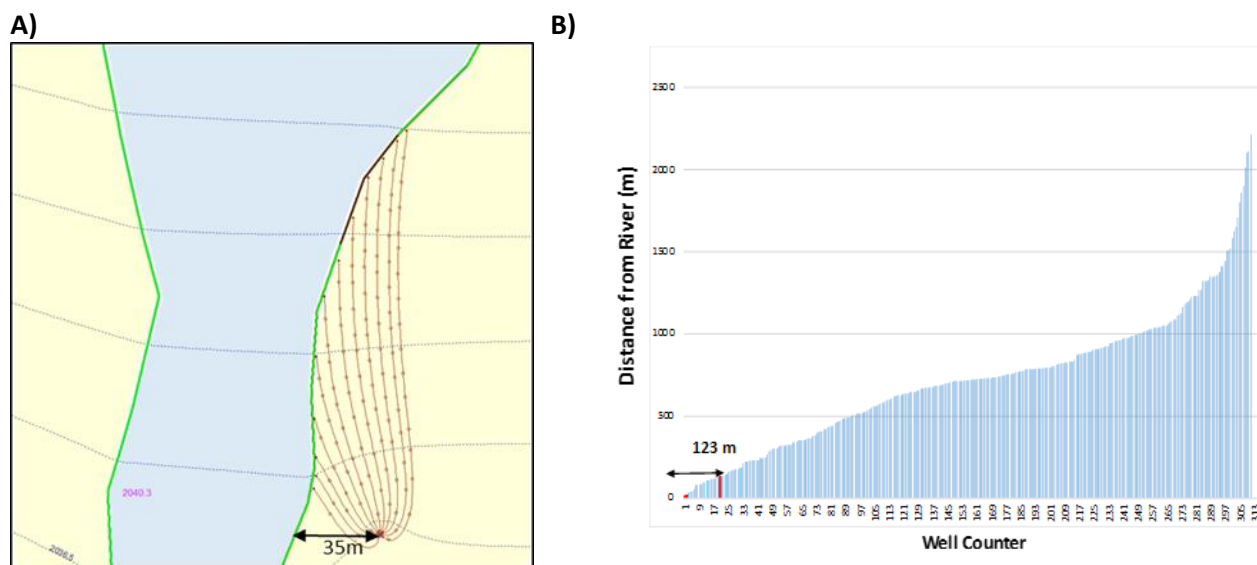


Figure D-30. GFLOW capture zone and solute breakthrough histogram for a mid-Animas River community well. GFLOW analysis of mid Animas River community well (35m-66km), high pumping ($Q_w = 2,616.5 \text{ m}^3/\text{d}$) and low porosity ($n=0.2$) A) particle tracking with 12 forward pathlines; B) time of arrival breakthrough, in days, are reported in a histogram, with a particle arriving in 25 days. Breakthrough time with same pumping but higher porosity ($n=0.35$) has a particle arriving in 44 days. Suggested peak river concentration is diluted to about 17% ($2/12$). Flushing of the aquifer in about 160 days.

Consideration of Uncertainty in the Groundwater Modeling

Mid Animas: Exploration of the steady-state modeling assumption

Analytical solution

Revisiting the issue of steady state modeling, recall Equation (4) for a dimensionless groundwater system response time τ :

$$\tau = \frac{SL^2}{4TP}$$

where S [-] is the aquifer storage coefficient, L [m] the distance between head specified boundaries, T [m^2/day] the aquifer transmissivity (product of aquifer thickness and hydraulic conductivity), and P [days] the period of a periodic forcing function. When considering seasonal variations in flow in an alluvial

aquifer, the definition of L is more conveniently defined as the distance between the river and the valley boundary (rock outcrop). Haitjema (2006) offers the following rules-of-thumb:

- $\tau < 0.1$ treat transient flow in the aquifer as successive steady state.
- $0.1 \leq \tau \leq 1$ transient flow cannot be meaningfully represented by a steady state model.
- $\tau > 1$ represent transient flow by a steady state model using average boundary conditions.

For select community wells in the mid Animas River floodplain, the calculations for τ are shown in Table D-9.

If the daily forcing of the community water supply wells is assumed (i.e., 1 day), then $\tau > 1$, independent of other properties, and steady state modeling can be applied using averaged river elevations and pumping rates. If the annual spring snow melt forcing is assumed (i.e., 365 days), then there are cases where $\tau < 0.1$, and successive steady state modeling can be applied, but also cases when $0.1 \leq \tau \leq 1$, and transient modeling would be required. In order to capture the full spectrum of capture zones with use of a steady state model, both actual and averaged pumping rates and river stages should encompass the full range of cases. This is explored in the sensitivity analysis presented in a later section.

Table D-9. Dimensionless time factor for mid Animas River floodplain wells.

Realization	Storativity, S, (-)	Distance, L, ft	Transmissivity, T, gpd/ft	Periodicity, P, days	τ
1	0.29	2,285	314,628	365	0.02
2	0.29	2,285	129,621	365	0.06
3	0.36	2,285	129,628	365	0.07
4	0.36	2,285	129,621	365	0.07
5	0.29	4,805	314,628	365	0.11
6	0.29	5,830	314,628	365	0.16
7	0.36	5,830	314,628	365	0.20
8	0.29	4,805	129,621	365	0.26
9	0.36	4,805	129,628	365	0.33
10	0.36	4,805	129,621	365	0.33
11	0.29	5,830	129,621	365	0.39
12	0.36	5,830	129,621	365	0.48
13	0.29	2,285	314,628	1	9.00
14	0.36	2,285	314,628	1	11.17
15	0.29	2,285	129,621	1	21.84
16	0.36	2,285	129,621	1	27.12
17	0.29	4,805	314,628	1	39.80
18	0.36	4,805	314,628	1	49.40
19	0.29	5,830	314,628	1	58.58
20	0.36	5,830	314,628	1	72.73
21	0.29	4,805	129,621	1	96.59
22	0.36	4,805	129,621	1	119.91
23	0.29	5,830	129,621	1	142.20
24	0.36	5,830	129,621	1	176.52

Note: The realizations indicated in green signify a situation where a steady state averaged condition groundwater model would suffice; the yellow realizations signify the situations for successive steady state modeling; the orange realizations signify where transient groundwater modeling would be suggested.

Modeling of Transient Flow

The numerical model MODFLOW is capable of simulating transient flow. The community well 1000m70km (Figure D-31) has pumping test data to support the parameterization of the transient simulation (WestWater Associates Inc, 2010). The regional steady-state GFLOW model has a MODFLOW grid extract feature to setup the initial conditions for the transient simulation (See Figure D-32). The GFLOW model was used to select the size of grid in that the outer boundary condition does not influence the local scale drawdowns of the pumping well. The reported data from the pumping test included 1) transmissivity equals 129,621-314,628 gpd/ft; 2) storage coefficient equals 0.006-0.003; and 3) specific yield equals 0.3616-0.2881. There were some complications experienced in conducting the pumping test; the ranges were reported reasonable for this type of geology.

The MODFLOW model representation of the initial condition is shown in Figure D-33. The transient pumping well is added to this solution and placed at the center of the refined grid. The transient “pulsed pumping” (i.e., 12 hours on daytime; 12 hours off night-time) 10-day capture zone, in comparison to the steady state solution, is somewhat bigger (See Figure D-34). The MODFLOW/MODPATH simulations may introduce some numerical dispersion.

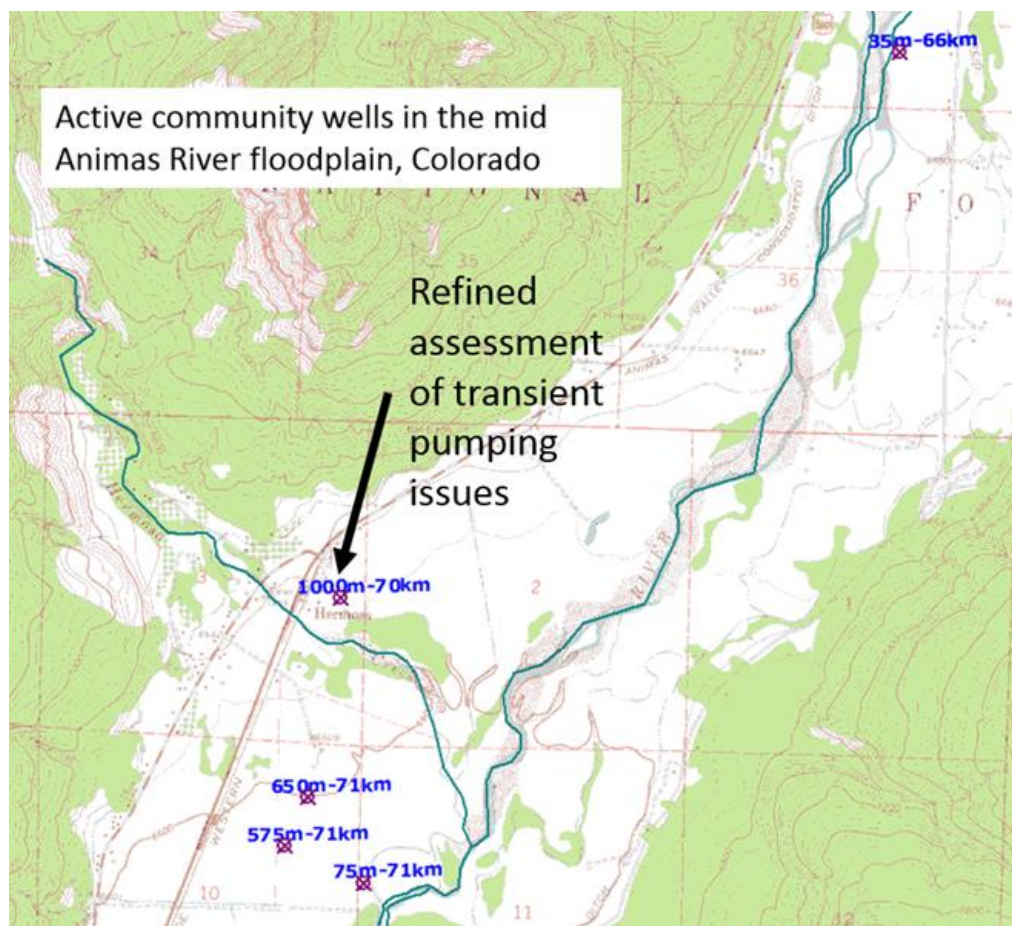


Figure D-31. The mid Animas River floodplain community well selected for exploration of transient flow. The well record included a pumping test.

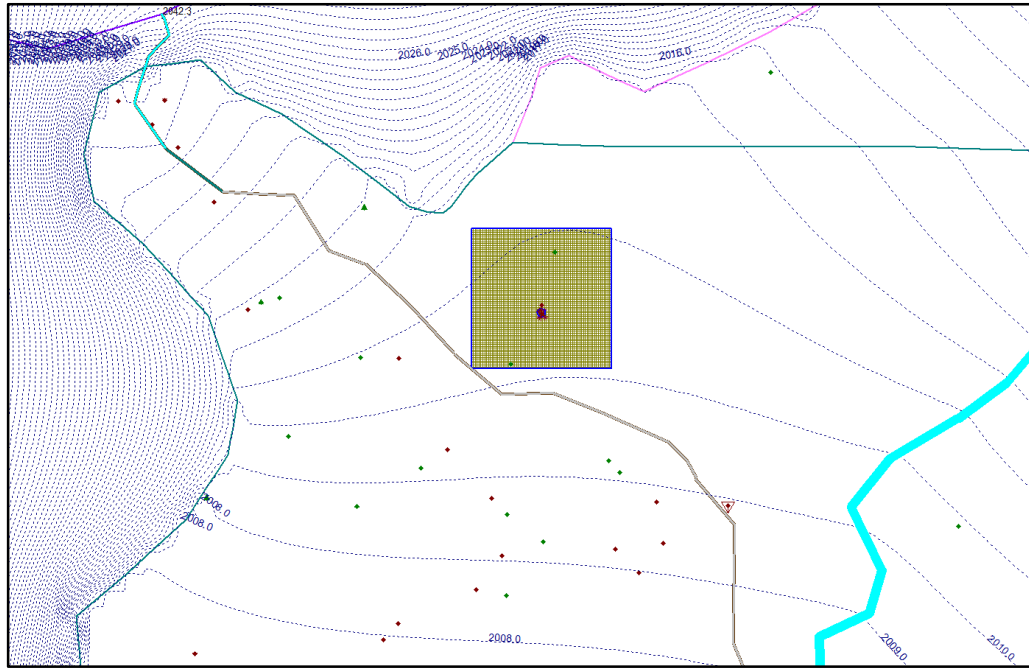


Figure D-32. The regional GFLOW model provides the initial heads to the outer cells of the MODFLOW model.

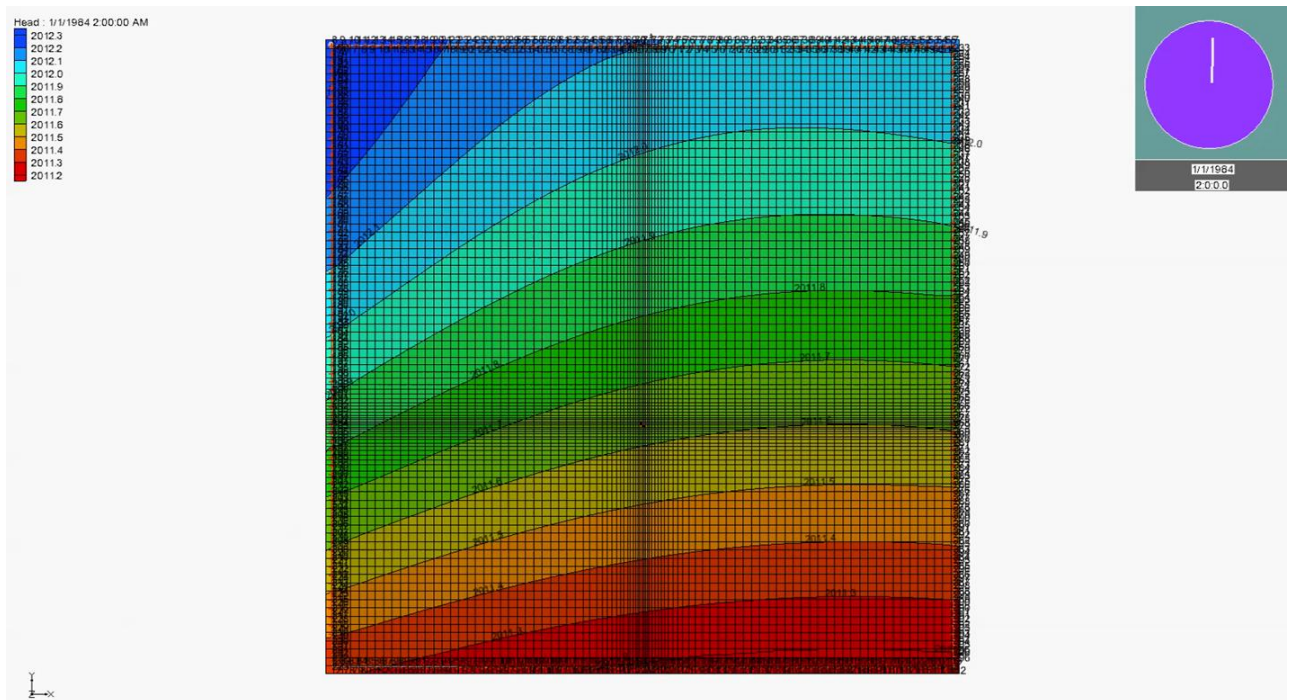


Figure D-33. The representation of initial (i.e., pre-pumping) hydraulic head conditions in the MODFLOW model.

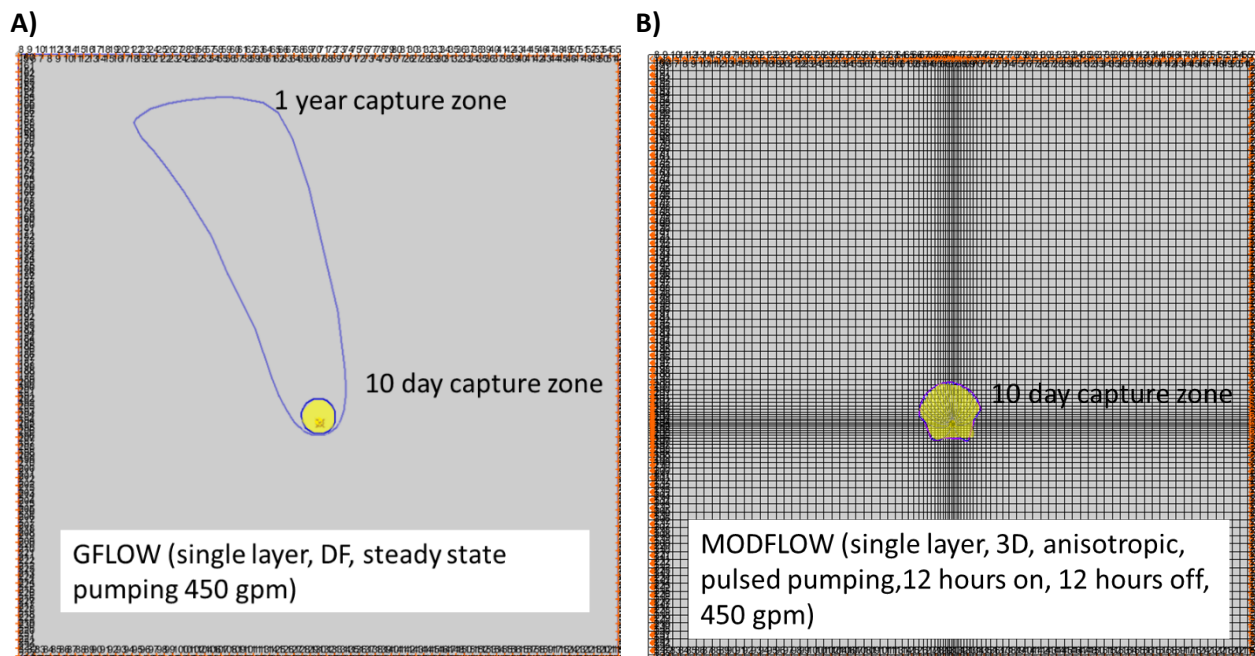


Figure D-34. GFLOW and MODFLOW models of capture zones for well 1000m70km. The pulsed and calibrated 10-day MODFLOW/MODPATH capture zone is assumed more realistic and is larger than the GFLOW steady state 10-day capture zone. This suggests there is some uncertainty in the simplified regional analysis.

Mid Animas: Exploration of Fully Three-Dimensional Flow vs. Dupuit-Forchheimer Flow

The numerical model MODFLOW is capable of simulating fully 3D flow, whereas the GFLOW model simulates 3D streamlines under the Dupuit-Forchheimer simplification that neglects resistance to vertical flow. The community well 35m66km (Figure D-35) has well driller’s log data to support the parameterization of the 3D simulation (Beeman Bros. Drilling, 1984). The regional steady state GFLOW model has a MODFLOW grid extract feature to setup the initial conditions for the numerical simulation (See Figure D-36). The GFLOW model was used to select the size of grid in that the outer boundary condition does not influence the local scale drawdowns of the pumping well. The MODFLOW grid in plan and cross-sectional view is shown in Figure D-37; the location of the well is in the center of the grid refinement.

The total depth of the well is 100 feet. The 35m66km well is screened from 67 feet below ground surface to the bottom. The initial static water level was 31 feet, 10 inches below ground surface. The well sustained yield was 480 gallons per minute (i.e., 2,616.5 m^3/day) with a drawdown to 38 feet below ground surface.

The resulting capture zone and breakthrough times for the 3D MODFLOW simulation for mid Animas River floodplain community well 35m66km are shown in Figure D-38. The well is pumping at averaged rates.

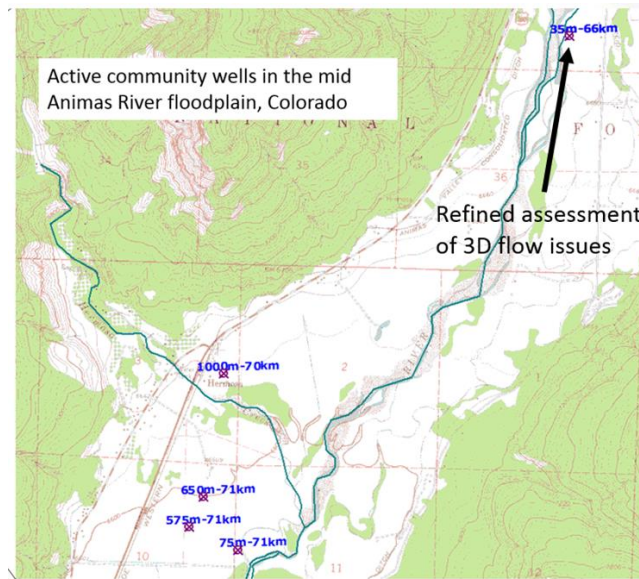


Figure D-35. The mid Animas floodplain community well selected for three-dimensional flow assessment.

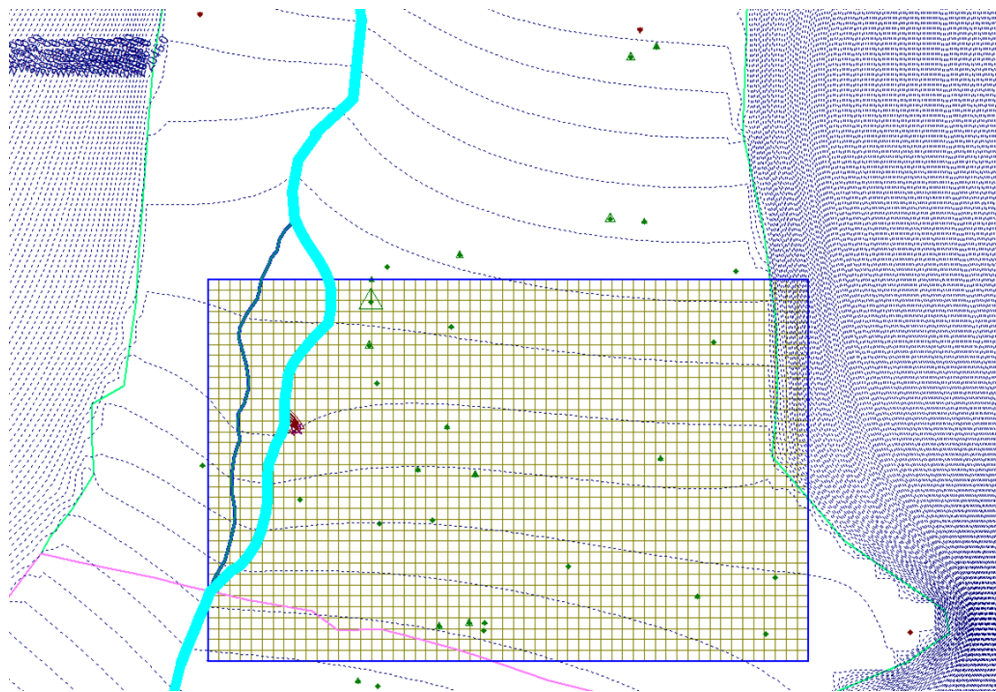


Figure D-36. The regional GFLOW model provides the hydraulic heads for the outer cells of the MODFLOW model. The boundary of the grid extract is 1,640 m by 1,020 m.

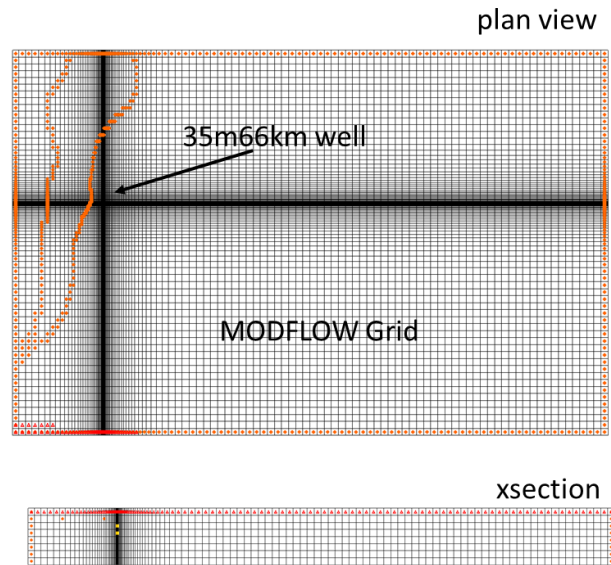


Figure D-37. The MODFLOW grid in plan view and cross-section view. The plan view cells are 1m x 1m in finest spatial resolution. Layers are 20-m thick. The well is represented in two stacked cells; the well discharge in each cell is proportional to the length of well screen in the associated layer.

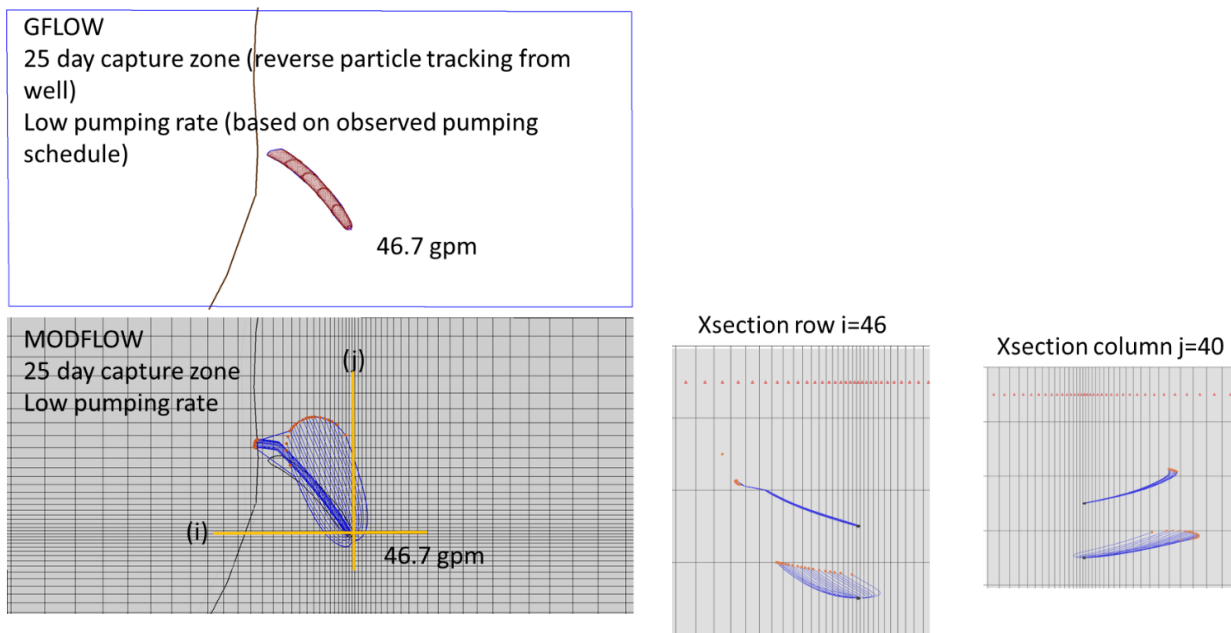


Figure D-38. The three-dimensional MODFLOW solution for the mid Animas community well. The simplified GFLOW model for well 35m66km is representative of the shallow transport pathways to the top of the well screen; the MODFLOW model shows a more complex story including different pathways to the top of the well screen and the bottom of the well screen. In both models the well communicates with the river, solute breakthrough using forward particle tracking in GFLOW is about 30 days and in MODFLOW is about 20 days.

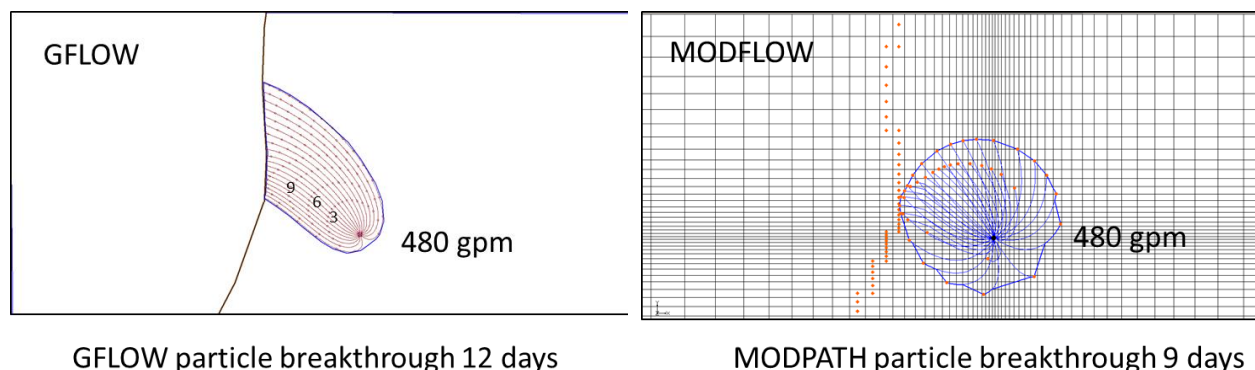


Figure D-39. The influence of pumping rate on shallow breakthrough time, GFLOW in comparison to MODFLOW. Maximum pumping rates based on rated yield from driller's log. At the higher pumping rates, the 3D solution (MODFLOW) is closer in shape and breakthrough times to the DF solution (GFLOW). The 3D solution has earlier breakthrough times.

The simplified GFLOW model had comparable results for the shallow capture zone associated with the top of the well screen, although MODFLOW conservative solute breakthrough was about 30 days and GFLOW breakthrough around 20 days. The MODFLOW model suggested a broader and slower forming deeper capture zone associated with water entering the lower half of the well screen. If the well is pumped at maximum (unrealistic) rates, the simulated shallow capture zones for GFLOW and MODFLOW are closer in comparison, as shown in Figure D-39.

As expected, the simplified GFLOW model does not capture the local complexity of the MODFLOW model. The previous discussion suggested that the Dupuit-Forchheimer (DF) GFLOW model would overestimate the extent of capture. For the 35m66km well, the GFLOW model and MODFLOW/MODPATH model gave similar results for the shallow capture zone; MODFLOW suggested a broader and more slowly developing capture zone for the bottom of the well screen. The MODFLOW model would be expected to have lower head at the well than the DF model for the same discharge. The steeper hydraulic head gradients between the river and the well and thus an increase in velocities. The result would be earlier MODFLOW breakthrough times.

Mid Animas: Exploration of local scale aquifer heterogeneities and anisotropy

The presence of local scale aquifer heterogeneities, such as buried stream channels, or anisotropy introduced by layers of low permeable clays, might impact the interactions of nearby pumping wells with river waters. This section will focus on the 75m71km community well in the mid Animas River floodplain in order to evaluate the impact of heterogeneities on well capture zones and conservative solute breakthrough times (See Figure D-40).

A Google Earth image associated with the region around the 75m71km community well shows the Animas River and its immediate floodplain (See Figure D-41). A visual inspection suggests a potential buried alluvial channel associated with Hermosa Creek joining from the north. The photo interpretation suggests the boundaries to be represented in the local scale groundwater model.

The mid Animas regional GFLOW model provided the hydraulic heads on the outer domain boundary of the local scale AnAqSim model.

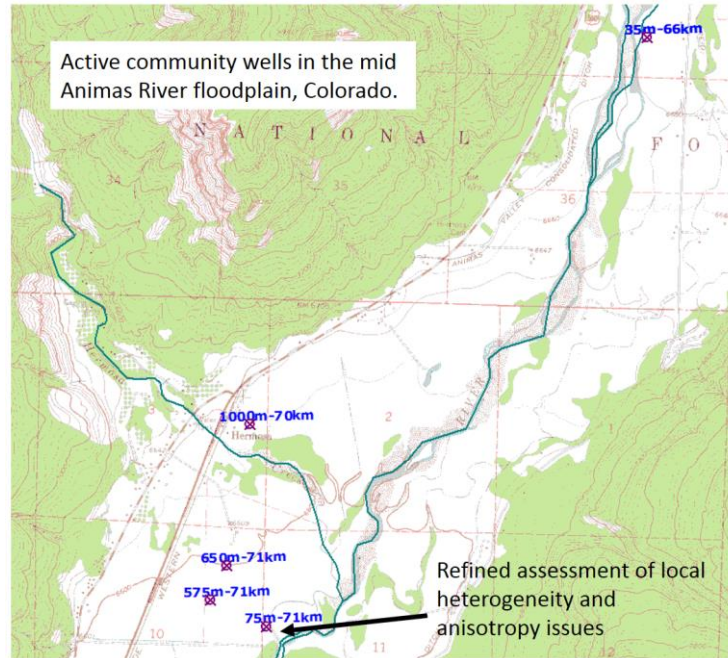


Figure D-40. The mid Animas River floodplain community well 75m71km selected for refined modeling of influence of local geologic heterogeneity.



Figure D-41. The domain of local scale heterogeneities to be detailed in the groundwater modeling of the 75m71km community well.

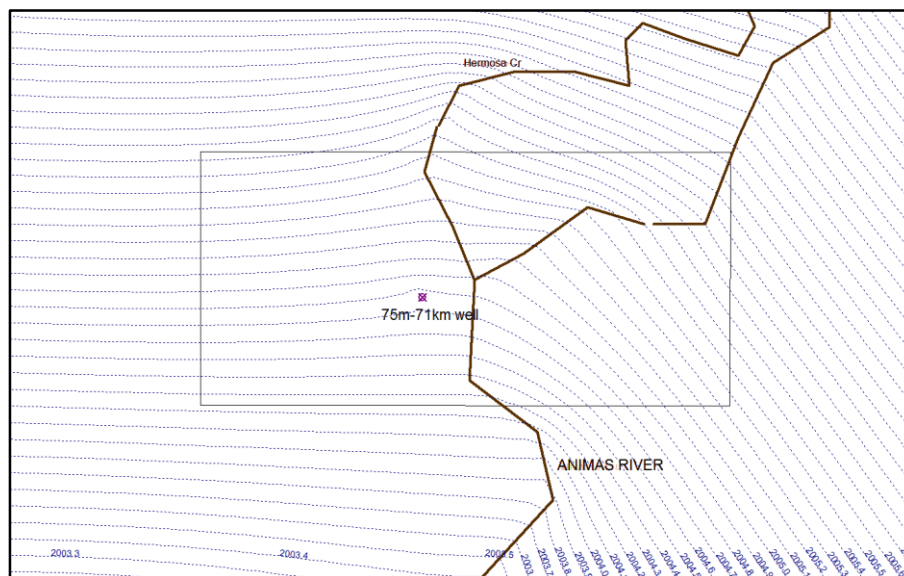
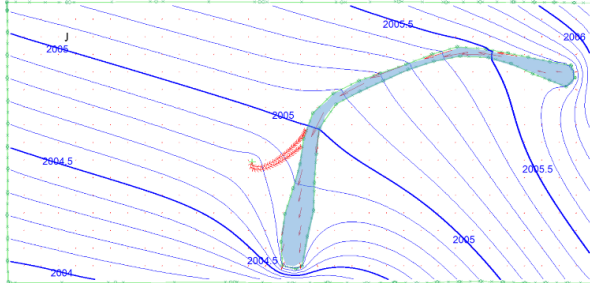


Figure D-42. The regional GFLOW model provides the heads on the boundary of the local scale AnAqSim model.

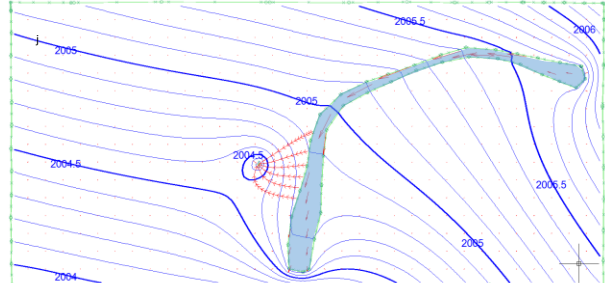
The AnAqSim model represents the local domain as a series of three potential subdomains. The Animas River channel is represented as a very high permeability (i.e., 1,000 m/day) subdomain. The Animas River floodplain subdomain is given a permeability of 100 m/day. The surrounding alluvium subdomain is given the permeability of 10 m/day. A series of scenarios are constructed based on average pumping rates (i.e., 145.74 acre-ft/yr=492.5 m³/day) and high pumping rates (445 gpm = 2425.7 m³/day) of the 75m71km community well. Porosity is assumed 0.25 in all domains. Also, all domains have anisotropic hydraulic conductivity (i.e., $k_h/k_v = 10$; See Figure D-43).

Under average pumping rates, the 75m71km community well would not be expected to source water from the Animas River. The scenario with no local scale heterogeneity is unlikely and presented for completeness. At the higher pumping rates, the community well is expected to receive Animas River water. The nature of the heterogeneity can cause a broad range of expected breakthroughs of a conservative solute from the river to reach the well, calculated by particle tracking, from 138 days to 289 days. Dilution is estimated to range from 25% to 33%.

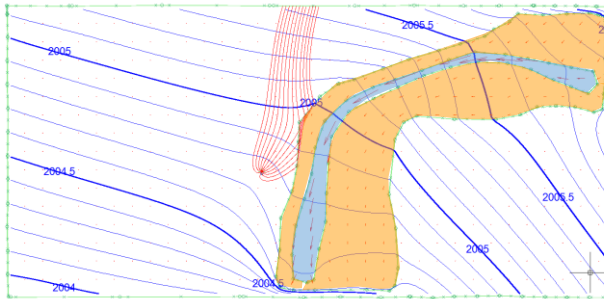
A) Avg Pumping, 1st arrival = 810 days, 17% dilution



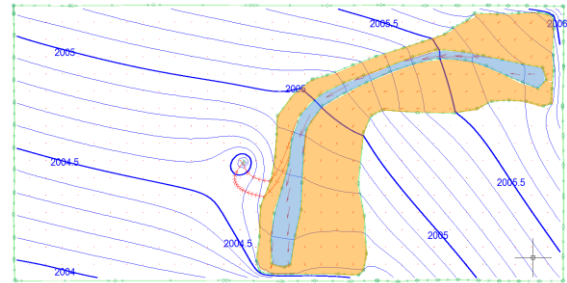
B) High Pumping, 1st arrival = 206 days, 50% dilution



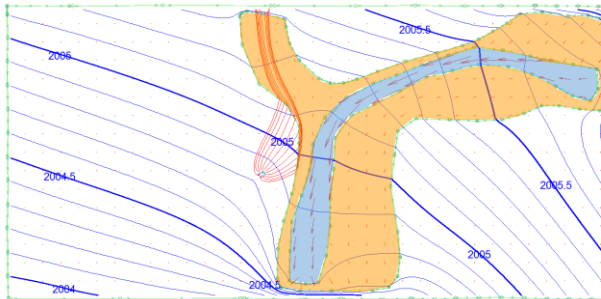
C) Avg Pumping, no river sourcing



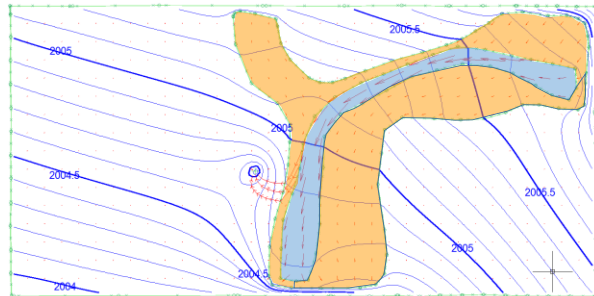
D) High Pumping, 1st arrival = 289 days, 25% dilution



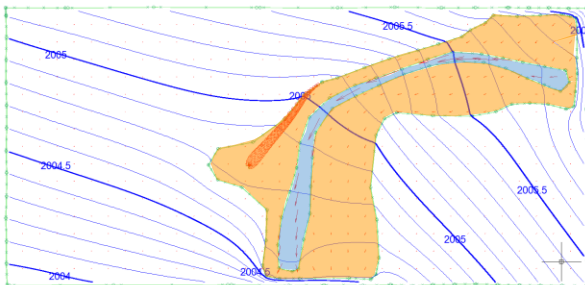
E) Avg Pumping, no river sourcing



F) High Pumping, 1st arrival = 176 days, 25% dilution



G) Avg Pumping, no river sourcing



H) High Pumping, 1st arrival = 138 days, 33% dilution

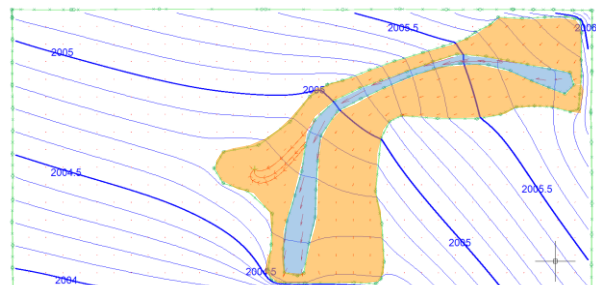


Figure D- 43. AnAqSim model runs exploring the influence of local scale heterogeneity on well capture, breakthrough times, and dilution of river-to-well source water.

Mid Animas: Sensitivity Analysis of Breakthrough Times of a Conservative Solute to a Pumping Well

Given the uncertainties in model conceptualization and parameterization, a sensitivity analysis was conducted to better understand the influence of major factors on capture zones and breakthrough times, including areal recharge, aquifer hydraulic conductivity, and well pumping rates. The mid Animas River floodplain community well 35m66km and the GFLOW model were used for the simulations. The summary of the runs is shown in Table D-10.

For this well and setting, a combination of high pumping rate, high aquifer hydraulic conductivity, and low seasonal recharge (i.e., August 2015 averaging) resulted in direct sourcing from the Animas River and the earliest dissolved solute breakthrough.

Table D- 10. The summary of GFLOW model simulations used for sensitivity analysis.

Run	Recharge Low N_{low}	Recharge High N_{high}	Hydraulic Conductivity Low k_{low}	Hydraulic Conductivity High k_{high}	Well Pumping Low Q_{low}	Well Pumping High Q_{high}	Source From River?	Model Predicted Breakthrough (days)
1							no	NA
2							no	NA
3							yes	154
4							yes	186
5							yes	66
6							yes	109
7							yes	25
8							yes	100

N_{low} = -1.165E-4 m/d; recharge low based on 8/1/2015 water balance, negative due to evapotranspiration possibly
 N_{high} =+3.915E-4 m/d; recharge high based on August-October 2015 water balance
 k_{low} =8.8 m/d; hydraulic conductivity alluvium low based on transmissivity from Smith well pumping test
 k_{high} =36.63 m/d; hydraulic conductivity alluvium high based on transmissivity from Smith well pumping test
 Q_{low} =190.2 m³/d; well pumping rate low based on reported diversions
 Q_{high} =2616.5 m³/d; well pumping rate high based on well driller reported yield

Empirical Evidence

Dissolved metals that are most useful as tracers associated with the GKM plume include primarily aluminum and iron, and also manganese, zinc, and cobalt. Together these metals represent about 95% of potentially toxic metals released to the rivers (Utah DEQ, 2015). This section will visit the hypothesis that dissolved metals in the GKM river plume may have impacted floodplain wells through examination of empirical data (i.e., well water quality sampling).

Mid Animas River Floodplain Community Wells

There are interesting chemical signals of dissolved metals at the mid Animas River floodplain community well 35m66km (Figure D-43). Dissolved background dissolved zinc concentrations in the upper Animas River near Elk Creek are expected to be around 0.08-0.20 mg/l as reported in Church et al (2007, Chapter E9 Quantification of metal loading by tracer injection and synoptic sampling, 1996-2000, Figure 17). The distinction between dissolved phase zinc and colloidal phase zinc in the Animas River is extensively

discussed in Church et al. (1997). The observed concentration of dissolved zinc in the plume in Cement Creek was around 30 mg/l.

The observed Animas River surface water quality observations by the Colorado Department of Public Health (CDPH) at the Baker's Bridge area after the passage of the GKM plume during August 12-18 show evidence that the dissolved zinc concentrations in the river had returned to background levels of 0.09-0.13 mg/l. The maximum observed dissolved zinc concentrations in the Animas River associated with the GKM plume near Baker's Bridge (RK 65) was about 1.7 mg/l.

Based on empirical observation and analysis the GKM plume would be expected to arrive in the 35m66km community well area early in the day of June 6 and take less than 24 hours to pass. The CDPH groundwater quality data at the 35m66km well indicated an elevated dissolved zinc concentration of 0.58 mg/l on August 14, with lower levels observed on August 9 and August 19. Other metals showing an elevated response on August 14 included dissolved copper, lead, and nickel. Metals not indicating an elevated response on August 14 were aluminum, manganese, arsenic, beryllium, cobalt, selenium. The pH and iron values were not reported. See Figure D-44.

The CDPHE water quality measurements available in the other mid Animas community wells 75m71km, 650m71km, and 575m71km did not have noteworthy changes suggesting impact by the acid mine drainage release.

Might the elevated dissolved zinc and other metals be indicative of GKM plume water entering the 35m66km well? The sensitivity modeling using GFLOW of solute breakthrough times ranged from 25 days to 187 days, based on choice of high or low recharge, hydraulic conductivity of the alluvium, pumping rate of the well, and aquifer porosity. The observed arrival of the dissolved zinc plume at the 35m66km community well was perhaps less than eight days.

The groundwater modeling analysis did not include complications such as transient pumping and transient river flows, aquifer heterogeneities that might influence dissolve solute dispersion, or reactive transport that would affect metals conversions between dissolved and colloidal forms. The groundwater modeling did not include the potential for clogging of the river bed sediments by algae or precipitated chemicals. The groundwater modeling at the 35m66km well did not include potential pumping interference from nearby private wells, or the influence of irrigation ditches. The modeling did satisfy fundamental continuity of flow and fundamental physical laws of groundwater mechanics, and included the primary process of advective transport of dissolved solute.

In the end, the results of the modeling and empirical evidence cannot rule out the hypothesis that the 35m66km well did pump Animas River water impacted by the GKM release of August 5, 2015.

The significance of the potential impact is not commented on here. The secondary drinking water standard for zinc, based on taste, is 5 mg/l, and the observed peak well concentration is an order of magnitude below this standard.

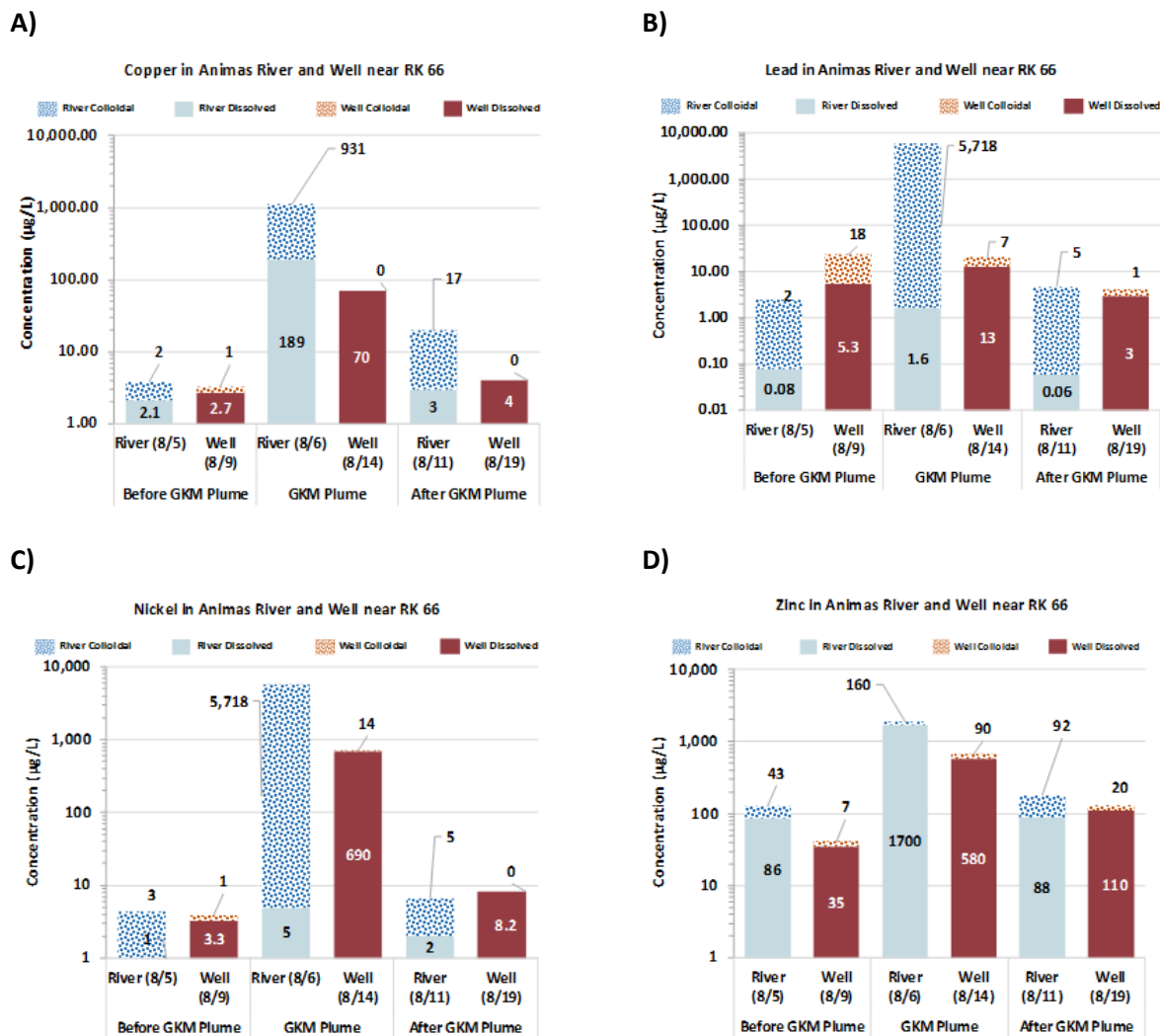


Figure D-44. River and well dissolved and colloidal metals concentrations around RK 66 of the mid Animas River in Colorado. The data are organized into before, during, and after plume time windows assuming the peak river plume passed the location on 8/6 and a potential 8-day lag in transport in the groundwater system before arrival at the well.

Lower Animas River Floodplain Community Wells

There was no clear evidence for water quality impact of the GKM plume on the community wells sampled in the lower Animas River floodplain, between Aztec and Farmington (i.e., near RK 163; See Figure D-45). The dissolved metals concentrations in the lower Animas River associated with the GKM release are much lower than was observed in the mid Animas River, somewhat due to dilution and dispersion, but more likely influenced by geochemistry as segregation into colloidal forms occurs. The community wells seem to indicate a fairly consistent groundwater quality concentration for copper, lead, nickel, and zinc, perhaps indicating the aquifer waters are in a state of equilibrium or long term mixing. The active spreading of river water via irrigation ditches may be a factor.

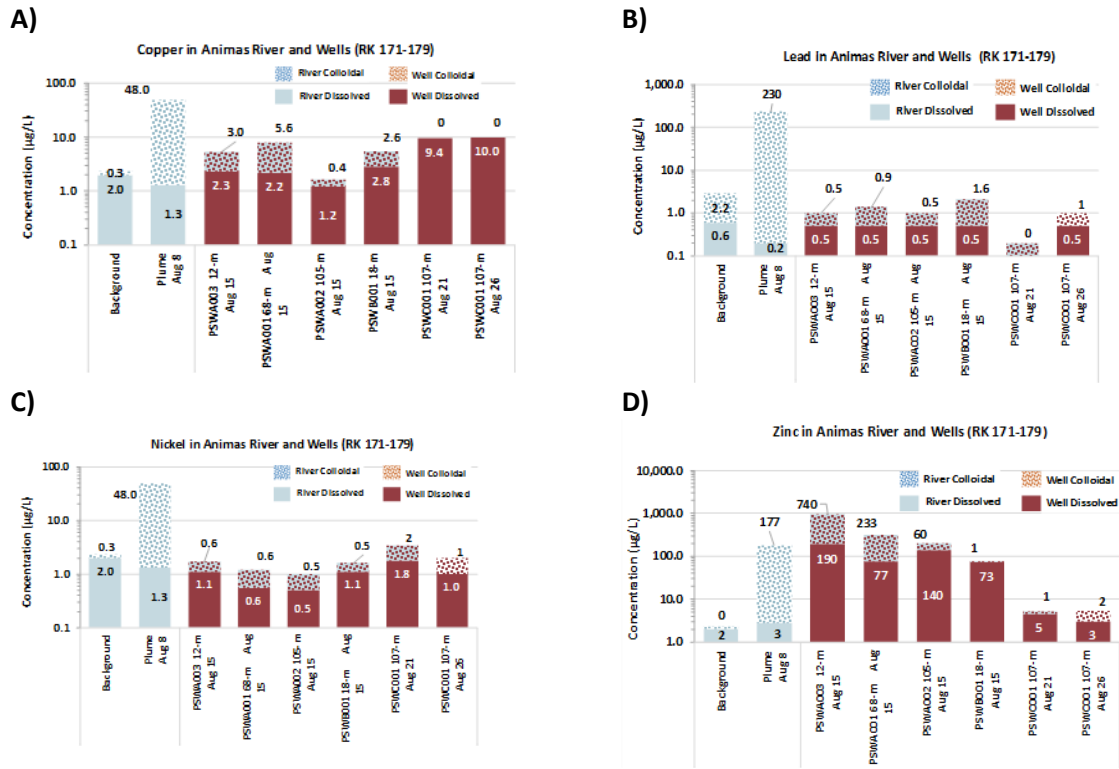


Figure D-45. River and well dissolved and colloidal metals concentrations around RK 163 of the lower Animas River in New Mexico.

Summary

The assessment of exposure of the floodplain wells to the GKM river plume evaluated the potential for the well to source its water directly from the Animas River, and if so, the expected breakthrough time of conservative river solutes to reach the well. In addition, dilution of direct river water compared to other sources of water in the well, such as rainfall recharge or deep aquifer contributions, were estimated. The empirical and computational methods used to evaluate the potential exposure were described in this Appendix. The results of the groundwater assessment are discussed in Chapter 8 of the main report and placed into context with the overall study.

References

- Beeman Bros. Drilling, 1984. Well Driller's Log, Permit No. 043554-F, <http://www.dwr.state.co.us/wellpermitsearch/>
- Blair, Robert W., Douglas B. Yager, 2002. Surficial geology along the Animas River quadrangle, Animas River watershed, La Plata County, Colorado, US Geological Survey, Digital Data Series 71, Plate 9.
- B.U.G.S., 2011 Animas River Watershed Based Plan, Bioassessment Underwater, GIS and Stats, Report August 2011. <http://animaswatershedpartnership.org/wp-content/uploads/2012/10/Final-Animas-Watershed-Management-Plan-12-22-11.pdf>
- CDPHE, 2015. Animas River spill incident – FINAL Drinking Water sample results, Colorado Department of Public Health & Environment, Laboratory Services Division, <https://www.colorado.gov/pacific/sites/default/files/WQ-Animas-DW-Data-FINAL-Update-12-08-15.pdf>
- Church, S.E., B.A. Kimball, D.L. Fey, D.A. Ferderer, T.J. Yager, and R.B. Vaughn, 1997. Source, transport, and partitioning of metals between water, colloids, and bed sediments of the Animas River, Colorado, US Geological Survey Open-File Report 97-151.
- Church, S.E., von Guerard, Paul, and Finger, S.E. eds., 2007. Integrated investigations of environmental effects of historical mining in the Animas River watershed, San Juan County, Colorado, US Geological Survey Professional Paper 1651, 1,096 p. plus CD-ROM (in two volumes).
- Craig, J. 2014. University of Waterloo lecture notes for course E661: Analytical methods in mathematical geology. Available at: http://www.civil.uwaterloo.ca/jrcraig/pdf/EARTH661_AEMLecture.pdf
- Fitts, C. R., 2010, Modeling Aquifer Systems with Analytic Elements and Subdomains, Water Resources Research, 46, W07521, doi:10.1029/2009WR008331.
- Fitts, C.R., 2012. Groundwater Science, 2nd Edition, Academic Press.
- Hasbrouk Geophysics, Inc., 2003. Animas Valley Gravity Survey, for Animas Water Company, Durango, Colorado., Final Report.
- Haitjema, H. M. 1995. Analytic element modeling of groundwater flow. Academic Press, Inc., San Diego, CA. 394 pp.
- Haitjema, H.M., 2006. Technical commentary/ the role of hand calculations in groundwater flow modeling, *Ground Water*, 44(6):786-791.
- Strack, O.D.L., 1984. Three-dimensional streamlines in Dupuit-Forchheimer models, *Water Resources Research*, 20:812-822.
- Strack, O. D. L. 1989. *Groundwater Mechanics*. Prentice Hall, Englewood Cliffs, NJ. 732 pp.
- Strack, O. D. L., and H. M. Haitjema. 1981a. Modeling double aquifer flow using a comprehensive potential and distributed singularities: 1. Solution for homogenous permeability. *Water Resources Research* 17(5): 1535-1549.
- Strack, O. D. L., and H. M. Haitjema. 1981b. Modeling double aquifer flow using a comprehensive potential and distributed singularities: 2. Solution for inhomogeneous permeabilities. *Water Resources Research* 17(5): 1551-1560.
- Sullivan, Kate, Michael Cyterski, Stephen Kraemer, Chris Knightes, Katie Price, Keewook Kim, Lourdes Prieto, Mark Gabriel, Roy Sidle, 2015. Case study analysis of the impacts of water acquisition for hydraulic fracturing on local water availability, EPA Office of Research and Development Report, EPA/600/R-14/179, <https://www.epa.gov/hfstudy/case-study-analysis-impacts-water-acquisition-hydraulic-fracturing-local-water-availability>

- Timmons, Stacy, Ethan Mamer, and Cathryn Pokorny, 2016. Animas River Long-term Monitoring: Summary of Groundwater Hydraulics and Chemistry from March 2016, New Mexico Bureau of Geology and Mineral Resources, Interim Technical Report June 2016.
- Townley, L.R., 1995. The response of aquifers to periodic forcing, *Advances in Water Resources*, 18(3):125-146.
- USEPA, 2016. EPA Gold King Mine Analysis of Fate and Transport in the Animas and San Juan Rivers: Response to Peer Review Comments, U.S. Environmental Protection Agency, Office of Research and Development Report, EPA/600/R-16/113, June 2016.
- Utah DEQ, 2015. Preliminary analysis of immediate effects of Gold King Mine release on water quality in the San Juan River, Utah, Utah Department of Environmental Quality, report final vol 2.
- Vincent, K.R., and J.G. Elliott, 2007. Stratigraphy of late Holocene channel and floodplain deposits exposed in a trench excavated across the Animas River valley floor 1.4 kilometers downstream of Eureka Townsite, San Juan County, Colorado, USGS PP 1651, Chapter E22, Plate 6.
- Wang, Hongqi , Shuyuan Liu, and Shasha Du, 2013. The Investigation and Assessment on Groundwater Organic Pollution, Organic Pollutants - Monitoring, Risk and Treatment, Prof. M.Nageeb Rashed (Ed.), InTech, DOI: 10.5772/53549. Available from: <http://www.intechopen.com/books/organic-pollutants-monitoring-risk-and-treatment/the-investigation-and-assessment-on-groundwater-organic-pollution>
- Ward, D. S., D. R. Buss, J. W. Mercer, S. S. Hughes. 1987. Evaluation of a groundwater corrective action at the Chem-Dyne hazardous waste site using a telescopic mesh refinement modeling approach. *Water Resources Research* 23(4): 603-617.
- WestWater Associates, Inc., 2010. Animas Water Company – Smith Well – Hydrology & Impacts, Permit No. 32370-F, <http://www.dwr.state.co.us/wellpermitsearch/>

Appendix E.
Empirical Data Analyses

Contents

Overview.....	2
Relationship Between Metal Concentrations and Flow.....	3
Annual Estimates of Metal Load.....	8
WASP Plume Modeling.....	11
Longitudinal Estimates of Plume Metal Mass and Maximum Concentration.....	12
Peak Concentration Curves.....	16

Overview

A great deal of data was gathered after the GKM release event on August 5, 2015. Appendix A of this report gives scope to the massive data collection effort that was undertaken by a variety of government agencies and NGO’s. The EPA team performed many data analyses and visualization tasks associated with its primary objectives, and this appendix attempts to capture the most important aspects of that supportive work that did not make it into the main report body.

Relationship Between Metal Concentrations and Flow

Data showed that dissolved and particulate (Note: dissolved + particulate = total) metal concentrations were related to streamflow for historic and post-event samples collected at Silverton (RK 16.4) and Durango (RK 94). These relationships are used in several ways in analyses: 1) to build daily metal load estimates from mean streamflow data in Chapter 6, 2) for plume analysis in Chapter 2, and 3) for post-event trend analysis in Chapter 8.

Total and dissolved metals have been measured at Silverton and Durango for a variety of studies, including the USGS Animas River acid mine drainage study (Church *et al.* 2007, see main text for reference) and EPA studies in support of acid mine drainage remediation. Metals concentration as a function of streamflow at Durango and Silverton for six important metals identified in the Gold King release is shown in Figures E-1 to E-4. Spring snowmelt data from 2016 is also shown on the graphs, although these data were not included in the regression relationships shown with each metal. The historic data were collected over a range of flow, up to 2,900 cfs or 82 m³/s, which is about equal to the long term average peak discharge during snowmelt.

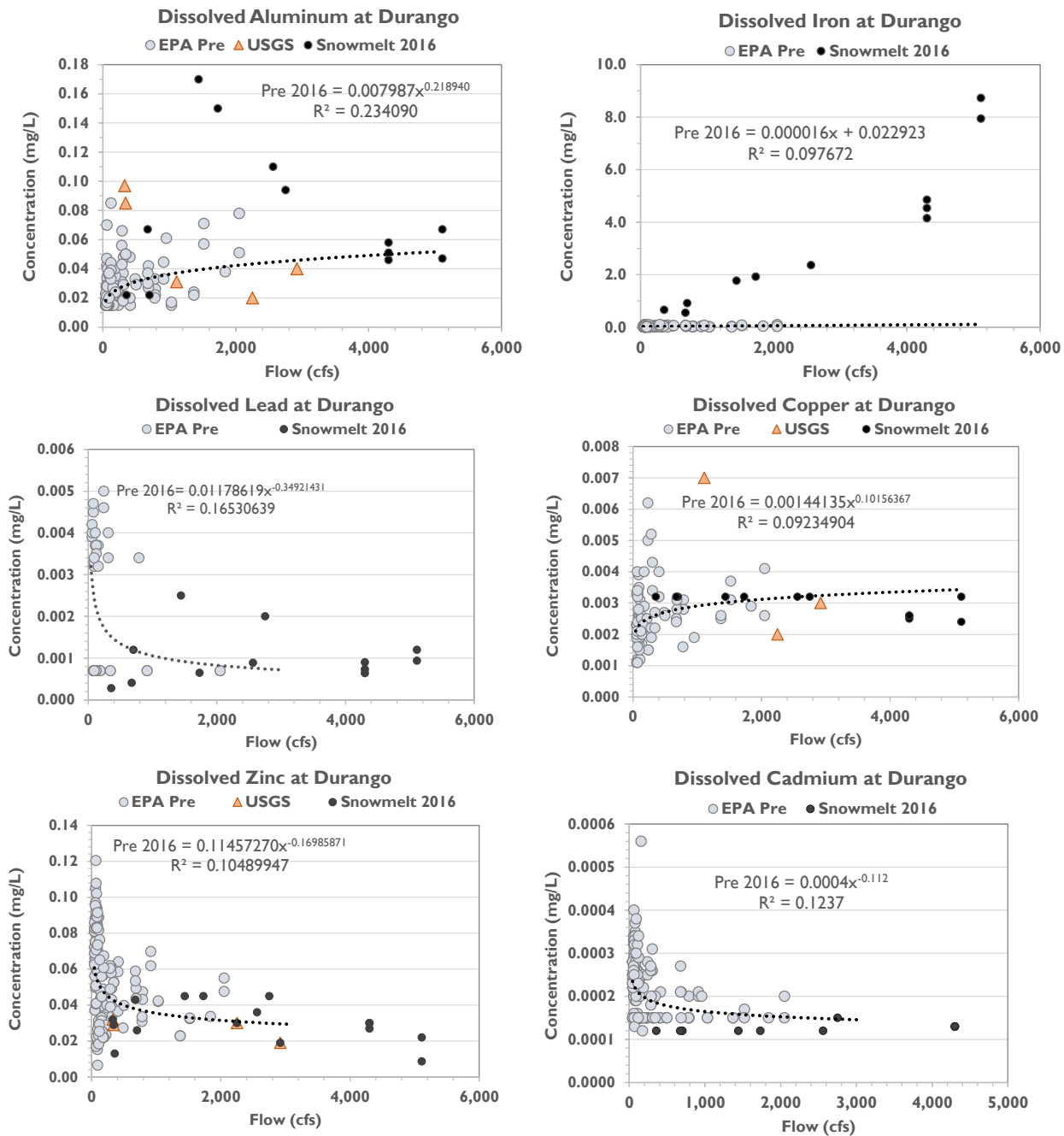


Figure E-1. Dissolved metal concentration in relation to discharge (cfs) at Durango. Regression equations are computed using pre-event data only. Samples collected during spring snowmelt in 2016 are shown as black dots. Orange triangles are data collected during snowmelt by Church et al. (1997) in 1995 and 1996.

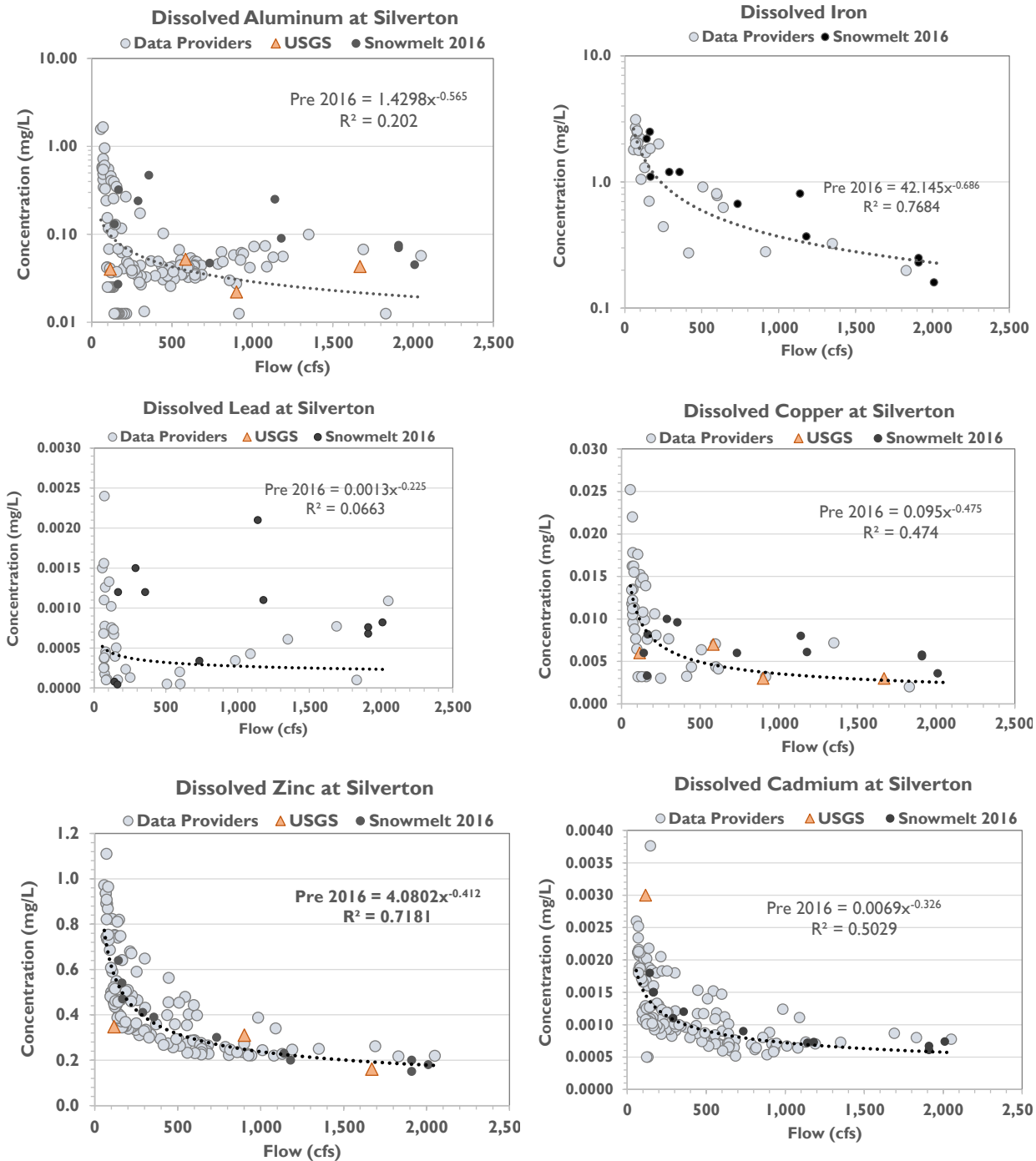


Figure E-2. Dissolved metal concentration in relation to discharge (cfs) at Silverton. Regression equations are computed using pre-event data only. Samples collected during spring snowmelt in 2016 are shown as black dots. Orange triangles are data collected during snowmelt by Church et al. (1997) in 1995 and 1996.

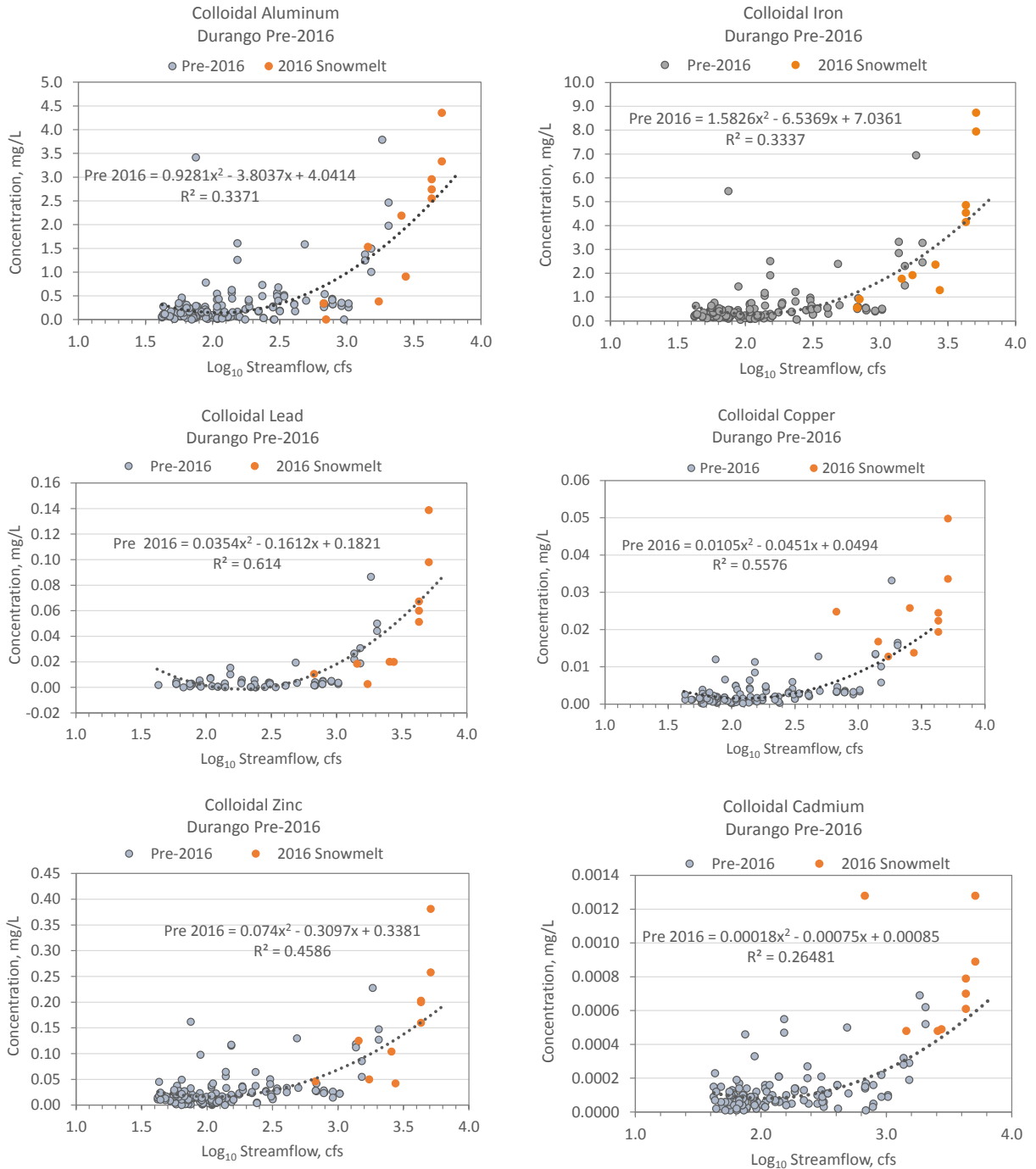


Figure E-3. Particulate metal concentration in relation to discharge (cfs) at Durango. Regression equations are computed using pre-event data only. Samples collected during spring snowmelt in 2016 are shown as orange circles.

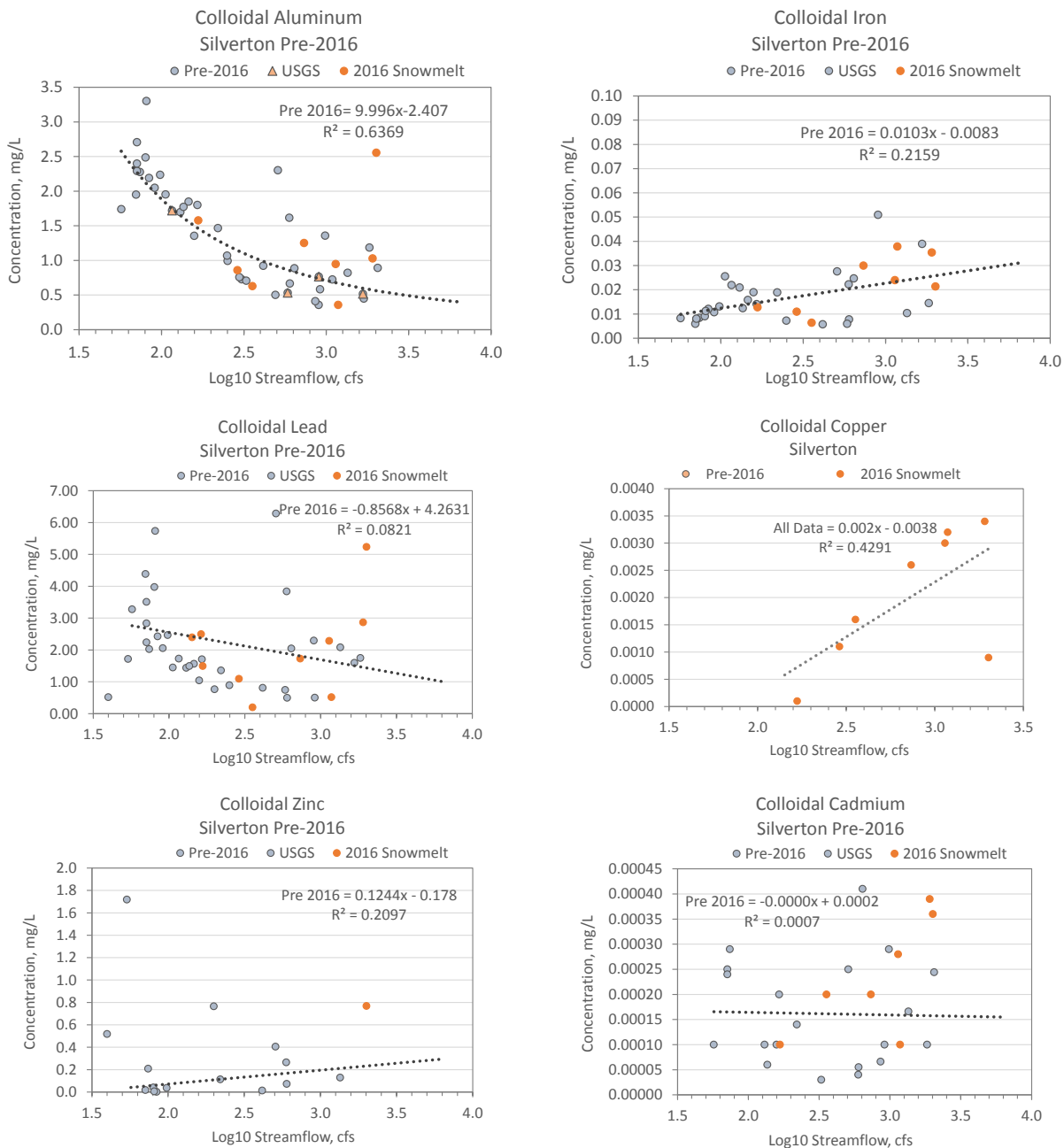


Figure E-4. Particulate metal concentration in relation to discharge (cfs) at Silverton. Regression equations are computed using pre-event data only. Samples collected during spring snowmelt in 2016 are shown as orange circles.

Annual Estimates of Metal Load

Computation of annual metal load (kg/yr) was based on modeled relationships between concentration and flow, as shown above, and developed using pre-event data. Loads were calculated for both dissolved and particulate fractions at Silverton and Durango. A mean daily flow series was published for the gauge's period of record by the USGS.

Figures E-5 shows how modeled concentrations of various metals, both dissolved and particulate, change with flow throughout the year at Silverton and Durango.

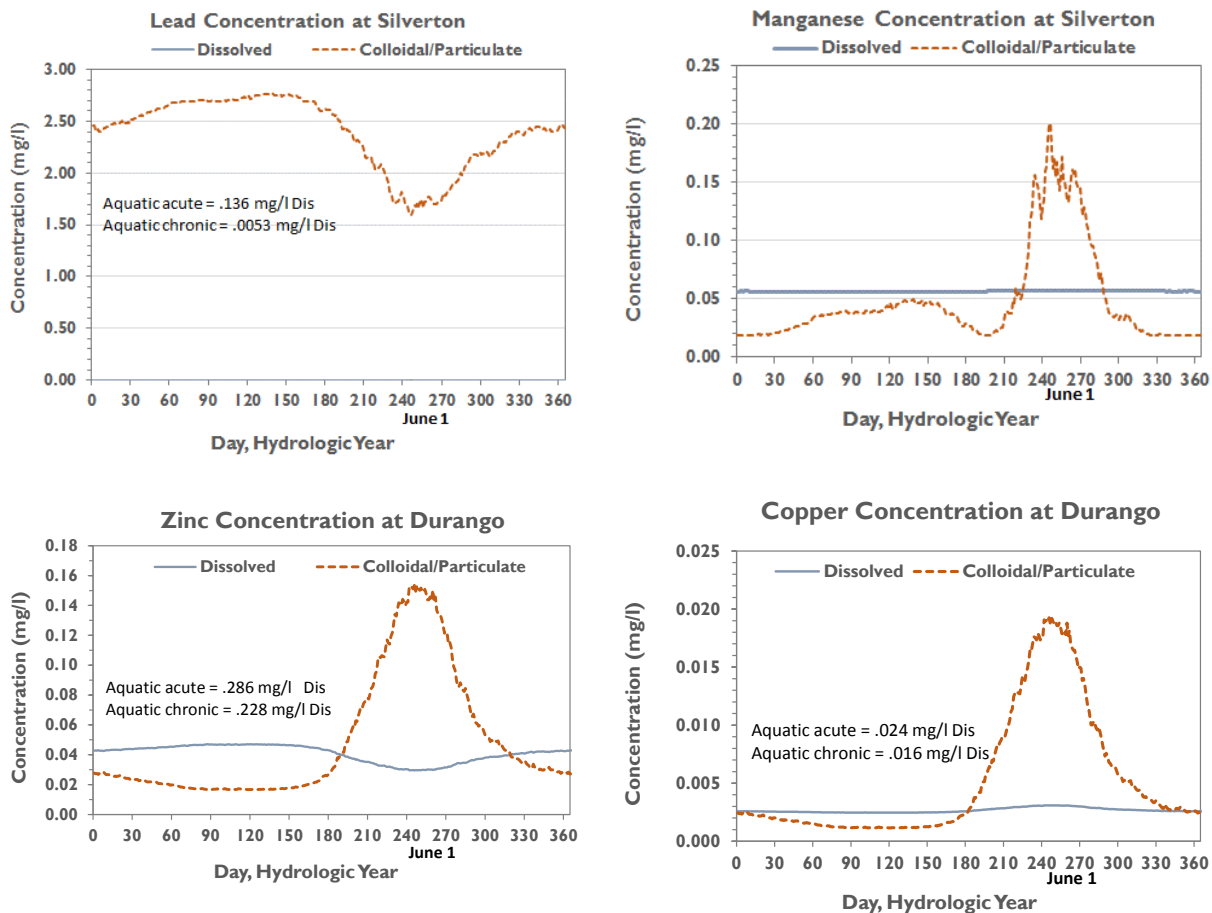


Figure E-5. Concentrations vary through the year with streamflow.

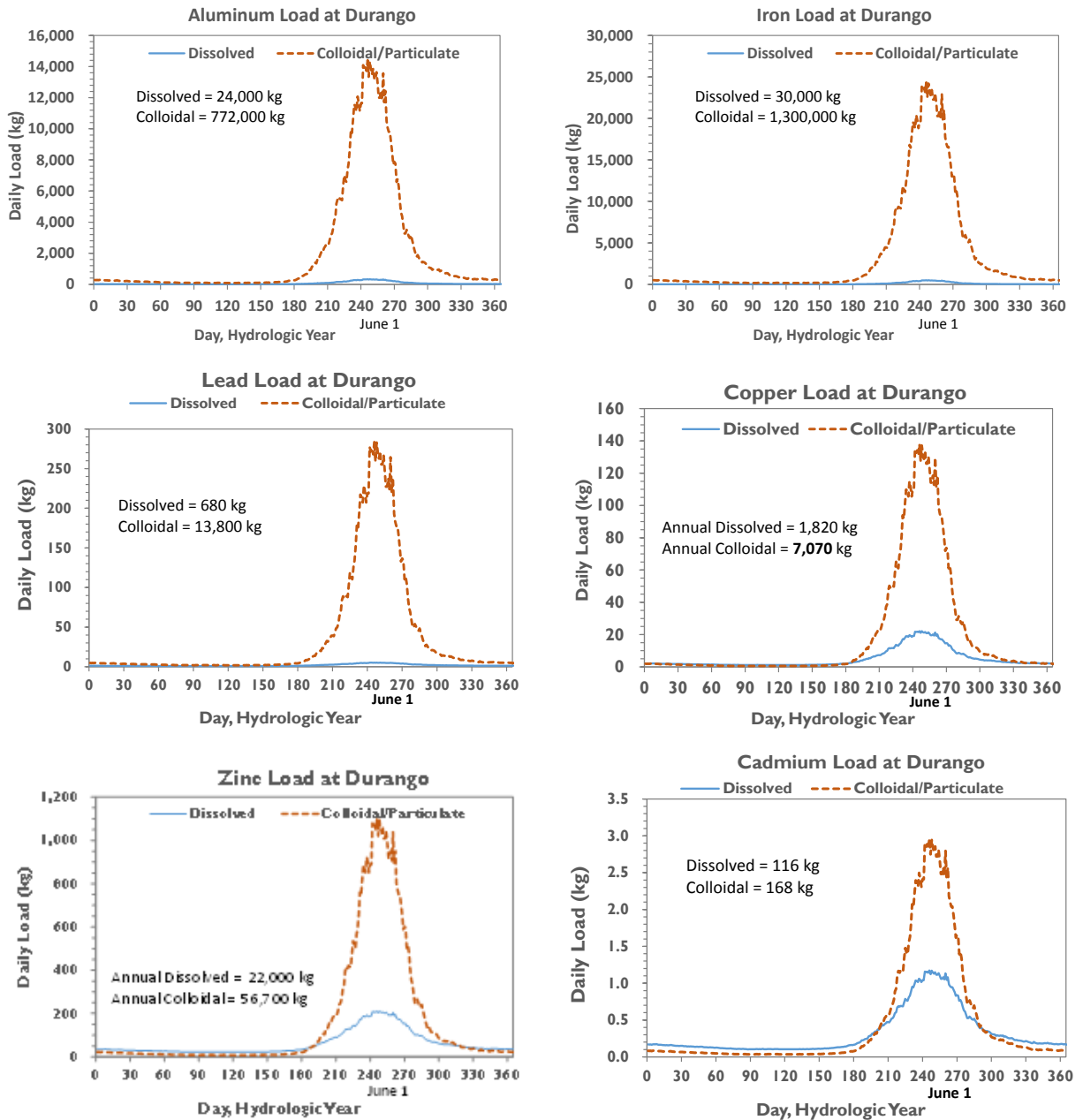


Figure E-6. Annual average loads at Durango computed with pre-event concentration regressions and annual flow daily flow statistics. Data are plotted for the hydrologic year (i.e., October 1 – September 30).

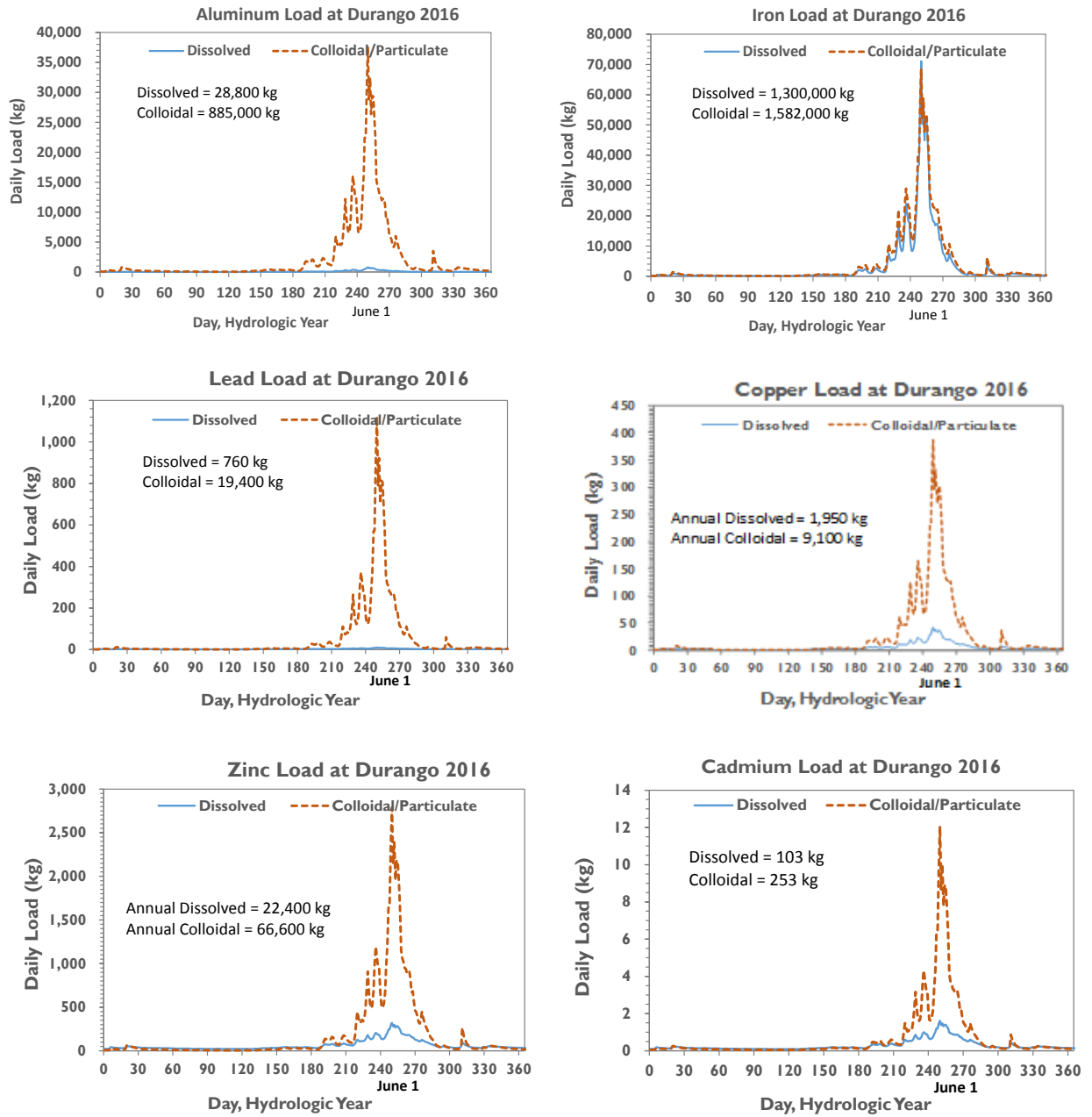


Figure E-7. Annual load at Durango for 2016 resulting from updated regressions using all data, including 2016 snowmelt samples, and 2016 daily flow. Data are plotted for the hydrologic year (i.e., October 1 – September 30).

WASP Plume Modeling

The table below provides estimates from the WASP model for the GKM plume duration (hours), time at plume peak (corresponding to maximum metal concentrations) and the elapsed time from the arrival of the plume at the mouth of Cement Creek to the peak concentration for numerous locations on the Animas and San Juan Rivers.

Table E-1. Plume duration and travel time to peak concentration and time of peak simulated by WASP at locations along the Animas and San Juan Rivers. Sites are ordered by distance from the Gold King Mine. The plume duration is defined as the time for 99% of the plume mass to pass, centered at the peak concentration.

River Distance (km)	Site	WASP Plume Duration (hrs)	Time to Peak Concentration (hr)	Date/Time of WASP Peak
12.5	Cement Creek near Silverton	24.2	0.5	8/5/15 13:04
16.4	Animas at Silverton	24.4	1.9	8/5/15 14:30
33.8	Animas in San Juan Forest	27.6	9.3	8/5/15 21:56
63.8	Animas at Baker's Bridge	30.7	20.1	8/6/15 8:43
94.2	Animas at Durango	37.2	37.9	8/7/15 2:29
104.2	Animas at So Utes (AR19.3)	37.9	40.8	8/7/15 5:22
109.0	Animas at So Utes (AR16)	38.2	42.7	8/7/15 7:17
129.6	Animas at Cedar Hill - USGS Gauge 9363500	39.6	48.9	8/7/15 13:31
131.5	Animas at So Utes (NAR06)	39.8	49.9	8/7/15 14:29
147.5	Animas near Cedar Hill (ADW 022)	40.8	55.4	8/7/15 19:59
164.1	Animas near Aztec	41.7	61.4	8/8/15 2:00
190.2	Animas at Farmington (FW040)	42.7	68.3	8/8/15 8:56
196.1	San Juan at Farmington (FW020)	43.4	69.8	8/8/15 10:23
204.5	San Juan near Farmington (LVW-030)	43.9	72.2	8/8/15 12:47
214.4	San Juan at Fruitland	44.4	75.1	8/8/15 15:39
246.3	San Juan at Shiprock	45.8	82.7	8/8/15 23:20
295.8	San Juan at Four Corners	48.7	98.5	8/9/15 15:09
298.7	San Juan near Hwy 160 Crossing	48.7	100.2	8/9/15 16:51
333.2	San Juan at McElmo Creek	51.3	111.5	8/10/15 4:08
345.8	San Juan at Montezuma Creek	52.7	116.1	8/10/15 8:41
364.8	San Juan near Swinging Footbridge	55.4	122.3	8/10/15 14:54
377.1	San Juan at Sand Island	57.1	125.9	8/10/15 18:32
421.3	San Juan at Mexican Hat	64.0	140.3	8/11/15 8:55
510.7	San Juan at Clay Hills Boat Ramp	77.9	171.7	8/12/15 16:20

Longitudinal Estimates of Plume Metal Mass and Maximum Concentration

Table E-2. Estimates of the total metal mass (kg) remaining in the plume as it passed through the Animas and San Juan Rivers. Whereas other metal masses decline along a longitudinal gradient once the Animas merges with the San Juan, the increase mass estimates for aluminum in the San Juan River (highlighted in green) are almost certainly an artifact of the increase in total suspended solids and turbidity in this system relative to the Animas River.

Location	River Km	Total*	Minor**	Aluminum	Antimony	Arsenic	Barium	Beryllium	Cadmium	Calcium	Chromium	Cobalt	Copper	Iron	Lead
Gold King Mine at Release Site	0.0	2,872	798	374	0.04	0.68	0.10	0.12	0.93	4,193	0.16	1.25	79	1,700	0.48
Cement Creek	12.5	490,404	16,186	41,132	14.16	358.36	417.56	6.01	7.69	30,484	30.59	17.68	1,615	433,086	7,658.3
Animas at Silverton	16.4	457,124	16,702	39,407	9.39	338.98	439.71	5.89	9.50	42,589	16.83	18.24	1,521	401,015	7,625.4
Animas at Baker's Bridge	63.8	155,396	7,075	15,411	8.71	104.59	162.53	2.18	3.02	111,399	5.54	6.45	463	132,909	2,241.3
Animas at Durango	94.2	79,760	2,942	10,007	7.90	46.21	203.83	2.00	2.52	160,916	7.46	3.51	247	66,811	803.2
Animas at So. Ute NAR06	132.0	72,828	2,724	12,146	6.85	43.24	221.03	0.92	1.76	198,486	5.48	3.05	187	57,957	885.7
Animas at Aztec	164.1	54,657	2,527	8,571	3.95	29.86	349.20	0.97	1.68	225,678	4.65	4.01	130	43,559	622.7
Animas at Farmington	190.2	52,907	2,632	9,448	4.02	29.56	422.92	1.01	1.42	297,196	6.72	4.38	135	40,826	573.4
San Juan at Farmington	196.1	41,389	5,290	16,265	1.36	8.81	406.62	1.36	2.03		8.81	6.78	41	23,720	210.1
San Juan at Shiprock	246.3	39,994	13,468	19,467	0.10	6.79	333.35	1.11	0.41		7.39	7.22	35	19,445	94.4
San Juan at Four Corners	295.8	26,396	8,993	13,092	0.18	4.94	245.24	0.91	0.21		6.91	6.06	12	12,506	64.3
San Juan at Bluff, Sand Island	377.1	25,784	13,834	13,579	0.09	3.70	230.30	0.95	0.19		7.06	6.14	18	11,492	27.7
San Juan at Mexican Hat	421.3	23,757	17,778	13,990	0.09	3.30	334.86	1.26	0.27		5.83	6.28	15	8,905	18.6

* All metals excluding major cations (Na, Mg, K, Ca)

** Metals excluding major cations, Fe and Al

Location	River Km	Magnesium	Manganese	Mercury	Molybdenum	Nickel	Potassium	Selenium	Silver	Sodium	Thallium	Vanadium	Zinc
Gold King Mine at Release Site	0.0	306	408	0.00	0.05	0.78	27.2	0.05	0.00	60	0.00	0.43	306
Cement Creek	12.5	15,891	3,599	0.81	86.82	12.47	11,853.8	11.22	47.45	1,427	5.61	237.83	2,059
Animas at Silverton	16.4	14,549	4,092	0.14	83.57	9.64	9,625.2	15.45	45.46	2,019	7.73	215.33	2,247
Animas at Baker's Bridge	63.8	21,559	1,533	0.07	28.07	6.36	12,272.8	5.56	15.62	5,696	2.77	71.58	2,414
Animas at Durango	94.2	24,449	921	0.13	17.00	5.19	9,202.0	6.88	9.38	28,233	2.97	37.53	619
Animas at So. Ute NAR06	132.0	31,669	735	0.17	13.62	5.48	15,109.7	3.28	6.46	38,564	0.64	28.22	577
Animas at Aztec	164.1	32,174	785	1.29	10.48	29.51	11,150.0	3.92	3.69	51,481	0.45	27.74	518
Animas at Farmington	190.2	39,448	861	1.94	10.40	7.58	12,329.6	5.51	3.88	71,119	0.47	26.98	536
San Juan at Farmington	196.1		549	0.05	2.71	10.50		1.14	1.36		0.24	31.17	122
San Juan at Shiprock	246.3		456	0.00	2.28	8.74		0.95	0.56		0.30	25.82	101
San Juan at Four Corners	295.8		365	0.03	0.79	8.45		0.40	0.46		0.15	19.65	63
San Juan at Bluff, Sand Island	377.1		342	0.00	0.46	8.12		0.72	0.20		0.16	17.50	49
San Juan at Mexican Hat	421.3		412	0.02	0.19	8.48		0.23	0.12		0.15	14.19	42

Table E-3. Estimates of the dissolved metal mass (kg) in the plume as it passed through the Animas and San Juan Rivers. Note that the dissolved mass remaining at Durango (~900kg) was nearly equivalent to the “background” dissolved mass that normally would pass through that site, meaning nearly all of the dissolved metals present at the mouth of Cement Creek had come out of solution by this point. Thus, the dissolved masses shown in this table for sites downstream of Durango (highlighted in green) represent primarily non-plume related quantities during plume passage.

Location	River Km	Total*	Minor Metals**	Plume Major Cations	Aluminum	Antimony	Arsenic	Barium	Beryllium	Cadmium	Calcium	Chromium	Cobalt	Copper
Gold King Mine at Release Site	0.0	2,872	798		374	0.04	0.68	0.10	0.12	0.93	4,193	0.16	1.25	79.3
Cement Creek	12.5	15,391	5,265	23,364	6,376	0.17	2.92	2.19	2.42	7.03	30,345	0.38	13.98	731.0
Animas at Silverton	16.4	17,768	6,938	22,831	8,034	0.37	2.27	18.96	3.09	12.28	38,070	0.75	21.84	1,162.9
Animas at Baker's Bridge	63.8	2,010	1,491	21,965	437	0.48	0.22	26.46	1.37	3.03	106,732	0.78	5.26	44.6
Animas at Durango	94.2	968	731	20,852	97	1.80	0.77	103.93	2.56	0.73	146,949	4.19	1.77	6.9
Animas at So. Ute NAR06	132.0	1,031	434	21,159	90	1.19	1.24	122.18	0.03	0.12	195,616	5.73	1.95	7.7
Animas at Aztec	164.1	534	338	21,204	119	1.80	2.30	236.42	0.68	0.19	276,199	4.50	0.54	7.2
Animas at Farmington	190.2	706	480	21,451	133	1.55	1.87	267.45	0.52	0.19	270,650	3.49	0.64	11.1
San Juan at Farmington	196.1	1,331	303		726	1.93	2.69	213.69	0.75	0.20	158,678	4.28	0.50	4.8
San Juan at Shiprock	246.3	154	9		86	0.05	0.06	5.36	0.02	0.01	3,635	0.12	0.03	0.2
San Juan at Four Corners	295.8	3,258	1,372		1,141	1.65	4.46	1,239.94	0.31	0.19	202,597	4.45	1.95	14.8
San Juan at Bluff, Sand Island	377.1	3,265	1,097		1,395	3.56	5.21	973.93	0.58	0.20	228,125	4.73	0.56	10.8
San Juan at Mexican Hat	421.3	5,519	1,228		2,997	3.91	5.70	1,082.52	0.48	0.19	190,429	4.32	5.30	14.7

* All metals excluding major cations (Na, Mg, K, Ca)

** All Metals minus Fe, Ir and major cations

Location	Iron	Lead	Magnesium	Manganese	Mercury	Molybdenum	Nickel	Potassium	Selenium	Silver	Sodium	Thallium	Vanadium	Zinc
Gold King Mine at Release Site	1,700	0.48	306	408	0.00045	0.05	0.8	27	0.05	0.001	60	0.003	0.43	306
Cement Creek	3,750	11.21	2,490	2581	0.00007	0.38	6.3	426	0.41	0.172	290	0.172	0.80	1904
Animas at Silverton	2,796	16.71	3,183	2958	0.00000	0.75	7.5	569	0.84	0.374	1225	0.374	1.50	2729
Animas at Baker's Bridge	83	0.54	12,388	743	0.51278	0.80	2.4	2321	0.74	0.348	4877	0.352	1.39	658
Animas at Durango	141	1.35	20,044	476	0.00776	2.05	2.5	5273	1.67	0.651	28294	0.794	2.87	121
Animas at So. Ute NAR06	507	3.69	27,031	246	0.00000	2.71	2.9	7159	1.19	0.068	37831	0.365	1.06	36
Animas at Aztec	77	0.82	37,295	26	0.24076	6.22	5.1	9896	4.07	0.450	63057	0.450	1.35	40
Animas at Farmington	94	1.31	36,194	26	0.21613	6.10	6.6	8944	4.62	0.358	65952	0.375	1.25	146
San Juan at Farmington	302	0.79	20,394	14	0.01095	5.44	4.3	7827	3.73	1.304	60721	0.521	1.78	42
San Juan at Shiprock	59	0.11	464	2	0.00284	0.11	0.1	198	0.09	0.040	1836	0.011	0.19	0.42
San Juan at Four Corners	745	1.15	26,957	16	0.35612	8.66	4.8	11232	2.27	0.445	143181	0.445	8.90	61
San Juan at Bluff, Sand Island	772	2.01	35,749	7	0.56794	10.14	4.7	12856	2.74	0.724	152793	0.371	9.86	60
San Juan at Mexican Hat	1,295	1.09	27,706	26	0.34580	9.25	5.1	13680	4.89	0.714	177495	0.297	17.82	45

Table E-4. Estimates of the maximum total concentrations (ug/l) of metals in the plume as it passed through the Animas and San Juan Rivers.

Location	River Km	Metals*	Minor Metals**	Aluminum	Antimony	Arsenic	Barium	Beryllium	Cadmium	Calcium	Chromium	Cobalt	Copper	Iron
Gold King Mine at Release Site	0.0	253.4	70.4	33.0	0.0037	0.060	0.01	0.011	0.082	370	0.014	0.110	7.00	150
Cement Creek	12.5	39683.0	1294.2	3335.9	1.1331	29.052	34.35	0.477	0.582	1603	2.492	1.356	129.55	35053
Animas at Silverton	16.4	11582.9	396.1	968.0	0.2022	8.475	11.41	0.149	0.229	551	0.404	0.438	37.54	10219
Animas at Baker's Bridge	63.8	521.0	17.4	61.1	0.0281	0.338	0.48	0.007	0.009	87	0.018	0.018	1.47	442
Animas at Durango	94.2	217.8	7.6	28.2	0.0156	0.137	0.31	0.002	0.005	212	0.012	0.008	0.65	182
Animas at So. Ute NAR06	132.0	103.1	3.5	15.8	0.0075	0.061	0.19	0.001	0.002	74	0.006	0.003	0.27	84
Animas at Aztec	164.1	63.6	2.7	9.2	0.0047	0.037	0.31	0.001	0.002	128	0.005	0.004	0.16	52
Animas at Farmington	190.2	64.1	2.6	6.7	0.0039	0.039	0.27	0.001	0.001	133	0.006	0.004	0.17	55
San Juan at Farmington	196.1	61.3	2.0	24.4	0.0020	0.013	0.61	0.002	0.003	68	0.013	0.010	0.06	36
San Juan at Shiprock	246.3	72.0	1.9	35.0	0.0002	0.012	0.60	0.002	0.001	46	0.013	0.013	0.06	35
San Juan at Four Corners	295.8	67.5	2.0	33.5	0.0005	0.013	0.63	0.002	0.001	98	0.018	0.016	0.03	32
San Juan at Bluff, Sand Island	377.1	65.8	3.0	33.0	0.0003	0.011	0.77	0.003	0.001	100	0.017	0.019	0.06	30
San Juan at Mexican Hat	421.3	196.4	3.6	108.8	0.0004	0.022	1.04	0.006	0.000	106	0.050	0.042	0.10	84

*Excluding major cations (Na, Mg, K, Ca)

**Excluding major cations, Fe and Al

Location	River Km	Lead	Magnesium	Manganese	Mercury	Molybdenum	Nickel	Potassium	Selenium	Silver	Sodium	Thallium	Vanadium	Zinc
Gold King Mine at Release Site	0.0	0.04	27.0	36.0	0.00004	0.004	0.069	2.4	0.0047	0.0001	5.3	0.0003	0.0380	27.0
Cement Creek	12.5	631.9	984.9	275.3	0.06778	7.095	0.974	748.4	0.8825	3.9183	82.6	0.4413	19.31	155.3
Animas at Silverton	16.4	182.8	234.1	98.7	0.00338	2.168	0.295	160.2	0.4044	1.2053	26.6	0.2022	5.48	45.9
Animas at Baker's Bridge	63.8	7.20	21.8	4.3	0.00021	0.094	0.027	15.1	0.0176	0.0533	4.9	0.0088	0.24	3.1
Animas at Durango	94.2	2.92	39.8	1.9	0.00032	0.039	0.006	20.6	0.0101	0.0246	29.3	0.0019	0.0919	1.5
Animas at So. Ute NAR06	132.0	1.30	12.7	0.8	0.00020	0.018	0.003	8.3	0.0030	0.0094	12.7	0.0005	0.0428	0.74
Animas at Aztec	164.1	0.79	17.4	0.8	0.00025	0.013	0.063	6.8	0.0018	0.0050	27.8	0.0004	0.0315	0.49
Animas at Farmington	190.2	0.83	18.2	0.7	0.00000	0.010	0.005	7.2	0.0019	0.0054	32.3	0.0003	0.0304	0.54
San Juan at Farmington	196.1	0.31	14.2	0.8	0.00008	0.004	0.016	8.5	0.0017	0.0020	26.8	0.0004	0.0467	0.18
San Juan at Shiprock	246.3	0.17	5.9	0.8	0.00001	0.004	0.016	1.5	0.0017	0.0010	33.1	0.0005	0.0465	0.18
San Juan at Four Corners	295.8	0.16	18.8	0.9	0.00008	0.002	0.022	9.2	0.0010	0.0012	28.0	0.0004	0.0503	0.16
San Juan at Bluff, Sand Island	377.1	0.08	20.8	1.2	0.000002	0.001	0.024	7.8	0.0009	0.0005	33.9	0.0003	0.0436	0.78
San Juan at Mexican Hat	421.3	0.09	28.9	1.8	0.00011	0.001	0.050	18.0	0.0044	0.0005	41.5	0.0010	0.1280	0.27

Table E-5. Estimates of the maximum dissolved concentrations (ug/l) of metals in the plume as it passed through the Animas and San Juan Rivers.

Site	RK	Metals*	Minor Metals**	Aluminum	Antimony	Arsenic	Barium	Beryllium	Cadmium	Calcium	Chromium	Cobalt	Copper	Iron
Gold King Mine at Release Site	0.0	253.45	70.45	33.0	0.0037	0.060	0.009	0.011	0.082	370	0.0144	0.1100	7.0	150
Cement Creek	12.5	1372.79	479.17	596.2	0.0123	0.297	0.167	0.230	0.647	2338	0.0294	1.2780	70.8	297
Animas at Silverton	16.4	254.78	97.66	124.4	0.0050	0.038	0.226	0.045	0.185	358	0.0100	0.3210	18.4	33
Animas at Baker's Bridge	63.8	5.34	3.87	1.28	0.0008	0.000	0.045	0.003	0.005	74	0.0015	0.0140	0.1	0.189
Animas at Durango	94.2	1.35	1.08	0.07	0.0008	0.000	0.038	0.003	0.001	119	0.0015	0.0025	0.0055	0.200
Animas at So. Ute NAR06	132.0	0.72	0.23	0.04	0.0005	0.000	0.033	0.000	0.000	69	0.0015	0.0003	0.0023	0.450
Animas at Aztec	164.1	0.15	0.09	0.03	0.0006	0.001	0.071	0.000	0.000	88	0.0015	0.0002	0.0019	0.025
Animas at Farmington	190.2	0.17	0.11	0.04	0.0006	0.001	0.091	0.000	0.000	87	0.0015	0.0002	0.0024	0.026
San Juan at Farmington	196.1	0.51	0.09	0.27	0.0004	0.001	0.070	0.000	0.000	51	0.0010	0.0002	0.0015	0.150
San Juan at Shiprock	246.3	1.77	0.11	0.99	0.0008	0.001	0.072	0.000	0.000	50	0.0017	0.0004	0.0027	0.664
San Juan at Four Corners	295.8	0.30	0.15	0.09	0.0004	0.001	0.134	0.000	0.000	53	0.0010	0.0001	0.0021	0.056
San Juan at Bluff, Sand Island	377.1	0.61	0.23	0.24	0.0007	0.001	0.205	0.000	0.000	48	0.0010	0.0001	0.0022	0.142
San Juan at Mexican Hat	421.3	0.14	0.10	0.03	0.0004	0.001	0.073	0.000	0.000	46	0.0010	0.0025	0.0024	0.017

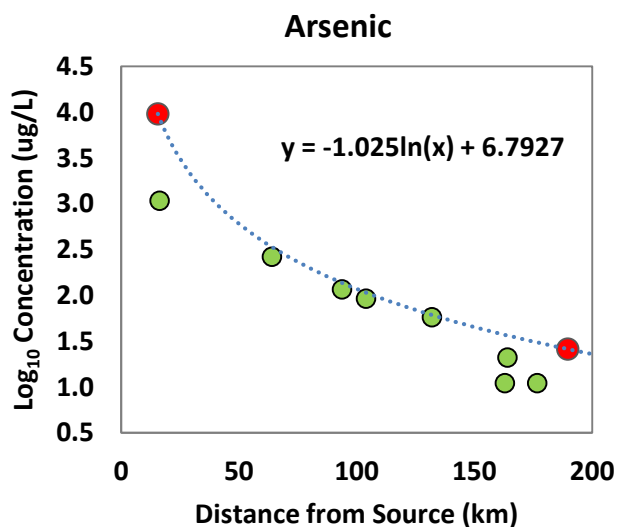
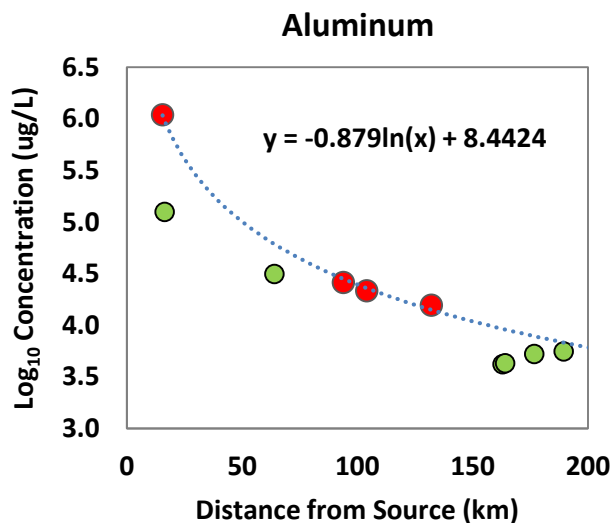
*Excluding major cations (Na, Mg, K, Ca)

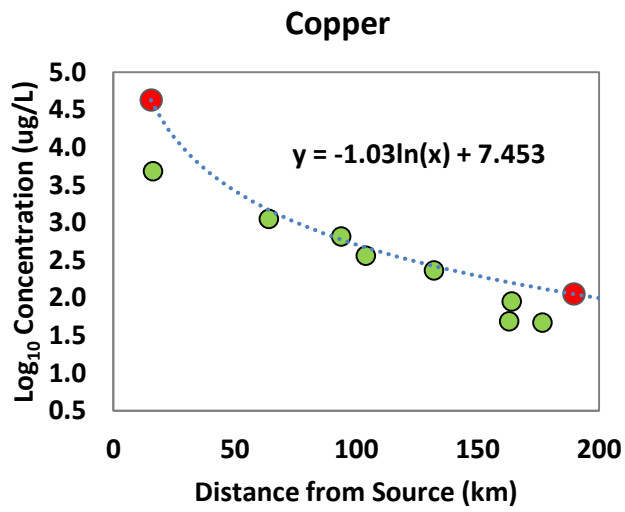
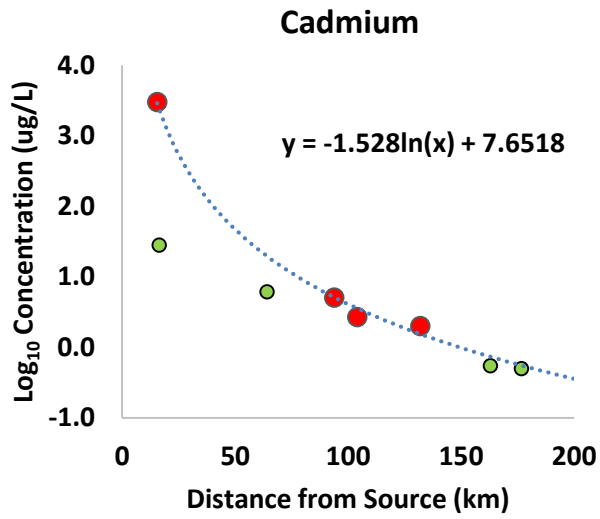
**Excluding major cations, Fe and Al

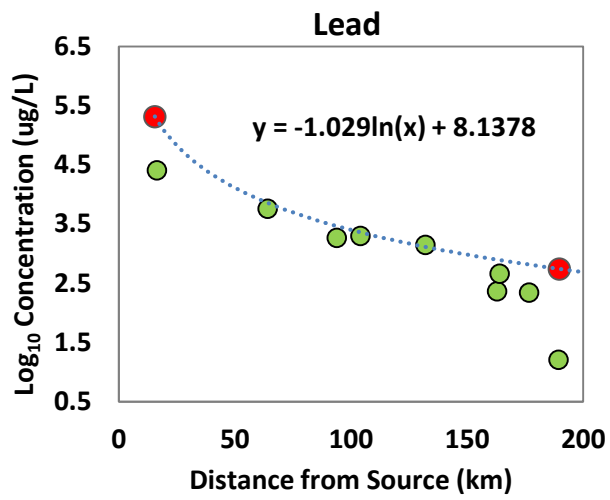
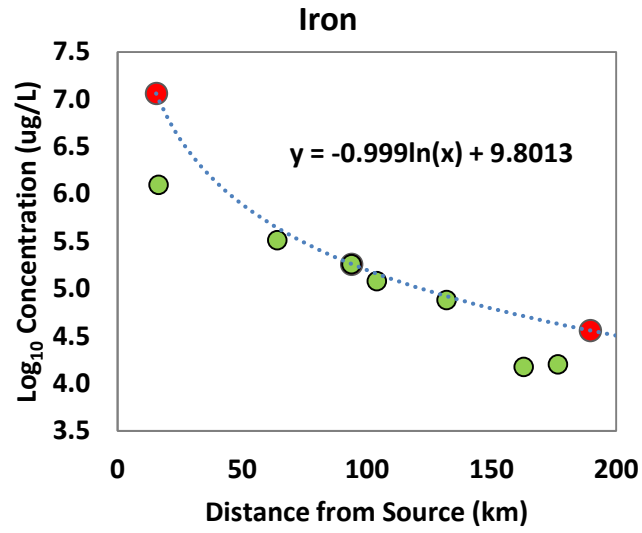
Site	RK	Lead	Magnesium	Manganese	Mercury	Molybdenum	Nickel	Potassium	Selenium	Silver	Sodium	Thallium	Vanadium	Zinc
Gold King Mine at Release Site	0	0.0420	27.0	36.0	0.000040	0.0042	0.0690	2.4	0.0047	0.0001	5.3	0.00029	0.0380	27.0
Cement Creek	12.5	0.9545	200.4	231.8	0.000000	0.0294	0.5632	35.8	0.0327	0.0123	11.2	0.01229	0.0637	172.2
Animas at Silverton	16.4	0.2289	30.1	38.4	0.000000	0.0100	0.1024	5.7	0.0114	0.0050	9.8	0.00500	0.0200	39.6
Animas at Baker's Bridge	63.8	0.0015	8.5	1.78	0.001500	0.0015	0.0054	1.5	0.0015	0.0008	3.1	0.00075	0.0030	1.874
Animas at Durango	94.2	0.0015	15.1	0.75	0.000000	0.0015	0.0023	3.8	0.0015	0.0008	19.2	0.00075	0.0030	0.271
Animas at So. Ute NAR06	132	0.0031	8.6	0.17	0.000000	0.0010	0.0000	2.2	0.0003	0.0000	11.1	0.00000	0.0000	0.011
Animas at Aztec	164.1	0.0002	11.7	0.0042	0.000116	0.0022	0.0017	3.2	0.0008	0.0001	20.3	0.00015	0.0004	0.004
Animas at Farmington	190.2	0.0003	12.8	0.0024	0.000122	0.0026	0.0027	3.3	0.0009	0.0002	24.3	0.00015	0.0005	0.004
San Juan at Farmington	196.1	0.0004	6.5	0.0035	0.000000	0.0018	0.0015	2.5	0.0006	0.0001	19.0	0.00015	0.0007	0.003
San Juan at Shiprock	246.3	0.0012	6.4	0.0191	0.000026	0.0016	0.0015	2.7	0.0015	0.0007	25.3	0.00017	0.0025	0.006
San Juan at Four Corners	295.8	0.0001	6.7	0.0043	0.000080	0.0019	0.0010	2.7	0.0009	0.0001	25.3	0.00010	0.0012	0.006
San Juan at Bluff, Sand Island	377.1	0.0004	7.6	0.0009	0.000120	0.0022	0.0010	2.7	0.0006	0.0001	32.0	0.00008	0.0020	0.013
San Juan at Mexican Hat	421.3	0.0001	5.4	0.0045	0.000080	0.0020	0.0013	3.1	0.0016	0.0001	37.2	0.00010	0.0020	0.003

Peak Concentration Curves

The following plots show the fitted curves used for predicting maximum total concentrations of major metals as the plume passed various locations. These estimates were necessary because sampling rarely coincided with peak metal concentrations. Red dots indicate samples that were near peak, and thus used for fitting the curves. Green dots show samples that were off-peak, and thus expected to exhibit lower concentrations than the maximum concentration that could have been measured at that site.







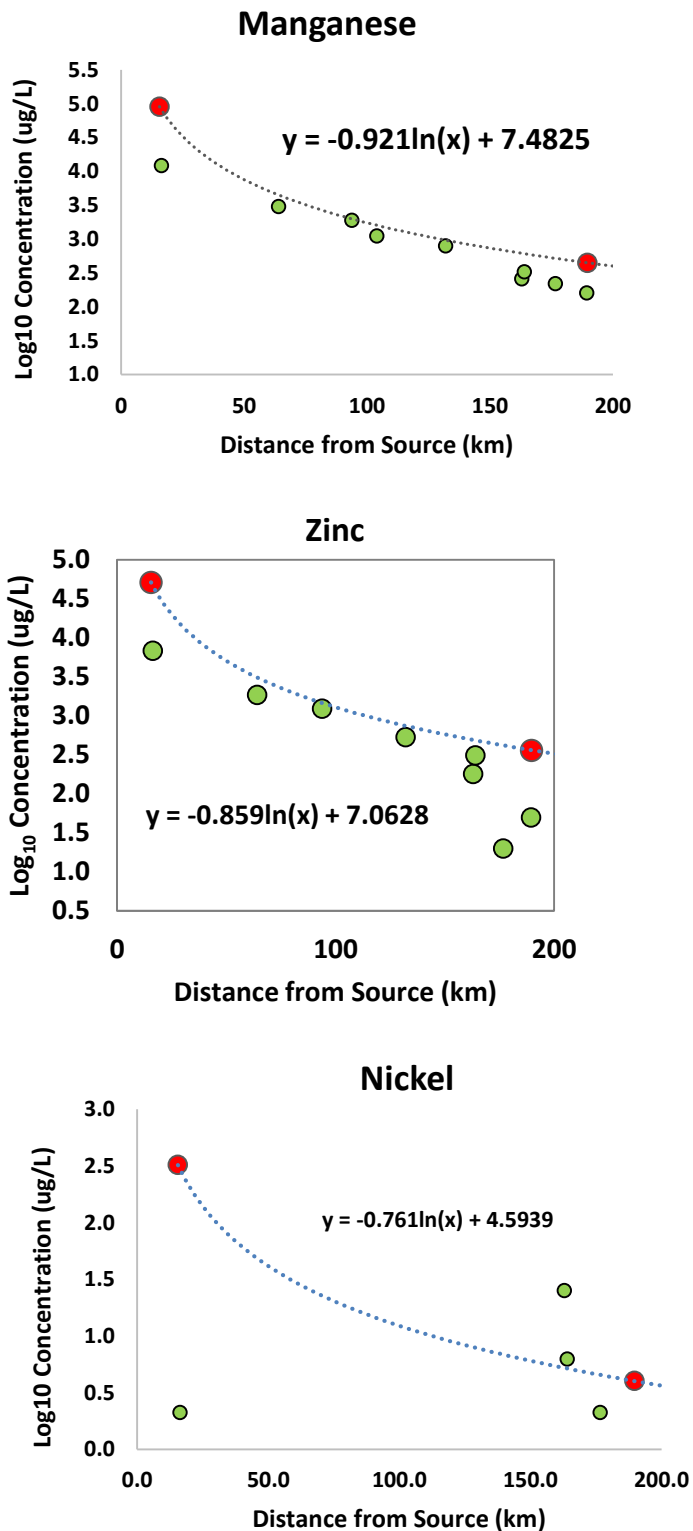
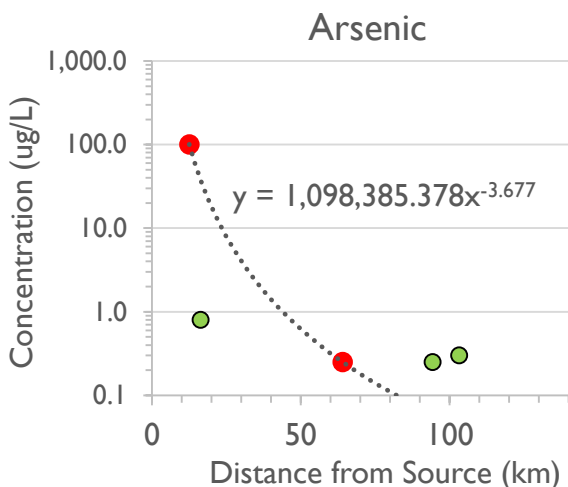
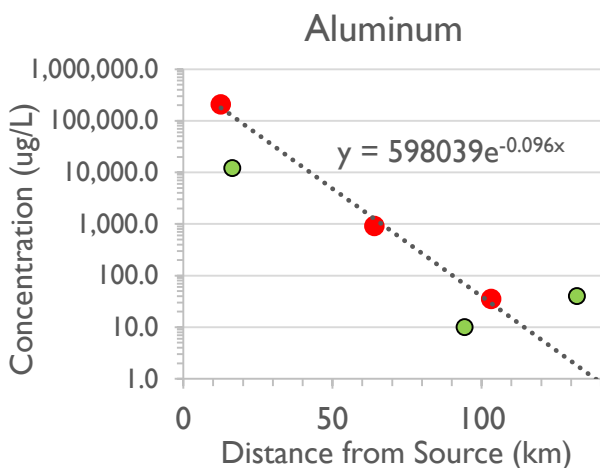
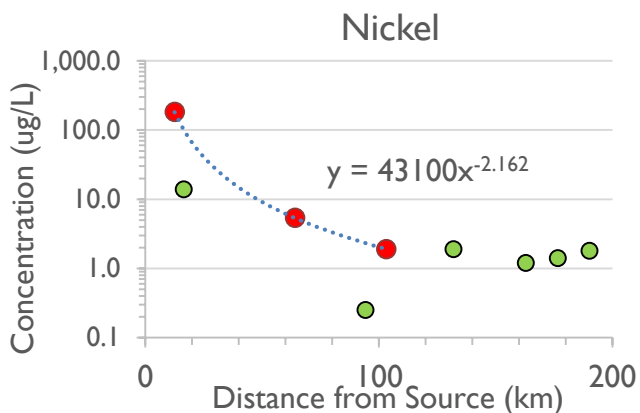
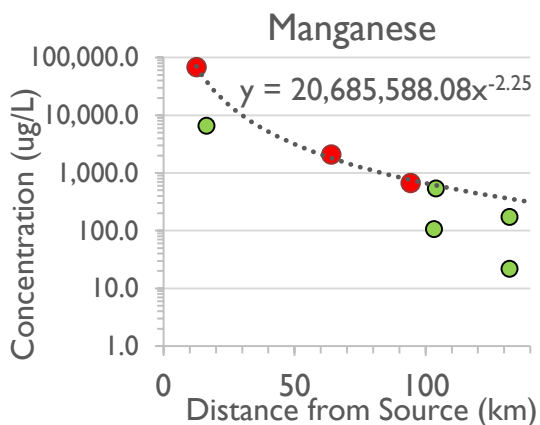
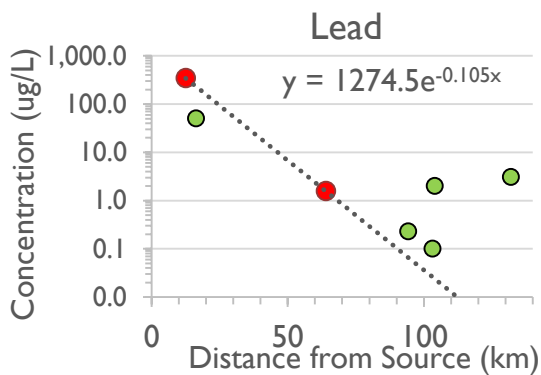
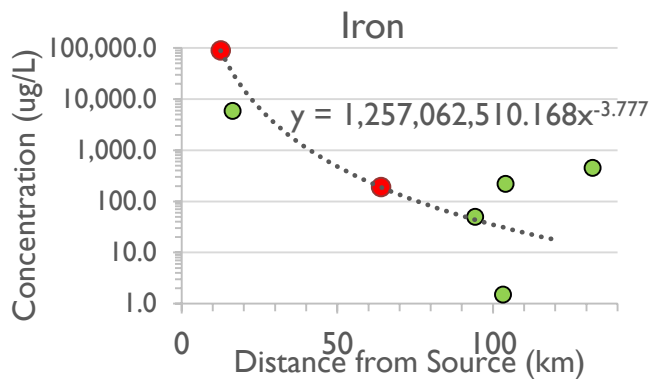
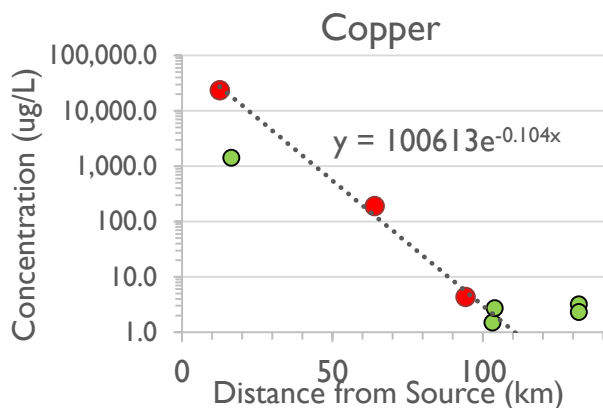
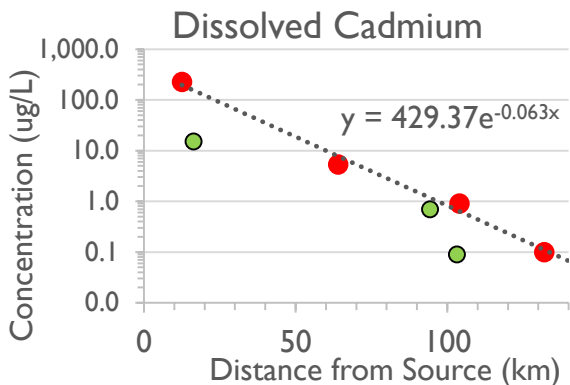


Figure E-8. Downstream attenuation in peak total metal concentrations during plume passage in the Animas.

The following plots show the fitted curves for predicting maximum dissolved concentrations of major metals as the plume passed various locations. These estimates were necessary because sampling rarely coincided with peak metal concentrations. Red dots indicate samples that were near peak, and thus used for fitting the curves. Green dots show samples that were either 1) off-peak, and thus expected to exhibit lower concentrations than the maximum concentration that could have been measured at that site, or 2) past the point where the dissolved mass of that metal species present at the bottom of Cement Creek was wholly converted to particulate/colloidal mass.

Dissolved concentrations of metals, more so than particulate/colloidal concentrations, naturally rise in certain places on the Animas River as tributaries enter the system (e.g., Florida River). The plots show that dissolved metal concentrations in the plume hit a minimum level at some point, and then begin to rise at lower sampling stations, likely due to additional sources entering the system. The exact location of the minimum for each metal species is dependent on geochemical reactions and specific properties of each metal. These plots support the ordering of the metal species along a pH-dependent sorption curve, as shown in the main report. Arsenic, lead, and iron look to have been most rapidly converted from dissolved to particulate/colloidal form, within the first 60-80km. The next group would include aluminum, copper, manganese, and nickel, which were converted by 100-120km. Dissolved cadmium and zinc persisted the longest, to 140-150km.





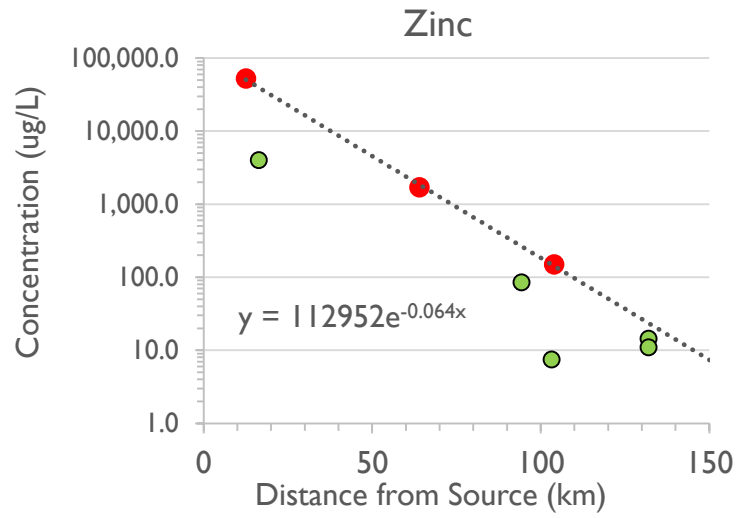


Figure E-9. Downstream attenuation in peak dissolved metal concentrations during plume passage in the Animas River.

Appendix F.
Quality Assurance-Quality Control

Contents

Overview.....	2
Data Acquisition.....	2
Analytics.....	3
Assessment of Data Quality & Completeness.....	4
Product Review.....	10
References.....	12

Overview

This project has followed quality assurance procedures described in the Quality Assurance Project Plan (QAPP) titled “Modeling Impacts of Mine Waste Release into the Animas River.” The QAPP addresses:

- data source quality and documentation,
- general analytical approach applied to acquired data,
- modeling quality assurance,
- data management and project archival record keeping
- product review

Project implementation involved gathering information and data from city, tribe, non-governmental organization (NGO), state and federal agency websites, along with modeling the fate and transport of metals, geochemistry of the release event, and impacts to groundwater. The project generated no new data though laboratory or field projects. Both post-event and historic, pre-event data were acquired. Acquired and modeled data were summarized according to project scientific design.

Data Acquisition and Processing

The project team gathered pre-event, event, and post-event data on water quality and stream sediments taken from many locations along Cement Creek, the Animas River, and the San Juan River. These data were collected by NGO, local, tribal, state, regional and federal government agencies. A comprehensive list of data sources is provided in Appendix A. All data acquired may not have been used in final data products presented in this report, but have been archived with project materials.

A master data file was created from the collation of original data files capturing event and post-event sampling efforts. Because of the project’s focus on analyzing metal concentrations associated with the event and post-event period, not all fields from original data files were retained in the master file. However, interested users can trace any record from the master file back to its comprehensive original data file using information contained in the master file, such as sample identifier (ID), site ID, sample date/time, collection agency, etc.

The EPA does not make any claims as to the quality or accuracy of the data gathered from the state, federal, and industry data sources used in the project. The project team applied quality assurance and quality control measures to acquired data to ensure that the analyses performed were properly conducted and that the data used in this report faithfully represented the original data obtained from all data sources. Acquired data were reviewed, but were used as received. Inspection occasionally identified significant outliers and peculiarities that suggested data error in the original files. The project team corrected obvious errors or consulted with source data owners to verify or correct data in the master file. Edited data are notated in supporting documentation with justification for doing so.

Some gathered data consisted of the geographic coordinates of sampled sites. Not all sites contained information on the horizontal datum associated with their coordinates. For these sites, we followed the following conventions: sites with Gold King Mine (GKM) event-related data were assumed to be using the World Geodetic System of 1984 (WGS84) horizontal datum; sites with historic data were assigned either the North American Datum of 1983 (NAD83) or the North American Datum of 1927 (NAD27), depending on when the data had been collected. This is documented in the “Notes” column of the sampling sites master list excel file.

A master shapefile and table were created of the sites associated with event and post-event sampling efforts. When combining sites with different horizontal datums into the shapefile, sites with different datums were first re-projected to a common horizontal datum using appropriate geographic transformations.

Secondary or ancillary geospatial data was also gathered primarily from federal, state, and local government agencies. These sources are detailed in Appendix A. Most of these data were used without modification; on occasion, changes (e.g., clipping, re-projecting, polygon merging) were made for mapping or analysis purposes. This is documented in the “Readme” files associated with the individual shapefiles.

Analytics

The project QAPP describes analytical approaches for assessing and summarizing water quality samples. Samples were used not only to empirically estimate metals mass in the GKM plume as it traveled down the Animas and into the San Juan (primarily accomplished via Excel files and statistical analyses in R), but also to inform simulation modeling of the fate and transport of the metals contained in the plume (i.e., WASP, groundwater, geochemistry). Modeling methods and calibration results are described in detail in Appendices B and D.

Empirical modeling was accomplished using measurements of metal concentrations in surface waters and stream sediments at a wide array of sites and times during and after plume passage. In addition, statistical comparisons with pre-event samples indicated where and when post-event conditions returned to a pre-event state. Recorded streamflow at USGS gauges were used at many locations to inform the empirical and simulation models, and techniques were used to extrapolate streamflow at several ungauged locations from observed flow at gaged sites. Streamflow estimation procedures are discussed in Chapter 2. Groundwater impacts were assessed at nearby well locations using multiple groundwater models including GFLOW™, GMS MODFLOW, WhAEM, and AnAq.

Non-Detect Methodology. Many samples taken during the post-event sampling period were below laboratory minimum detection limits (MDL). There was variability in these MDL’s depending on the analytical method and analyte, and sometimes original data did not include any MDL. In the “Result” column of the Master Data File created from all data gathered for this project, the EPA team denoted any non-detect measurement as “ND_” plus the minimum detection limit, if given. If no detection limit accompanied the measurement in the original data, the result was set to “ND.”

Many observations also included a lower reporting limit (LRL), which was always greater than or equal to the MDL. However, the MDL was reported more often than the LRL, which is the primary reason the team chose to designate non-detects using this value, rather than the LRL.

When data were pulled from the master file for analysis of plume fate and transport, or for statistical analyses on pre-event versus post-event comparisons, non-detects were set to their MDL if available. If the MDL was not available, the non-detects were set to the most common MDL for the analyte and analytical method, if known.

Because metal concentrations were elevated as the plume passed through the system, non-detections did not factor significantly into the analyses of this period. Non-detections were more prevalent in the data used to make pre-event versus post-event comparisons. In Chapter 9, the statistical result tables note when statistical analyses were avoided because the EPA team decided a large number of non-detections in the data were affecting the comparison results, especially because detection limits in the pre-event period were not typically the same as detection limits used in the post-event period (Note: the former tended to be greater than the latter).

All statistics and graphing were performed with R Statistical Software, version 3.3.1 (R Core Team 2013) or Microsoft Excel (2012, 2016). Versions of modeling software used during analysis are provided in Table 2-11.

Data files are managed in project electronic archives as defined in the QAPP (U.S. EPA 2015).

Assessment of Data Quality & Completeness

Data quality for surface water samples was evaluated by selecting samples with reported sulfate values because these samples allowed for the most complete suite of analyses. This criterion was satisfied for 233 out of approximately 3,200 water quality samples. These samples were subjected to tests for quality and completeness of the analytical suite by three methods: i) cation-anion charge balance; ii) comparison of sum of analytes, total dissolved solids and total dissolved solids estimated from the field measures of specific conductance and temperature; and iii) ratios of dissolved to total analytes.

Cation-anion charge balance: When water analyses are accurate and complete, the sum of cationic charge should balance anionic charge, consistent with the samples maintaining electro-neutrality (Stumm and Morgan 1981). In detail, trace metals can complicate the balance because several possess multiple valences and many of them can be bound by major solutes to produce a variety of charged complexes, with the resulting complex being a sensitive function of setting (e.g., oxy-anions). Commonly, these trace metals are present at orders of magnitude lower concentration than the major solutes, so their effect on overall balance is small. Considering these factors, and that the team is evaluating 233 samples drawn from a variety of settings, here the team examines the balance of the major solutes. Anions included in this balance include SO_4^{2-} , Cl^- , Br^- , H_2PO_4^- , F^- and OH^- . With a $\text{pK}_a \sim 7.2$ (Lindsay 1979), H_2PO_4^- was approximated as monovalent. Cations included Ca^{2+} , Mg^{2+} , Na^+ , K^+ , Al^{3+} , Fe^{2+} and Mn^{2+} . The cation Fe^{2+} does not complex with OH^- considerably, and Fe^{3+} complexes as FeOH^{2+} at $2.2 < \text{pH} < 5.7$ (Lindsay 1979) so a $2+$ approximation for the pH range in which Fe^{3+} is likely to be concentrated. The cation Al^{3+} was taken as trivalent, which is reasonable below its $\text{pK}_a \sim 5$ (Nordstrom et al. 1984), where its concentrations might be high. For these approximations, the cation/anion balance is depicted in Figures F-1 and F-2.

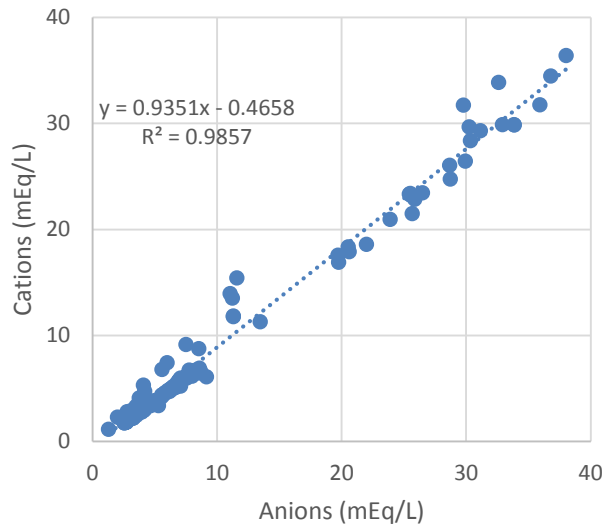


Figure F-1. Cation charge vs. anion charge. With a slope of 0.94 nearing the ideal of 1.0 and an R^2 of 0.99, charge balance supports that these analyses were reasonably accurate and complete.

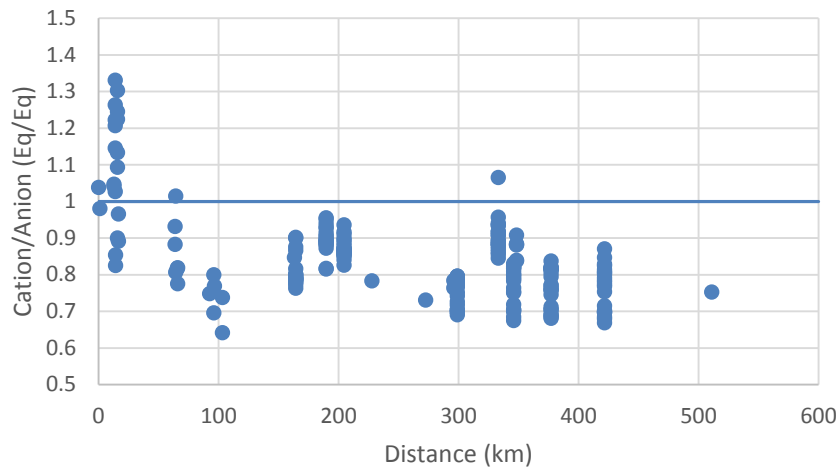


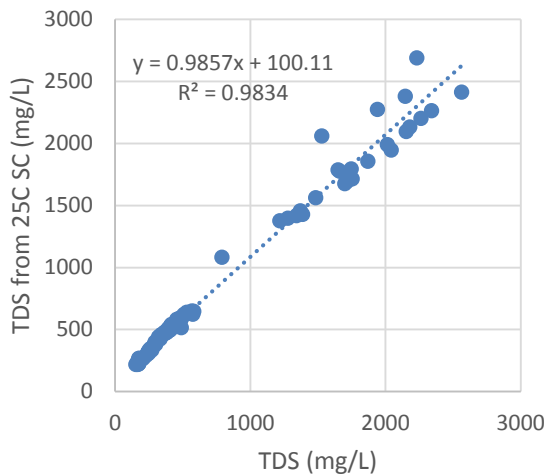
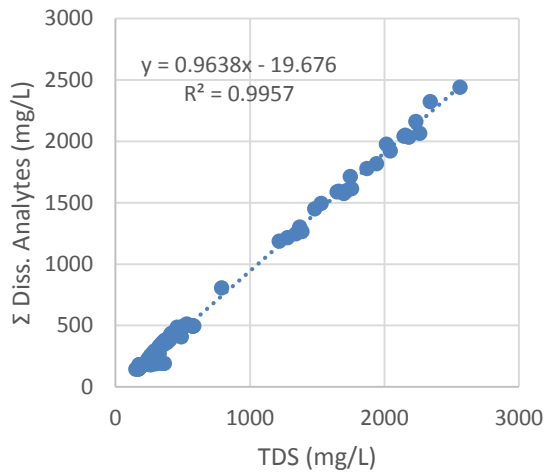
Figure F-2. Cation/Anion charge ratio vs distance from GKM. The large majority of samples fell with 30% of the ideal unity, a reasonable range. There appears to be more high cation/anion ratios near Gold King and excess anions more distant from the mine, perhaps reflecting an effect from neglecting trace solutes.

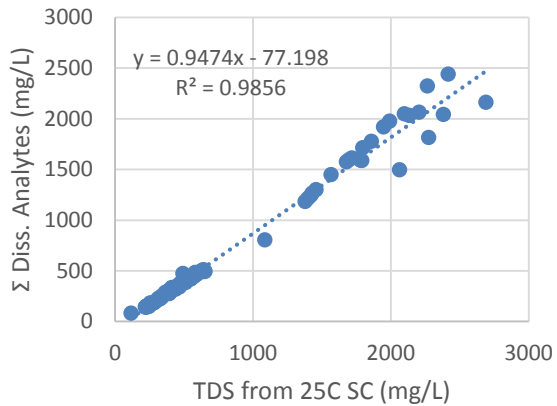
Comparison of sum of analytes, total dissolved solids and specific conductance: Total dissolved solids (TDS) commonly are reported by adding a filtered water sample to an accurately weighed container, weighing the water plus container, evaporating it to dryness, then reweighing the container to obtain the dissolved solids in that mass of water. When chemical analyses of water samples are complete and accurate, the sum of analytes should be close to the same value as TDS.

Because electric charge is carried through water by dissolved ions, field specific conductance (SC) has been shown to be roughly proportional to TDS (Hem 1989). The effect of temperature on SC is removed by applying a 2% correction per degree centigrade (Hem 1989):

$$SC_{25\ C} = SCT(1+0.02(25-T)) \tag{1}$$

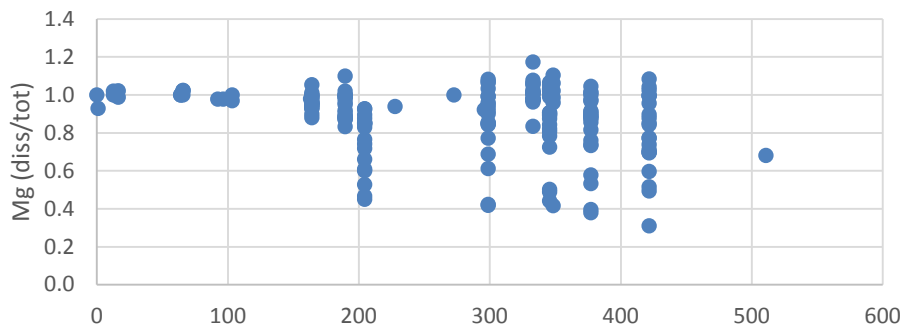
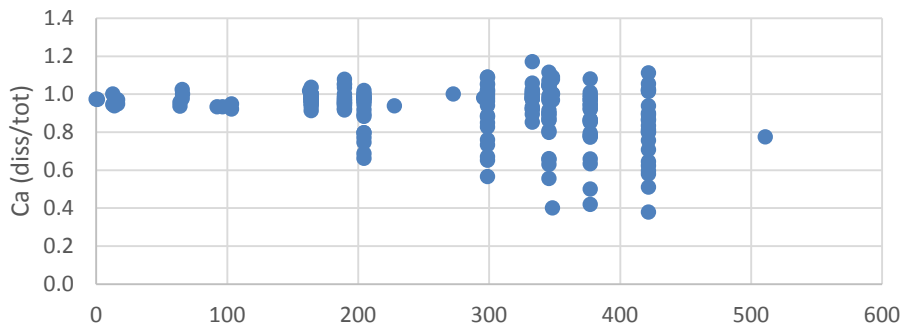
Although there is variation in the relationship between concentration and SC among ions, in natural waters TDS (mg/L) often falls close to 0.059 SC_{25 C} (μS/cm) (Hem 1989). Given all this, TDS, sum of analytes, and TDS estimated from SC are compared in Figures F-3a, F-3b and F-3c. These comparisons are supportive of reasonable completeness and accuracy for these data.

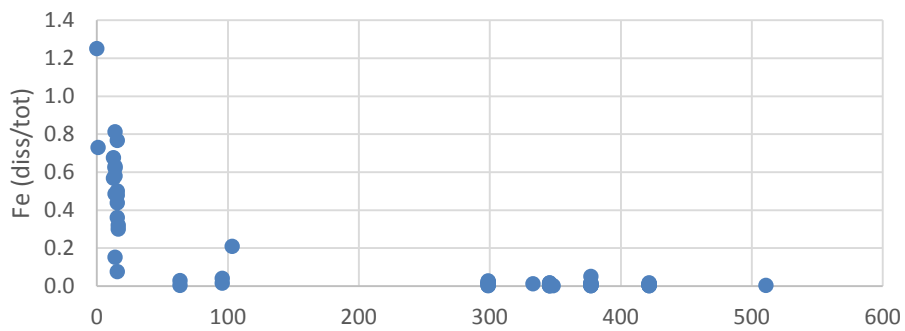
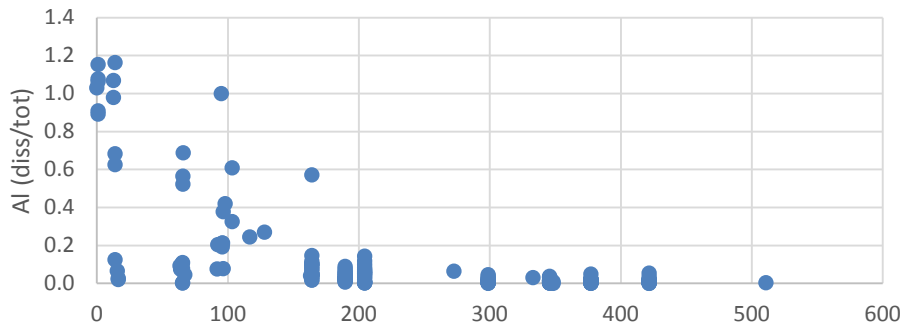
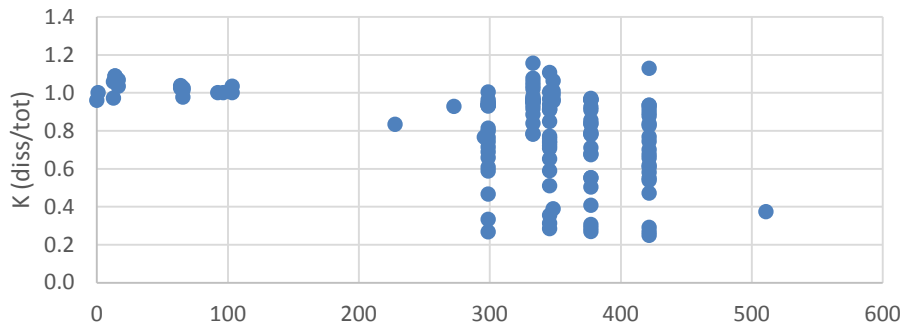
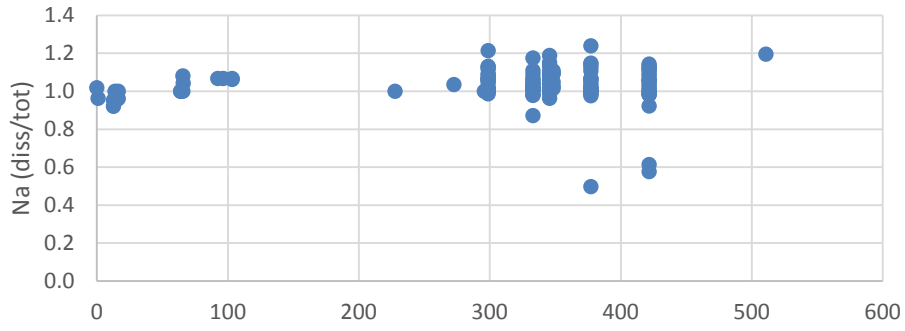


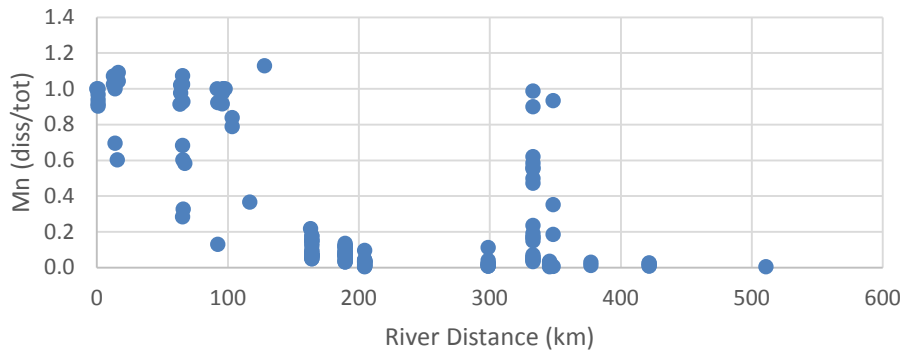


Figures F3 a-c. Estimates of dissolved solids by various methods. With slopes of 0.95 to 0.99 being close to the ideal of unity and $R^2 = 0.98$ to 0.99 , these comparisons suggest acceptable accuracy and completeness.

Ratios of dissolved to total analytes: When a water-sample source is well-mixed, the ratio of dissolved to total for analytes ideally should fall at unity or less than one. Because of uncertainties regarding mixing at the source, and sampling and analytical artifacts, and considering the objectives for the data use, values for this ratio of <1.3 can be considered reasonable. Here, the team evaluates major cations by this criterion (Figures F-4a through F-4g). Results of this evaluation suggest reasonable internal consistency of dissolved and total major cations. Although not presented, trace metals have been evaluated by this method as well.







Figures F-4 a-g. Dissolved/total major analyte ratios versus distance from GKM. Almost all values fall below 1.2, suggesting reasonable internal consistence between dissolved and total major solute analytes.

In addition to these analyses, the EPA team also examined all samples in the dataset for which dissolved and total concentrations of various analytes were measured concurrently (n= 1,415 total samples). Out of this population, they identified 60 samples for which the dissolved concentration of at least one analyte exceeded the total concentration by 30% or more. For most of these cases, the team was able to find a reasonable explanation for the higher dissolved measurement, including: 1) the original data incorporated into the master data file were later re-issued with dissolved and total concentrations transposed to reflect their correct magnitudes; 2) the team had attributed an incorrect detection limit for a non-detect outcome; and 3) either the dissolved or total concentration were flagged as an estimated value, not an actual measurement. In these cases, the dissolved and/or total concentrations were transposed or changed so as to reflect their correct magnitudes. For the small number of samples that remained, the team transposed the dissolved and total concentrations in the master data file, but noted this in the “Comment” column of the master data file for these measurements so they could be easily identified.

Duplicate samples: The EPA team identified duplicate samples in the master data file, representing the situation where two samples were collected and processed at the same location and time for various analytes. They chose to disregard samples where one or both measured values were below detection limits, as sometimes these limits were not identical for the paired measures, sometimes no detection limit was given, and sometimes obvious errors in detection limit reporting were found. After doing this, the team had 1,845 pairs of sediment samples, 1,832 pairs of total surface water samples, and 1,378 pairs of dissolved surface water samples.

For each pair of values, the team calculated the absolute % difference of the two values (i.e., the absolute value of their difference divided by the mean of the two values) as a measure of reliability and uncertainty in the measurement of metal concentrations. Variability could arise from a number of sources (e.g., field sampling and collection activities, laboratory preparation and analyses), but the team did not have enough information to specifically attribute variability amongst these various sources. They found that the average % difference for sediment samples was 20%, while the average % difference for both total and dissolved surface water samples was 14%. They also found that 93% of all of the paired samples were less than 50% different from one another, and 81% were less than 25% different. The team deems the data on measured metal concentrations to have good reliability based on these results.

Product Review

The project's QAPP (U.S. EPA 2015) was approved by the EPA project quality assurance manager on October 6, 2015. Minor deviations from the approved QAPP were documented by individual researchers and resulted in no impact on data quality.

A project specific Technical Systems Audit (TSA) was conducted on January 12-13, 2016 which assessed implementation of the project's QAPP. Additionally, team members participated in an internal laboratory competency audit (LCA) conducted July 19-21, 2016 which reviewed documentation practices and conformance to Agency policies and procedures. Findings identified during either assessment were determined to not adversely impact data quality. Corrective actions were identified and implemented.

The modeling included in this report was reviewed with a mid-course panel peer consultation in February 2016. Versar, Inc. (Versar), an independent contractor, assembled five scientific experts with expertise in the following areas: (1) geochemistry, (2) fate and transport (water/sediment), (3) water quality analysis simulation (WASP) modeling, (4) groundwater modeling, (5) geospatial analysis (EnviroAtlas modeling), and (6) bioaccumulation. The reviewers met in Athens, Georgia for three days to evaluate the scientific integrity of EPA's analysis and characterization of the fate, transport, and potential impacts of acid mine drainage (AMD) release in the Animas and San Juan Rivers. The EPA scientists presented their analysis and findings to the reviewers, then each reviewer provided his individual written response to a set of charge questions.

The five reviewers were screened by Versar for scientific qualifications and any conflicts of interest. The peer consultation followed procedures specified in EPA's Peer Review Handbook, 4th edition. The selected reviewers are listed below:

Brian S. Caruso, Ph.D., P.E

U.S. Geological Survey
Denver, CO

Charles R. Fitts, Ph.D.

Fitts Geosolutions, LLC
Scarborough, ME

Henk M. Haitjema Ph.D.

Haitjema Consulting, Inc.
Bloomington, IN

D. Kirk Nordstrom, Ph.D.

U.S. Geological Survey
Boulder, CO

William A. Stubblefield, Ph.D. (chair)

Oregon State University
Corvallis, OR

The modeling was updated based on feedback provided during the peer consultation, and developed into a final report. EPA also prepared a written response to the peer consultation. The final report was categorized as Influential Scientific Information (ISI), as defined by the OMB Peer Review Bulletin, and the report underwent a thorough peer review. It was also listed on EPA's publicly available Peer Review Agenda.

Peer review of this document occurred via a letter review that was independently managed by Versar. Four reviewers were chosen to review the report and respond to charge questions pertaining to hydrology, geochemistry, fate and transport, and potential impacts from the GKM release. The same set of scientific expertise was represented as had occurred in the mid-course peer consultation. Versar conducted a thorough COI screening for each reviewer and met with EPA staff to discuss any actual or potential COI. The peer reviewers each provided written responses to a set of charge questions. Following receipt of the Peer Review Report, this document was revised to reflect suggested changes and clarifications from the peer reviewers. Versar's Peer Review Report and EPA's response to peer review are posted on EPA's Peer Review Agenda. The four selected reviewers are listed below:

Charles Fitts, Ph.D.

Fitts Geosolutions
Scarborough, Maine

Glenn C. Miller, Ph.D.

University of Nevada
Reno, Nevada

Ronald L. Schmiermund, Ph.D.

Economic & Environmental Geochemistry, Inc.
Lakewood, Colorado

Mark A. Williamson, Ph.D.

Geochemical Solutions, LLC
Loveland, Colorado

Quality assurance (QA) review of this document was conducted by a team of EPA quality assurance managers and consisted of review of associated datasets used to generate original EPA table and figures. Reviews focused on ensuring that rows, columns, and tables were properly labeled, units were identified, transcription errors were addressed, and errors in calculations were corrected. The QA reviewers each provided written comments for each reviewed table and figure. Following receipt of these comments, project team members determined whether any comments impacted tables or figures and then revised datasets as needed prior to the release of this report.

References

- FGDC (Federal Geographic Data Committee). 1998. Content Standard for Digital Geospatial Metadata, FGDC-STD-001-1998. <http://www.fgdc.gov/standards/projects/FGDC-standards-projects/metadata/base-metadata/index.html>.
- Hem, J. D. 1989. Study and Interpretation of the Chemical Characteristics of Natural Water. Washington, D.C., U.S. Geological Survey.
- Lindsay, W. L. 1979. Chemical equilibria in soils. New York, NY, John Wiley & Sons.
- Luedke, R. G. and W. S. Burbank (1999). Geologic map of the Silverton and Howardsville quadrangles, southwestern Colorado. U. S. G. Survey.
- Nordstrom, D. K., S. D. Valentine, J. W. Ball, L. N. Plummer and B. F. Jones. 1984. Partial compilation and revision of basic data in the WATEQ programs. Water-Resources Investigation Report 84-4186. Menlo Park, CA, U.S. Geological Survey: 43.
- R Core Team. 2013. R: A language and environment for statistical computing. R Foundation for Statistical Computing, Vienna, Austria. ISBN 3-900051-07-0, URL <http://www.R-project.org/>
- Stumm, W. and W. W. Morgan. 1981. Aquatic Chemistry. New York, NY, Wiley-Interscience.
- U.S. EPA (Environmental Protection Agency) 2007. Geospatial Metadata Technical Specification Version 1.0. Office of Information Collection Office of Environmental Information, Environmental Protection Agency, November 2007. <http://www.epa.gov/geospatial/policies.html>.
- U.S. EPA (Environmental Protection Agency). 2015. Peer Review Handbook, 4th edition. https://www.epa.gov/sites/production/files/2015-10/documents/epa_peer_review_handbook_4th_edition_october_2015.pdf
- U.S. EPA (Environmental Protection Agency). 2015. Modeling Impacts of Mine Waste Release into the Animas River, Quality Assurance Project Plan, Version 1.1. 42 pp.

